PROPERTIES AND BEHAVIOUR OF PROGENITOR CELLS IN THE EMBRYONIC CHICK RETINA

NANNA LIEBACH LÜNEBORG

A thesis submitted for the degree of
Doctor of Philosphy
in the
University of London

Department of Physiology
University College London

April 2005

UMI Number: U592267

All rights reserved

INFORMATION TO ALL USERS
The quality of this reproduction is dependent upon the quality of the copy submitted.

In the unlikely event that the author did not send a complete manuscript
and there are missing pages, these will be noted. Also, if material had to be removed,
a note will indicate the deletion.

UMI U592267
Published by ProQuest LLC 2013. Copyright in the Dissertation held by the Author.
Microform Edition © ProQuest LLC.
All rights reserved. This work is protected against
unauthorized copying under Title 17, United States Code.

ProQuest LLC
789 East Eisenhower Parkway
P.O. Box 1346
Ann Arbor, MI 48106-1346

ABSTRACT

During embryonic development, interactions between extracellular signalling molecules and intracellular transduction pathways are involved in the regulation of cell proliferation, differentiation and migration. This thesis investigates the properties and behaviour of cells in the developing neural retina of 4-9 day old chick embryos. In addition, it describes the expression of amino acid transmitter receptors and gap junctional communication amongst progenitor cells and newly differentiated neurons at these early times.

The membrane properties of progenitor cells and postmitotic neurons were investigated using whole-cell patchclamping of cells in retinal slices. The results show that E5-E8 progenitor cells, but not postmitotic neurons, respond to GABA and glutamate and are coupled via gap junctions to neighbouring cells. Postmitotic neurons, but not progenitor cells, express time-dependent, voltage-gated currents.

Progenitor cells are characterized by extensive gap junctional coupling, which gradually increases from E4-E6, and decreases towards the end of neurogenesis, from E7-E9. Postmitotic cells are excluded from the coupled clusters. The expression of Cx43 and Cx36 is consistent with a role for these connexin proteins in mediating the coupling between proliferating cells, and interference with Cx43 expression resulted in a reduction in gap junction coupling.

The interkinetic nuclear migration and division of progenitor cells was followed in real time using confocal microscopy. The movement of these cells is saltatory, and characterized by stationary phases interspersed with rapid movements in both directions, to produce an average rate of movement of around 20μm per hour. The maintenance of normal rates of migration is dependent on intact gap junctional communication. Unopposed gap junction hemichannels were found to

play a role in migration. The effect of neurotransmitters on interkinetic nuclear migration was also investigated. Agonists and antagonists of GABA-, glutamate-, ACh-, and purine-receptors were found to have minor effects on interkinetic nuclear migration.

CONTENTS

Chapter 3

Membrane properties and neurotransmitter responses of cells in the ventricular zone of the embryonic chick retina

Chapter 4

Gap junctional coupling of progenitor cells during early development of the chick retina

Chapter 5

The properties of interkinetic nuclear migration in embryonic chick retina and its modulation by gap junctions, hemichannels and neurotransmitters

List of Figures

List of Tables

Supplementary Material

Acknowledgements

I would like to thank my supervisor, Peter Mobbs, for his guidance, encouragement and support throughout my PhD. I am also grateful to Marina Catsicas, Rachael Pearson, David Attwell and David Becker for teaching me and giving me advice on experiments and analysis. I would also like to thank Rachael for her contributions to the collaboration in Chapter 5, as well as all manner of helpful PhD-survival tips.

A big thanks to all my fellow lab rats, past and present, for all their help and inspiration, for providing such good company, making the long days of doing analysis go a little quicker, and making the summer lunchtimes and evenings, in the quad and on the roof, a lot of fun: Nicky Allen, Danni Billups, Martine Hamaan, Celine Auger, David Rossi, Paikan Marcaggi, Ines Hans, Pauline Cavalier, Jo Kittler, Jenga Karadottir, Claire Peppiat, Clare Howarth, Manuela Lahne, Jamie McCutcheon, Louise Whiteley, Lata Ramakrishnan and Anna Simoni.

Thanks also to Rachel Hammond, Catharine Winstanley, and everyone in the Wellcome-gang: Tom Nielsen, Paul Miller, Catherine Hall, Laura von Hertzen, Ronnie Gee and Susan Griffin, for many hilarious evenings in the pub and in New Orleans, and for being such fun fellow sufferers on all things neuroscience and PhD related.

Finally, a special thanks to Oleg, Johannes and my parents for all their invaluable support and encouragement throughout, and for their never-ending faith in me.

This work was supported by the Wellcome Trust.

Chapter 1

INTRODUCTION

1.1 Aims of current study

During the development of an embryo, the central nervous system develops from a single population of stem cells. These stem cells divide and form specialized regions that will give rise to the different parts of the mature nervous system. One such region is the optic cup, where the retina begins as a single layer of cells. These cells undergo multiple rounds of division to form the mature structure. In the adult chick, the retina contains around two hundred million cells, nearly all of which are produced in the 10-day period following the formation of the optic cup, corresponding to the production of around 250 cells per second. These cells must be produced in the correct number, adopt the correct fate, migrate to their final destinations, and form the appropriate synaptic connections with other cells. To ensure the proper function of the adult retina, these processes must be tightly regulated. While the development of the visual pathways from the retina to other parts of the brain has been extensively studied, much less is known about the regulation of the early stages of retinal development.

The experiments described in this thesis aim to define the properties and behaviour of progenitor cells in the embryonic chick retina. This chapter provides a brief introduction to retinal development and some of the factors thought to be involved in its regulation. Chapter 2 describes the methods employed in the experiments described in this thesis. Chapter 3 describes the membrane properties and the responses to neurotransmitters of cells in the embryonic retina. Chapter 4 examines the gap junctional coupling between cells in the developing retina. Chapter 5 describes live imaging experiments of retinal cell migration and cell division, and investigates the role of neurotransmitters and gap junctions in regulating migration.

1.2 The chick retina as a model

The chick retina provides an excellent model in which to study the development of the nervous system for a number of reasons. The timetable for chick retinal development is well documented, and the retina is easily accessible at all times during development. The adult structure has been extensively studied, so the different cell types, signalling pathways and anatomical structure are well described. Like other regions of the central nervous system, the retina is derived from the neural tube. Although other structures within the nervous system can be studied in isolation, the retina is unique in that within isolated preparations both structure and function are preserved relatively intact. The basic processes of mitosis, migration and differentiation resemble those found throughout the early neural tube, and the many commonalities between retinal and cortical neurogenesis mean that findings made using one tissue often apply to the other.

A limitation of studying the neural retina in isolation, without the pigment epithelium, is that this removes a source of both membrane-bound and diffusible signals between the tissues. The absence of the pigment epithelium has been shown to affect several different processes in development of the neural retina, including photoreceptor development (Hollyfield and Witkovsky, 1974) and the rate of mitosis (Pearson et al., 2002, Pearson et al., 2005).

1.3 Adult retina

1.3.1 Basic anatomy

The mature chick retina consists of six different types of neurons and one type of glial cell, the Müller cells. It is organised into three layers of cell bodies: the outer nuclear layer (ONL), inner nuclear layer (INL) and the ganglion cell layer (GCL). The ONL contains the cell bodies of the photoreceptors, of which there are two types, rods and cones, the outer segments of which lie adjacent to the retinal pigment epithelium (RPE) at the back of the eye. The ONL is separated from the INL by the neuropil of the outer plexiform layer (OPL). The INL contains the cell bodies of the Müller glia, along with those of three neuronal cell types, the amacrine, horizontal and bipolar cells. Bipolar cell axons and amacrine dendrites are located in the inner plexiform layer (IPL), along with the dendrites of the retinal ganglion cells (RGCs). The axons of RGCs form the most superficial layer at the front the retina (the fibre layer (FL)), and represent the output pathway for signalling to the optic tectum in the brain. Some RGCs are found in the INL, and are termed 'displaced' RGCs, and similarly 'displaced' amacrine cell bodies may be found in the GCL (Figure 1.1B). Unlike the mammalian retina, which contains both astrocytes and Müller glial cells, the chick retina contains only Müller glia, which extend processes to the outer and inner limiting membranes of the retina (Figure 1.1B).

The circuitry of the retina is organised into vertical and lateral pathways. In the vertical pathway, photoreceptors transduce the changes in light intensity into an electrical signal, and synapse with bipolar cells, which in turn synapse with the output cells of the retina, the RGCs. One or many photoreceptor cells may form synaptic connections with a single bipolar cell, one or many of which may contact a RGC. The degree of convergence of inputs to a single output varies with the central-to-peripheral gradient across the retina, with the highest resolution (and the least convergence of inputs) in the central area of the retina,

the fovea. The horizontal and amacrine cells form lateral pathways at the level of the OPL and IPL, respectively, mediating lateral inhibition, and modulating the transfer of information from the photoreceptors to the RGCs.

1.3.2 Information processing in the retina

The response to a visual stimulus begins with the absorption of a photon by the visual pigment within a photoreceptor. Rod photoreceptors are highly sensitive and mediate vision in dim light, whereas cone photoreceptors operate in bright light and provide colour vision. In the chick, cone photoreceptors vastly outnumber rods, and contain one of four different visual pigments, red, blue, green and violet. Avian cones contain oil droplets in their inner segments that differ in color and size, depending on the cone subtype. These oil droplets sharpen the tuning of the cones by reducing the window of the receptor's spectral responses (reviewed in Okano et al., 1995). The absorption of a photon leads to a conformational change in the visual pigment, and this initiates a transduction cascade leading to the hydrolysis of cGMP. In the dark, cGMP gates a cation-permeable channel in the outer segment of the photoreceptor, producing the so-called 'dark current', which maintains the photoreceptor cell in a depolarised state, causing tonic release of glutamate from the photoreceptor terminal. The dark current is carried mainly by influx of Na^+-ions through the cGMP-gated channel, which is balanced electrically by an influx of K^+-ions in the inner segment, and electrochemically by the Na^+/K^+-ATPase. The light-induced hydrolysis of cGMP causes the channel to close, reducing the dark current and hyperpolarising the cell, leading to a reduction in the level of tonic glutamate release from the photoreceptor terminal.

Outside of the fovea, bipolar and horizontal cells receive convergent inputs from multiple photoreceptors, and respond to the light-induced reduction in glutamate with graded, sustained potentials. Bipolar cells may be ON-centre, and

depolarise in response to light, or OFF-centre, and hyperpolarise in response to light. Bipolar cells in turn form glutamatergic synapses onto the dendrites of RGCs and amacrine cells in the IPL. RCGs respond to light with either an increase or a decrease in membrane potential, depending on whether they are driven by an ON-centre or OFF-centre bipolar cell input. Horizontal cells hyperpolarize in response to light, leading to a decrease in the rate of tonic release of the inhibitory transmitter γ-amino-butyric acid (GABA). The lateral interactions formed by the inhibitory input of horizontal cells to bipolar cells and photoreceptors provide the centre-surround receptive fields, which form the basis for the detection of contrast. The lateral inhibition of RGCs by amacrine cells in the IPL is dependent on rapid changes in the input signal, which provides a mechanism for the detection of motion.

1.4 Retinal development

1.4.1 Early retinal development

The entire central nervous system originates from the neural plate, a derivative of the dorsal ectoderm of the gastrula. The nervous system starts as a sheet of neuroectodermal cells, the neural plate, which invaginates along its length to form the neural tube. This occurs between the four- and seven-somite stage in the chick, corresponding to Hamburger and Hamilton (1951) stage 8-9. The neural tube is compartmentalised into different regions, to give rise to different parts of the nervous system. This segmentation along the anterior-posterior axis is orchestrated by the homeobox (*hox*) genes (for review, see Mey & Thanos, 2000). The optic vesicles are formed through evagination of the neural tube in the region destined to form the forebrain (Figure 1.1A). In the chick, this occurs at Hamburger and Hamilton (1951) stage 9, which corresponds to 29-33 hours post-fertilization. The base of each vesicle constricts until its connection to the brain is reduced to a narrow stalk. Subsequently, the optic vesicles invaginate to form a two-layered structure, the optic cup (Figure 1.1A). The thickened inner layer of this undergoes repeated cycles of division to form the multilayered neural retina, while the outer layer remains a single cell layer thick, and forms the retinal pigment epithelium (RPE). Within the neural retina, cell division is confined to the region adjacent to the RPE, the ventricular zone. Pigmentation of the RPE begins around E3 (Hamburger & Hamilton (1951) stage 18-19), although RPE cells can be induced to transdifferentiate into neuronal cell types until E4.5 (Coulombre & Coulombre, 1965). The decision to adopt epithelial or neural cell fate depends on the positional information in signals released from the surrounding tissue. Culture experiments have shown that fibroblast growth factors (FGFs) from the surface-ectoderm play a pivotal role in facilitating neural retinal differentiation from the alternative RPE default fate (Pittack et al., 1991; Pittack et al. 1997). The entire process of retinal development lasts around 3

weeks and is essentially complete at the time of hatching (20-21 days post-fertilization).

1.4.2 Cell proliferation

Cell division is controlled by regulating the timing of two critical events in the cell cycle: nuclear DNA replication and mitosis. The cell cycle can be divided into four sequential steps: G_1 (gap 1), S (synthesis), G_2 (gap 2), and M phase (mitosis). M phase is subdivided into prophase, metaphase, anaphase, telophase and cytokinesis. Replication of DNA occurs during S-phase. During mitosis the genetic material is equally partitioned (in anaphase) and two new daughter cells are born (telophase and cytokinesis). Passage through the cell cycle is controlled by cyclin-dependent kinase complexes (CdkCs). For example, during G_1, CdkCs activate transcription factors to express enzymes necessary for DNA replication and induce degradation of S-phase inhibitors to prepare for and initiate the next phase. During S-phase, other CdkCs control DNA replication, and in G_2, mitotic CdkCs are synthesised. The degradation of proteins by CdkCs drives the cell cycle in one direction because of the irreversibility of protein degradation. S-phase, G_1 and G_2 are collectively known as interphase. Upon exit from the cell cycle, the cell enters the quiescent G_0 stage, and, in the case of neurons, becomes post-mitotic, i.e. unable to re-enter a proliferative state (reviewed by Lodish et al., 2000). The cell cycle duration in the developing retina increases with time and ranges from 6-18 hours (Morris & Cowan, 1995).

1.4.3 Progenitor cells undergo interkinetic nuclear migration

Progenitor cells in the developing retina, as well as the developing cortex, undergo a process called interkinetic nuclear migration (INM) as they pass

through the cell cycle (Figure 1.2A). Progenitor cells have bipolar morphology, extending processes to both surfaces of the tissue (Figure 1.2B). During G_1, the soma moves from the ventricular zone to the vitreal surface, where S-phase takes place, and returns to the ventricular zone in G_2, and undergoes mitosis. After terminal division, newly differentiated cells migrate from the ventricular zone to a location appropriate to their fate. At later times in development, there is evidence to suggest that a small population of mitotic cells divides in the inner part of the neuroblastic layer or, after the outer plexiform layer has formed, in the inner nuclear layer, resembling the subventricular zone in the developing cortex. Cells dividing there are fewer in number than those at the ventricular zone, and show little nuclear movement between S- and M-phases of the mitotic cycle (Robinson et al., 1985). However, at early times, mitosis predominantly occurs within the ventricular zone, and thus factors affecting the rate of interkinetic nuclear migration also affect proliferation. The role and regulation of INM in neurogenesis to date has not received much attention. Murciano et al. (2002) used mathematical modelling to analyse the influence of INM on neurogenesis. In the absence of INM, the model predicted an increase in the number of cells leaving the cell cycle, due to the reduction in the influence of inhibitory signals. The enhanced level of neurogenesis led to a predicted diminution of the neuroepithelium and a reduction in the later production of neurons, suggesting that INM might be important for maintaining proliferation, and thus for the efficient and continued production of neurons.

1.4.4 Cell divisions can be symmetric or asymmetric

All cells in the mature retina derive from a single population of multi-potential progenitor cells, with a single progenitor giving rise to a clone of mixed cell types (Turner & Cepko, 1987; Turner et al., 1990). The process of proliferation overlaps with differentiation. Cell divisions are either symmetric or asymmetric. Early in development, most divisions are symmetric, producing two identical

daughter progenitor cells, to enlarge the pool of dividing cells. At the onset of neurogenesis, some divisions become asymmetric, generating one progenitor daughter, which re-enters the cell cycle, and one post-mitotic cell, which differentiates and migrates to its final destination (as shown in figure 1.2A). Finally, towards the end of neurogenesis, symmetric terminal divisions occur, in which both daughter cells exit the cell cycle and become post-mitotic (Takahashi et al., 1993 and 1994; Caviness et al., 1995).

1.4.5 Progenitor morphology during cell division

It has generally been believed that retinal and cortical progenitors retract their basal process as they progress through mitosis (Figure 1.2A), and that the two daughter cells, regardless of fate, re-extend a process following cytokinesis, either for migration out of the VZ, or to resume INM. However, recent evidence has questioned this view. Noctor et al. (2001), using time-lapse imaging of cortical progenitor cells, did not observe any examples of process retraction. They suggest instead that the process becomes very thin, yet is maintained throughout mitosis. However, the frequency of image-acquisition they employed did not allow them to rule out the occurrence of process retraction and re-extension, since this may have occurred in the interval between image frames. Saito et al. (2003) used timelapse-imaging of DiI labelled cells in cultured slices of E14-17 mouse retinae, and also observed cell division without process retraction, including divisions generating two progenitor daughters, suggesting that asymmetric process inheritance does not preclude a functionally symmetric division.

1.4.6 Different cell types are generated in a conserved sequence

Prada and colleagues (1991) used [^{3}H]-thymidine injections in chick embryos to

chart the timing and sequence of neurogenesis. The first cells to withdraw from the cell cycle, at E2, are ganglion cells, followed, by amacrine, horizontal, photoreceptor, Müller glia, and bipolar cells (see Figure 1.3), which withdraw in phases that substantially overlap one another. Neurogenesis is complete around E12. This sequence of development of the different cell types is conserved across all species studied so far, including *Xenopus*, mouse, rat, rabbit, ferret and monkey (Cepko et al., 1996; Livesey & Cepko, 2001).

1.4.7 Cell death

In virtually all developing tissues that have been examined, substantial cell death occurs. Cell death has been suggested as the default pathway for all cells, unless they receive the appropriate survival signal, a trophic factor. It is not well understood what the benefit is of an initial massive overproduction of cells, followed by extensive cell death, but it is a widely observed phenomenon, and plays an essential part in normal development, serving to regulate the final number of cells. Studies of cell death in the nervous system have focused on postmitotic neurons as they form synaptic targets, and compete for target-derived trophic factor, leading to cell death of up to 50% or more of many types of neurons. However, mitotically active cells can also undergo programmed cell death (for review, see Oppenheim, 1991; Raff et al., 1993). In the chick retina, at least two discrete periods of programmed cell death have been described: an early period around E5-E7 (Frade et al., 1997), and a later period of major cell death around the time of tectal innervation (embryonic day 10-14). In the early period, apoptosis is induced by nerve growth factor (NGF) acting via the p75 receptor, and can be prevented by application of brain-derived neurotrophic factor (BDNF). BDNF is expressed in both the RPE and neural retina from E4, along with a BDNF receptor, TrkB, in the neural retina, suggesting that early cell death regulates the neurogenesis of retinal ganglion cells (which is the main cell type generated at this stage) and is regulated locally by BDNF (Frade et al.,

1997). The later period of cell death in the retina occurs around the time of tectal innervation by the retinal ganglion cells, which compete for target-derived trophic factors; if the optic fibres are transected, or the tectum is lesioned, the corresponding ganglion cells undergo apoptosis (Hughes & McLoon, 1979; for review, see Raff et al., 1993). Spontaneous activity in the tectum and the retina serves to fine-tune retinotopic maps in the tectum and connectivity within the retina, and inappropriate connections are eliminated by cell death. However, not all cell types in the retina undergo programmed cell death. Cook et al. (1998) used propidium iodide staining of pyknotic nuclei and TUNEL-labelling to investigate apoptosis in the chick retina at different developmental stages, and did not find any evidence of apoptosis in the outer nuclear layer, showing that programmed cell death is not universal amongst different retinal cell types. Similarly, in the developing mouse retina, Young (1984) found that while ~50% of ganglion, amacrine and bipolar cells are eliminated by cell death, this was only true for ~5% of photoreceptor cells.

1.4.8 Intrinsic and extrinsic mechanisms control development

Neurogenesis is regulated by signalling pathways that integrate extracellular signals concerning the identity and number of neighbouring cells, and intracellular cues about cell size and developmental stage. Several models involving a feedback mechanism of neuronal fate choice have been put forward, whereby differentiated neurons release a factor to either inhibit the generation of additional cells of the same type, or promote different cell types. Lesioning of specific cell layers during embryonic development results in the generation of new cells in proportion to the degree to which each cell type was destroyed, rather than those generated in normal development (Reh, 1987). Co-culturing progenitor cells from E4 chick retina with cells from older retinae reduces the number of cells that differentiate to become RGCs, an effect that increases with the age of the older cell population, and that has been shown to be due to a

diffusible factor, rather than direct cell-cell interactions (Waid & McLoon, 1998). Similarly, co-culturing rodent E16 retinal progenitors with a P0 population, which has been depleted of amacrine cells, leads to an increase in the number of amacrines generated by the E16 progenitors (Belliveau & Cepko, 1999). Experiments using dissociated cultures grown in the presence of various transmitter agonists and antagonist show that taurine, acting via GABA- and glycine-receptors promotes differentiation of rod photoreceptors, and this was confirmed *in vivo* by targeted knockdown of the glycine-receptor in question, the α2-subtype (Altschuler et al., 1993; Young & Cepko, 2004). The development of ganglion, horizontal, amacrine, bipolar, rod and cone photoreceptor cells have all been shown to be regulated by extrinsic cues (Altschuler et al., 1993; Belliveau & Cepko, 1999; Belliveau et al., 2000; Waid & McLoon, 1998).

Intercellular signalling via direct cell-cell interactions, in particular Notch-Delta signalling, have been shown to play a role in regulating proliferation in many different tissues, including the retina (Gridley, 1997; Perron & Harris, 2000). Delta is the membrane-bound ligand for the Notch-receptor. Notch activation can affect regulation of transcription factors via cleavage of the intracellular part of the receptor, which translocates to the nucleus. In the chick retina, Notch signalling has been shown to be necessary for maintaining a proliferative state. If Notch signalling is suppressed in early retino-genesis, an overproduction of ganglion cells occurs, as too many progenitors leave the cell cycle and differentiate (Austin et al., 1995).

However, cell fate does not simply depend on the balance of extracellular cues; there is a progressive restriction of fate competences as development proceeds. The following lines of evidence support this notion. Firstly, lesions made at later stages do not lead to regeneration of early-born cell-types, as is the case if the lesion is made early in development, despite continued proliferation of later-born cell types (Beazley et al., 1987). Secondly, while co-culture of labelled, late retinal progenitor cells with early progenitor cells does

lead to a change in the proportion of cells adopting different fates, with an increase in bipolar cells and a decrease in rods, none of the late progenitors adopt the ganglion, horizontal or amacrine cell fates, which are usually adopted by the daughters of early progenitors (Belliveau & Cepko, 1999; Belliveau et al., 2000). These findings support a 'competence model' of cell-fate determination, whereby progenitors pass through intrinsically determined competences, at each stage being able to generate a subset of possible cell types, the balance of which is determined by the extracellular cues in the environment (Livesey & Cepko, 2001; Adler & Belecky-Adams, 1999).

1.5 Are radial glia progenitor cells?

The traditional view of radial glia in the developing cortex is that they are postmitotic cells that act as a scaffold for the migration of neurons generated by progenitor cells (Rakic, 1972). Recently, the distinction between radial glial cells and progenitor cells has been blurred, by findings suggesting that radial glial cells are neuronal progenitor cells (for reviews, see Parnavelas & Nadarajah, 2001; Campbell & Götz, 2002; Goldman, 2003). In both cortex and retina, there are striking morphological similarities between radial glial cells and the bipolar progenitor cells seen in development. In the developing cortex, radial glia have been shown to be able to give rise to neurons. Malatesta and colleagues (2000) used fluorescent-activated cell sorting of radial glial cells expressing GFP under the control of a glial fibrillary acidic protein (GFAP) promoter, to show that these cells could give rise to clones of differentiated cells *in vitro*, including neurons. Noctor and colleagues (2001) confirmed this *in vivo*, showing that GFP-expressing radial cells in developing cortex are the only mitotically active cells, that they express vimentin as a marker of their radial glia identity, and that they give rise to neuronal progeny. Using timelapse imaging of cultured brain slices with GFP-expressing radial glia, they found that the same radial glial cell could give rise to a neuron by asymmetric division, and subsequently act as a guide for the migration of the neuron out of the ventricular zone, demonstrating that, in the embryonic cortex, radial glial cells can fulfil both their traditional role as 'guides' for migratory cells and also act as progenitors. In the retina, it has not been proven that Müller glia can act as progenitor cells during normal development. However, Blackshaw and colleagues (2004), using serial analysis of gene expression combined with in situ hybridisation in the embryonic rodent retina, found very extensive overlap between the gene expression profiles of progenitor and Müller cells. Of the genes identified as being specifically expressed in Müller glia after the first postnatal week, 68% were found to be enriched in mitotic progenitor cells, in contrast to only 14% of genes specific to photoreceptors. Over two-thirds of Müller-glia-enriched genes were also

enriched in progenitors, relative to other cell types, and virtually all Müller-glia-enriched genes were expressed at detectable levels in progenitor cells. Müller glial cells are one of the last cell types to be generated, and in some cases in response to injury in the postnatal chick retina, they have been induced to re-enter mitosis (Fischer & Reh, 2001). After re-entering the cell cycle, these cells express transcription factors such as Pax6 and Chx10, which are commonly expressed by embryonic progenitors, and whilst the majority remained undifferentiated, some gave rise to amacrine or bipolar cells. So far, the focus has been on the proliferative potential of Müller cells, but if they and progenitor cells are indeed one and the same, another question also emerges, namely whether progenitor cells show any of the properties usually associated with Müller cells, such as neurotransmitter uptake. In the developing mouse cortex, Anthony et al. (2004) used Cre-loxP mediated recombination to fate-map radial glial progenitors *in vivo*, and found that the vast majority of neurons in all brain regions were derived from radial glia, which expressed both the progenitor marker Nestin and the glutamate-aspartate transporter, GLAST. GLAST is also the dominant glutamate-transporter expressed by Müller cells.

1.6 Cell migration in the developing nervous system

1.6.1 Neuronal migration

As described in section 1.4.3, proliferating cells in the developing cortex and retina undergo INM, and mitosis is restricted to the ventricular zone; thus, any change in the speed of INM can affect the rate of proliferation. However, despite the implications of this, research on cell migration in development has focused on newly differentiated neurons, rather than progenitor cells. Using confocal microscopy in acute cerebellar slices, Komuro and Rakic (1992; 1995; 1998) have studied the migratory behaviour of newly generated granule cells. Granule cells are generated in the external granule layer, and migrate through the molecular and Purkinje cell layers to reach their final destination in the internal granule cell layer. After the final mitotic division, newborn granule cells become bipolar, and extend a leading process across the molecular layer, through which the cell moves its soma during migration to the Purkinje cell layer (Komuro & Rakic, 1995; 1998). Komuro and Rakic found that granule cells migrated through the molecular layer at rates of ~10 μm/hr in 7-d-old mice, increasing to ~18 μm/hr in 13-d-old mice. However, while the average rates of movement were stable at a given time in development, the detailed paths of individual cells were characterised by short, saltatory bursts of movement in either a forward or backward direction, interspersed with stationary periods. Upon entering the Purkinje cell layer, the granule cells round up and remain stationary for a prolonged period, after which they again become more spindle-shaped, and resume migration. Thus, the migration of granule cells closely parallels the movement of the nucleus of a progenitor cell, as it cycles through INM. In both cases, the movement takes place through a heterogeneous environment of both proliferating and differentiated cells, where both surface adhesion molecules and diffusible factors may affect migration, and in both cases, the cell migrates by extending a process, assuming a spindle-like shape, through which the soma is translocated.

1.6.2 Neurotransmitters and voltage-gated ion channels influence migration

Physiological and pharmacological approaches have revealed that the activity of voltage-gated ion channels and neurotransmitter receptors regulate migration. In particular, extracellular Ca^{2+}-influx through N-type voltage-gated Ca^{2+}-channels (Komuro & Rakic, 1992; 1996) and NMDA-receptor activation regulates migration of newborn cerebellar granule cells (Komuro & Rakic, 1993, 1998; Rossi & Slater, 1993; Farrant et al., 1994), and newborn cortical neurons (Behar et al., 1999). Experiments using Ca^{2+} indicators, such as Fluo-4, to monitor intracellular Ca^{2+}-fluctuations in migrating granule cells, has shown a correlation between dynamic changes in $[Ca^{2+}]_i$ and movement of the cell body (Komuro and Rakic, 1996). Behar and colleagues (1998, 2000) have shown that GABA can act to stimulate migration of cortical neurones during rat cortical histogenesis. When cortical slices were cultured in the presence of BrdU, to label ventricular zone cells in terminal mitosis, and a GABA-receptor antagonist, effects on migration were dependent on the GABA-receptor blocker employed; Bicuculline enhanced migration towards the cortical plate, whereas in picrotoxin-treated slices, most cells remained in the ventricular or subventricular zone. Application of saclofen, a $GABA_B$-receptor antagonist, resulted in an accumulation of cells in the intermediate zone, suggesting that as cortical cells differentiate, changing receptor expression modulates the migratory responses to GABA (Behar et al., 2000).

The development of the structure of the adult retina depends on both the nuclear translocation of progenitor cells during INM and the migration of newly generated neurons as they exit the cell cycle and migrate out of the ventricular zone. However, the possible regulation of these processes by neurotransmitters and voltage-gated ion channels has not previously been investigated.

1.7 Neurotransmitters and their receptors

Below, I present a brief overview of the transmitter systems studied in this thesis.

1.7.1 Glutamate

Glutamate is the main excitatory transmitter, as well as the most abundant amino acid in the nervous system, and acts as a regulatory signal during development via metabotropic and ionotropic receptors (for review, see Collingridge & Lester, 1989). Ionotropic receptors are ion channels that are directly gated by ligand binding. Ionotropic glutamate receptors are commonly classified into NMDA- and non-NMDA-receptors on the basis of their selective responses to synthetic ligands. Non-NMDA-receptors are further subdivided into AMPA- and kainate-receptors.

The AMPA receptor subunits were the first to be cloned, named GluR1-4, any combination of which forms functional receptors, which mediate a small, fast conductance. AMPA receptors are low affinity glutamate receptors that respond strongly to the rapid increases in [Glu] associated with vesicular release. A slow rise in [Glu] leads to desensitisation rather than activation of the receptor. Part of the GluR2 subunit (and also the subsequently discovered GluR5 and GluR6 subunits) is subject to RNA editing, causing a glutamine in the protein to be substituted for an arginine. This alteration changes the permeability of the receptor to divalent cations, notably Ca^{2+}, from permeable to impermeable. ~99% of GluR2 subunits exist in the edited form, and in the adult, the GluR2 subunit is ubiquitous in AMPA receptors, which are thus impermeable to Ca^{2+}. However, the expression of the GluR2 subunit is regulated through development, its prevalence increasing with age, meaning that at early times, most AMPA receptors are Ca^{2+} permeable (for review, see Hollmann & Heinemann, 1994).

Kainate receptors differ from AMPA receptors in being non-desensitising. Subunits GluR5-6 and KA1-2 form heteromeric receptors. KA1-2 subunits have a high affinity for kainate and respond selectively to it, whereas GluR5-6 subunits have a low affinity for this ligand. Antagonists at both AMPA and kainate receptors include NBQX and CNQX.

NMDA-receptors form heteromers of NR1 and NR2 subunits. The NR1 subunit is subject to alternative splicing (deletion of exons) on the N- and C-terminal of the protein, leading to 8 different splice variants. NR2 subunits are found in 4 different isoforms, NR2A-D. The ion channel of NMDA receptors is permeable to both monovalent and divalent cations, notably Ca^{2+}. Another important feature of NMDA receptors is the external block by Mg^{2+} at negative potentials, resulting in a gating mechanism that requires coincident membrane depolarisation and ligand binding. NMDA-receptors have a very high affinity for glutamate, which gates a large, non-desensitising conductance. As a result of these special properties, the NMDA receptor plays a pivotal role in synaptic plasticity and cytotoxicity. Combinations of NR1 splice variants and NR2 isoforms endows the receptor with varying degrees of Ca^{2+}-permeability and channel conductance, and their expression and distribution is highly developmentally regulated. DL-AP5 is a potent, selective NMDA-receptor antagonist (for review, see Hollmann & Heinemann, 1994).

Metabotropic glutamate receptors (mGluRs) are G-protein linked receptors, although they show little sequence homology to other G-protein linked receptor families. mGluRs are subdivided into 3 main groups, I, II and III, based on sequence homology and second messenger coupling. Group I mGluR activation stimulates phospholipase C, leading to IP_3 synthesis and intracellular Ca^{2+} release from IP_3-sensitive, intracellular stores, whereas activation of mGluRs Group II and III leads to a decrease in adenylyl cyclase activity. ACPD

is a selective agonist at Group I and II mGluRs, whereas L-AP4 is a selective Group III agonist (for review, see Nakanishi, 1994).

1.7.2 Glutamate receptors in the retina

In the adult vertebrate retina, glutamate is the main neurotransmitter of RGCs, bipolar cells and photoreceptors. In the chick, all AMPA/kainate subunits and the NR1 subunit are found in the INL and GCL, mostly on amacrines and RGCs (Silveira dos Santos Bredariol & Hamassaki-Britto, 2001), from as early as E5 through to post-hatching stages. Electrophysiological studies have shown ionotropic glutamate responses in RGCs from E6 (Allcorn et al., 1996).

In the adult retina, bipolar (Snellman & Nawy, 2002), Müller (Lopez et al., 1998), amacrine (Gomes et al., 2004) ganglion and photoreceptor (Yang, 2004) cells have all been shown to express functional mGluRs (for review, see Yang, 2004). The expression pattern of mGluRs in the developing retina has not been systematically investigated, but Price et al. (1995) found that injection of the mGluR antagonist L-AP3 in newborn rats caused profound degenerative changes to all cell types in the retina, which is still immature in the newborn rat. The most mature cell type, the RGCs, was most resistant to these effects. The authors speculate that either all cell types at this stage express AP3-sensitive mGluRs, which mediate growth or survival signals via second messenger systems, or alternatively, a single cell type, such as the Müller cells, express mGluRs which mediate a supportive function on which all retinal neurons depend.

1.7.3 GABA

In the adult nervous system, γ-amino-butyric acid (GABA) is the dominant

inhibitory transmitter. However, during development, GABA often produces an excitatory response (Owens et al., 1996). GABA is derived from glutamate via the enzyme glutamic acid decarboxylase (GAD). There are three main types of GABA-receptors: $GABA_A$- and $GABA_C$-receptors, which are both ionotropic, and gate an anion channel, and $GABA_B$-receptors, which are metabotropic. Both $GABA_A$- and $GABA_C$-receptors are part of the super-family of ionotropic receptors, which includes the nicotinic acetylcholine receptor, and consist of five subunits that assemble to from an ion channel. $GABA_A$-receptors are hetero-pentamers, the majority comprising two α-, two β- and one γ-subunit, although other classes of subunits exist as well. At least six α-, three β- and three γ-subunits have been cloned so far, and receptors exhibit distinct pharmacological and gating properties depending on their subunit composition (for review, see Sieghart, 2000). The molecular components of $GABA_C$ receptors are the ρ-subunits, and five types have been identified: ρ1-5. There is a high degree of sequence homology (~90%) across species, whereas 60-74% sequence homology is exhibited between the various ρ-subunit types. The subunits form functional homomeric receptors (formed from ρ1-, ρ2- or ρ3-subunits) or pseudo-heteromeric receptors (e.g. a combination of ρ1- and ρ2-subunits) (for review, see Chebib, 2004). $GABA_B$-receptors are G-protein coupled receptors with a distinctive structure, where two related receptor splice variants, $GABA_{B(1)}$ and $GABA_{B(2)}$, hetero-dimerize to form a functional $GABA_B$-receptor. The pharmacological profiles of the splice variants examined to date do not show marked differences (Billinton et al., 2001; Brauner-Osborne & Krogsgaard-Larsen, 1999).

The pharmacology of GABA-receptors is extensive with multiple modulatory binding sites for each receptor class, which are the targets of many therapeutic compounds, details of which are beyond the scope of this introduction (for review, see Bormann, 2000). Briefly, the $GABA_A$-receptor is characterised by fast activation and inactivation, a high single channel conductance and short open time, and can be reversibly blocked by bicuculline. Selective agonists at

the $GABA_A$-receptor include isoguvacine and THIP (tetra-hydro-isoxazolo-pyridine). In contrast, the $GABA_C$-receptor is bicuculline insensitive, shows slow activation and inactivation, low single channel conductance and only very weak desensitisation, and a ~10-fold higher sensitivity to GABA than $GABA_A$-receptors. Both $GABA_A$- and some $GABA_C$-receptors (dependent on subunit composition) are blocked by picrotoxin. $GABA_B$-receptors are selectively activated by baclofen, a GABA analogue, and are coupled to Ca^{2+}- and K^+-channels.

1.7.4 GABA receptors in the retina

All three types of GABA-receptors are found in the retina, although their expression patterns in development have not been systematically studied. In the adult retina, $GABA_C$-receptors are expressed in horizontal cells and, in particular, in bipolar cells, where they mediate lateral inhibiton. The $GABA_C$-receptors are ideally suited to this due to their slow and sustained responses that do not show marked desensitisation. The graded membrane potentials of the non-spiking cells in the outer retina may preclude the rapidly desensitising, fast $GABA_A$-responses from serving such a role. In the mouse retina, $GABA_C$-receptor subunits were detected from postnatal day 6, and functional receptors at P9, which correlates with bipolar cell differentiation and eye opening (Greka et al., 2000). Immunostaining for GAD in the developing chick retina showed ~20% of GAD-expressing cells are born between E3-E6, with the remainder born from E6-E9, periods which overlap the profile for amacrine and horizontal cell generation (da Costa Calaza et al., 2000). Yamashita & Fukuda (1993) found Ca^{2+}-responses to GABA-application from E3 in the chick retina, which could be blocked by bicuculline, indicating a $GABA_A$-receptor mediated response. $GABA_B$-receptors have also been shown to be involved in development, and there is some dynamic regulation of splice variant expression: in the rat retina, the $GABA_{B1a}$ variant is predominant in neonatal

and adult retina, whereas $GABA_{B1b}$ is expressed only late in postnatal development and in the adult retina. Since $GABA_{B1a}$ is expressed at high levels before functional synapses are formed, this specific receptor subtype might be involved in the maturation of the retina (Benke et al., 2002). Catsicas & Mobbs (2001) found $GABA_B$-receptors and the GABA-transporter, GAT-1, to be present from the onset of synaptogenesis, around E8 in the chick retina, and located on RGCs and amacrine cells.

1.7.5 Acetylcholine

Acetylcholine (ACh) is a major excitatory neurotransmitter, and influences many different aspects of development through two main classes of receptors, nicotinic and muscarinic ACh-receptors. Nicotinic ACh-receptors (nAChR) are ionotropic receptors, gating a cation channel permeable to Na^+, K^+ and Ca^{2+}, and are termed muscle and neuronal nAChRs, depending on location, and their properties and pharmacology vary with subunit composition (for review, see Dajas-Bailador & Wonnacott, 2003). Muscarinic ACh-receptors (mAChR) are metabotropic receptors, and form part of the superfamily of 7-transmembrane G-protein coupled receptors. mAChR subtypes M_1, M_3 and M_5 are linked to phosphoinositide hydrolysis and Ca^{2+}-release from intracellular stores. In contrast, subtypes M_2 and M_4 are linked to adenylyl cyclase and reduce cAMP levels. All mAChRs are activated by muscarine and carbachol, and antagonized by atropine at low concentrations, whereas pirenzipine is a selective antagonist at the M_1 receptor. The action of ACh at the synapse is predominantly terminated by enzyme cleavage of ACh by acetylcholinesterase, and, in the embryonic avian retina also butyrylcholinesterease (Layer & Sporns, 1987).

1.7.6 Cholinergic receptors in the retina

In the chick retina, both nAChRs (Keyser et al., 1988) and mAChRs (Fischer et al., 1998) are expressed extensively in the INL and GCL on amacrine cells and RGCs. In addition, mAChRs are widely expressed during development, and the expression of different receptor subtypes is dynamically regulated (Nadler et al., 1999). The expression of a particular receptor subtype can be altered by addition of culture medium from mature retinal cultures. A potentially novel and developmentally regulated factor, called MARIA (muscarinic acetylcholine receptor-inducing activity), which is secreted by Müller cells, may cause the induction of the M2 mAChR (Belmonte et al., 2000). The appearance of the M2 receptor in vivo occurs concomitantly with the appearance of significant numbers of Müller cells in the developing retina, and administration of this factor prior to the appearance of Müller cells induces precocious expression of M2 receptors (Belmonte et al., 2000). This is an example of the way in which factors released by differentiated cells may influence the development of other cell types.

1.7.7 Purinergic agonists and receptors

In addition to its key role in cellular metabolism, the purine nucleotide adenosine triphosphate (ATP) also functions as a potent extracellular messenger producing its effects via the activation of a family of distinct cell surface receptors, the P2 receptors. In addition, uridine triphosphate (UTP), adenosine diphosphate (ADP) and uridine diphosphate (UDP) also modulate cell function via P2 receptor activation. These molecules play key roles in a number of tissue functions including fast excitatory neurotransmission and neuromodulation. P2 receptors exist as two distinct families: the P2X receptors, which are ligand-gated ionotropic channels involved in fast excitatory neurotransmission, and the P2Y receptors, which are metabotropic, G-protein coupled receptors, the

activation of which affects either the PLC-IP_3-Ca^{2+} pathway or adenylyl cyclase, depending on the subtype. P2X receptors are composed of subunits as trimeric homomers and heteromers, and gate a non-selective cation channel. Eight members of the P2X receptor family with a number of splice variants and approximately eleven P2Y receptors have been cloned and expressed. Of these, seven P2X receptors ($P2X_{1-7}$) and six P2Y receptors ($P2Y_1$, $P2Y_2$, $P2Y_4$, $P2Y_6$, $P2Y_{11}$, and $P2Y_{12}$) are molecularly distinct entities that can elicit functional responses, and the remainder are either species variants or lack a functional response. Agonist potency varies at different receptor subtypes, and some have higher sensitivity to pyrimidine nucleotides, e.g. $P2Y_2$, $P2Y_4$, and $P2Y_6$.

ATP is co-released with a number of neurotransmitters including ACh, GABA and glutamate. Once released, ATP is degraded to ADP, AMP, and adenosine by a family of approximately 11 ectonucleotidases, limiting the extracellular actions of the nucleotides and producing the pharmacologically active nucleoside, adenosine (for review, see Burnstock & Williams, 2000).

The pharmacology of purinergic receptors is complex, and there are currently few readily available selective agonists or antagonists, and none that are subtype specific. Pharmacological characterization of P2 receptors has generally been based on their rank order of activation by agonists related to ATP and UTP since the majority of available P2 receptor antagonists are relatively weak and only marginally selective for one P2 receptor subtype over another. These antagonists also interact with other ATP recognition sites and with other receptor classes and signal transduction systems (Williams & Jarvis, 2000). Suramin is a broad-spectrum purinergic antagonist, blocking the $P2Y_1$, $P2Y_2$, $P2Y_3$, $P2Y_6$ and $P2Y_{11}$ receptors, but not the $P2Y_4$ receptor. Reactive Blue blocks all bar the $P2Y_2$ subtype, and PPADS blocks the $P2Y_1$ and $P2Y_6$ receptors.

1.7.8 Purinergic signalling in the retina

Purinergic signalling plays a pivotal role in regulating development. In the chick, purinergic and cholinergic receptors are expressed as early as Hamburger & Hamilton stage 3-5, corresponding to 12-22 hours post-fertilisation, and activation leads to IP_3-mediated intracellular Ca^{2+}-release (Laasberg, 1990). Studies using Ca^{2+}-imaging in the developing chick retina have shown large Ca^{2+} responses to ATP from E3 onwards, which decline towards E8 and decrease further until E11-13, suggesting that the Ca^{2+} mobilisation by ATP via purinoceptors is characteristic of early embryonic retinal cells, and may be involved in modulating proliferation (Sugioka et al., 1996, Sakaki et al., 1996). Multiple P2Y and P2X receptor subtypes have been reported to be expressed and dynamically regulated in multiple cell-types in both adult (Jabs et al., 2000; Wheeler-Schilling et al., 2000; Wheeler-Schilling et al., 2001) and developing rodent retina (Cheung & Burnstock, 2002).

1.8 Gap junctions

1.8.1 Gap junctions are formed by connexins

Gap junctions contain hydrophilic membrane channels that allow direct communication between two neighbouring cells, coupling them electrically and permitting the diffusion between them of metabolites and small intracellular signalling molecules less than 1 kDa in size, such as Ca^{2+}, cAMP and IP_3. Electron microscopy and X-ray crystallographic studies show that gap junctions are composed of connexin subunits, six of which are packed together in a hexagonal array to form a hemichannel (also termed a connexon). Each cell donates a hemichannel to the gap junction formed between them (for review, see Wei et al., 2004).

A single connexin molecule has four transmembrane domains, and so far ~20 connexin genes have been identified in both the mouse and human genome, and these have named according to the predicted molecular weight of the proteins, eg Cx26, Cx36 and Cx43. Connexons may be homomeric (identical subunits) or heteromeric (more than one connexin isotype), and when associated end to end, form membrane channels that may be homotypic or heterotypic. Most cells and tissues express more than one connexin isotype. The ability to form homomeric/heteromeric and homotypic/heterotypic channels provides greater complexity in the regulation of gap junctional communication (for review, see Wei et al., 2004), and the conductance and permeability of a channel varies with subunit composition. Connexins are highly dynamic proteins with half-lives ranging from 1.5 to 5 hours (Thomas et al., 2003) and studies of cells in culture have shown gap junctions to be formed between cells within ~ 1 minute of contact, suggesting that pre-existing connexons are available in the membrane (Rook et al., 1990).

1.8.2 Modulation of gap junctions

Gap junctions can be differentially gated by a variety of mechanisms. Closure of the gap junction channel has been observed in the presence of μM concentrations of $[Ca^{2+}]_i$, which suggests that it can be modulated by calcium-dependent cellular events. Calmodulin has been proposed as a mediator for this effect because it can bind Cx32, and the depletion of calmodulin reduces the sensitivity of gap junctional communication to elevated calcium levels in *Xenopus* oocytes (Peracchia et al. 1996). Gap junction conductance can also be regulated by intracellular pH, as well as trans-junctional voltage (the difference between the internal voltages of the interconnected cells). Most connexins are sensitive to trans-junctional voltage and form closed channels when large trans-junctional voltages are applied. Cx26, Cx43, and Cx45 also display trans-membrane voltage dependence. Different homotypic and heterotypic gap junction channels exhibit voltage gating to different degrees and the voltage-gating properties of a connexin may also be species-specific (Revilla et al., 2000). Neurotransmitters, including dopamine and glutamate, may also modulate gap junctions, usually via intracellular second messengers rather than by affecting channel properties directly. In the retina, dopamine released from amacrine cells in response to an increase in ambient light binds to D_1 receptors on horizontal cells and AII amacrine cells and activates their adenylyl cyclase. This leads to an increase in cAMP concentration and activation of cAMP-dependent protein kinase (PKA). PKA-mediated phosphorylation of connexins reduces the probability of channel opening, thus lowering the conductance of gap junctions between horizontal cells (Piccolino et al., 1984).

1.8.3 Gap junctions interact with other proteins

Gap junction proteins may interact with a number of other cellular proteins, and

several studies have indicated a close association between gap junctions and cadherin-based adherens junctions. Cadherins are comprised of a major family of transmembrane glycoproteins known to play an important role in the regulation of cell adhesion and cell motility. Inhibition of cadherin function can disrupt gap junction formation and inhibit cell-cell coupling, suggesting that localization of cadherin to cell-cell contact sites may be a prerequiste for gap junction formation. Conversely, inhibition of Cx43 can block adherens junction formation (Meyer et al. 1992). Studies in neural crest cells suggest that Cx43 and cadherin may modulate cell motility by engaging in a dynamic cross-talk with the cell's locomotory apparatus (Xu et al. 2001). There are also indications that Cx43 can interact directly with actin filaments and microtubules, suggesting gap junctions may regulate cytoskeletal proteins (Giepmans et al., 2001).

1.8.4 Gap junction blockers

Blockers of gap junction channels include octanol, arachidonic acid, glycerrhetinic acid and carbenoxolone, which are lipophilic agents, thought to act by intercalating into the membrane surrounding the connexon, or into the hydrophobic domains of the connexin protein. However, none of these blockers are very specific, and all have been shown to have other effects, for example, carbenoxolone inhibits voltage-gated calcium channels (Vessey et al., 2004).

1.8.5 Gap junctions in the retina

In the adult retina, gap junctions mediate lateral connections, coupling neurons of a single type or subtype into an extended, regular array or mosaic in the plane of the retina. In addition, heterologous coupling exists between bipolar and amacrine cells, between rod and cone photoreceptors, and between amacrine and ganglion cells. Gap junctions play important roles in the

processing of visual information in the retina by functioning as electrical synapses that are dynamically modulated by neurotransmitters and the level of ambient illumination (for review, see Sterling et al., 1986).

Gap junction communication is thought to play a key role during development in a number of processes, including proliferation, cell death, differentiation and migration. Numerous studies have shown extensive coupling of progenitor cells in the developing cortex, dynamic regulation of connexin expression, and an overall decrease in coupling with maturation (LoTurco & Kriegstein, 1991; Nadarajah et al., 1996; Bittman et al., 1997; Nadarajah et al., 1997; Bittman et al., 2002). The changes in coupling strength and pattern coincide with differentiation and commitment of cells to a certain fate, suggesting that gap junction coupling at early times enables signalling molecules to diffuse between cells, thereby preventing premature cell cycle exit and differentiation (for review, see Naus & Bani-Yaghoub, 1998). In the embryonic neocortex, Bittman et al. (1997) found that progenitor cells and radial glia form coupled clusters that extend radially through the VZ, and exclude differentiated cells. They speculate that coupling within these radial clusters serves to coordinate cell cycle events.

Electron microscope studies of sections of developing chick retina have shown an increase in the number of gap junctions from E3 to E5-6, followed by a sharp decrease between E7.5 and E9, a time course that parallels the period of neurogenesis and differentiation (Fujisawa et al., 1976). Immunolabelling of Cx26, Cx32 and Cx43 in the developing chick retina showed the expression of these connexins to be dynamically regulated, with major changes in expression patterns correlating with events such as proliferation, migration and synaptogenesis (Becker et al., 1998; 2002). Antisense oligodeoxynucleotide (asODN) treatment directed at Cx43 in the E2-4 chick eye caused an overall reduction in eye size, which was not due to apoptotic cell death, but more likely due a decrease in the rate of proliferation (Becker & Mobbs, 1999).

In the rodent retina, gap junctions have been shown to mediate so-called bystander cell death, by diffusion of an apoptotic signal, which could be prevented with gap junction blockers (Cusato et al., 2003). In the chick retina, connexin expression declines around E9-12, the main period of cell death, and increases again during the period of synaptogenesis and circuit formation around E14-18 (Becker et al., 1998). Gap junctions are also thought to mediate the spontaneous calcium waves that traverse the thickness of the retina at this time, and are involved in circuit formation (Catsicas et al., 1998).

1.8.6 Hemichannels

A hemichannel in the cell membrane is generally closed before docking with a hemichannel in another cell; both hemichannels then open in a ligand-gating reaction where the ligand and the gate are identical molecules. However, in addition to their function in forming gap junction channels, recent studies suggest that under some conditions connexin proteins may also mediate signalling via unopposed hemichannels. In isolated, solitary horizontal cells from the catfish retina, hemichannels were shown to mediate a Ca^{2+}- and dopamine-sensitive current (DeVries & Schwartz, 1992). Other studies, mostly in isolated cells in culture, have confirmed that a reduction in extracellular Ca^{2+} can cause hemichannels to open, and have suggested a role for hemichannel signalling in Ca^{2+}-wave propagation in astrocytes, involving the release of small signalling molecules, such as ATP or NAD^{+}, through hemichannels (for review, see Goodenough & Paul, 2003; Bennett et al., 2003).

Recently, Weismann et al (2004) have shown that spontaneous Ca^{2+}-waves in radial glia in slices of embryonic cortex require ATP release via hemichannels, $P2Y_1$ receptor activation and IP_3-mediated $[Ca^{2+}]_i$ release. The disruption of these Ca^{2+}-waves was associated with a decrease in the rate of proliferation during the peak of neurogenesis. In the embryonic chick, ATP has been shown

to be released from the RPE via hemichannels that face the ventricular surface of the neural retina (Pearson et al., 2005, in press). ATP has previously been shown to modulate the rate of mitosis in the chick retina (Pearson et al., 2002). However, it is not known if hemichannel signalling within the neural retina may also play a role in regulating development.

1.9 Membrane properties of progenitor cells

1.9.1 Properties of cells in the developing neocortex

The membrane properties of embryonic progenitor cells have so far received little attention. LoTurco and colleagues (1991) made whole-cell patch-clamp recordings from cells in the developing neocortex of E16-P12 rats, and found three types of cells, which were presumed to be, 1) radial glia-like cells, found in the ventricular zone; 2) immature, migrating neurons in the ventricular and subventricular zone, and 3) more mature neurons with inward sodium currents in the cortical plate. The radial glia-like cells had relatively low input resistances, between 200 and 400 MΩ, no apparent time-dependent voltage-gated currents, and did not respond to NMDA. In contrast, both immature and mature neurons had much higher input resistances, ranging from 0.8-3 GΩ, and generated fast inward currents in response to depolarising voltage steps. In addition, almost all cells in the cortical plate showed responses to NMDA. The radial glia-like cells may now, in view of recent findings, be presumed to be cortical progenitor cells, but no immunolabelling was carried out to confirm their identity.

1.9.2 Properties of adult progenitor cells

Recently, the membrane properties of progenitor cells in the adult brain in the hippocampus, the subventricular zone and the rostral migratory stream have been characterized. Using expression of GFP linked to a nestin-promoter to do fluorescence guided recordings in the adult mouse hippocampus, Fukuda and colleagues (2003) found two distinct classes of progenitor cells: cells of Type I that had a low input resistance and no voltage-gated currents, and cells of Type II that had a high input resistance and obvious time-dependent, voltage-gated currents. Immunohistochemistry identified cell Types I and II as early and late neural precursors, respectively, and the authors hypothesize that in adult

neurogenesis, progenitors go through a partial neuronal differentiation before the final mitosis. Wang et al. (2003a; 2003b) examined the biophysical properties of progenitor cells from the adult subventricular zone and rostral migratory stream, which supply neurons to the olfactory bulb, where neuronal regeneration continues in the adult. They found these cells to have high input resistances (around 4 GΩ), to show depolarising responses to GABA via $GABA_A$-receptors, to express both Ca^{2+}- and voltage-dependent K^+-currents, and to possess, in ~60% of cells, inward Na^+-currents. These cells were both nestin- and TuJ1-positive, features that identify them as neuron-specific progenitors. How the properties of progenitor cells found in the adult compare to those in the embryo, and how the changes in membrane properties observed by Fukuda and colleagues relate to cell cycle exit, has yet to be investigated.

1.9.3 Properties of immortalized retinal precursors

In the retina, immortalized R28 precursor cells have been studied, and shown to lack voltage-gated currents, but to possess depolarizing responses to NMDA, non-NMDA, $GABA_A$ and $GABA_B$-receptor agonists. Immunolabelling confirmed the presence of glutamate receptor subunits GluR1-3 and NMDAR2C, and $GABA_A$-receptors (Sun et al., 2002). However, it is unknown how the phenotypes of immortalized, cultured progenitor cells relate to those of progenitor cells *in vivo*.

1.10 Spontaneous Ca^{2+}-activity and Ca^{2+}-waves in development

Transient increases in $[Ca^{2+}]_i$, either in individual cells or as coordinated wave-activity, play a key role in development in all parts of the nervous system. $[Ca^{2+}]_i$ transients are thought to be important in the control of cell proliferation, differentiation, migration, gene expression and synapse formation. Spontaneous $[Ca^{2+}]_i$ activity is controlled by the expression of voltage- and ligand-gated ion channels, neurotransmitters and gap junctional coupling, and Ca^{2+} may in turn provide a feedback signal to regulate differentiation and maturation of different cell types. Gu & Spitzer (1995) imaged $[Ca^{2+}]_i$ activity in the spinal neurons of *Xenopus* embryos, and identified two types of spontaneous $[Ca^{2+}]_i$ activity, Ca^{2+}-spikes and Ca^{2+}-waves, which occur at different frequencies. Ca^{2+}-spikes require Ca^{2+}-influx through voltage-gated Ca^{2+}-channels and evoke Ca^{2+}-induced Ca^{2+}-release, producing a large, brief increase in $[Ca^{2+}]_i$. These $[Ca^{2+}]_i$ changes were shown to regulate the maturation of K^+-channel and neurotransmitter expression. Neuronal differentiation is altered when spikes are eliminated by preventing Ca^{2+} influx, or when spontaneous Ca^{2+} elevations are suppressed of by intracellular loading of the Ca^{2+}-chelator, BAPTA. Reimposing different frequency patterns of Ca^{2+} elevation demonstrated that natural Ca^{2+}-spike activity is sufficient to promote normal neurotransmitter expression and channel maturation. Ca^{2+}-waves produced a slower, smaller magnitude increase in $[Ca^{2+}]_i$, which was shown to modulate neurite extension, and this finding was subsequently replicated *in vivo* (Gomez & Spitzer, 1999). Spitzer and colleagues have also shown that neurotransmitter expression may be altered by interfering with the pattern of spontaneous Ca^{2+}-transients in spinal *Xenopus* neurons, without altering the expression of cell-type specific markers. Suppression of Ca^{2+} spikes by overexpression of an inward rectifier K^+ channel led to an increase in the number of neurons expressing excitatory transmitters, such as glutamate and ACh, and a decrease in inhibitory transmitter phenotypes, such as GABA and glycine. Conversely, enhancing spike activity by overexpressing a Na^+-channel

had the opposite effect, leading to an increase in inhibitory phenotypes and a decrease in excitatory phenotypes. The authors speculate that levels of spontaneous activity provide a homeostatic mechanism which is important in determining transmitter expression in embryonic spinal neurons (Borodinsky et al., 2004; for review, see Spitzer et al., 2004).

In the developing cortex, Owens & Kriegstein (1998) have shown that precursor cells in the ventricular zone undergo both individual Ca^{2+}-transients and coordinated wave-activity. The wave-activity propagates through gap junctions, and is independent of voltage-gated sodium channels, voltage-gated calcium channels, or amino acid neurotransmitter receptors. Recently, it has been suggested that these waves regulate the rate of proliferation via hemichannel-mediated ATP-release (Weismann et al., 2004).

In the developing retina, spontaneous Ca^{2+}-transients have been shown to occur both in individual cells and as coordinated wave activity. At early times in the chick retina (E4-6), cells in the ventricular zone show spontaneous Ca^{2+}-activity in individual cells, cell pairs, and in clusters of up to a dozen cells. This activity is modulated by the endogenous release of neurotransmitters, and regulates the rate of mitosis (Pearson et al., 2002).

From E8 in the chick retina, prior to the formation of synapses, the GCL shows coordinated waves of calcium-activity. These waves are abolished by gap junction blockers, and thus propagate through gap junctions. The waves are modulated by endogenous transmitters, including ACh, dopamine, glycine and GABA, acting via $GABA_B$-receptors. The waves propagate into the depth of the retina, suggesting that they are not restricted to ganglion and amacrine cells (Catsicas et al., 1998; Catsicas & Mobbs, 2001). Recently, a correlation between calcium waves in the inner retina (IR) and in the VZ has been described in the developing rabbit retina. Syed et al. (2004) used two-photon imaging of the VZ combined with multielectrode-array recordings in the ganglion

cell layer to show that waves in the IR and VZ had similar frequency and propagation speed, and that all drugs blocking the IR waves also blocked the VZ waves, but not vice versa, suggesting that the waves in the VZ are likely initiated by waves in the IR, and further, that the signalling pathway involves cholinergic stimulation of muscarinic receptors in the VZ.

At later times, spontaneous electrical activity takes the form of rhythmic bursts of action potentials that spread between adjacent ganglion and amacrine cells and produce transient elevations in $[Ca^{2+}]_i$. These transients are necessary for the formation of the appropriate synaptic connections between RGCs and cells in the lateral geniculate nucleus or optic tectum, and the appropriate segregation of inputs from the two eyes (McLaughlin et al., 2003; Grubb et al., 2003). These waves have been described for both mammalian (Meister et al., 1991) and chick (Catsicas et al., 1998; Wong et al., 1998) retina. Spontaneous bursting activity also modulates synapse formation within the retina, and has been demonstrated to regulate the formation of RGC receptive fields (Sernagor & Grzywacz, 1996).

1.11 The role of neurotransmitters in development

In addition to the roles in modulating neuronal migration discussed in section 1.6.2, and cell-fate choices, discussed in section 1.4.8, neurotransmitters are known to regulate many other aspects of development, prior to the formation of synapses. Progenitor cells in the developing cortex and retina express neurotransmitter receptors before exiting the cell cycle, and neurotransmitters have been shown to affect proliferation, survival and neurite outgrowth. LoTurco et al. (1995) used whole-cell patch-clamping, and Ca^{2+}-imaging, in embryonic rat cortical slices to test the responses of ventricular zone cells to GABA and glutamate. They found that the number of cells responding to these transmitters increased from 0% at E13-14 to ~40% at E15, and 100% at E16. Both GABA and glutamate produced a depolarizing response, the former acting via AMPA/kainate receptors and the latter via $GABA_A$ receptors. The depolarizing response to GABA in development is due to a high $[Cl^-]_i$ concentration, leading to an efflux of Cl^- upon $GABA_A$-receptor activation (Owens et al., 1996). Both GABA and glutamate produce an increase in $[Ca^{2+}]_i$ in ventricular zone cells, through activation of voltage-gated calcium channels. Exposing cortical explants to GABA and glutamate caused a decrease in the incorporation of [^{3}H]thymidine, and conversely, the antagonists CNQX and bicuculline caused an increase in [^{3}H]thymidine incorporation, suggesting that the presence of endogenous transmitters can regulate the rate of DNA synthesis. Depolarization with KCl mimicked the effects of agonist application, reinforcing the notion that GABA and glutamate exert their actions via membrane depolarization. Haydar et al. (2000) also found that GABA and glutamate act via AMPA/kainate and $GABA_A$ receptors to influence proliferation in the neocortex. However, rather than producing an overall decrease in proliferation, they found different effects of the transmitters in the ventricular and subventricular zones. BrdU labelling showed an increase in cell proliferation in the ventricular zone upon GABA/glutamate stimulation but a substantial decrease in the subventricular zone. Haydar and colleagues speculate that the overall decrease reported by

LoTurco and colleagues was due to the pooling of the different effects on the two populations.

In cultured neural precursor cells from the striatum, Nguyen et al. (2003) also found that $GABA_A$-receptor stimulation produced a decrease in proliferation, mediated by the GABA-induced depolarization and calcium-entry via voltage-gated calcium channels. A downstream target of the increase in $[Ca^{2+}]_i$ is mitogen-activated protein (MAP) kinase (Rosen et al., 1994), which is involved in the regulation of cell cycle progression in neuronal progenitor cells (for review, see Wilkinson & Millar, 2000). The $GABA_A$-receptor antagonist SR95531 produced a significant increase in proliferation, but this effect could be substantially blocked by a MAP-kinase inhibitor. In addition, the precursor cells were shown to produce and release GABA, thus regulating precursor cell division via a GABA-mediated autocrine/paracrine signalling loop (Nguyen et al. 2003). Cortical precursor cell proliferation was also found to be stimulated by ACh via muscarinic receptor activation (Ma et al., 2000). The growth-regulatory signal was found to involve an increase in $[Ca^{2+}]_i$ and MAP kinase, which increased DNA synthesis and neuronal differentiation.

In the E3 chick retina, the activation of P2 purinoceptors by ATP was found to regulate DNA synthesis by inducing Ca^{2+} mobilization, and the purinergic Ca^{2+} response was found to decline in parallel with the decrease in mitotic activity during retinal development (Sugioka et al., 1999). The purinergic antagonists, suramin and PPADS, both inhibited [^{3}H]-thymidine incorporation, which could be enhanced by exogenous ATP. In addition, in the medium of E3 retinal organ cultures, the concentration of ATP increased 25-fold within 1 hour of incubation and this concentration was kept for at least 24 hours, indicating autocrine or paracrine release of ATP is involved in the regulation of DNA synthesis in the neural retina.

Neurotransmitters have also been shown to regulate the outgrowth of neurites. In cultured hippocampal neurons, glutamate receptor agonists produced a decrease in neurite outgrowth, and, at increasing concentrations, a decrease in neuronal survival, which was found to be due to calcium-entry via voltage-gated calcium-channels following depolarization (Mattson et al., 1988). Similarly, in retinal cultures from E8 chick, activation of Ca^{2+}-permeable AMPA with glutamate, AMPA or kainite caused a reduction in neurite outgrowth (Catsicas et al., 2001). In contrast, GABA increased the complexity of the dendritic arbors of cultured cerebellar granule neurons via depolarization and activation of voltage-gated calcium channels. Blockers of CAM-kinase II and MAP-kinase implicated these kinases in the intracellular pathways involved in the neuritogenic effect of GABA (Borodinsky et al., 2003).

A

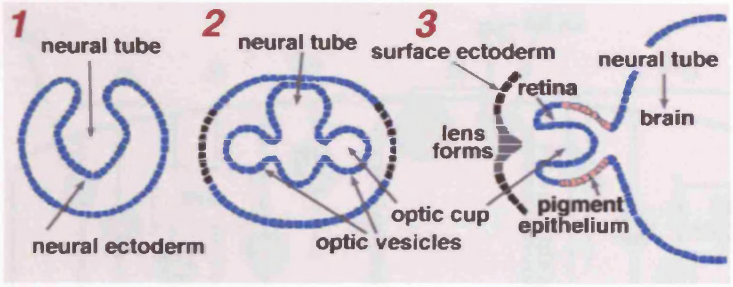

B

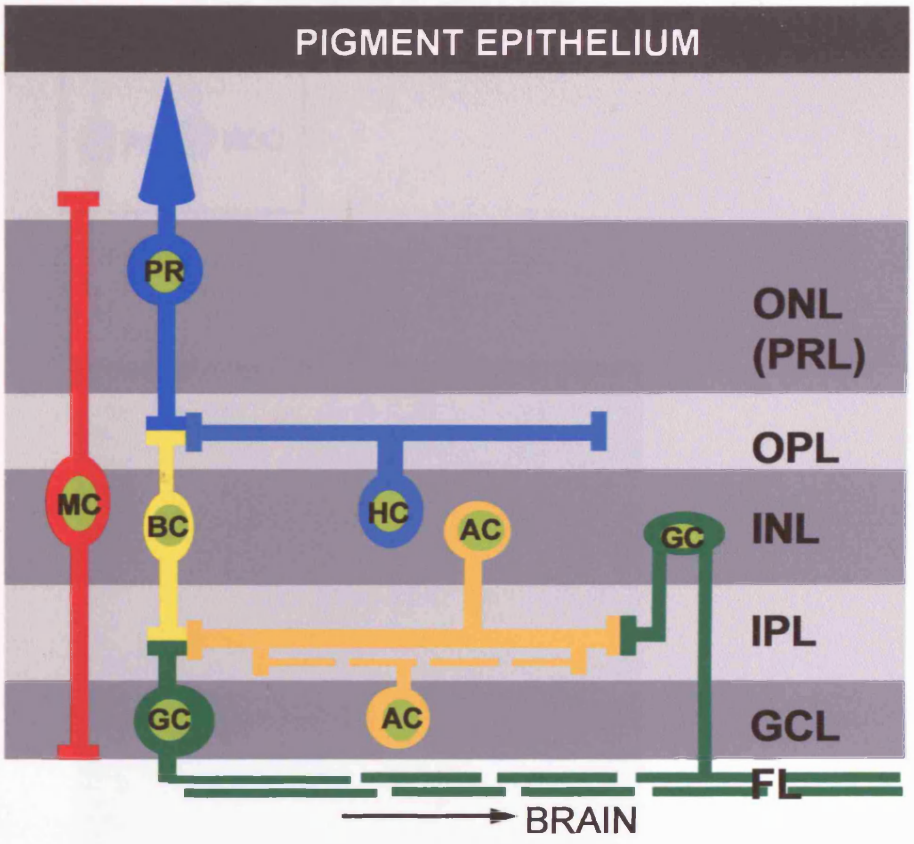

Figure 1.1 The development and anatomy of the retina. A, The retina derives from the neural tube. The neural retina starts as a single layer of progenitor cells, and repeated cycles of cell division generate all the cell types in the mature retina. *B*, Anatomy of the mature chick retina. The mature chick retina contains 6 types of neuron and 1 type of glial cell, the Müller cells (MC, red). Photoreceptors (PR, light blue), of which there are two types, rods and cones, bipolar cells (BC, yellow) and ganglion cells (GC, green) constitute the vertical pathway for information flow through the retina. Action potentials are conveyed to the brain by the ganglion cell fibres (FL). Horizontal cells (HC, dark blue) and amacrine cells (AC, orange) modulate the vertical pathway at the level of PR-BC and BC-GC synapses, respectively. PRL: photoreceptor layer; ONL: outer nuclear layer; OPL: outer plexiform layer; INL: inner nuclear layer; IPL: inner plexiform layer; GCL: ganglion cell layer; FL: fibre layer.

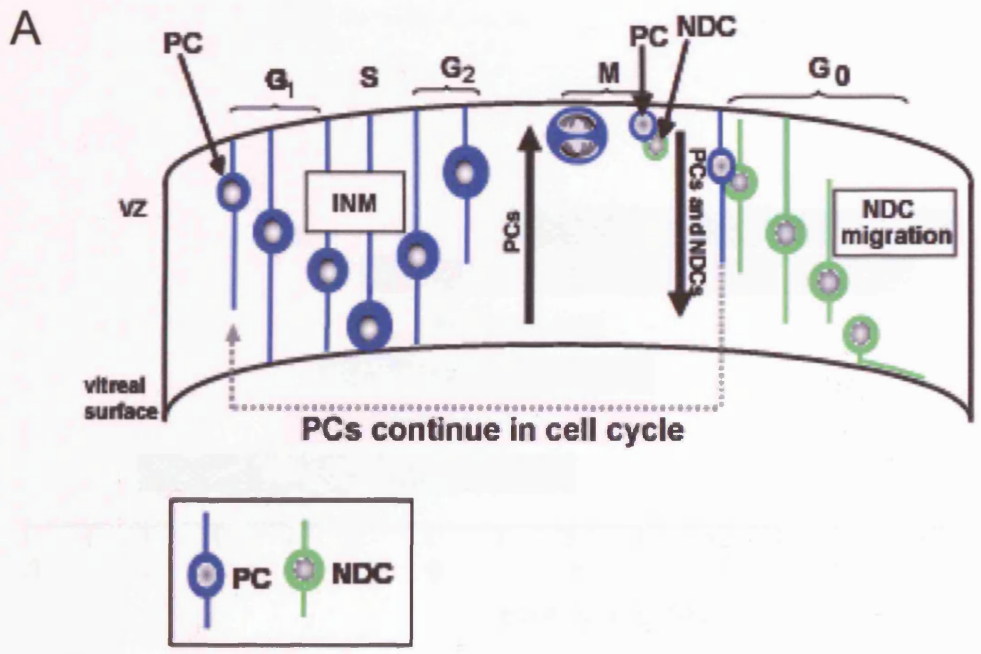

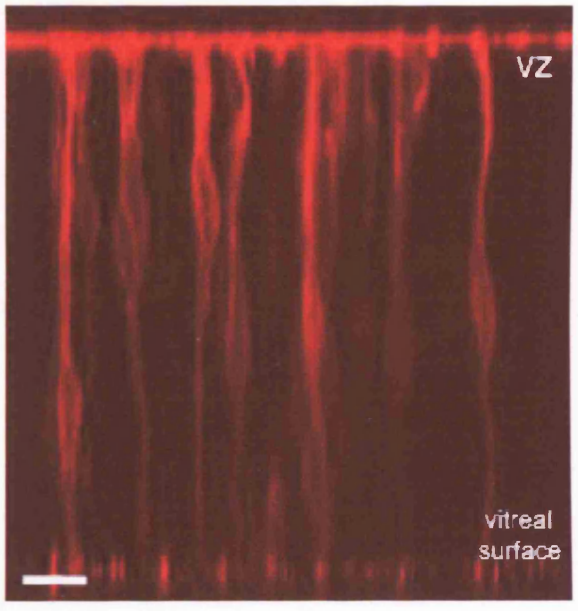

Figure 1.2 The cell cycle in the chick retina. A, Progenitor cells (PCs, *blue*) undergo interkinetic nuclear migration: The nucleus moves between the ventricular zone, which is permissive for mitosis (M), and the vitreal surface. The nucleus moves toward the vitreal surface in G_1, replicates its DNA (S-phase) and returns toward the ventricular zone in G_2. Progenitor cells can either undergo symmetrical division in which both daughter cells continue in the cell cycle, or divide asymmetrically, to give rise to a progenitor cell and a newly differentiated cell (NDC, *green*) that then migrates to its final location. *B*, DiI-labeled retinal cells. Note that processes extend to either side of the retina. Scale bar 10μm.

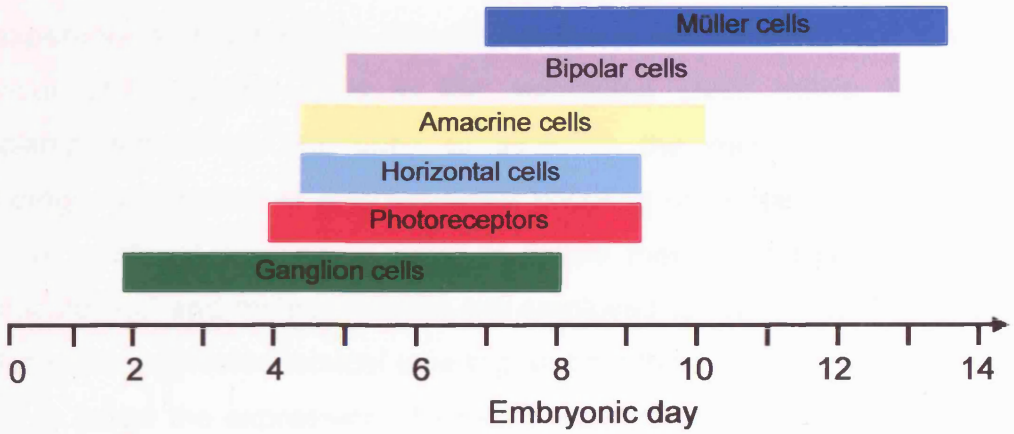

Figure 1.3 Cell birth in the chick retina based on ^{3}H-thymidine labelling studies (Kahn, 1974; Prada et al., 1991). Neural development involves two main phases: proliferation and differentiation. Differentiation occurs in several overlapping waves, with RGCs emerging earlier than any other cell type followed by photoreceptors, horizontal, amacrine, bipolar and Müller cells.

Chapter 2

METHODS

The experiments described in this thesis aim to define the properties and behaviour of progenitor cells in the embryonic chick retina. Whole-cell patchclamp recordings are used to examine the membrane properties, morphology, and extent of gap junctional coupling of retinal progenitor cells, while live confocal imaging is used to follow their migratory movements. Pharmacological and molecular tools are employed to investigate intercellular signalling. Immunohistochemical labelling and confocal imaging of fixed tissue is used to follow the expression of specific markers of neuronal development and gap junction proteins.

2.1 Preparation of retinal tissue

Fertile White Leghorn chicken eggs were incubated at 36°C. Animals from embryonic day (E) 4-9 were killed by decapitation. Embryos aged E4-E5 were staged according to Hamilton and Hamburger (1951). E4 corresponds with stages 23-25, E5 with 26-28. Embryos aged E6 and older were staged according to size. Embryos that had not reached the appropriate stage of development were discarded.

The head of the embryo was placed in Krebs' solution (see table 2.1) at room temperature, and the eyes removed. The neural retina was isolated using a pair of fine forceps. The sclera and RPE were gently peeled off, the lens cut out, and the vitreous humour carefully removed. By making 3-4 small radial incisions, the retina can be flattened out as a sheet, with either ventricular or vitreal surface facing up. For experiments using paired controls, one retina was dissected out and used immediately, while the other eye was kept in gassed Krebs' solution for up to two hours, and the retina dissected out immediately before use. The order of control/drug condition was alternated between experiments.

2.2 Preparation of drug stock solutions

The following drugs were made up in distilled water at concentrations ranging from 1 to 100mM, depending on solubility: acetylcholine chloride (Ach); carbachol; pirenzepine; uridine 5'-triphosphate (UTP); 4-[[4-Formyl-5-hydroxy-6-methyl-3-[(phosphonooxy)methyl]-2-pyridinyl]azo]-1,3-benzenedisulfonic acid tetrasodium salt (PPADS); carbenoxolone (CBX); γ-aminobutyric acid (GABA); tetrodotoxin (TTX); bicuculline; glycine; taurine; strychnine; isoguvacine; 4,5,6,7-tetrahydroisoxazolo[5,4-c]pyridin-3-ol hydrochloride (THIP); tetraethylammonium chloride (TEA); 4-aminopyridine (4AP); glutamate (all Sigma, UK); (RS)-α-Amino-3-hydroxy-5-methyl-4-isoxazolepropionic acid (AMPA); 2,3-Dioxo-6-nitro-1,2,3,4-tetrahydrobenzo[f]quinoxaline-7-sulfonamide disodium salt (NBQX); D-(-)-2-Amino-5-phosphonopentanoic acid (D-AP5); 1-(4,4-Diphenyl-3-butenyl)-3-piperidinecarboxylic acid hydrochloride (SKF-89976A) (all Tocris, UK). Due to its low solubility DL-*threo-b*-Benzyloxyaspartic acid (TBOA) (Tocris, UK) was made up directly in the Krebs' solution. Picrotoxin and 18-α-glycerrhetinic acid were made up in ethanol, and retinoic acid was made up in dimethyl sulfoxide (DMSO) (all Sigma, UK). Where experiments involved drugs made up in DMSO or ethanol, these solvents were included in the control solution at the appropriate concentration.

2.3 Whole-cell patchclamp recording

2.3.1 Recording of membrane currents

Whole-cell patchclamp recording (Hamill et al., 1981) is used here to describe the voltage and transmitter gated currents present in cells, to establish their morphology and the extent of their gap junctional coupling to neighbouring cells. The basic principle of whole-cell patchclamping is that by obtaining a high resistance seal to the cell membrane, and a low resistance access pathway to the cytoplasm, the voltage across the cell membrane can be accurately controlled (voltage-clamped) thereby enabling the study of voltage dependent membrane conductances. Unlike voltage clamp techniques that employ sharp high resistance glass electrodes, the low access resistance to the interior of the cell via the patch pipette means that the solution the pipette contains rapidly exchanges with the contents of the cell enabling the experimenter to both control the intracellular ionic environment and introduce large molecules such as dyes.

In practice, thick-walled glass pipettes, prepared as described below, are filled with a solution mimicking the internal milieu. These are lowered through the bath solution and pushed against the cell membrane. During the process of moving the pipette through the bath, light positive pressure is exerted on it to prevent the end becoming fouled with debris that would otherwise prevent the formation of a tight seal between the cell membrane and the glass of the tip. In order to monitor seal formation small voltage pulses are applied to the pipette solution and the corresponding current flow continuously monitored. Once the pipette is in contact with the cell membrane, gentle suction is applied, and the pipette voltage lowered, to encourage seal formation. When the seal resistance reaches a steady level of several giga-ohms, the capacity currents through the electrode glass are electronically subtracted and a sharper pulse of suction applied. This causes the patch of membrane under the tip to be disrupted but leaves the high resistance seal with the membrane intact. Since the currents evoked by the voltage pulses at the electrode can now flow through the membrane capacitance of the cell, the rupture of the membrane

patch is marked by a sudden change in the appearance of these currents. A feedback circuit in the head-stage and amplifier allows the potential across the cell membrane to be controlled at a given value by injection of current. This value, the command potential, is set by the experimenter, hence the term 'voltage-clamped'. By keeping the voltage constant, the changes in membrane current are linearly proportional to the membrane conductance. The current is converted to a voltage by the current-to-voltage converter in the head-stage, and measured with reference to an earth electrode via an Ag/AgCl pellet in the bath solution. By altering the membrane potential or the concentration of ion-channel ligands in a controlled fashion, the changes in membrane conductance in response to these stimuli can be measured, and the presence of voltage- or ligand-gated ion-channels in the cell membrane determined. A diagram illustrating the setup for whole-cell patchclamp recordings in whole retinae, and the equivalent circuit for the whole-cell patchclamp configuration are shown in Figure 2.1.

2.3.2 Introduction of fluorescent dyes

In the experiments described in this thesis, the solution in the patch-pipette contained, in addition to a mixture of salts designed to mimic the intracellular milieu, fluorescent dyes to delineate the morphology of the recorded cells. A combination of two dyes, Neurobiotin (MW 323; Vector Laboratories, UK), and either FITC-dextran or Alexa 568-dextran (both MW 10 000; Molecular Probes, UK), was used to investigate gap junctional coupling. These dyes diffuse into the cell during whole-cell recording but only the smaller Neurobiotin molecule can diffuse through gap junctions. Thus, the dextran-linked dyes mark the recorded cell and the Neurobiotin any cell coupled to it. A diagram illustrating the setup for dye-filling using patch-clamp electrodes, and an example of a retina labelled in this way are shown in Figure 2.2. In other experiments, a single, low molecular weight dye was used, either Alexa 488 hydrazide (MW 570; Molecular Probes, UK) or Lucifer Yellow (MW 521; Sigma, UK). To further aid in the identification of dye-filled and other cells, retinae were fixed

and subject to treatment with antibodies directed at molecules diagnostic of neuronal or progenitor cell phenotype (see below).

2.3.3 Tissue preparation

Retinae were dissected out as described, and flattened out as a sheet, with the ventricular surface facing up. For experiments on whole-mounts of retina, this was done directly in the recording chamber, and the retina was held in place by a nylon mesh glued to a platinum harp. For experiments using retinal slices, the retina was placed on a 13mm Millipore nitrocellulose membrane filter paper (see Figure 2.3A) and cut into ~300 µm thick slices with a guillotine-operated razor blade. The slices were then rotated through 90°, and placed on a glass coverslip by embedding the Millipore (to which the slices remained attached) in two lines of Vaseline to hold the slice so that the cut edge of the retina was visible (Figure 2.3B-C). The coverslip was then transferred to the recording chamber and covered with Krebs' solution.

2.3.4 Optical and mechanical setup

The recording chamber was placed on the stage of an upright microscope (Olympus BX50WI) and connected to perfusion inlet and outlet, to allow constant superfusion of the tissue with gassed Krebs' solution. The inlet was either gravity fed from 50 ml syringes or via a peristaltic pump at a constant flow rate of approximately 1 ml/s. The outlet was connected to a vacuum pump.

The tissue was viewed under a 40X or a 60X water immersion objective, using white light illumination or differential interference contrast (DIC) (Nomarski optics). The microscope was equipped with a xenon lamp and appropriate filters for epifluorescence illumination (Lucifer Yellow; excitation: 425 nm, emission: 515 nm, and FITC/Alexa 488; excitation: 475 nm, emission: 535 nm). The microscope was also equipped with a CCD camera (Hamamatsu multiformat CCD C4880-80), and a Sutter filter wheel (Lambda 10-2 filter

device, Sutter Instruments) controlled via Kinetic Imaging acquisition software (AQM Advance 6), to allow acquisition of both white light and epifluorescence images following patch-clamp recording.

2.3.5 Patch pipettes and recording set up

Patch pipettes were pulled from thick-walled borosilicate glass with internal filaments (Clark Electromedical, GCF10) which facilitate filling them with internal solution. A two-step vertical puller was employed (Narishige PC-10) to produce pipettes with a resistance of 4-15 MΩ. Several different internal solutions were used (Table 2.2); the choice of solution depended on the purpose of the experiment. For experiments to record membrane currents, K-Gluc solution (Table 2.2) was used, except where otherwise stated. For experiments to assess gap junctional coupling with FITC-dextran and Neurobiotin, Cs-Gluc solution (Table 2.2) was used. The fluorescent dye containing internal solutions (Lucifer Yellow 0.5mg/ml, Alexa 488 hydrazide 0.2mg/ml, FITC-dextran, Alexa-568-dextran and Neurobiotin all 0.1 mg/ml, unless otherwise stated) were loaded into the pipette tip by back-filling from the shank. To enable a connection to be made with the silver/silver chloride electrode in the pipette holder, the remainder of the pipettes' length was filled with internal solution without dye. The patch pipette was mounted in the holder and attached to an electronically controlled stepping motor-driven micromanipulator (SMI, Luigs-Neumann). The holder was connected to an Axoptach 200B amplifier and the data digitised using a Digidata 1200 interface and pClamp software (both Axon Instruments) and stored on a PC.

2.3.6 Series resistance

Series resistance is the resistance represented by the pathway between the interior of the cell and that of the pipette in the whole-cell patchclamp configuration. A low series resistance implies a good electrical and diffusion pathway into the cell. The presence of the series resistance introduces an error between the command potential and the membrane potential of the cell,

due to the voltage drop across the pipette tip. If the series resistance is high or the current flow is large, this voltage error becomes significant, and should be corrected for - see below.

2.3.7 Capacitance measurements

Where voltage-gated currents do not contribute to the membrane current, the series resistance, input resistance and the membrane capacitance can be established from a capacity transient, the current response to a small voltage step at a holding potential of -60 or -70 mV. The cell can then be treated as a capacitor and a resistor connected in parallel, with an additional resistor connected in series that represents the pathway from the patch pipette's interior to that of the cell (the series resistance, see Figure 2.1B for equivalent circuit). The change in current, ΔI, predicted by this model circuit is (Tessier-Lavigne et al, 1988):

$$(2.1) \quad \Delta I(t) = V(1 + R_{in}e^{-t/\tau} / R_s) / (R_{in} + R_s)$$

t : time from onset of voltage step
V : voltage step amplitude
R_{in} : input resistance (membrane resistance)
R_s : series resistance
τ : current decay time constant

The current transient follows a single exponential, the slope of which reflects the decay time constant. The decay time constant is related to the membrane capacitance, C_m:

$$(2.2) \quad \tau = C_m (R_s R_{in}) / (R_s + R_{in})$$

The peak of the transient at time t = 0, the onset of the voltage step, correlates with the series resistance, which is given by:

(2.3) $R_s = V / I_{(t=0)}$

Since it is not possible to measure the transient peak at t = 0, a single exponential curve can be fitted using Clampfit software, to obtain the projected value at t = 0 to calculate R_s, as well as value of the time constant, τ. Having determined R_s, recordings can be corrected accordingly using a spreadsheet.

At steady state, i.e. as $t \sim \infty$, the capacitor is fully charged, and no current flows through it. The steady state current is then given by:

(2.4) $I_{(t=\infty)} = V / (R_{in} + R_s)$

(since e^{-t} approaches 0 as t increases, $R_{in}e^{-t/\tau} / R_s$ becomes zero at $t = \infty$)
and thus R_{in} is given by:

(2.5) $R_{in} = (V / I_{(t=\infty)}) - R_s$

The steady state current reflects the membrane resistance - the higher the input resistance, the less current will flow.

Having determined the values for R_{in}, R_s and τ, C_m can be calculated by rearranging equation (2.2):

(2.6) $C_m = \tau (R_{in} + R_s) / (R_{in} R_s)$

2.3.8 Diffusion of substances from the pipette to the cell

In the whole-cell recording mode, the cell interior is in direct contact with the pipette solution, which diffuses into the cell. The time constant, τ, for equilibration of ions from the pipette to the cell is determined by the diffusion coefficients of the ions involved, the size of the cell, the resistivity of the pipette solution, and the size of the pore between the cell and the pipette - the series resistance:

(2.7) $\tau = (V_{cell} \cdot R_s) / (D \cdot \rho)$

where V_{cell} is the cell volume, R_s is the series resistance, D is the diffusion coefficient of the ion in question, and ρ is the resistivity of the pipette solution (Hille, 2001; Billups, 2002). For a small ion, such as Na^+ and K^+, the diffusion coefficient is of the order of $10^{-9}\ m^2s^{-1}$. Using an average cell diameter of 10μm, a series resistance of 5MΩ and a solution resistivity of 0.1Ωm (Hille, 2001), the time to reach equilibrium between the cell and the pipette solution will be ~ 26 seconds. Since V_{cell}, D and ρ remain relatively constant across experiments, a 5-fold increase of R_s to 25MΩ will produce a directly proportional increase of τ, to ~ 2 minutes. Thus, shortly after entry into the whole-cell mode, the ionic composition of the cell interior is set by the intracellular solution used.

2.3.9 Drug application

Drugs were generally applied via bath perfusion, using a multi-barrelled inlet tube which was gravity fed from 50 ml syringes, allowing rapid solution change (<3 sec). In some cases, puff-application was used instead of bath-application; a patch pipette was filled with the drug-containing external solution, and placed in a micromanipulator. The puff pipette was connected to a pressure micro injector (PMI-100, Cornerstone Series, Dagan).

2.3.10 Analysis of membrane currents

Recorded currents were analysed using pCLAMP 9.2 Clampfit software (Axon Instruments). All calculations were done in Excel. Graphs were plotted using Excel and SigmaPlot 2000 Version 6.0 (SPSS).

2.3.11 Fixation of tissue and processing for confocal microscopy

Preparations to be processed for immunohistochemistry were fixed in 0.1 M phosphate-buffered saline (PBS) containing 4% paraformaldehyde (PFA), either overnight at 4°C, or for 30 mins-2 hours (depending on the age of the preparation) at room temperature on a shaking table. Following fixation, the preparation was washed 3 x 10 mins in PBS on a shaking table, and processed for immunohistochemistry as described below. For dye filling experiments investigating gap junction coupling, the preparation was left on the stage of the microscope for 30 minutes following the last dye-fill, to allow sufficient time for the Neurobiotin to diffuse through the coupled network, prior to fixation.

2.4 Manipulation of the expression of gap junction proteins

2.4.1 Antisense-treatment

In addition to pharmacological gap junction blockers, such as carbenoxolone, 18-α-glycerrhetinic acid and retinoic acid, the expression of a specific gap junction protein, Cx43, was modulated using antisense-oligodeoxynucleotide treatment (asODNs) (Becker & Mobbs, 1999; Becker et al., 1999). The asODN sequence used, DB1, is proprietary. The sequence was selected on the basis of being specific for Cx43, of not forming homodimers, hairpins or stem loops, and of preliminary screens to avoid toxicity. It was designed to work as a mouse antisense sequence to the Cx43 gene, and has four mismatches with the chick Cx43 gene, but is still effective in reducing chick Cx43 expression (Becker et al., 1999). 30% Pluronic F-127 gel (BASF Corp) in PBS was used to deliver Cx43-specific unmodified antisense ODNs (Sigma-Genosys, UK) at a concentration of 5 μM. Pluronic gel is liquid between 0-4°C but sets at warmer temperatures. Retinas were dissected out as previously described and mounted on Millipore nitrocellulose filters. Keeping the gel, pipette tips and other tools on ice, so the gel is kept liquid, the gel was rapidly spread onto the preparation, where it sets in place on the ventricular surface of the retina. asODNs are slowly released by diffusion from the gel, which is also a mild surfactant and thus expedites ODN penetration into cells. The preparations were transferred to a 6-well plate with tissue culture inserts and ~1 ml culture medium (Table 2.3) and incubated at 36°C for 4-8 hours. Knockdown was assessed by comparing GAP1 staining in antisense- and sense-control-treated preparations.

2.4.2 Electroporation with pIRES2-eGFP constructs

Another method employed to manipulate connexin expression in the retina was by electroporation with a pIRES vector, which uses cyclomegalovirus (CMV) to promote the expression of a green fluorescent protein (EGFP), and either wild type Cx43 or a dominant negative form of Cx43 (Becker et al.,

2001). Constructs were obtained from D Becker (UCL, UK). Acutely dissected E5 neural retinas were mounted onto 13mm diameter Millipore nitrocellulose filters with the vitreal surface contacting the filter. Filters were lifted out of the bathing media and any extra media removed with blotting paper, before being placed on a coiled platinum wire electrode. 2-3µl of construct-containing solution (1µg/µl) was placed onto the ventricular surface of the retina. A second platinum electrode was brought close enough to the retinal surface to cause it to form a meniscus with the construct-containing solution, but not so close as to touch the tissue. A series of 50 V current pulses of 50 ms duration were applied at a frequency of 100Hz as the electrode was moved laterally over the ventricular surface of the retina. This process was carried out swiftly in order to avoid the retina drying out. Three eGFP-pIRES2 vectors were used; a dominant negative version (dnCx43), wildtype Cx43 or eGFP alone (Becker et al. 2001). Following electroporation, retinas were placed in culture medium (Table 2.3) and incubated at 36°C for 8-10 hours.

2.5 Manipulation of hemichannel function

In whole gap junctions, each of the coupled cells contributes a hemichannel (or connexon), a hexamer of connexin proteins. In addition to gap junctions, functional hemichannels, i.e. unopposed connexons, have recently been shown to play significant roles in development. However, there are no standard pharmacological tools commercially available to specifically manipulate hemichannel function rather than gap junctions. Here, two different approaches were employed to target hemichannels.

2.5.1 Peptide block of hemichannel function

A connexin mimetic peptide was employed to test the role of hemichannels. This peptide, Gap26, blocks Cx43 hemichannels by mimicking a 13 amino acid sequence (VCYDKSFPISHVR) on the first extracellular loop of Cx43, but does not affect coupled gap junctions (Braet et al., 200.3; Leybaert et al., 2003; Figure 5.19 in this thesis). The mimetic peptides Gap26 (VCYDKSFPISHVR) and a scrambled version of Gap26 used as a control (PSFDSRHCIVKYV) (Severn Biotech, UK) were acetylated and amidated in order to mimic the peptide in situ within the protein. Mimetic peptides were applied for 30 minutes prior to the experiment.

2.5.2 Dye-uptake and -efflux for assessment of hemichannels

To test if functional hemichannels are present in the embryonic neural retina, a technique of monitoring dye-efflux in varying external Ca^{2+}-concentrations was employed. This method was used by Pearson et al. (2005a) to probe the presence of functional hemichannels in the retinal pigment epithelium (RPE). The rationale of this technique is based on the observations that, in isolated cells in culture, a reduction in extracellular Ca^{2+} can cause hemichannels to open (Bennett et al., 2003), and open hemichannels pass small dye-molecules (Weissman et al., 2004). To measure dye efflux, acutely dissected

retinae were loaded with 0.1 mg/ml Alexa 488 (a low molecular weight fluorophore (MW 570) small enough to pass through open hemichannels) in Ca^{2+}-free Krebs' solution (see Table 2.1) for ~30 minutes, then in 2mM Ca^{2+}-Krebs' for ~10 minutes prior to imaging on a confocal microscope, while perfusing with varying external Ca^{2+}-concentrations. If the rate of dye efflux is controlled by hemichannels, varying the $[Ca^{2+}]$ in the perfusate should produce a corresponding variation in the rate of fluorescence decrease.

Another way to asses the presence of hemichannels is to compare the extent of dye uptake in the presence of varying Ca^{2+} concentrations or gap junction and hemichannel blockers, as described by Weissman et al. (2004). When open, hemichannels pass small dye-molecules. Acutely dissected retinae were incubated for ~30 min with 0.3mg/ml Neurobiotin, and subsequently fixed and processed to reveal the Neurobiotin, and imaged on a confocal microscope. To assess the extent of dye uptake in the presence or absence of gap junction blockers or connexon mimetic peptides, these were applied for 30 minutes prior to Neurobiotin loading.

2.6 Imaging of cell migration using dye-labelling

2.6.1 Confocal imaging of cell migration

Live confocal imaging of cells labelled with a membrane dye, DiI, was used to follow their migration in real time. DiI (Molecular Probes, UK) is a carbocyanine dye which is incorporated irreversibly into the plasma membrane of cells that contact the dye but does not spread from labelled to unlabeled cells (Honig and Hume, 1986; Lumsden et al., 1991). Retinae from 5-day old embryos were dissected out as previously described, and cells labelled using one of two methods: the biolistic technique described by Gan et al. (2000) or by bath immersion of retinal preparations in Krebs' solution containing DiI. The aim is to achieve a sufficiently sparse labelling of the tissue to allow the movements of individual cells to be followed over time by use of time-lapse confocal imaging. Labelled retinal wholemounts were transferred to a gas-, humidity- and temperature (36°C)-controlled closed chamber on the stage of a confocal microscope (LSM 510, Zeiss, UK or SP2, Leica, UK), and positioned with the VZ facing the objective and held flat with a harp consisting of nylon strands glued to a platinum frame. Labelled cells were located using epi-fluorescence illumination. The fluorescence of DiI was excited using the 543nm line of the argon-krypton laser. XY images (in the plane of the retinal surface) of labelled preparations were taken at 1μm steps, throughout the depth of the retina and ~5μm on either side. This was repeated at 30s-15mins intervals for periods up to 6 hours, depending on the experiment. Following acquisition, the individual XY scans were built into a XYZ stack to give a 3D image of the retina for each timepoint. Individual image stacks were rotated about the x-axis and projected to give an XZ image series over time, from which the movements of individual cells could be followed and quantified as described below. The rates of movement were not affected by the method of labelling.

2.6.2 DiI-labelling using a biolistic technique

To label the retina with DiI, a modified protocol for the BioRad Gene Gun was used. To make the 'bullets', BioRad Goldcoat ™ plastic tubing was pre-coated for 2-3 minutes with 100mM polyvinylpyrrolidone (PVP, Sigma, UK) dissolved in ethanol, and then partially dried with a flow of nitrogen for 15-20 minutes. 80 mg of tungsten particles (1μm diameter, BioRad, UK) were coated with 2mg DiI suspended in 400 μl dichloromethane (Sigma, UK) by mixing and spreading out on a glass slide. After drying for 3-4 minutes, the particles were scraped off and poured dry into the PVP-coated tubing, and distributed by gently shaking the tube with both ends sealed off. The tube was cut into suitable pieces to be loaded into the GeneGun, and stored at 4°C in the dark until use. The dissected retina was placed ventricular zone side up in a dish, and excess liquid removed. The particles were fired at the retina with helium gas at approx. 60psi, with the gun held at an approx distance of 2.5 cm from the retina, with a Millipore cell culture filter insert in between to prevent large clumps of particles hitting the retina. A diagram of the setup for biolistic labelling is shown in Figure 2.4.

2.6.3 Immersion labelling of DiI

A stock solution of DiI (Molecular Probes, UK) was prepared (1μg/μl DMSO, Sigma). 1-2μl of this DiI solution was mixed with 100μl of Krebs's solution. DiI is highly hydrophobic, dissolving readily in the solvent DMSO. When added to Krebs', the dye solution forms minute droplets that may settle on the surface of the tissue, labelling the cells beneath. The DiI-Krebs's mixture was gently pipetted over the surface of the flattened retina, and incubated for a few minutes at 36°C.

2.6.4 Image analysis employed in migration experiments

Images were analyzed off-line using either LSM (Zeiss, UK), Leica Lite (Leica) or Metamorph software (Universal Imaging, PA, USA). The individual XY scans were built into a XYZ stack to give a 3D image of the retina. Individual image stacks were rotated about the x-axis and projected to give an XZ image series over time. Where appropriate, image stacks were 'cut' into smaller virtual sections to allow individual cells to be followed. Measurements of the position of cell nuclei were made relative to the ventricular surface. The centre of the cell body was defined as the intersection of two diagonal lines drawn between the corners of a box fitted to the bulge containing the cell nucleus. The distance between this point and the outer edge of the VZ was measured for each time point and the speed of migration determined, as illustrated in Figure 2.5.

2.7 Immunohistochemistry

2.7.1 Tissue preparation

Following fixation, a solution of PBS with 0.05% Triton X-100 and 1% L-Lysine (both Sigma, UK) was used to permeabilise the cell membrane to allow access to antigens and block non-specific binding (blocking solution). The blocking solution was applied for 1-4 hours (depending on the preparation) at room temperature on a shaking table, or overnight at 4°C.

2.7.2 Neurobiotin histochemistry

Neurobiotin was revealed by incubation in blocking solution with streptavidin coupled to CY3 (1:100, Jackson ImmunoResearch Laboratories, USA) for 4 hours at room temperature on a shaking table, or overnight at 4°C.

2.7.3 TuJ1 staining

An antibody against neuron specific Class III β-tubulin was used to identify post-mitotic neurons. A monoclonal antibody raised in mouse (1:500; Covance Research products, USA) was applied in blocking solution for 5 hours at room temperature on a shaking table or overnight at 4°C. After rinsing with PBS for 3 x 15 mins, a secondary antibody, either anti-mouse-CY5 (1:200; Amersham Biosciences, UK), or anti-mouse-FITC (1:100, Chemicon, UK), or anti-mouse-Alexa 633 (1:200; Molecular Probes, UK), was applied in blocking solution for 4 hours at room temperature on a shaking table. This treatment was followed by a final wash, 3 x 15 mins in PBS on a shaking table.

2.7.4 Vimentin staining

Vimentin is an intermediate filament protein, and although it is not a specific marker for progenitor or stem cells, it has been shown to be expressed by many different types of progenitor cells (Raff et al., 1984; Haque et al., 1996), including those of the developing chick tectum (Herman et al., 1993). An antibody against vimentin raised in mouse was used to identify progenitor cells (H5 supernatant, 1:10; Developmental Studies Hybridoma Bank, University of Iowa, USA). The antibody was applied in the blocking solution for 48 hours at 4°C. After rinsing with PBS for 3 x 15 mins, a secondary antibody, anti-mouse-CY5 (1:200; Amersham Biosciences, UK), or anti-mouse-FITC (1:100, Chemicon, UK), was applied in blocking solution for 4 hours at room temperature on a shaking table.

2.7.5 Combined TuJ1 and vimentin staining in retinal slices

In order to simultaneously label vimentin and TuJ1 in the same preparation, a polyclonal antibody against neuron specific Class III β-tubulin raised in rabbit was used (1:2000; Covance Research products, USA), in combination with the vimentin antibody raised in mouse. To reveal the rabbit polyclonal TuJ1 antibody, a biotinylated anti-rabbit secondary was used (1:100; Vector Laboratories, UK), followed by streptavidin-CY3 (1:100; Jackson ImmunoResearch Laboratories, USA) or streptavidin-CY5 (1:100; Amersham Biosciences, UK).

2.7.6 Connexin staining

A monoclonal mouse antibody raised against a peptide sequence specific to Cx43, GAP1A (Becker et al., 1995), and a rabbit polyclonal antibody raised against the rodent Cx36 was used to assess the expression level of these connexins (both 1:100, gift from D Becker, UCL, UK). A rabbit polyclonal antibody, Gap7M raised against a peptide sequence on the first external loop

of Cx43, which is only exposed on unopposed gap junction hemichannels and so does not bind to complete gap junctions was used to asses the presence of hemichannels (1:200, gift from D Becker, UCL, UK). The antibodies were applied in the blocking solution for 4 hours at room temperature on a shaking table or overnight at 4°C. Preparations were then rinsed 3 x 15 minutes in PBS, and the location of the primary revealed using secondary antibodies as described above.

2.8 Imaging of dye-filled cells and immunohistochemical labelling

2.8.1 Confocal imaging

Following immunohistological processing, retinal whole-mount preparations were mounted in Citifluor, an anti-fading mountant (Citifluor, UK), and held in place with a coverslip glued on with nail varnish, before imaging on a confocal microscope using oil-immersion objectives (Zeiss LSM 510, Zeiss Pascal or Leica SP2). Occasionally, the vital chromatin dye Hoechst 33342 (2 μM, Molecular Probes, UK) was included in the final PBS wash prior to mounting, to aid in the identification of mitotic cells and orientation of the tissue. Due to the fragile nature of the retinal slice preparations, these could not be mounted. Instead, the fixed slice preparations were placed in a petridish and imaged using water-immersion objectives. Dye-filled cells were located using epifluorescence, and XY-sections (in the plane of the retina in the case of wholemounts, and in the plane of the slice in the case of retinal slice preparations) were taken, 1-1.5 μm apart, through the depth of the tissue, averaging each line 2-4 times. The image resolution was 512 x 512 or 1024 x 1024. Hoechst 33342 was excited using the 351nm line of the UV laser, and the emitted light collected using a 385-470nm bandpass filter. FITC and Alexa 488 were excited using the 488nm line of the Argon laser, and the emitted light collected using a 505-530nm bandpass filter. Cy3 and Alexa 568 dextran were excited using the 543nm line of the HeNe laser, and the emitted light collected using a 560-615nm bandpass filter. Cy5 and Alexa 633 were excited using the 633nm line of the HeNe laser, and the emitted light collected using a 655nm longpass filter. Individual fluorophores were imaged sequentially to avoid bleed-through between the channels. Where the experiment included a control condition, such as negative controls for antibody-staining, or pluronic gel only treatment for antisense preparations, the experimental and control preparations were imaged using the same laser intensity, gain and contrast settings.

2.8.2 Image analysis of cells filled with Neurobiotin to assess gap junction coupling

Images were viewed and analysed using Zeiss Image Browser, Zeiss LSM software (both Zeiss, UK) and Metamorph software (Universal Imaging, PA, USA). Image stacks could be viewed in a number of different ways: As single XY-sections (one pixel thick, representing a ~ 1 µm thick section of the retina), or projected to produce a single image view through the entire stack in the XY-plane. Alternatively, the image stack could be rotated to produce a side-view of the retina, called an XZ-section (a single pixel thick), or an XZ-projection (through the entire stack). In young retinae (< E8) where cells were labelled with FITC and Neurobiotin, the coupled cluster was usually too dense to enable individual cells to be counted. Instead, the numbers of coupled cells was determined by measuring the radius of the cluster at the widest and narrowest point to determine the volume of the cluster, and dividing by the volume of a single cell to give an estimate of the number of cells in the cluster*. The boundary of the cluster was determined by measuring the intensity of the Neurobiotin signal along a line through a single XY-section, as illustrated in Figure 2.6A. Using LSM software, the absolute intensity values could be mapped against distance along the length of the line (Figure 2.6B). These values could be copied to an Excel spreadsheet. The background fluorescence was determined by measuring the intensity along the first 20 µm of the lines from either edge of the image, and the change in fluorescence, $\Delta F/F$, determined using the average value of these values. $\Delta F/F$ was plotted against distance along the length of the line (Figure 2.6C), and the boundary of the cluster was set at $\Delta F/F>5$. The boundaries in the example shown in Figure 2.6 are shown by the blue and red lines/circles on the plots/image, and yield a radius of 47 µm for this cell cluster.

The cluster of coupled cells was not always cylindrical (see example in Figure 2.7A). Therefore, the radius was measured at the minimum and maximum

* While a limitation of this method is the implicit assumption that all cells within the radius of the cluster are included in the coupling (which is not consistent with the observed pattern of labelling), the advantage of enabling a quantitative approach to comparing changes in coupling over time was deemed sufficiently important to apply this method despite this caveat.

point. Since the volume of a cone is given by:

(2.8) $V_{cone} = {}^1/_3 \pi r^2 h$

where r is the radius and h is the height of the cone, the volume of the cluster can be determined by:

(2.9) $V_{cluster} = {}^1/_3 \pi (r_2^2 a_2 - r_1^2 a_1)$

where r_1, r_2, a_1 and a_2 represent the measurements shown in Figure 2.7B. As illustrated in Figure 2.7C,

(2.10) $r_2/r_1 = a_2/a_1$

and thus

(2.11) $a_1 = a_2 r_1 / r_2$

$V_{cluster}$ can be expressed as:

(2.12) $V_{cluster} = {}^1/_3 \pi a_2 (r_2^3 - r_1^3) / r_2$

Since

(2.13) $h = a_2 - a_1$

substituting a_1 for (2.11) and re-arranging gives

(2.14) $a_2 = h / (1 - r_1/r_2)$

substituting a_2 for (2.14) and re-arranging gives

(2.15) $V_{cluster} = {}^1/_3 \pi h (r_2^3 - r_1^3) / (r_2 - r_1)$

The number of cells contained in a cluster was estimated by dividing the volume obtained using equation (2.15) with the volume of a single cell. The single cell volume was determined by using images of single FITC filled cells, as shown in the example in Figure 2.8. Due to the high signal to background ratio of these images, image thresholding could be used to accurately determine their volume, using Metamorph software. Once the threshold is set, the total volume of the thresholded area is automatically calculated by the software, and by applying the image calibration, the cell volume can be measured. The volume of a single cell ranged from 850-1716 μm^3, with a mean value of 1184 μm^3 (n=24, ranging in age from E4-E9). The cell volume did not vary significantly with embryonic age, and the same mean value was used for all ages examined.

Table 2.1 External solutions

External solution	**Krebs'**	**Ca^{2+}-free Krebs'**	**Ba^{2+}-Krebs'**
	mM	**mM**	**mM**
NaCl	100.0	100.0	98.0
$NaHCO_3$	30.0	30.0	30.0
KCl	6.0	6.0	5.0
$MgCl_2$	1.0	2.0	1.0
$CaCl_2$	1.0		1.0
NaH_2PO_4	1.0	1.0	
Glucose	20.0	20.0	20.0
$BaCl_2$			5.0
NMDG-EGTA		0.5	
pH	7.4[†]	7.4[1]	7.4[1]

Table 2.2 Internal solutions

Internal solution	**K-Gluc**	**Cs-Gluc**	**CsCl**
	mM	**mM**	**mM**
NaCl	10.0		
K-Gluconate	130.0		
Cs-Gluconate		103.0	
CsCl			120.0
HEPES	10.0	40.0	10.0
K_2EGTA[‡]	1.1		
NMDG[§]-EGTA		5.0	1.1
TEA-Cl[**]			5.0
$MgCl_2$	1.0	2.0	
$CaCl_2$	0.1	0.1	
Na_2ATP	1.0		
MgATP		1.0	4.0
NaGTP			0.5
Phosphocreatine disodium			14.0
pH	7.0[††]	7.0[‡‡]	7.0[6]

[†] gassed with 95% O_2 / 5% CO_2
[‡] EGTA is ethylene glycol-bis(2-aminoethylether)-N,N,N',N'-tetraacetic acid
[§] NMDG is N-Methyl-D-Glucamine
[**] TEA-Cl is tetraethylammonium chloride
[††] with KOH
[‡‡] with CsOH

Table 2.3 Culture medium

Culture medium	
DMEM (Dulbecco's Modified Eagle Medium, Sigma), supplemented with:	
L-glutamine	4 mM
Fetal Bovine Serum	10 %
Penicillin	100 units per ml
Streptomycin	100 µg per ml

A

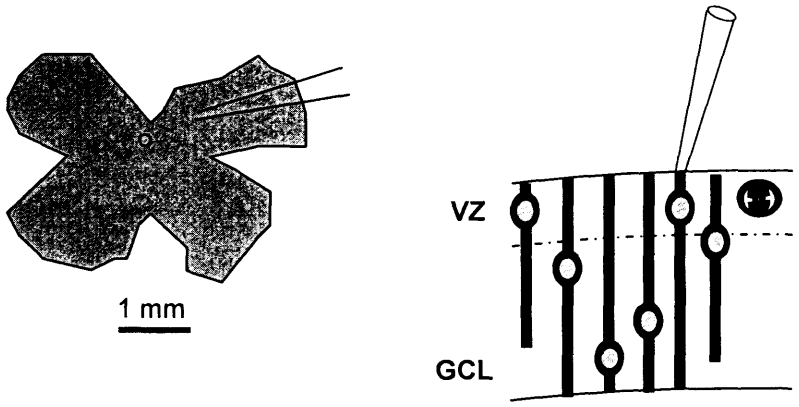

B

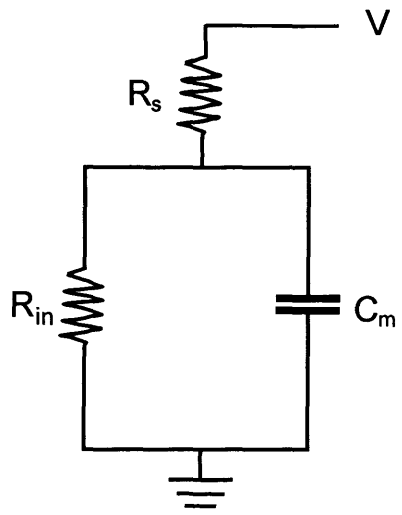

Figure 2.1 The setup for whole-cell patchclamp recordings in whole retinae and the equivalent circuit. A, This diagram illustrates the setup for whole-cell patchclamp recordings in whole retinae. Following dissection, 3 to 4 incisions were made in the retina to allow it to be flattened out as a sheet, with the ventricular surface facing up. The processes of cells on the ventricular surface could then be targeted for patchclamp recording. *B*, The equivalent circuit for the whole-cell patchclamp configuration, where R_{in} is the input (membrane) resistance, R_s is the series resistance, and C_m is the membrane capacitance

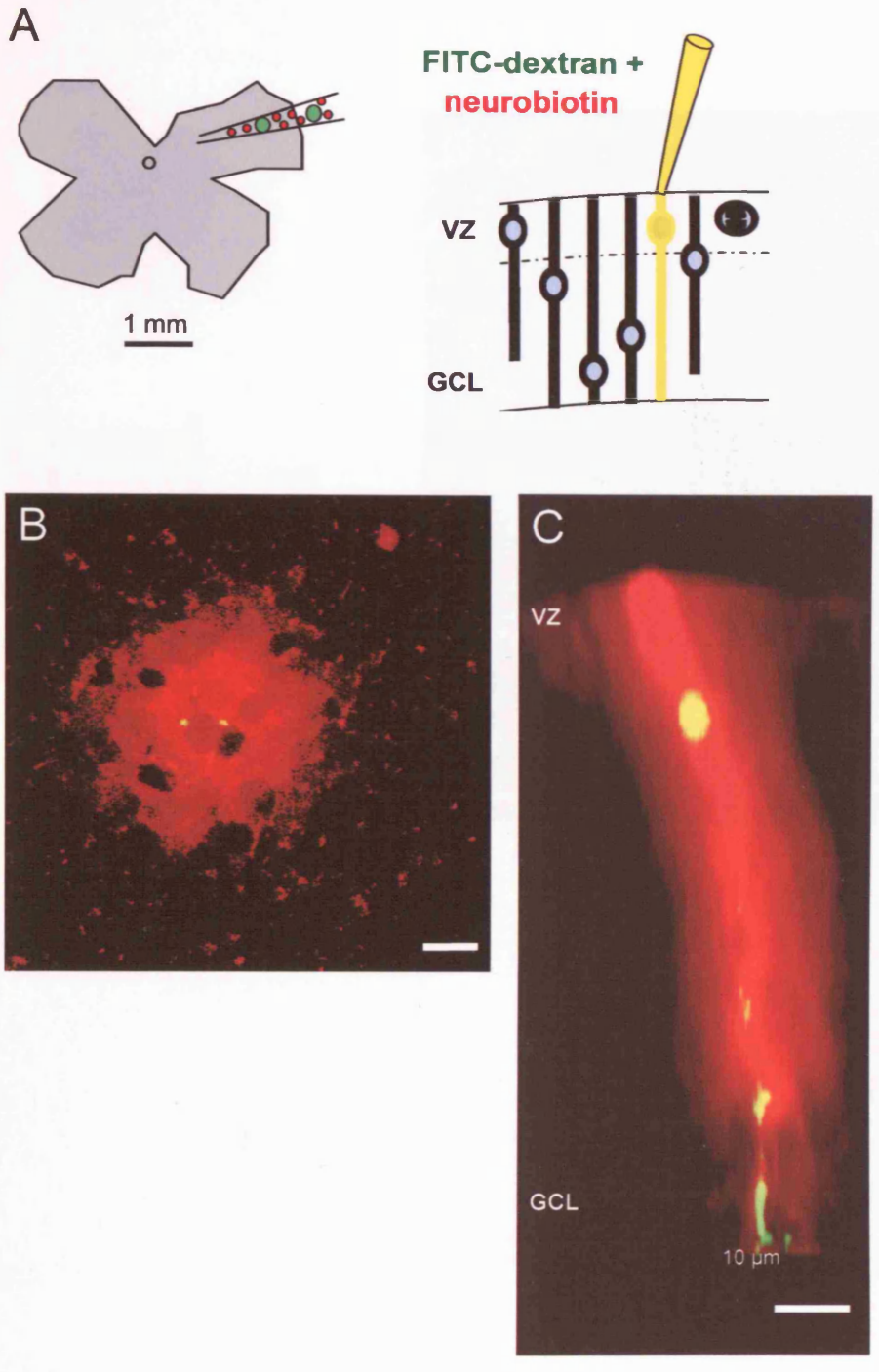

Figure 2.2 Dye-labelling using whole-cell patchclamping A, As shown in this diagram, cells in the isolated neural retina could be labelled with a mixture of Neurobiotin and FITC-dextran (*yellow*) via thin processes that terminate at the ventricular surface. Following dye-labelling, the retina was fixed and processed for Neurobiotin, and imaged on a confocal microscope. *B,* Confocal image at the level of the VZ through a cluster of coupled cells in an E5 retina. The processes of the injected cells (two in this case) are seen as yellow (Neurobiotin, *red*, and FITC, *green*), whereas coupled cells are red (Neurobiotin only) *C*, The image stack rotated through 90° to give an XZ projection, showing the injected cell (*yellow*) surrounded throughout its length by Neurobiotin only-filled cells (*red*).

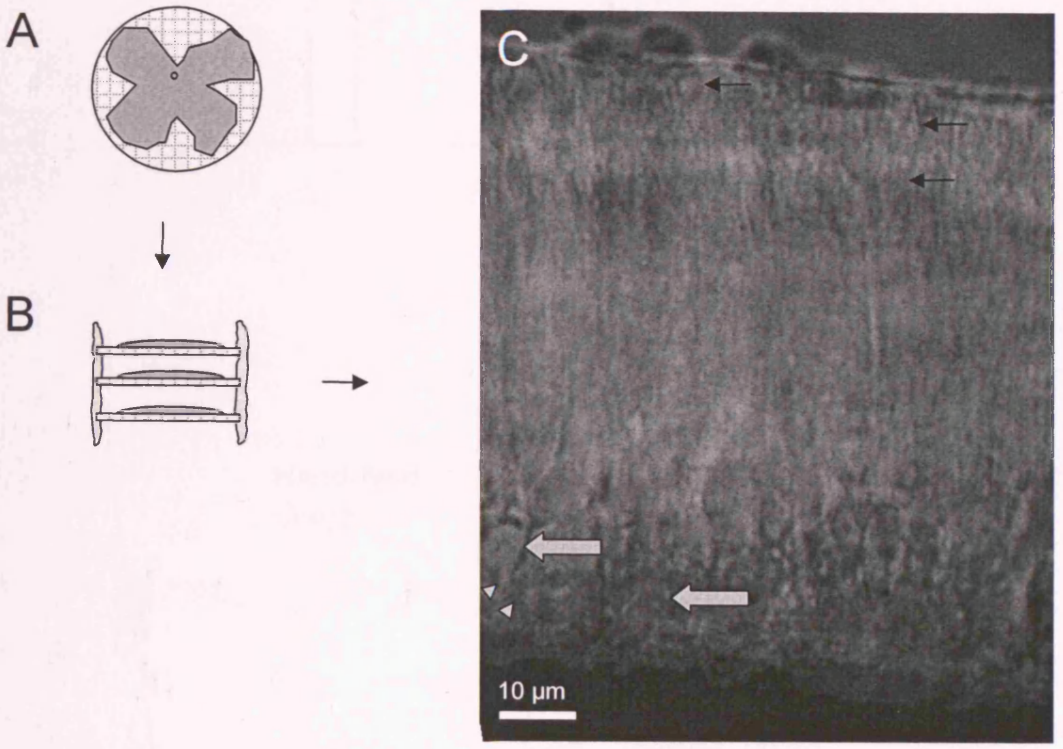

Figure 2.3 Preparation of retinal slices A, The retina was flattened onto a Millipore filter paper, with the ventricular surface facing up, and cut into ~300 µm thick slices with a guillotine-mounted razor blade. *B,* The slices were rotated through 90°, and the ends of the Millipore filter paper were embedded in lines of Vaseline to hold the slice so that the cross-section of the retina was accessible for patchclamping. *C,* DIC image of an E5 retinal slice. Small black arrows indicate the spindle-shaped cellbodies of the presumptive progenitors in or near the ventricular zone, whereas the light arrows indicate the larger, rounded cell bodies of the presumptive ganglion cells. The axon of the RGC indicated on the left is highlighted by arrowheads.

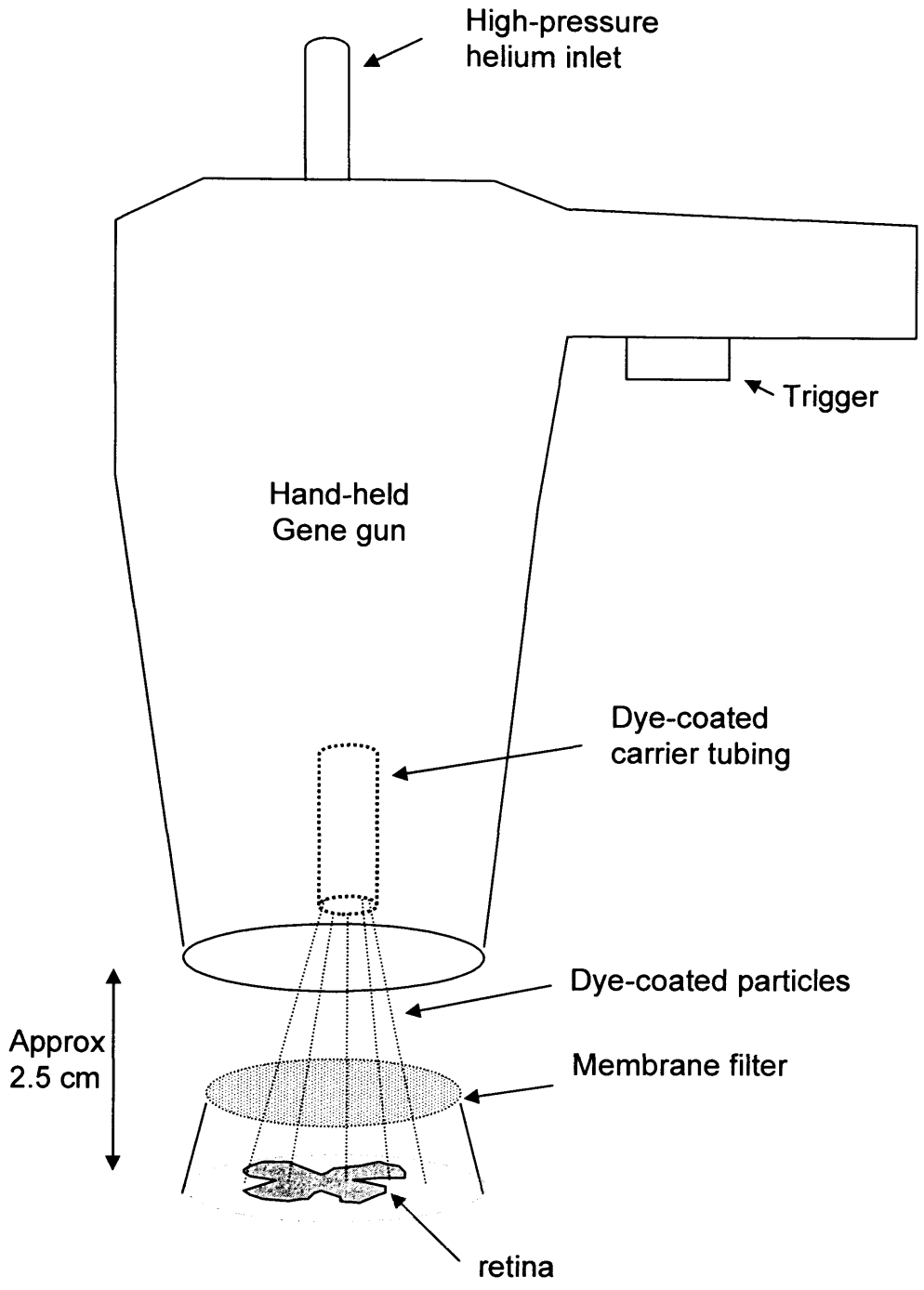

Figure 2.4 Set-up for biolistic labelling. Dye-coated particles are fired at the retinal surface using a handheld GeneGun. The 'bullets' are propelled using pressurised helium. A membrane filter (tissue culture insert) is placed between the gun and the retina to avoid large clumps of particles hitting the tissue and damaging it.

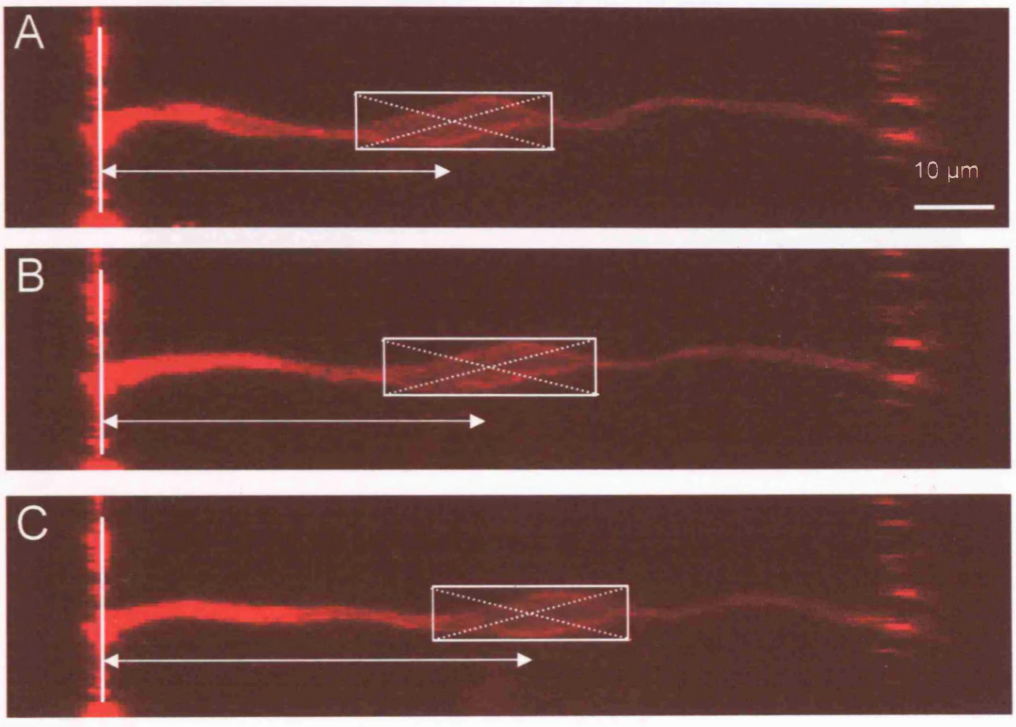

Figure 2.5 Measurement of interkinetic nuclear migration. A box was drawn around the bulge containing the nucleus, and the distance between the centre of the box and the ventricular surface (vertical line) was measured at each time point (A-C).

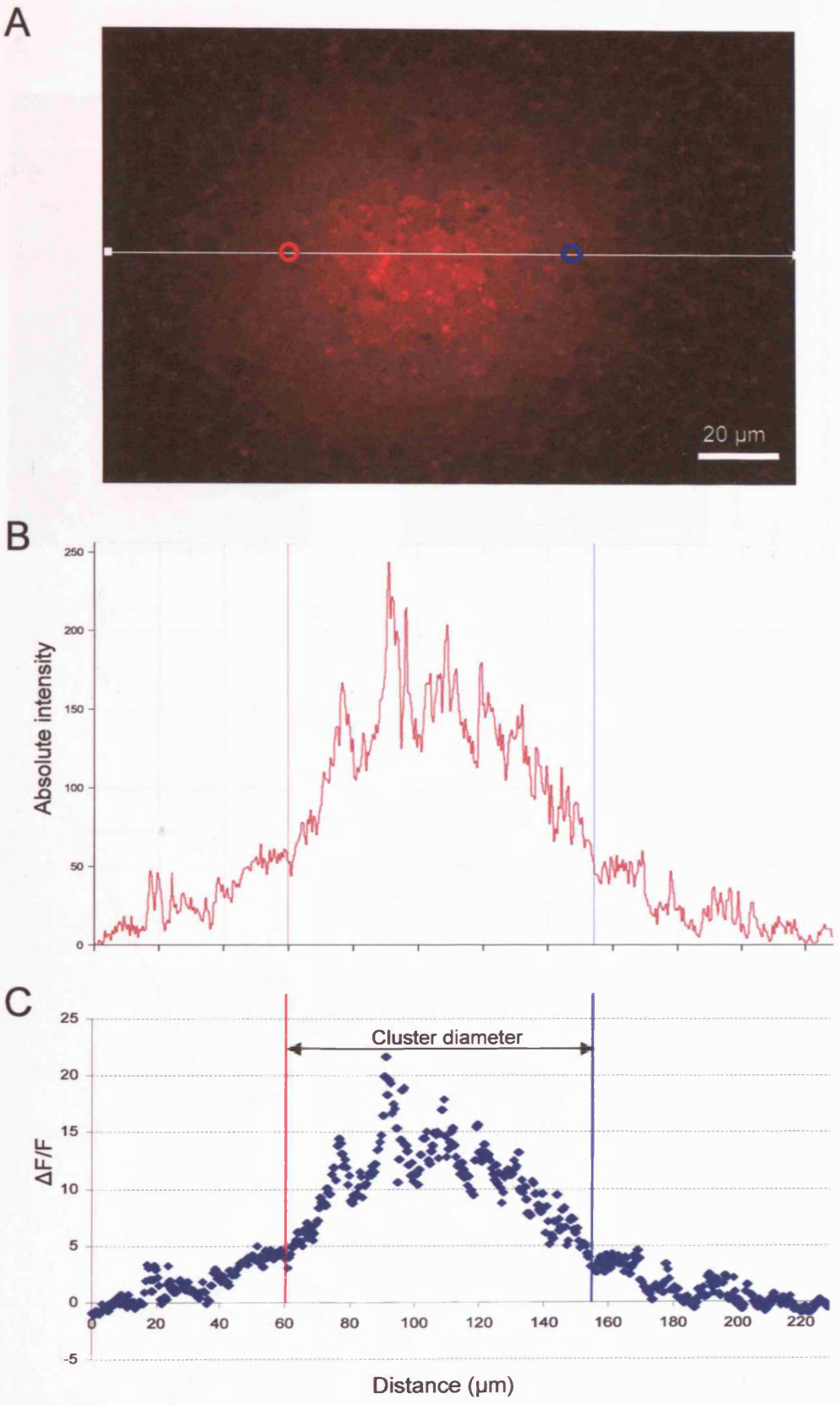

Figure 2.6 Measurement of the extent of dye-coupling. Using Zeiss LSM software, a line was drawn through the dye-coupled cluster in a single XY-section *(A)*. The intensity was plotted against distance (*B*), and this set of values was saved to a spreadsheet. The background fluorescence was calculated by averaging the intensity of the first 20 µm from either side of the image, and ΔF/F determined using this value *(C)*. The boundary of the cluster was set at ΔF/F>5, as indicated by the red and blue circles/lines on the image/plots. In the example shown here, the radius of the cluster at this level was 47 µm.

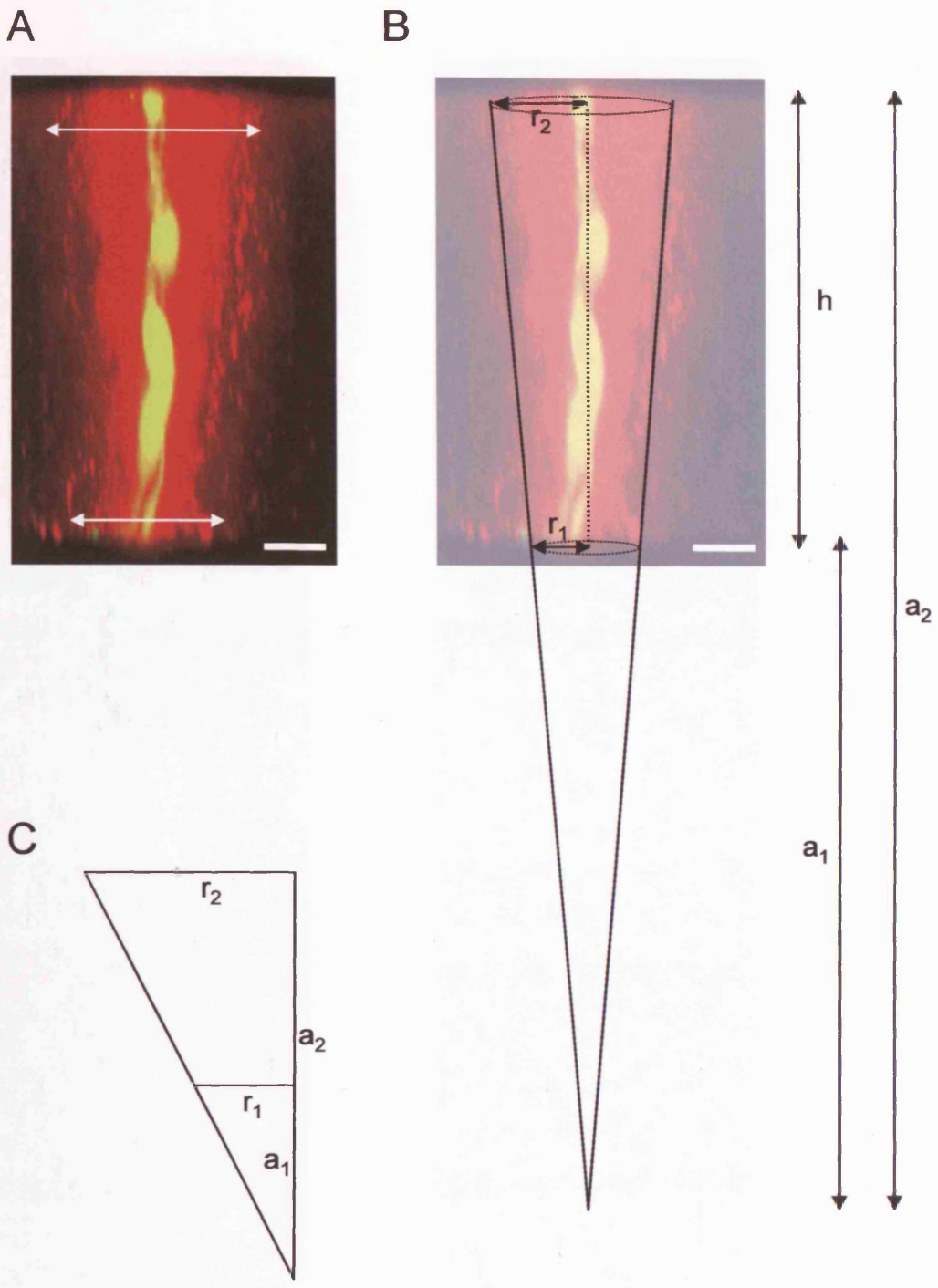

Figure 2.7 Measurement of the volume of a coupled cluster. A, An E5 retina injected with FITC and Neurobiotin shows extensive coupling. The radius of a coupled cluster of cells is not always constant at all levels of the retina. Scale bar 10 µm. *B-C,* The volume of a coupled cluster can be determined from the volume of a cone. For further details, see text.

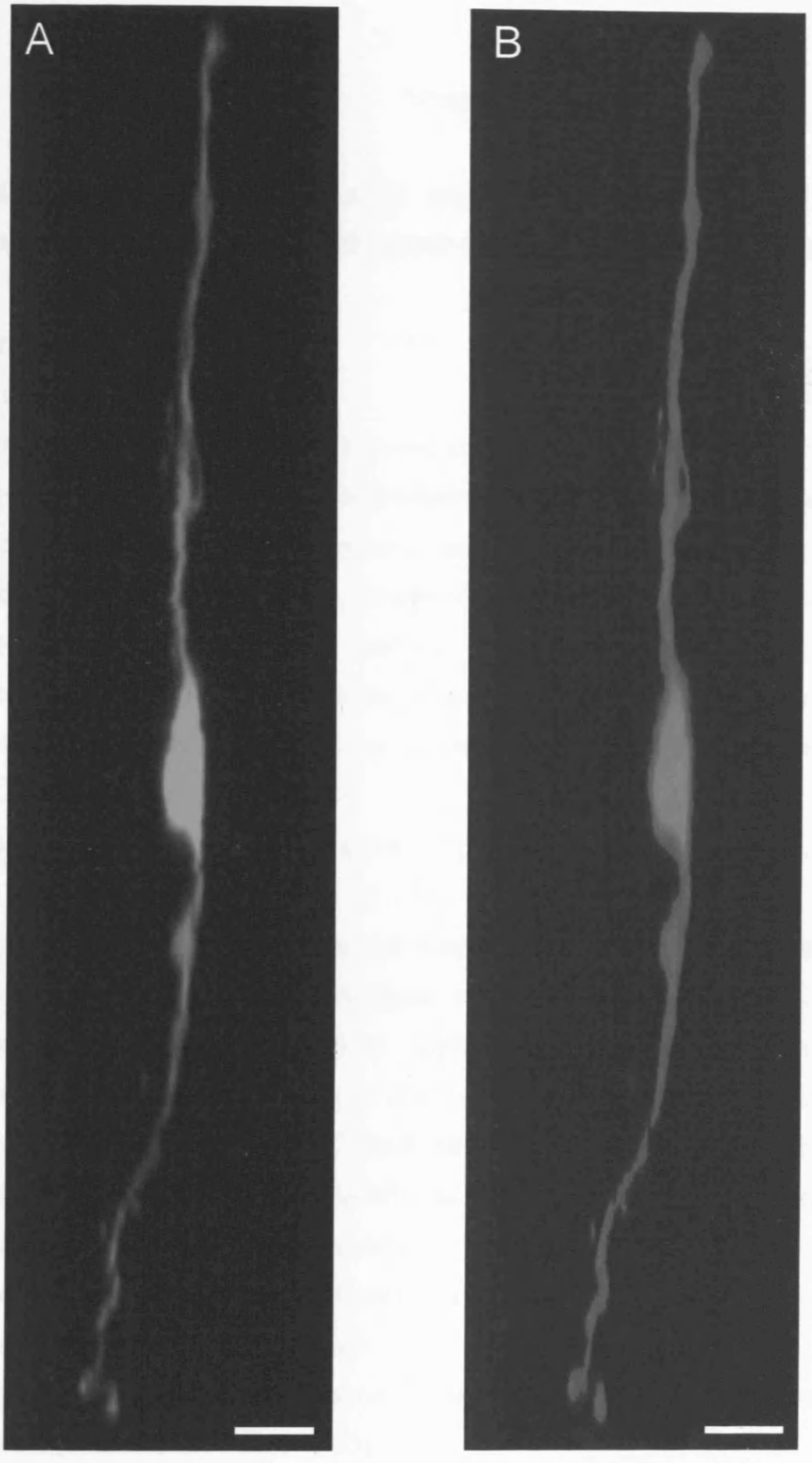

Figure 2.8 Measurement of the volume of a single cell using thresholding. A, Projection of a single FITC-filled cell from an E8 retina. *B*, The same cell as shown in *A* after thresholding. The thresholded area is shown by the pink mask. The volume of the thresholded area could be calculated using Metamorph software (Universal Imaging, PA, USA). Scale bar 10 µm.

Chapter 3

MEMBRANE PROPERTIES AND NEUROTRANSMITTER RESPONSES OF CELLS IN THE VENTRICULAR ZONE OF THE EMBRYONIC CHICK RETINA

3.1 Introduction

During neurogenesis in the embryonic neural retina, mitosis occurs only within the ventricular zone (VZ). Here, asymmetric divisions of progenitor cells give rise to one progenitor cell and one postmitotic cell, while symmetric divisions produce two daughter progenitor cells. Proliferation, migration and differentiation are all subject to modulation by both intrinsic and extrinsic factors. Previous work has demonstrated roles for neurotransmitters, and the membrane voltage changes they evoke, in such modulatory functions at early times in development.

In cortical progenitors, the depolarizing actions of GABA and glutamate have been shown to affect the rate of DNA synthesis (LoTurco et al., 1995), and to have differential effects on the cell cycle time in the VZ and the subventricular zone (Haydar et al., 2000). Nguyen et al. (2003) show that $GABA_A$-receptor activation in neural progenitors from the striatum can inhibit cell cycle progression. Confocal imaging of Ca^{2+}-signals in mitotic cells within the VZ has shown that spontaneous Ca^{2+}-fluctuations can be modulated by endogenous transmitter release, and that this affects the rate of mitosis (Pearson et al., 2002). In addition, neurotransmitters and/or electrical activity may also affect the differentiation and migration of postmitotic cells. The rate of migration of newly differentiated cerebellar granule cells has been shown to be modulated by glutamate acting via NMDA receptors, and the activation of voltage-gated calcium channels (Komuro & Rakic, 1993).

Ca^{2+}-signals in embryonic spinal neurons are known to be important for K^+-channel expression, which in turn is involved in the maturation of the action

potential (Gu & Spitzer, 1995, Vincent et al., 2000). In amphibian neurons, electrical excitability is acquired within 8 hours of the final round of DNA synthesis. The early action potentials in the cells are of long duration, are Ca^{2+}-dependent, and occur spontaneously, producing increases in cytosolic calcium which regulate differentiation, including the development of K^+-currents. The development of K^+-currents is required for the switch from Ca^{2+}- to Na^+-dependence of the inward current of the action potential (for review, see Spitzer & Ribera, 1998).

Several recent papers have investigated the properties of neural progenitor cells in adult mice, namely those of the subgranular zone in the hippocampus, and those of the subventricular zone (SVZ) adjacent to the lateral ventricle, that migrate to the olfatory bulb via the rostral migratory stream to become olfactory interneurons. Wang et al. demonstrate that progenitor cells in the SVZ respond to GABA, which may modulate proliferation and/or migration via $GABA_A$-receptors (2003a). Fukuda et al. (2003) investigated the membrane properties of progenitor cells in the hippocampus of the adult mouse, and found that these could be divided into sub-categories of early and late progenitor cells with distinct membrane properties. Here, whole-cell patch-clamping is used to investigate the expression of voltage- and transmitter gated channels in cells in the developing retina. This technique is combined with immunohistochemistry to show whether the cells are progenitors or postmitotic cells.

3.2 Methods

The methods employed are described in detail in section 2.3. Briefly, acutely dissected retinae were placed with the VZ facing upwards in a recording chamber. The retina was held flat with a nylon- and platinum harp, and transferred to the stage of an upright microscope, where the tissue was continuously superfused with Krebs' solution. A series of taps and reservoirs enabled solution exchanges between control- and drug-containing Krebs' solution. The tissue was visualised using bright field illumination and differential contrast optics. The internal solution used to fill the patch pipette (K-Gluc, Table 2.2, unless otherwise stated) contained a fluorophore to allow the detailed morphology of the recorded cell to be examined using epifluorescence illumination following recording. Membrane currents were measured in the whole-cell clamp configuration to examine the expression of voltage- and transmitter-gated channels, and current-traces were stored on a PC for subsequent analysis. The resting membrane potential was measured by switching the amplifier to the current clamp mode with no current injection. In order to gain better access to the membranes of progenitor cells for recordings, a method of guillotine slicing of very young embryonic retina was developed. The retinae were mounted on Millipore membrane filters, and cut into slices, which could be rotated and held in place in the recording chamber with strips of Vaseline. By targeting the cells within the VZ exposed in these slices, possible cell-types are restricted to progenitors or postmitotic cells that have just exited the cell cycle. Following recording and dye-labelling of the cells, the tissue was fixed in PFA, processed for immunohistochemistry, and viewed on a confocal microscope.

Results are presented as means ± standard error of the mean, unless otherwise indicated. Statistical significance was tested using an unpaired Student's t-test.

3.3 Results

3.3.1 Properties of cells in the VZ in whole, flatmounted E5 retinae

Initial recordings were made in whole E5 retinae, flattened out with the ventricular surface facing up (Figure 2.1A). Following entry into the whole-cell mode, the cells' input resistance (R_{in}), capacitance (C_m) and series resistance (R_s) were determined from the current responses to -10 mV steps from the holding potential (Figure 3.1A). The decay of the transient could be fitted by a single exponential, and the series resistance calculated from the time constant (see section 2.3.7 in the Methods chapter for further details). 24 cells in 15 retinae were recorded. These cells had a mean R_{in} of 134±19MΩ and a mean resting membrane potential (V_m) of -49±2mV. The presence of gap junctions coupling cells in the VZ was expected to contribute significantly to the low input resistance. This was tested by making the recording in the presence of carbenoxolone (CBX), which was added by bath-perfusion for 5 minutes prior to recording. As shown in Figure 3.1, the presence of CBX caused a significant increase in the input resistance of the cells, to a mean value of 495±100MΩ.

Recordings from cells in the VZ of flat-mounted retinae were short-lived, because the electrode can only access the ends of the cell processes that cover the ventricular surface, rather than the cell bodies. In this situation, the smallest movement of the electrode causes the process to break away from the pipette, thus ending the recording. For this reason, it was not possible to test the effects of drug applications on the membrane currents of cells and examine the expression of ligand- and voltage-gated ion-channels using flatmounted preparations.

3.3.2 Membrane properties of cells in the VZ in E5 retinal slices

In order to overcome the obstacles encountered when recording from cells in flatmounted retinae, a retinal slicing procedure was adopted. This permits access to the cell bodies of VZ cells (Figure 3.2), rather than their processes, and allows longer lasting recordings to be made. In order to restrict possible cell-types to progenitors or postmitotic cells that have just exited the cell cycle, rather than more mature retinal neurons, recording were made by targeting cell bodies within the VZ. Recordings made from retinal slices revealed the existence of two distinct populations of cells. One type of cell was without any obvious time-dependent, voltage-gated currents, with largely ohmic responses to depolarising voltage-steps (Type 1), and other cells (Type 2) showed outward, time-dependent currents in response to depolarising voltage steps. Neither cell type showed any obvious spontaneous electrical activity. Examples of the electrical responses to depolarising voltage-steps of these two cell types are shown in Figure 3.3. While some cells with intermediate properties were also found, the majority fell clearly into one of these two groups. In addition to the difference in the expression of time-dependent currents, Type 1 cells had a low input resistance, whereas Type 2 cells had a high input resistance. The distribution of input resistance by cell type is shown in Figure 3.4. Although the two populations are slightly overlapping, the difference between the mean R_{in} for the two cell types was highly significant (Type 1, 165±21MΩ; Type 2, 1252±145MΩ; $p<0.0001$).

The two cell types were of similar bipolar morphology and both extended a process toward both the ventricular and vitreal surfaces of the retina. In cases where the cell body was juxtaposed to the ventricular surface, only a single process was present. The distribution of membrane capacitance by cell type is shown in Figure 3.5, and does not vary significantly between the groups (Type 1, 2.5±0.2pF; Type 2, 2.7±0.1pF; $p=0.51$).

The introduction of Alexa 488 into the cells showed that the extent of gap junction coupling to other cells varied with cell type. Cells of Type 1 were usually part of a coupled cluster, containing between one and ten other cells. In contrast, cells of Type 2 were mainly uncoupled, or, in a few cases, coupled to one other cell.

The resting membrane potential (V_m) did not vary between the two groups. The distribution of resting membrane potential by input resistance and cell type is shown in Figure 3.6. The V_m for each cell type varies across a similar range, and the mean V_m for cells of Type and Type 2 were not significantly different (Type 1, -43.5±1.4mV; Type 2 -40.4±1.4mV; $p = 0.13$).

3.3.3 Properties of voltage-gated currents of Type 2 cells in E5 retinal slices

The emergence of electrical excitability is a critical step in neuronal differentiation, and has been shown overall to follow a stereotyped pattern across species and cell types, although there is significant variation in the specific properties of the ionic conductances expressed (for review, see Robinson & Wang, 1998). The general rule governing the development of voltage-gated currents appears to be that K^+-channels, which act to hyperpolarize the cell and restore membrane potential following excitation, are expressed prior to channels mediating inward currents, such as voltage-gated Na^+-channels, required for the generation of fast action potentials (for review, see Spitzer et al., 2000). In amphibian neurons, the expression of K^+-channel mediating the delayed rectifier K^+-current, I_K, precedes that of the transient, inactivating K^+-current, I_A (Desarmenien et al., 1993), whereas in other cell types, I_A precedes the delayed rectifier (Beck et al., 1992). Studies using injections of antisense into *Xenopus* oocytes demonstrated that the expression of the delayed rectifier current is required for the maturation of the action potential (Vincent et al., 2000). In the developing retina, studies of voltage-gated current expression has focused on the development of spiking in retinal ganglion cells (RGCs), which is a prerequisite

for activity-dependent refinement of retino-tectal projections, and has been studied mainly in RGCs in developing cat and ferret (for review, see Robinson & Wang, 1998). In the embryonic cat retina, at E30, a time when RGCs are still being generated, electrical stimulation elicited spikes in only a third of cells, and none were capable of repeated spiking in response to maintained depolarization. The proportion of spiking RGCs increased such that by E55, all RGCs generated spikes, and the majority were capable of repetitive firing (Skaliora et al., 1993). For K^+-currents in cat RGCs, a decrease in the proportion of cells expressing I_A was observed during a similar period, from E31 through to early postnatal stages (Skaliora et al., 1995). In embryonic *Xenopus* motoneurons, and in cultured cortical neurons from embryonic chick, early action potentials are largely calcium-dependent (Spitzer & Lamborghini, 1976; Mori-Okamoto et al., 1983), whereas in cat RGCs they are sodium-dependent from the outset (Skaliora et al., 1993).

A characteristic feature of the Type 2 cells described here is the presence of outward, voltage-gated currents, consisting of a fast, transient component and a slower, sustained component (in the following description, the fast transient component is termed I_A, and the slower sustained component is termed I_K). As illustrated in Figure 3.7, these currents were almost completely suppressed by a combination of the pharmacological blockers, 4AP and TEA. Residual voltage-gated current activated in the presence of these pharmacological blockers could be blocked by increasing the holding potential to -30mV (Figure 3.7D), which causes voltage-dependent inactivation of the sustained current (C-type inactivation). These features identify them as voltage-gated K^+-currents. In contrast to the classical pattern of K^+-channel blockade from studies in invertebrate neurons, where 4AP blocks the transient I_A current, and TEA blocks the delayed I_K current (Hille, 2001; Thompson, 1982), in these experiments both agents affected both the transient and the sustained component of the voltage-gated K^+-conductance. K^+-currents with similar properties to those described here were found in embryonic cat RGCs (Skaliora et al., 1995).

Figure 3.8 illustrates the averaged peak current amplitude for 18 cells of Type 2 at different membrane potentials, after subtraction of leak-current and appropriate voltage corrections. The peak amplitude for the I_K component ranged from 154pA to 1052pA, with a mean peak amplitude of 670±61pA, whereas the peak amplitude for the I_A component ranged from 890pA to 2240pA, with a mean peak amplitude of 1484±153pA. The peak current density for the I_K component ranged from 44pA/pF to 526pA/pF, with a mean of 267±31pA/pF. The peak current density for the I_A component ranged from 254pA/pF to 845pA/pF, with a mean of 541±67pA/pF.

If the K^+-currents were suppressed using a combination of Ba^{2+} in the external solution (Ba^{2+}-Krebs' in Table 2.1) and Cs^+ in the internal solution (CsCl solution in Table 2.2), a rapid, inward voltage-gated current could be seen in some Type 2 cells, as illustrated in Figure 3.9. This current had a rapid time course, activated between -30 and -20mV, and could be blocked by the presence of TTX, features which identify it as a Na^+-current. However, as seen in Figure 3.9, the Na^+-current was very small in amplitude, and was only observed in 2 out of 16 cells tested, in contrast to the large outward K^+-currents, which were seen in all Type 2 cells.

3.3.4 Membrane properties of cells in the VZ in E8 retinal slices

Fukuda et al. (2003) have shown that nestin-positive progenitor cells in the adult mouse hippocampus comprise two distinct cell types, identified as early and late neural progenitor cells, which have distinct membrane properties. Here, to examine how the distribution of cell types and their properties change during development in the retina, recordings were made from retinal slices at E8. All cells recorded at this stage had features characteristic of the Type 1 cells seen at E5. Examples of typical responses of an E8 Type 1 cell, and an E5 Type 1 cell, are shown in Figure 3.10. In both cases, the cells have a low R_{in}, and respond

ohmically to a series of depolarizing voltage steps. In addition, both E8 and E5 Type 1 cells show gap junctional coupling to neighbouring cells.

The distribution of R_{in} for E8 and E5 Type 1 cells is shown in Figure 3.11. Although the R_{in} values at E5 span a larger range than at E8, there is no difference in the mean R_{in} between the two groups (E5 Type 1, 145±12MΩ; E8, 119±15MΩ; $p = 0.29$).

The distribution of membrane capacitance for E8 and E5 Type 1 cells is shown in Figure 3.12. Although the C_m values at E5 span a larger range than at E8, the mean C_m of the two groups are similar (E5 Type 1, 2.5±0.17pF; E8, 2.6±0.29pF; $p = 0.70$)

Figure 3.13 shows the distribution of V_m against R_{in} for E8 and E5 Type 1 cells. The V_m values of E5 cells range from -14 to -75mV, whereas for E8 cells, the V_m values cluster around -50 to -60mV. The mean V_m of type 1 cells at E5 is significantly more positive than the mean V_m at E8 (E5, -44±1.4mV; E8, -54±1.6mV, $p < 0.0001$).

3.3.5 Responses to glutamate in VZ cells at E5 and E8

In the developing cortex, glutamate acts via AMPA/kainate receptors to depolarize VZ cells, and decrease the rate of DNA synthesis (LoTurco et al., 1995). Whole-cell patch-clamp recording of RGCs in embryonic chick retina have shown that at E6 (the earliest time tested), 20% of these cells respond to AMPA. By E8, almost all RGCs recorded showed responses to both AMPA and NMDA (Bonness, 1999). Using confocal imaging and Ca^{2+}-dyes, Pearson (2003) found that ~40% of cells within the VZ of the chick retina at E6 respond to application of 100μM glutamate, a response that was predominantly mediated via AMPA-

kainate receptors. In contrast, using non-confocal Ca^{2+}-imaging, Yamashita & Fukuda (1993) report the same cells to be glutamate insensitive at E3.

Here, I have tested the responses to glutamate of whole-cell patchclamped VZ cells in retinal slices at E5 and E8. Cells were tested at holding potentials of -70mV, and then at more depolarized voltages.

At E5, none of the 23 Type 2 cells tested showed any response to glutamate. In contrast, 28% of E5 Type 1 cells (n=39) responded to glutamate with a sustained, inward current. At E8, when all VZ cells are of Type 1, 93% responded to glutamate (n=14). The current evoked by glutamate was not blocked by the NMDA receptor antagonist AP5 and showed no sign of Mg^{2+} block at more depolarized potentials. Thus, these responses are likely to be mediated by non-NMDA receptors.

However, application of NBQX, a potent antagonist at AMPA/kainate receptors, only reduced the current response by ~50%. In addition, the current response to glutamate did not reverse even at very positive potentials. Application of TBOA, a non-selective inhibitor of the glutamate transporters (EAAT1-5), in the presence of NBQX, produced an additional reduction in the inward current response, suggesting that the response is mediated partly by an AMPA/kainate-receptor and partly by the electrogenic action of a glutamate transporter. An example of this is shown in Figure 3.14A. When glutamate was applied in the presence of TBOA, the response showed a linear current voltage relation with a reversal potential of -2.6 mV (Figure 3.13B).

As shown in Figure 3.15, the mean amplitude of the response to glutamate was greater at E8 than at E5, although the difference was not statistically significant (E5, -57±13pA; E8, -82±12pA; $p = 0.17$). The current density was also greater at E8 than at E5, although this was also not statistically significant (E5, -28±7pA/pF; E8, -44±10pA/pF; $p = 0.19$).

3.3.6 Responses to GABA in VZ cells at E5 and E8

Wang et al. (2003) found depolarizing responses to GABA via $GABA_A$-receptors in progenitor cells in the adult rodent subventricular zone and rostral migratory stream. Similarly, LoTurco & Kriegstein (1991) and Owens et al (1996) reported depolarizing effects of GABA in VZ cells in cortical slices. Whole-cell patch-clamp recordings of RGCs from embryonic chick retina showed responses to GABA from E6 (the earliest time tested), where 25% of RGCs show $GABA_A$-receptor mediated responses, increasing to 100% at E12 to E14 (Bonness, 1999). In studies using non-confocal calcium-imaging of embryonic chick retina, Yamashita & Fukuda (1993) report that $GABA_A$-receptor mediated depolarization produce calcium-responses from E3 (the earliest time tested). Using confocal calcium-imaging, Pearson (2003) reports that, at E6, ~35% of cells within the VZ of chick retina respond to application of 100 µM GABA, a response which could be reversibly blocked by bicuculline.

Here, the responses to GABA were tested by puff- and bath-application of GABAergic agents to whole-cell patchclamped cells in retinal slices. At E5, none of the Type 2 cells tested showed any response to GABA (n=26). In contrast, 97% of Type 1 cells at E5 (n=60) and 100% of Type 1 cells at E8 (n=15) showed an inward current in response to application of GABA at -70mV. As shown in Figure 3.16A, the response to GABA could be reversibly blocked by application of bicuculline, suggesting that it is mediated by a $GABA_A$-receptor. The presence of $GABA_A$-receptors in these cells was confirmed by application of the selective $GABA_A$-receptor agonists, isoguvacine and THIP, both of which produced inward currents at negative potentials (Figure 3.16B). The current responses to these agents were smaller in amplitude, probably reflecting both the lower efficacy of these agonists compared to GABA (Mortensen et al., 2004), and desensitization caused by the initial application of GABA (full functional recovery from desensitization following prolonged agonist exposure can be of the order of 5-10 minutes (Im et al., 1995)).

Since the $GABA_A$-receptor gates an anion-channel, which is mainly permeable to Cl^--ions, the predicted reversal potential can be calculated by the Nernst equation:

(3.1) $E_{Cl} = (RT / F) * \ln (Cl_i / Cl_e)$

where R is the gas constant, T is absolute temperature, and F is Faraday's constant. At 25° C, RT / F = 25.69. The concentrations of Cl^- in the internal and external solutions are 12.2 and 110 mM, respectively:

(3.2) $E_{Cl} = 25.69 * \ln (12.2/110) = -56.5$ mV

If the inward current generated by GABA-application is mediated by a $GABA_A$-receptor, the current should reverse at a membrane potential close to this value. However, in practice the GABA-current was large near the calculated reversal potential, and became smaller at more positive potentials. In Figure 3.17A, the peak response to bath-applied GABA in Type 1 cells at E5, averaged for 8 cells, is plotted as a function of the holding potential. The GABA evoked current did not reverse in any of the cells examined. The extrapolated reversal potential from these data is +39mV, in comparison to the calculated reversal potential of -56.5mV.

A potential problem with bath-applying the drug at different holding potentials is incomplete recovery from desensitization between each application (Im et al., 1995). To overcome this, a rapid voltage-ladder of increasingly depolarising voltage-steps was applied in control solution, and in the presence of GABA, to examine the current-responses at all membrane potentials within the first few seconds of the response. The GABA-evoked current was obtained by subtracting the control trace from the GABA-trace. An example of this experiment is shown in Figure 3.17B, where the GABA-evoked current reverses at +14mV, ~70 mV

positive to the calculated value of E_{Cl}. Several different approaches were employed to test the possibility of a non-$GABA_A$-mediated mechanism contributing to the response.

Despite the pharmacological evidence indicating a $GABA_A$-receptor mediated response, the potential involvement a $GABA_B$-receptor was considered. $GABA_B$-receptors are known to modulate the release of other transmitters (for review, see Kuriyama et al., 2000). If GABA-application to VZ cells was to result in the release of a depolarizing agent this could be the cause of the apparently anomalous reversal potential of the GABA response described above. However, co-application of GABA and CGP35348 (100µM), a potent $GABA_B$-receptor antagonist, did not generate the outward current expected under this hypothesis (n=3). Application of baclofen (10µM), a $GABA_B$-receptor agonist, was also without effect (n=3).

Given the actions of $GABA_A$-receptor agonists and antagonists, it seems that, in contrast to glutamate, it is unlikely that the GABA-response is mediated in part by a transporter. GABA-transporters are electrogenic through coupling with Na^+ (for review, see Kanner, 1994). The GAT-1 transporter is widely expressed in the adult retina of many species, including rat (Brecha & Weigmann, 1994), guinea pig (Biedermann et al., 2002) and rabbit (Hu et al., 1999a). During retinal development, GAT-1 immunoreactivity was detected from P3 in the rabbit (Hu et al., 1999b) and from E6, the earliest time tested, in the chick (Catsicas & Mobbs, 1998). To exclude to possibility that activation of GAT-1 contributes to the GABA-evoked response, the effect of SKF89976A (50µM), a potent GAT-1 inhibitor, was tested. SKF89976A had no effect on the GABA-evoked current (n=5). SKF89976A is selective for GAT-1, so it can not be ruled out that other transporter are involved. However, calcium-waves occurring at E8, which are modulated by GABA, are profoundly affected by application of SKF89976A, suggesting that this is the predominant GABA transporter expressed at this time (Catsicas & Mobbs, 1998).

On the basis of these findings, the most likely explanation for the unusual responses to GABA-application is the extensive gap junctional coupling of Type 1 cells at this time. While the [Cl^-] in the recorded cell is set by the pipette solution, the [Cl^-] in coupled cells is not. Previous studies have shown that the reason for the depolarizing actions of GABA during development is the high $[Cl^-]_i$ (Owens et al., 1996), which in turn is due to the relatively later expression of the Cl^--exporter, KCC2 (Rivera et al., 1999). In addition, the control the patchclamp apparatus exerts over the membrane voltage is poor within a coupled network, since the current introduced to hold the membrane voltage constant leaks into neighbouring cells.

The mean peak amplitude of the GABA-evoked current at E5 was -126±12pA, a large current for small embryonic cells. Inward GABA-evoked currents of similar amplitude (-186±12pA) were observed in cortical progenitors in brain slices from E16 fetal rats. Like the Type 1 cells described here, these cells are also extensively coupled. The amplitude of the GABA-currents recorded in cortical progenitors was approximate 10-fold larger than that of GABA-currents elicited in cells in the cortical plate, which are uncoupled (LoTurco & Kriegstein, 1991). These authors speculate that the large currents observed in progenitor cells arise from the summation of currents generated by several coupled cells. At E8, mean peak amplitude of the GABA-evoked current was -70±11pA, significantly lower than at E5 (Figure 3.18A). The mean current density was also significantly higher at E5 (-78±11pA/pF) than at E8 (-38±10pA/pF), as shown in Figure 3.18B. However, the distribution of GABA-evoked current densities shows variation across a large range, from -10pA/pF to -268pA/pF, as shown in Figure 3.19. This large variation in current density is consistent with the hypothesis that the current arises from coupled cells, the amplitude and density varying with the numbers of cells contributing to the response.

3.3.7 Responses to other neurotransmitters of VZ cells

A range of other neurotransmitters have been shown evoke responses in early embryonic cells. In studies that utilized calcium-imaging of embryonic chick retina, Fukuda and colleagues reported calcium-responses from E3 (the earliest time tested) to ATP and UTP via P2U purinoceptors (Sugioka et al., 1996), and to ACh via muscarinic receptors, which peaked at E3-E5, then rapidly declined until E8 (Yamashita et al. 1994). Pearson et al. (2002) also reported calcium-responses in the VZ of E4-E6 chick retinae to purinergic and muscarinic agonists. Glycine and taurine responses have been reported in early embryonic cells in several species. Using whole-cell patchclamping of neurons in the ganglion cell layer, Bonness (1999) found glycine responses in ~25% of cells at E6, increasing to ~60% at E8. Recently, taurine has been demonstrated to act on retinal progenitors in mouse via $GABA_A$-receptors and ionotropic glycine-receptors to promote rod photoreceptor development (Young & Cepko, 2004).

Here, carbachol, UTP, glycine and taurine (all 100 µM) were tested by bath-application to whole-cell patchclamped cells in retinal slices. However, none of these agents evoked a current response in any of the cells tested. The responses to all neurotransmitters tested are summarized in Figure 3.20.

3.3.8 Expression of immunohistochemical markers

Immunohistochemistry was used to identify cells in the developing retina. Figure 3.21 shows single confocal sections from an E5 retinal slice preparation labelled with antibodies for TuJ1 and vimentin. The TuJ1-antibody labels neuron-specific β-tubulin and thus marks postmitotic neurons. Vimentin is an intermediate filament expressed by both glial cells and progenitor cells. As expected at early stages in development, the vast majority of cells at E5 are $vimentin^+/TuJ1^-$, and the majority of $TuJ1^+$ cells are found in the putative ganglion cell layer (Figure

3.21, indicated by the yellow arrows). However, some TuJ1$^+$ cells are also visible in the VZ, (Figure 3.21, indicated by the white arrows), and in the neuroblastic layer (Figure 3.21, indicated by the green arrows). The morphology of TuJ1$^+$ cells and vimentin$^+$ cells is indistinguishable at this stage. The pattern of TuJ1/vimentin staining shows that, at E5, the VZ contains a mixed population of vimentin$^+$ progenitor cells and TuJ1$^+$ post-mitotic cells, at this stage most likely RGCs.

3.3.9 Correlation between antigen expression and cell type

Following patch-clamp recording and dye-filling, retinal slices were fixed in PFA and labelled with antibodies for TuJ1 and vimentin. The two cells types observed at E5 fell clearly into two separate groups as indicated by these markers. In general, Type 1 cells were vimentin$^+$/TuJ1$^-$, whereas Type 2 cells were TuJ1$^+$/vimentin$^-$. Figure 3.22 shows a typical E5 Type 1 cell filled with Alexa 488 during patchclamp recording, where the retina has subsequently been stained for vimentin (red) and TuJ1 (blue). A projection of several confocal sections illustrates the extensive coupling seen between neighbouring progenitor cells, as revealed by the diffusion of Alexa 488 from the recorded cell (Figure 3.22A). Single confocal sections show that the recorded cell and most of the neighbouring cells are vimentin$^+$/TuJ1$^-$ (Figure 3.22B-C). The same pattern of staining was seen whenever a Type 1 cell was filled with Alexa 488, and two further examples of Alexa-filled Type 1 cells are shown in Figure 3.23. All three Type 1 cells shown in Figures 3.22-3.23 form coupled clusters with neighbouring cells, and are vimentin$^+$/TuJ1$^-$. In contrast, Type 2 cells, when filled with Alexa, proved not to be coupled to any neighbouring cells (Figure 3.24A), and were generally vimentin$^-$/TuJ1$^+$ (Figure 3.24B-E). Figure 3.25 shows a further typical example of a Type 2 cell. Whilst the cell body expresses vimentin (Figure 3.25C), the process is TuJ1$^+$ (Figure 3.25E). Again, it is not coupled to any neighbouring cells (Figure 3.25B). The pattern of staining, and the location of the cell body in

the ventricular surface (Figure 3.25A), suggests that this cell may have recently completed mitosis, and started to differentiate as a neuron.

Figure 3.26 shows an E8 Type 1 cell labelled with Alexa 488. Such cells show similar patterns of staining to that seen in E5 Type 1 cells, which have a bipolar morphology and are extensively coupled to neighbouring cells. Cells within the coupled cluster are vimentin^{+}/TuJ1^{-}. Thus, Type 1 cells at E8 have the same membrane properties as Type 1 cells at E5, and, as at E5, express vimentin, but not TuJ1.

3.4 Discussion

3.4.1 Whole-cell patchclamp recordings in the VZ of the developing retina

The pattern of development in the retina follows a highly stereotyped pattern, with a conserved order of neurogenesis and migration. The accessibility of the retina at early times in development makes it an attractive preparation in which to study the properties of early, embryonic progenitor cells.

A growing body of evidence suggests that shown both ligand- and voltage-gated ion channels play pivotal roles in development prior to synapse formation. Maturation of K^+-channel expression, and development of a fast, inward Na^+-current, is a critical step in neuronal differentiation and the maturation of the action potential (Gu & Spitzer, 1995; Vincent et al., 2000). In the adult hippocampus, Fukuda et al. (2003) demonstrated a dynamic change in membrane properties of progenitor cells as they progress from early to later stages of neurogenesis. Neurotransmitters have been shown to regulate a number of developmental processes in a paracrine fashion, including migration (Rossi & Slater 1993; Komuro & Rakic, 1993), proliferation (LoTurco et al., 1995; Haydar et al., 2000; Pearson et al., 2002; Nguyen et al., 2003) survival and cell fate (Altshuler et al., 1993; Young & Cepko, 2004). Recently, it has been suggested that transmitters may have similar effects on adult progenitors; Brazel et al. (2005) report that increased levels of glutamate caused by ischaemia enhanced the survival and proliferation of progenitor cells in the subventricular zone of newborn rats.

A number of neurotransmitter receptors are thought to be expressed by embryonic chick retinal cells prior to synapse formation. Responses have been observed to exogenous application of ACh, GABA, glutamate and purine nucleotides and these responses are developmentally regulated (Yamashita and Fukuda, 1993; Bonness, 1999; Sakaki et al., 1996; Sugioka et al., 1996; 1999;

Pearson, 2003). There is also evidence of endogenous neurotransmitter release in the early embryonic chick retina. Components of the exocytotic mechanism, such as synaptotagmin and syntaxin, are expressed in the chick retina as early as E4 (Bergmann et al., 2000). Release of ACh, GABA, ATP and glutamate has been demonstrated in cultures of dissociated chick retinal cells and organotypic retinal cultures (Bonness, 1998; Duarte et al., 1996; Sugioka et al., 1999; Santos et al., 1998; 1999).

Previous studies in the retina have either focused on RGCs, and investigated how their voltage- and transmitter-gated channels develop, especially during the time of activity-dependent refinement of synaptic connectivity, or used calcium-imaging methods that are unable to resolve the identity of the cells that respond. The methods developed here, of using embryonic retinal slices to study the properties of individual VZ cells at very early times in development, allows a more detailed investigation of the membrane properties of embryonic progenitors and newly postmitotic cells, at earlier times than could previously be investigated. Previous studies of the development of the membrane conductances of retinal cell have targeted cells identified by virtue of their location in the retina within the GCL (Bonness, 1999), or by retrograde labelling with fluorescent dyes from the lateral geniculate nucleus (Skaliora et al., 1993; 1995). These studies have been restricted to cells in the GCL that have assumed their final phenotype and location. The retinal slicing procedure adopted here allows both newly postmitotic cells and progenitor cells to be recorded from the earliest stages of development. The combination of electrophysiology and immunohistochemistry employed provides a powerful method of correlating the membrane properties of individual cells with their expression of developmentally regulated markers and changes in their morphology.

3.4.2 Gap junction coupling of VZ cells

Cortical VZ progenitor cells are known to be extensively coupled via gap junctions, which enable Ca^{2+}-transients to pass between cells as waves (Owens & Kriegstein, 1998). In the chick retina, the coupling of RGCs one to another increases with time (Bonness, 1999). While it was possible to make patch-clamp recordings from the ventricular surface of whole-mounted E5 retinae, which show that these cells are extensively coupled to one another, the technique is insufficiently robust to allow enough time to assess membrane properties of the cells in more detail. The extent and developmental profile of gap junctional coupling in progenitor cells is the subject of chapter 4, and will not be discussed further here.

3.4.3 Membrane properties of VZ cells in retinal slices reveal two distinct cell types

Two distinct cell types were observed in the VZ in E5 retinal slices. Cells of Type 1 had a low R_{in} (mean 165MΩ), showed no obvious expression of time-dependent, voltage-gated currents, and were extensively coupled to neighbouring cells. Cells of Type 2 had a high R_{in} (mean 1252MΩ), expressed time-dependent voltage-gated K^+-currents, and, occasionally, fast inward Na^+-currents, and showed no, or very limited, gap junctional coupling to neighbouring cells. Neither cell type demonstrated spontaneous electrical activity. Although cells of Type 1 are extensively coupled, and the voltage-control during patch-clamp experiments in a large coupled network is poor due to the buffering by neighbouring cells within the coupled network, the marked differences in the response to series of depolarising voltage-steps by the two cell types make it unlikely that this is an artefact of the gap junctional coupling. These results show striking similarities to those of Fukuda and colleagues (2003), in their study of nestin-positive progenitor cells in the adult dentate gyrus, where they also describe two distinct

cell types. In the study by Fukuda et al. (2003), Type I cells had a low R_{in} (mean 77MΩ) and little in the way of voltage-gated current expression. By comparison, Type II cells had a high R_{in} (mean 2110MΩ), and showed both transient outward K^+-currents and fast inward Na^+-currents. No spontaneous electrical activity was observed in either cell type. The findings presented here show that progenitor cells in the embryonic retina show similar patterns in the development of their membrane properties to progenitor cells in the adult hippocampus, suggesting this may be a general feature of progenitor cell maturation.

3.4.4 Type 2 cells express voltage-gated K^+-currents

Cells of Type 2 expressed outward K^+-currents, which contained a transient and a sustained component, I_A and I_K. These currents were sensitive to the K^+-channel blockers, TEA and 4AP, and showed voltage-dependent inactivation. The properties of the Type 2 cell K^+-currents were similar to those reported in fetal cat RGCs by Skaliora et al. (1993), and the peak current amplitudes and densities fell within the range reported by these authors. In amphibian neurons, I_K precedes expression of I_A (Desarmenien et al., 1993), whereas in other cell types, I_A precedes I_K (Beck et al., 1992). Skailora and colleagues (1993) found that, at E31, 82% of RGCs expressed both I_A and I_K, compared to only 55% of postnatal RGCs expressing both I_A and I_K, the remainder only expressing I_K. Here, both components were expressed by all cells investigated at E5. The I_K current has been shown by Vincent et al. (2000) to play a role in maturation of the action potential, and its consistent expression in the Type 2 cells observed in this study strongly suggests these cells are differentiating along a neuronal path. At this stage in development, the majority of postmitotic cells are most likely fated to become RGCs. Skaliora et al. (1993) speculate that the decrease in the proportion of RGCs with transient K^+ currents is due to their preferential elimination during ontogeny. The findings described here neither contradict nor support this hypothesis. An alternative hypothesis is that I_A plays a particular role

in the development of the firing properties of mature RGC, after which the channel is down-regulated. It would be interesting to follow the development of K^+-currents in chick RGCs at later stages, to see if a change in the composition of their membrane currents occurs, following a similar pattern to that observed in the cat, which would suggest a more general mechanism.

3.4.5 Some Type 2 cells express voltage-gated Na^+-currents

In some Type 2 cells, the presence of a fast, TTX-sensitive, inward Na^+-current was observed. In general, previous studies have found that K^+-channels, which act to hyperpolarize the cell and restore membrane potential following excitation, appear before voltage-gated Na^+-channels, which are required for fast action potential generation (reviewed in Spitzer et al., 2000). The expression of voltage-gated Na^+-currents is seen as a hallmark of neuronal differentiation. The findings presented here are consistent with this pattern, and also support the notion that Type 2 cells represent postmitotic cells, that have begun neuronal differentiation.

3.4.6 Type 1 cells respond to glutamate

28% of E5 Type 1 cells responded to glutamate with a sustained, inward current, whereas at E8, almost all Type 1 cells responded to glutamate. The glutamate response was partly blocked by NBQX, indicating an AMPA/kainate-receptor mediated mechanism. The reversal potential of the response blocked by NBQX was -2.6mV, a value similar to that of embryonic chick RGCs (Bonness, 1999) and rabbit starburst amacrine cells (Zhou & Fain, 1995).

In studies using confocal imaging of retinae loaded with Ca^{2+}-sensitive dye, Pearson (2003) found ~20% of cells in the VZ at E5 responded to glutamate with an increase in $[Ca^{2+}]_i$. This figure rose to around 35% at E6, and these responses

could be blocked by NBQX. However, neither glutamate nor glutamate antagonists affected the rate of mitosis in the VZ at E5, determined by measuring the time spent in metaphase, or the number of mitotic profiles following *in ovo* injections of the drugs (Pearson et al., 2002; Pearson, 2003). The findings described here confirm that glutamate causes a depolarizing response in cells within the VZ, and present the question of what the role of glutamatergic signalling is in these cells. In the developing cortex, glutamate acts via AMPA/kainate receptors to depolarize VZ cells, raise $[Ca^{2+}]_i$ and decrease the rate of DNA synthesis (LoTurco et al., 1995). Glutamate has also been shown to regulate the rate of migration of postmitotic cells. Given that progenitor cells go through different stages of the cell cycle in different locations within the retina, it is possible that glutamate regulates the cell cycle in retinal progenitors through an effect on interkinetic nuclear migration. This hypothesis will be investigated in chapter 5.

3.4.7 The glutamate response is partly mediated by a glutamate transporter

An unexpected finding of this study was the sensitivity of the glutamate response to TBOA, a blocker of glutamate transport. In the mature retina, Müller glial cells provide the main source of glutamate uptake via the glial glutamate/aspartate transporter, GLAST or EAAT1 (Rauen et al, 1996), although other cell types, including bipolar, horizontal, amacrine and photoreceptors cells, also express glutamate transporters (Kugler & Beyer, 2003). In situ hybridization studies show extensive expression of EAAT1 and EAAT2 mRNA in the cortical VZ of the E15 mouse embryo, and this pattern persists in the adult (proliferative) subventricular zone (Sutherland et al., 1996). This raises the intriguing possibility that progenitor cells in the embryonic retina, and possibly in the cortex, express EAAT1, a glutamate-transporter thought to be glial-specific. This notion adds support to the growing body of evidence suggesting that progenitor cells and radial glia share many common features. Indeed, it may no longer be meaningful to distinguish

between these two cell types. In keeping with this, it has recently been shown that fetal human Müller cells express the progenitor cell marker nestin in both proliferating and differentiated retina (Walcott & Provis, 2003).

3.4.8 Type 1 cells respond to GABA

Almost all Type 1 cells recorded at both E5 and E8 responded to GABA with a depolarizing, inward current. The GABA-evoked response could be reversibly blocked by bicuculline, and mimicked by the selective $GABA_A$-receptor agonist, THIP and isoguvacine. These findings indicate that the GABA-response in these cells is mediated by a $GABA_A$-receptor. Activation of the $GABA_A$-receptor is associated with the opening of an anion-channel, which is mainly permeable to Cl^-. Thus, a $GABA_A$-receptor mediated current is expected to reverse around the equilibrium potential for Cl^-, E_{Cl^-}. However, in the experiments described above the GABA-mediated current did not reverse at the predicted voltage. Attempts were made to elucidate if a non-$GABA_A$-receptor mediated component was contributing to the GABA-response, by blocking $GABA_B$-receptors and the GAT-1 GABA-transporter, but these blockers were without effect. Gluconate was used in the patch pipette, but the permeability of GABA channels for gluconate is thought to be low (Fatima-Shad & Barry, 1993). On the basis of these findings, the most likely explanation for the unusual responses to GABA-application is the extensive gap junctional coupling of Type 1 cells at this time. While the $[Cl^-]$ in the recorded cell is set by the pipette solution, the $[Cl^-]$ in coupled cells is not. Thus, if the coupling between cells is strong, a major determinant of the reversal potential in the recorded cell will be the $[Cl^-]$ in the cells coupled to it. The strength of coupling between cells is determined by the number and type of gap junction channels between them. The unitary conductance of a single gap junction channel depends on the specific connexin composition, and varies across a range of 15-300pS, and is approximately 100pS for Cx43 (Harris, 2001). Previous studies have shown that the reason for the depolarizing actions of GABA during

development is the high $[Cl^-]_i$ (Owens et al., 1996), which in turn is due to the relatively later expression of the Cl^--exporter, KCC2 (Rivera et al., 1999). In addition, the voltage-control during patch-clamp experiments in a large coupled network is poor. Thus, neither the $[Cl^-]_i$ nor the membrane potential of the coupled cells is controlled in the experiments described here, and therefore the voltage dependence of the GABA response can not be predicted by the E_{Cl^-} calculated on the basis of the solutions used.

The hypothesis that the GABA-response observed in these experiments arises from summation of currents from the coupled cluster of cells was further supported by the large amplitude of the GABA-current (mean 126pA at E5) which was similar to that observed in cortical progenitors by LoTurco & Kriegstein (1991), and approximately 10-fold greater than that of GABA-currents elicited in uncoupled cortical cells. Furthermore, at E8, the amplitude of the GABA-response was significantly smaller than at E5 (mean 70pA at E8). The results presented in chapter 4 of this thesis show that cells at E5 are more extensively coupled than those at E8. Finally, the current density observed was highly variable, an observation which is also consistent with the hypothesis that the current arises from coupled cells, the amplitude and density varying with the numbers of cells contributing to the response. Together, these findings suggest that the GABA-currents in Type 1 cells described here arise from multiple coupled cells, and are mediated by $GABA_A$-receptors.

In studies using non-confocal calcium-imaging, Yamashita & Fukuda (1993) reported $GABA_A$-receptor mediated calcium-responses could be evoked in embryonic chick retina from E3. In E4 retina, Pearson (2003) showed, using confocal calcium-imaging, that ~10% of cells in the VZ to respond to GABA with an increase in $[Ca^{2+}]_i$. The number of cells responding rose to 15% at E5 and 35% at E6. These responses could be blocked by bicuculline. However, neither GABA nor bicuculline affected the rate of mitosis in the VZ at E5, as determined by imaging the time spent in metaphase, or counting the number of mitotic

profiles following *in ovo* injections of these drugs (Pearson, 2003; Pearson et al., 2002). The present findings confirm that GABA causes a depolarizing response in cells within the VZ, but raise the question of why all cells show an inward current response to GABA, but only a small subset show an increase in $[Ca^{2+}]_i$ in response to GABA. The calcium-response evoked by GABA-application is thought to be mediated by depolarization, leading to the opening of voltage-gated calcium-channels. In the developing cortex, where GABA acts via $GABA_A$-receptors to depolarize VZ cells, and decreases the rate of DNA synthesis, the role of voltage-gated calcium-channels has been confirmed by blocking the response with La^{3+} (LoTurco et al., 1995). The discrepancy between the proportion of cells in the VZ of the chick retina that shows GABA-evoked currents, and that which shows $[Ca^{2+}]_i$ response may be due to a difference in the expression of voltage-gated calcium-channels. Nguyen et al. (2003) show that $GABA_A$-receptor activation in neural progenitor cells from the striatum can inhibit cell cycle progression via a mechanism involving MAP kinase, which is involved in the regulation of cell cycle progression in neuronal progenitor cells (Rosen et al., 1994). The present findings are consistent with a possible role for GABA in regulating cell proliferation in the retina, although currently there is no evidence for this. As for glutamate, it is possible that GABA affects interkinetic nuclear migration in progenitor cells. Behar and colleagues (1998, 2000) have shown that GABA can stimulate migration of newborn cortical neurones during rat cortical histogenesis. The role of GABA in the regulation of migration in the retina is investigated in chapter 5.

3.4.9 VZ cells do not respond to taurine, glycine, UTP or carbachol

The neurotransmitter taurine is especially abundant during development (Macione et al., 1974), and has been shown to have important roles in development in several mammalian species, including cats, primates and rodents (reviewed in Sturman, 1993). When pregnant cats were deprived of dietary

taurine, most of the embryos aborted, and those born had severe malformations in the brain and retina, which appeared to stem from problems with the differentiation and migration of developing neurons (Imaki et al., 1986). A well described action of taurine in the retina is the induction of rod photoreceptor differentiation (Altshuler et al., 1993). Recently, it has been demonstrated that taurine exerts its actions in the developing mouse retina through activation of ionotropic glycine receptors and $GABA_A$-receptors to induce exit from mitosis (Young & Cepko, 2004). Surprisingly, despite the ubiquitous expression of a $GABA_A$-like receptor, application of exogenous taurine to chick retinal VZ cells failed to produce any effects. Thus it would appear that the GABA-receptors expressed by progenitor cells in the E5-E8 chick retina are not sensitive to taurine. The difference between mouse and chick may be due to a species-specific difference in GABA receptor subunit expression. The findings of the experiments described here do not prelude that taurine plays a role in chick retinal development via a non-ionotropic mechanism.

Glycine is released endogenously in the chick retina from E4 (the earliest time tested), and in decreasing amounts to E14 (Bonness, 1999). Exogenous application of glycine produced responses in 27% of chick RGCs at E6, rising to 60% at E8 and 100% at E12-14, and these responses were blocked by strychnine (Bonness, 1999). In the VZ of developing mouse retina, GlyRα2 subunits were detected at P0, but not at E16, and this receptor was shown to mediate the induction of rod photoreceptor differentiation. If forced expression of GlyRα2 was induced at E16, progenitor cells exited prematurely from the cell cycle and started to differentiate to rod photoreceptors (Young & Cepko, 2004). In the experiments described here, exogenous application of glycine or strychnine was without effect at either of the two stages tested. However, it may be that glycine receptors are expressed at later times in retinal development in the chick. In the developing mouse retina, production of rods continues to early postnatal times (Young, 1985), but the first rods are born around E12 (Cepko et al., 1996), much earlier than GlyRα2 is expressed, so rod differentiation at early times in

development must proceed via a non-GlyRα2 dependent signalling pathway. Thus, despite the fact that rod photoreceptors in the chick are being generated during the period tested here, at times when glycinergic signalling appears to be absent, glycine may be involved in cell fate determination at the later stages in development.

Pearson et al. (2002) found that activation or blockade of purinergic receptors affected the rate of mitosis of cells in the VZ of E4-E6 chick embryos. In the experiments described here, exogenous application of UTP was without effect. This suggests that ionotropic purine-receptors are not expressed during this period of retinal development, and that the effects of purinergic signalling are mediated solely through metabotropic P2Y-receptors.

Pearson et al. (2002) report oscillatory Ca^{2+}-responses to muscarinic agonists in VZ cells at E4-6, which modulate the rate of mitosis. In the present experiments, application of carbachol, a cholinergic agonist with a high potency at mAChRs, and with lower potency at nAChRs, failed to evoke any response in VZ cells held in voltage-clamp. This result is consistent with previous findings that cholinergic effects in the developing retina are mediated via metabotropic rather than ionotropic receptors.

3.4.10 Antigen expression is correlated with cell type

In general, Type 1 cells were vimentin$^+$/TuJ1$^-$, whereas Type 2 cells were TuJ1$^+$/vimentin$^-$. This pattern of staining strongly supports the notion that Type 1 cells are proliferating progenitors, and that Type 2 cells are postmitotic neurons. If the Type 2 cells were found within the ganglion cell layer, these results would be unsurprising, however, all cells included in this study had their cell bodies within the VZ, a result that implies that neuronal differentiation begins before cells leave the VZ. Experiments using BrdU and antibody-labelling of RA4, a ganglion cell

specific protein, show that this marker of ganglion cells is expressed within minutes of the final mitosis (Waid & McLoon, 1995). Culture experiments, where retinal progenitors are allowed to differentiate *in vitro*, suggest that the ganglion cell fate is the default pathway of neuronal differentiation early in retinal development (reviewed in Adler & Belecky-Adams, 1999). Thus, cell fate may be decided before or during the final mitosis, and hence differentiation can proceed rapidly following the final cell division, before migration out of the ventricular zone takes place.

In their study of adult progenitors in the dentate gyrus, Fukuda et al. (2003) found early stage progenitors, which had membrane properties similar to the Type 1 cells described here, and had radial processes which stained positive with anti-glial fibrillary acidic protein antibody. In contrast, late stage progenitors, similar to the Type 2 cells described here, were positive for PSA-NCAM, a specific marker for immature neurons in the hippocampus.

In summary, the pattern of immunohistochemical staining seen here in the chick retina, and in the study by Fukuda et al. (2003) of the adult dentate gyrus, support the notion that Type 1 cells are proliferating progenitors, and that Type 2 cells are postmitotic neurons.

3.4.11 Why are Type 2 cells absent at E8?

An unexpected finding was that, at E8, all cells recorded within the VZ had characteristics of Type 1 cells, the progenitor cell type. This was surprising, since more divisions should be generating postmitotic cells at later stages in development. Given the pattern of antigen-expression seen in the chick retina and the similarity in the expression of voltage-gated currents to those seen in other studies, it seems unlikely that the identities of the two groups are the opposite to those in other brain regions, i.e. that Type 2 cells should be

proliferating progenitors, and Type 1 cells should be postmitotic cells. Evidence in the literature on birthdating suggests an alternative explanation. Window-labelling is a technique that utilizes initial injection of [^{3}H]thymidine, followed 5 hours later by injection of BrdU, repeated as necessary as the embryos are developing. Cells born before [^{3}H]thymidine injection are unlabelled, cells born after BrdU are labelled with both, whereas only cells born in the 5-hour window between the two injections are [^{3}H]thymidine$^+$/BrdU$^-$. Thus, the time of birth of specific cell types can determined within narrowly defined time-periods. These studies show ganglion cell birth occurs between E3 and E6, peaking at E5 (Adler & Belecky-Adams, 1999). In addition, there is evidence that the ganglion cell fate is the default pathway early in development, and that RGC differentiation occurs within minutes of the final mitosis, before migration out of the VZ (Waid & McLoon, 1995). In contrast, for other cell fates, cell-to-cell signalling from the surrounding cells is required for differentiation to occur. If differentiation to other cell types requires more input form the surrounding cells, differentiation may take place later, relative to the time of the final mitosis, and occur in parallel with or following migration out of the VZ. This might explain why at E5, at the peak of ganglion cell generation, lots of new-born ganglion cells are encountered within the VZ, whereas at E8, despite the generation of more postmitotic cells within the VZ, the cells encountered during patchclamp recordings have yet to express the membrane conductances typical of more mature cell types, and thus have the properties of Type 1 cells.

3.5 Further studies

At early times in development, cells are not distinguishable on the basis of their morphology, so cell type identification is only possible post-recording, using immunohistochemical techniques. While this is possible, it is both time-consuming and difficult, and has a low success-rate because the retinal slices are fragile, and often do not all survive the several days it takes to process them in antibody- and blocking-solutions. Further, not all cells can be recovered for confocal imaging, because they have lost the Alexa dye during the immunohistochemical processing. One way to overcome these problems would be to use GFP as a marker, linking the expression to a cell type specific promoter. It is possible to transfect the chick embryo *in ovo* using electroporation, so the retina could still be allowed to develop *in vivo* up to the time of recording. This would provide a more efficient way to study specific cell types, and avoid the limitation of only being able to study cells within the VZ. The expression of membrane receptors and ion channels is likely to change during the cell cycle. Such changes could not be resolved using the methods described here. However, the embryonic retinal slice preparation provides a powerful tool to investigate the properties of very early embryonic cells, and it would be interesting to follow the pattern of development of membrane properties at other times, both for progenitor cells and for newly postmitotic neurons.

A surprising finding was that Type 1, progenitor cells, but not Type 2, postmitotic cells, responded to neurotransmitters. The majority of Type 2 cells are most likely newborn RGCs. These findings suggest that while proliferating cells respond to GABA and glutamate, these receptors are down-regulated upon exit from the cell cycle. Application of AMPA, GABA or glycine to RGCs, recorded from the RGC layer, were found to produce responses in around 20% of cells at E6, increasing to 85% in the case of AMPA, and ~50% for GABA and glycine at E8 (Bonness, 1999). It would be interesting follow the expression of these receptors in RGCs in

relation to their position in the retina, and examine if their expression is up-regulated again when the RGCs reach their final destination in the RGC layer.

A limitation in these experiments was that the Type 1 cells are extensively coupled, which means that responses from neighbouring cells can contribute to the responses. In order to eliminate the contribution of coupled cells to the neurotransmitter-evoked responses, it would be interesting to test the responses in isolated cells. Preparation of isolated cells from the embryonic retinae was attempted, but it was not possible to do so without destroying the processes, which prevented morphological identification of the cells. Another preparation in which to investigate this would be outside-out patches, where the properties of single receptor channels can be assessed.

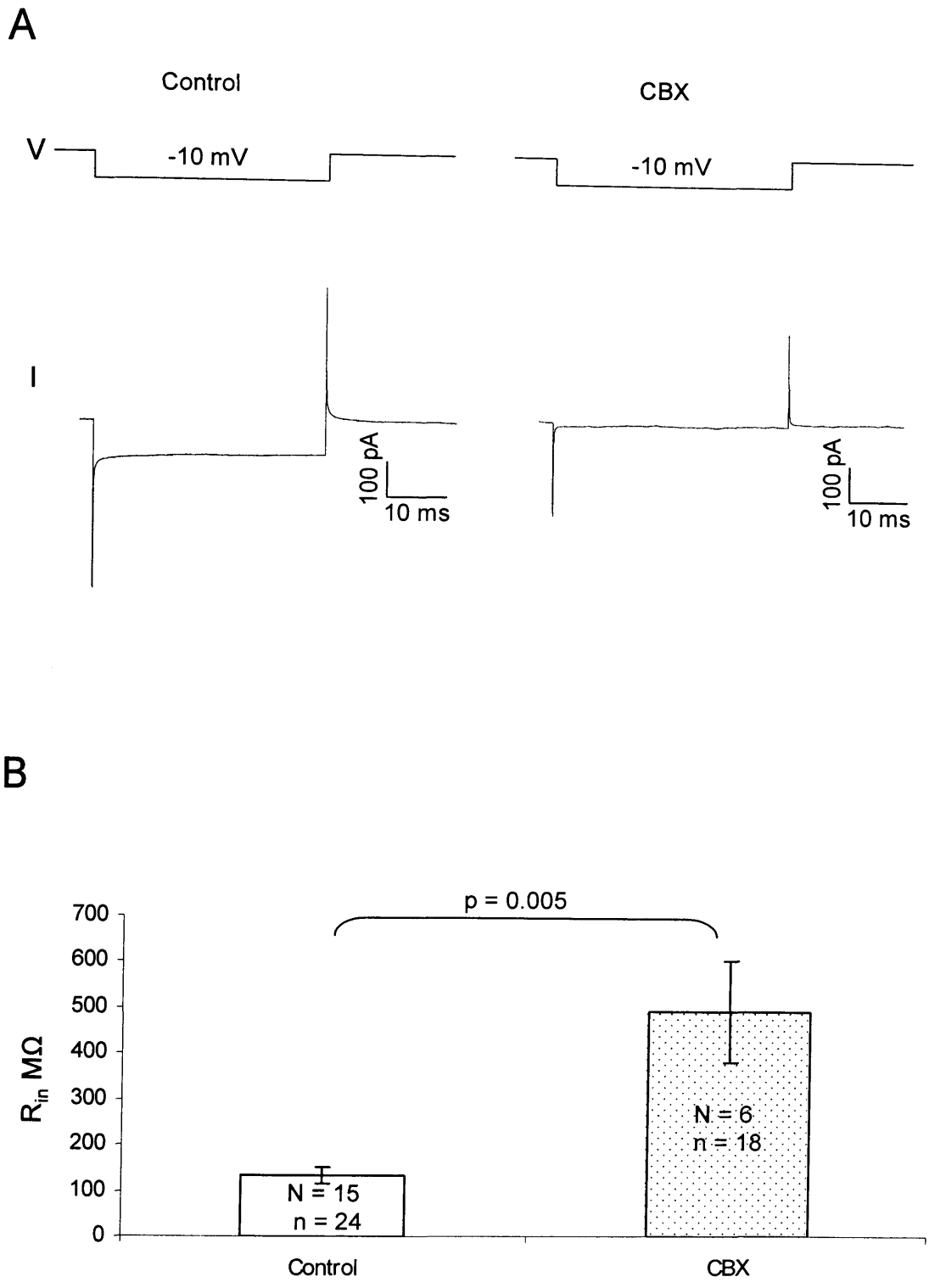

Figure 3.1 Gap junctional coupling between cells in the VZ affects R_{in}
A, Example of the current response of a cell in a whole-mounted E5 retina (lower trace) to a -10mV depolarising step (upper trace) in control Krebs' solution (R_{in}=91MΩ) or in 100μM CBX (R_{in}=1430MΩ)
B, The mean input resistance of cells in the VZ in E5 whole-mounted retinae is significantly increased in the presence of carbenoxolone (mean R_{in} in control: 134±19MΩ; in CBX: 495±110MΩ. (N = number of retinae, n = number of cells).

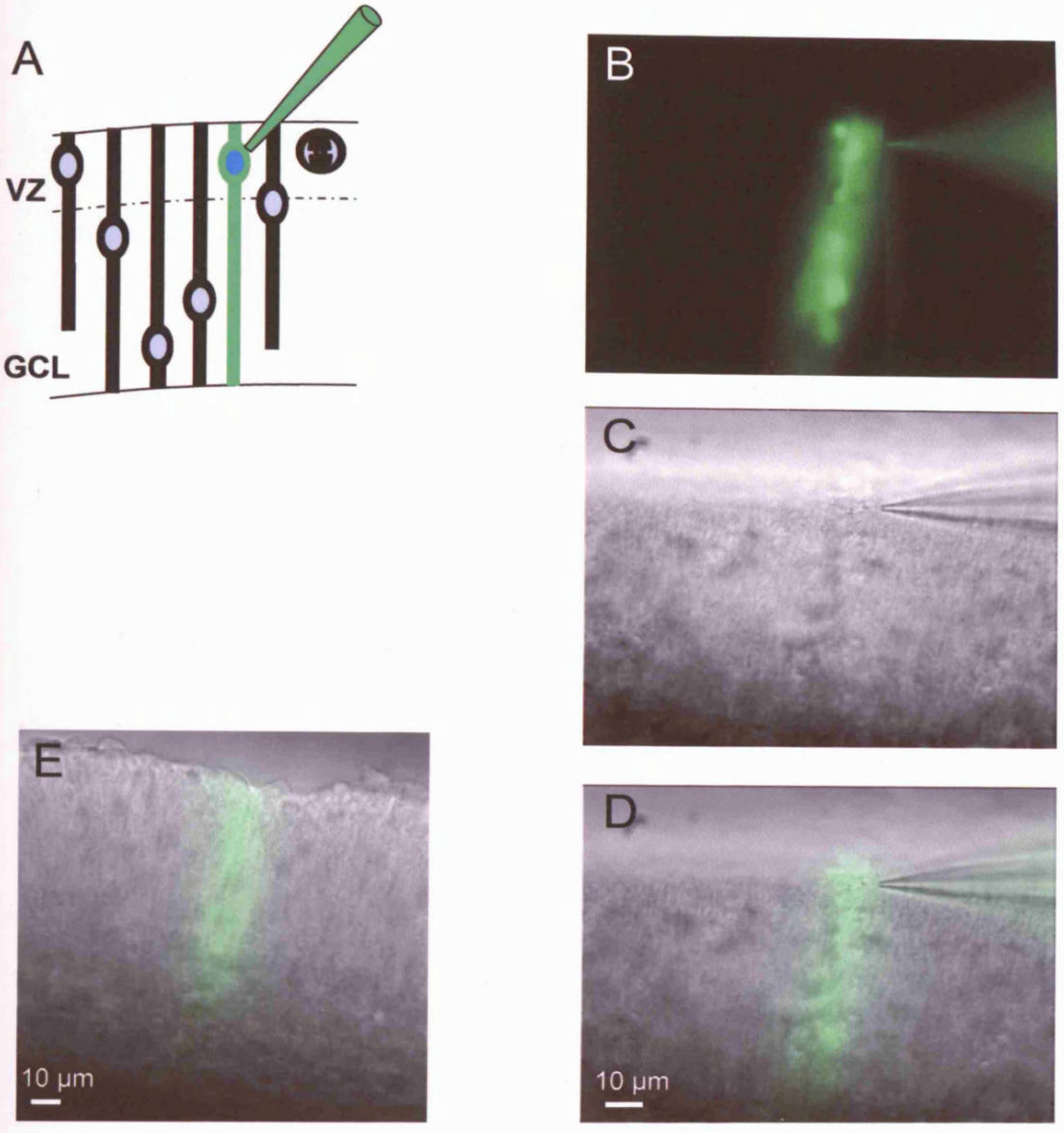

Figure 3.2 Retinal slices allow the cell bodies of VZ cells to be targeted for recording. *A*, As illustrated in this diagram, the retinal slice preparation allows access to the cellbodies, rather than the processes, of the progenitor cells for patchclamping. For these experiments, Alexa 488 was included in the internal solution to allow the position of the cell body and the presence of gap junction coupling to be established. *B*, Epifluorescence image of a patched cell in an E5 retinal slice. The Alexa 488 in the internal solution delineates the recorded cell and coupled neighbours. *C*, DIC image of the slice in *B*. *D*, Overlay of *B* and *C*. *E*, Overlay of DIC image and epifluorescence image of the cells filled during recording in an E8 retinal slice.

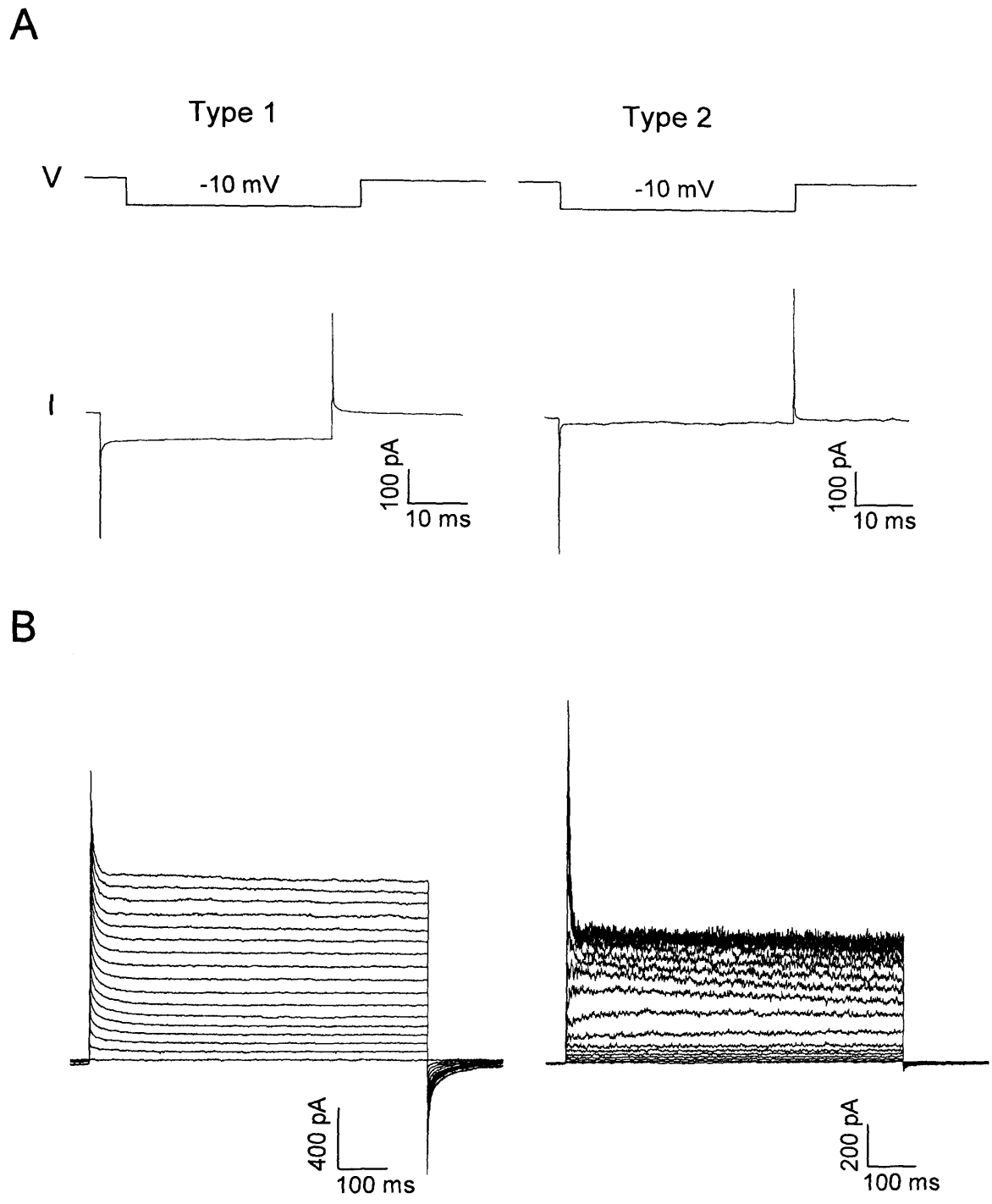

Figure 3.3 Recording in the VZ in E5 retinal slices reveals two different cell types
A, Current response to a -10 mV voltage step from a holding potential of -70 mV shows cells of Type 1 to have a low input resistance (this cell: 120 MΩ), and cells of Type 2 a high input resistance (this cell: 1430 MΩ). *B,* Current response to a series of depolarising voltage steps (10 mV increments) from a holding potential of -70 mV of the same two cells shown in *A*. Type 1 cells respond ohmically, whereas Type 2 cells express voltage- and time-dependent currents.

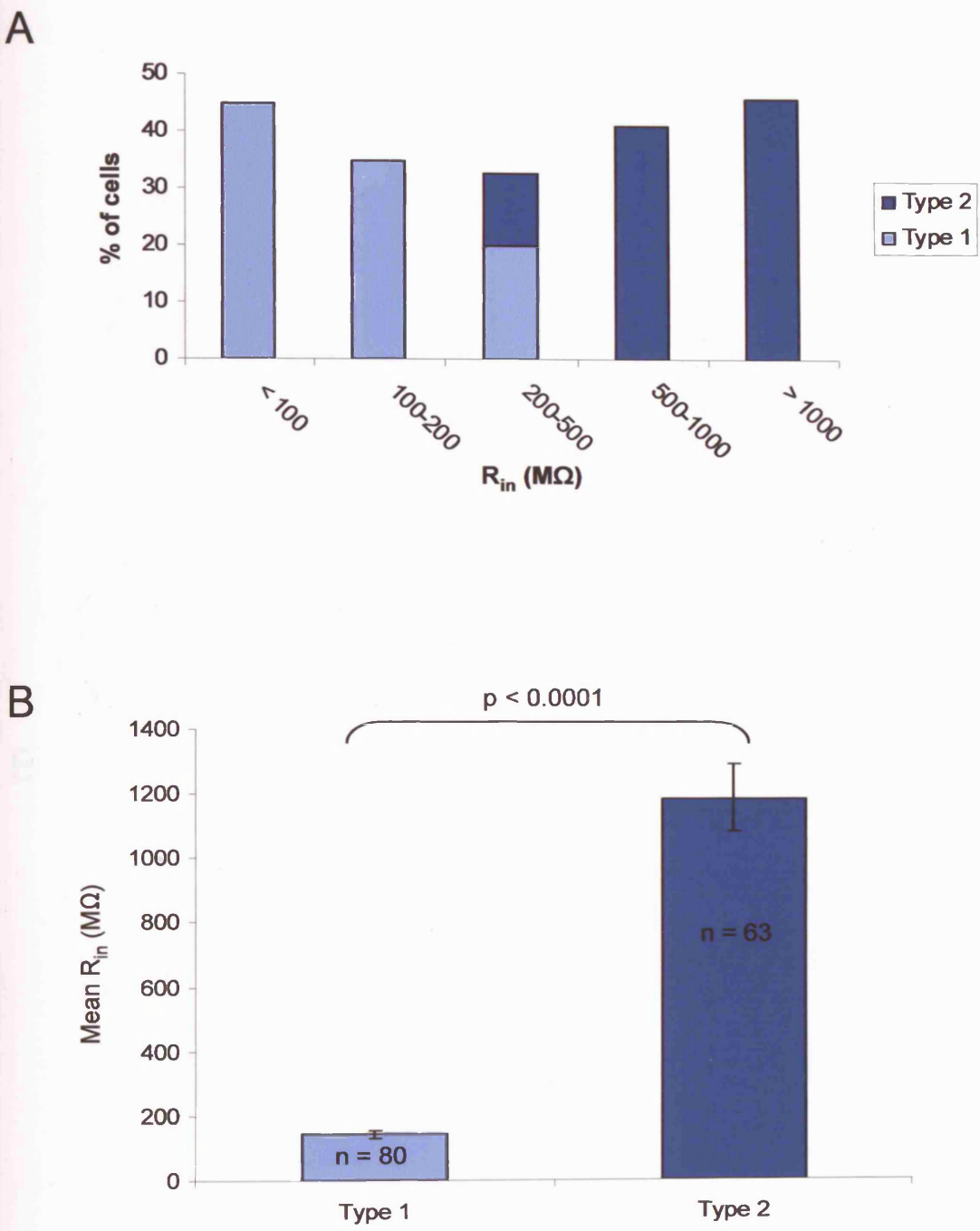

Figure 3.4 The input resistance of VZ cells at E5 varies with cell type
A, Histogram of the distribution of R_{in} shows two separate, but slightly overlapping populations. *B,* At E5, the mean R_{in} of Type 1 cells (145±12MΩ) is significantly lower than Type 2 cells (1187±104MΩ).

A

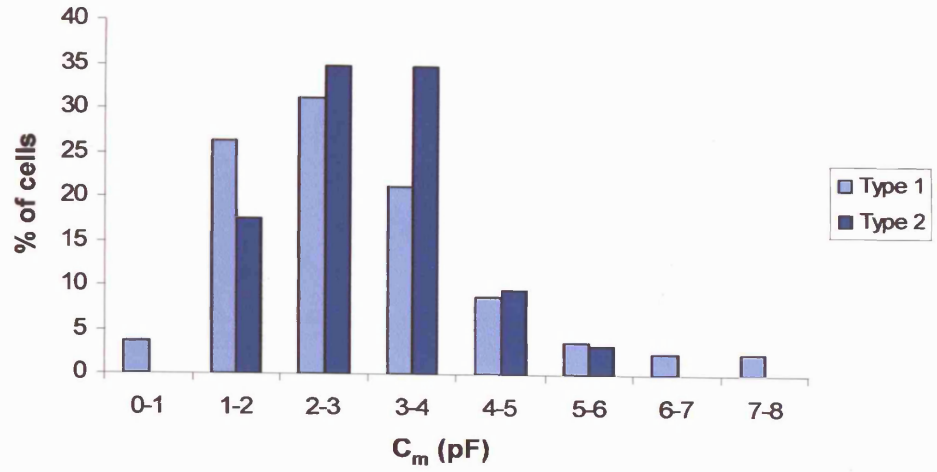

B

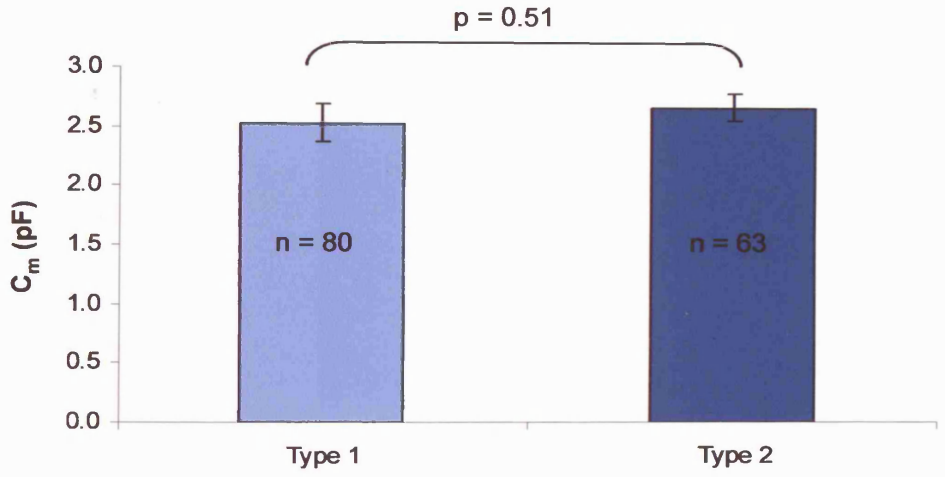

Figure 3.5 The membrane capacitance of VZ cells at E5 does not vary with cell type *A,* Histogram showing the distribution of membrane capacitance for each cell type. Although cells of type 1 show a slightly wider range of membrane capacitance, the two populations are largely overlapping. *B,* The mean C_m is similar for cells of Type 1 (2.53±0.17pF) and cells of Type 2 (2.66±0.11pF).

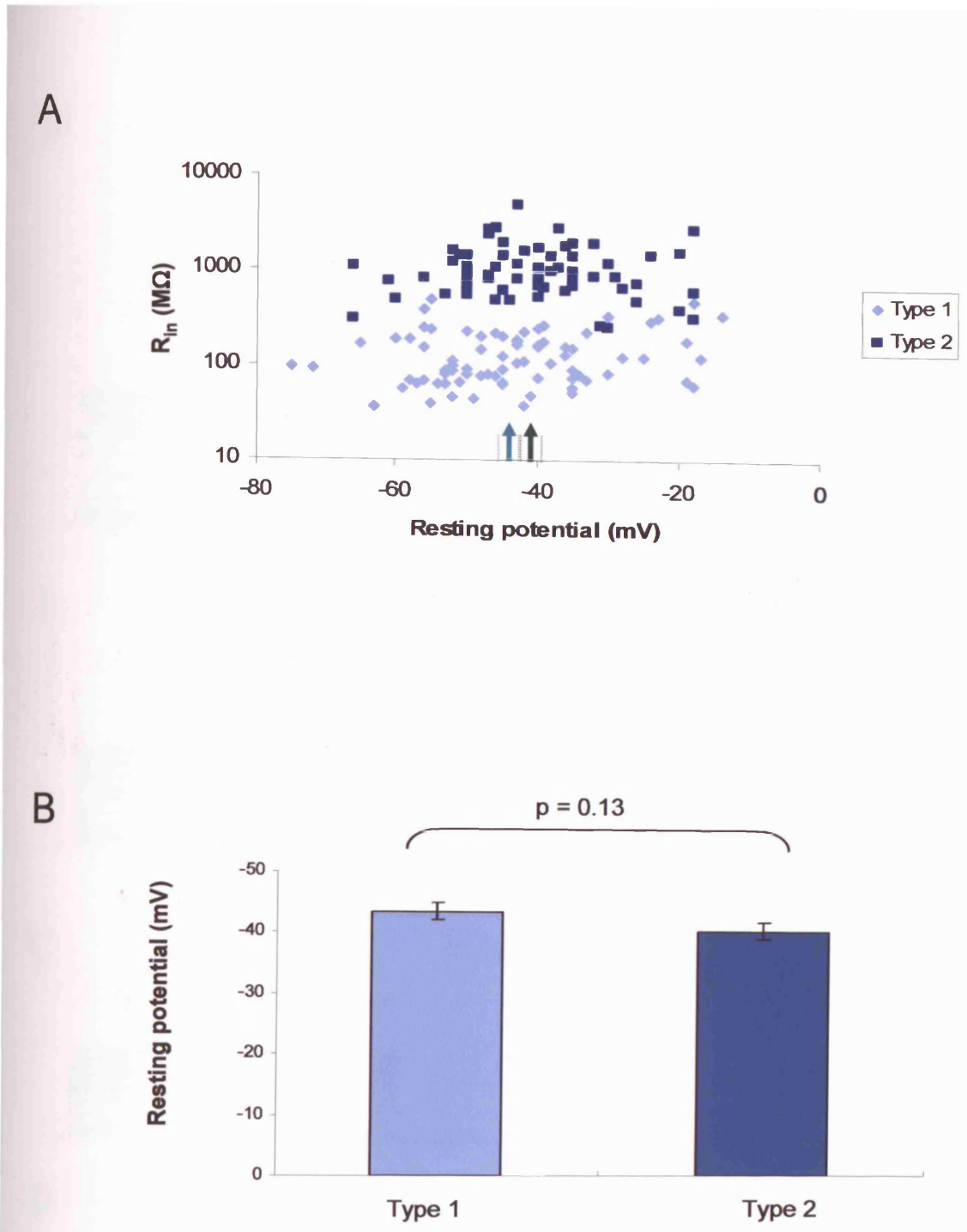

Figure 3.6 The resting potential of VZ cells at E5 does not vary with cell type
A, Scatter plot of input resistance (R_{in}) and resting potential (V_m); whilst R_{in} values for each cell type fall into separate halves of the plot, V_m values for each cell type show extensive overlap. Mean V_m values for cell types 1 and 2 are indicated by the light and dark green arrows, respectively, with dashed lines either side indicating s.e.m. *B,* The mean V_m of Type 1 cells (-43.5±1.4mV) did not differ significantly from that of Type 2 cells (-40.4±1.4mV).

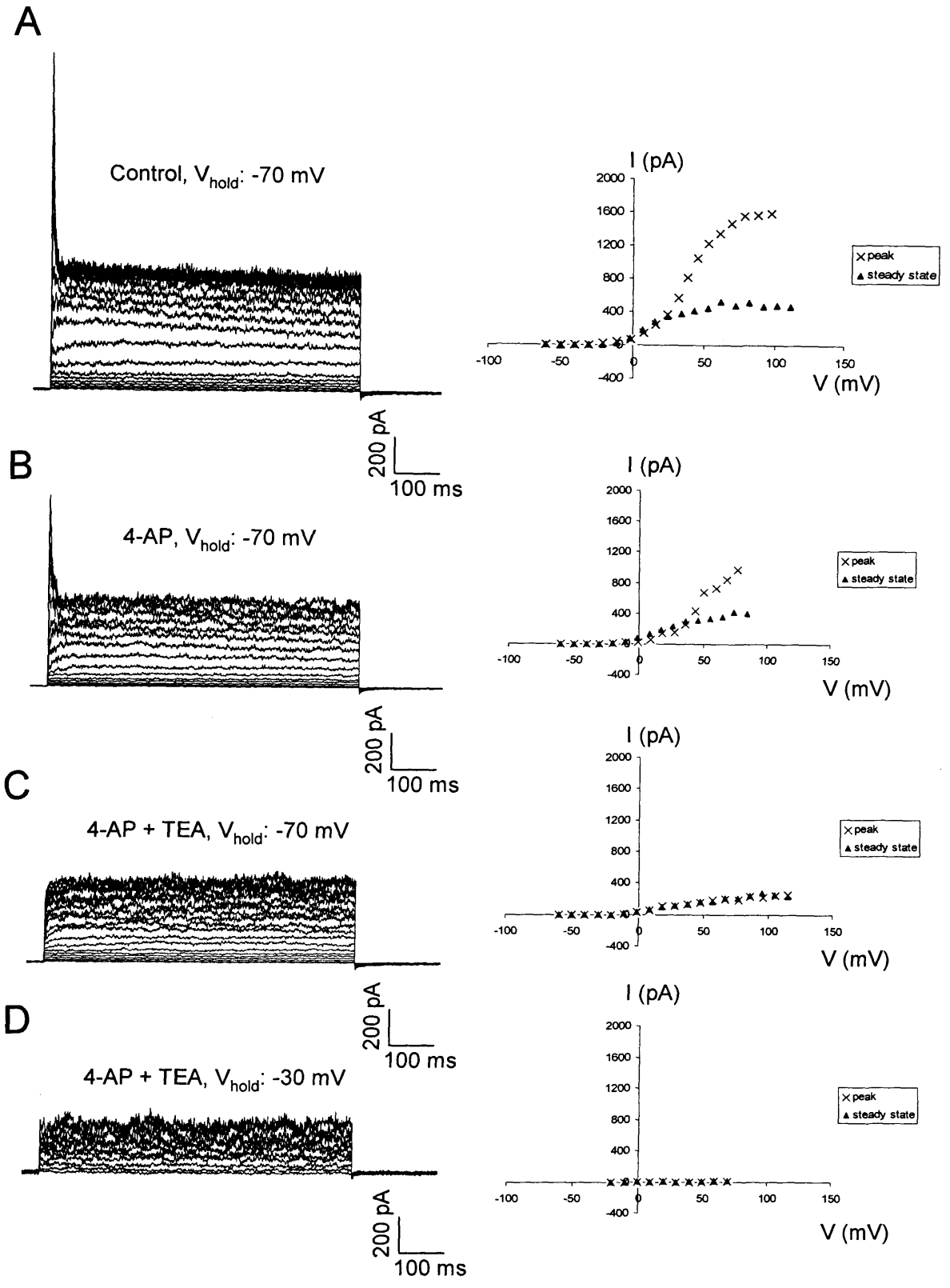

Figure 3.7 The outward voltage-gated currents in Type 2 cells are suppressed by 4AP and TEA. A,B,C, Left panel: Typical current responses of a Type 2 cell to a series of depolarising voltage steps (10 mV increments) from a holding potential of -70 mV in control, 4AP (5 mM), and 4AP + TEA (5 mM). Right panel: The IV relations for the currents depicted on the left are plotted at peak and steady state, following leak-current subtraction and correction for voltage error. *D,* Any residual voltage-gated currents are largely eliminated by increasing the holding potential to -30 mV.

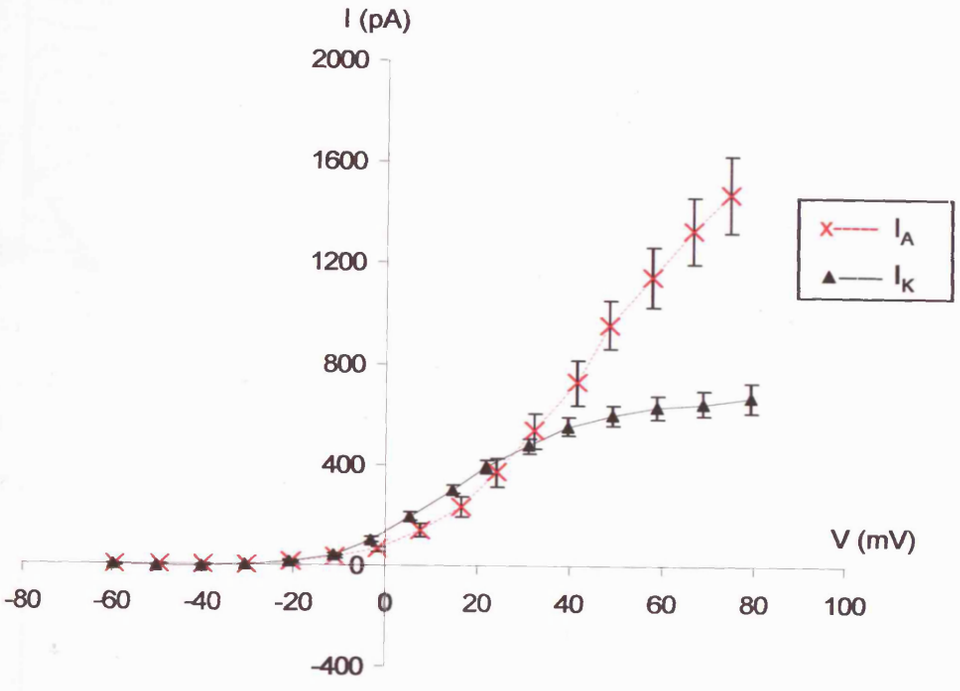

Figure 3.8 Amplitude of voltage-gated K^+-currents in Type 2 cells
IV curve constructed using data pooled from 18 Type 2 cells. Points show mean±sem. The data has been leak-subtracted and corrected for series resistance voltage error. The peak amplitude for the I_K component ranged from 154pA to 1052pA (mean peak amplitude 670±61pA). The peak amplitude for the I_A component ranged from 890pA to 2240pA (mean peak amplitude 1484±153pA). The peak current density for the I_K component ranged from 44pA/pF to 526pA/pF (mean peak current density 267±31pA/pF). The peak current density for the I_A component ranged from 254pA/pF to 845pA/pF (mean peak current density 541±67pA/pF).

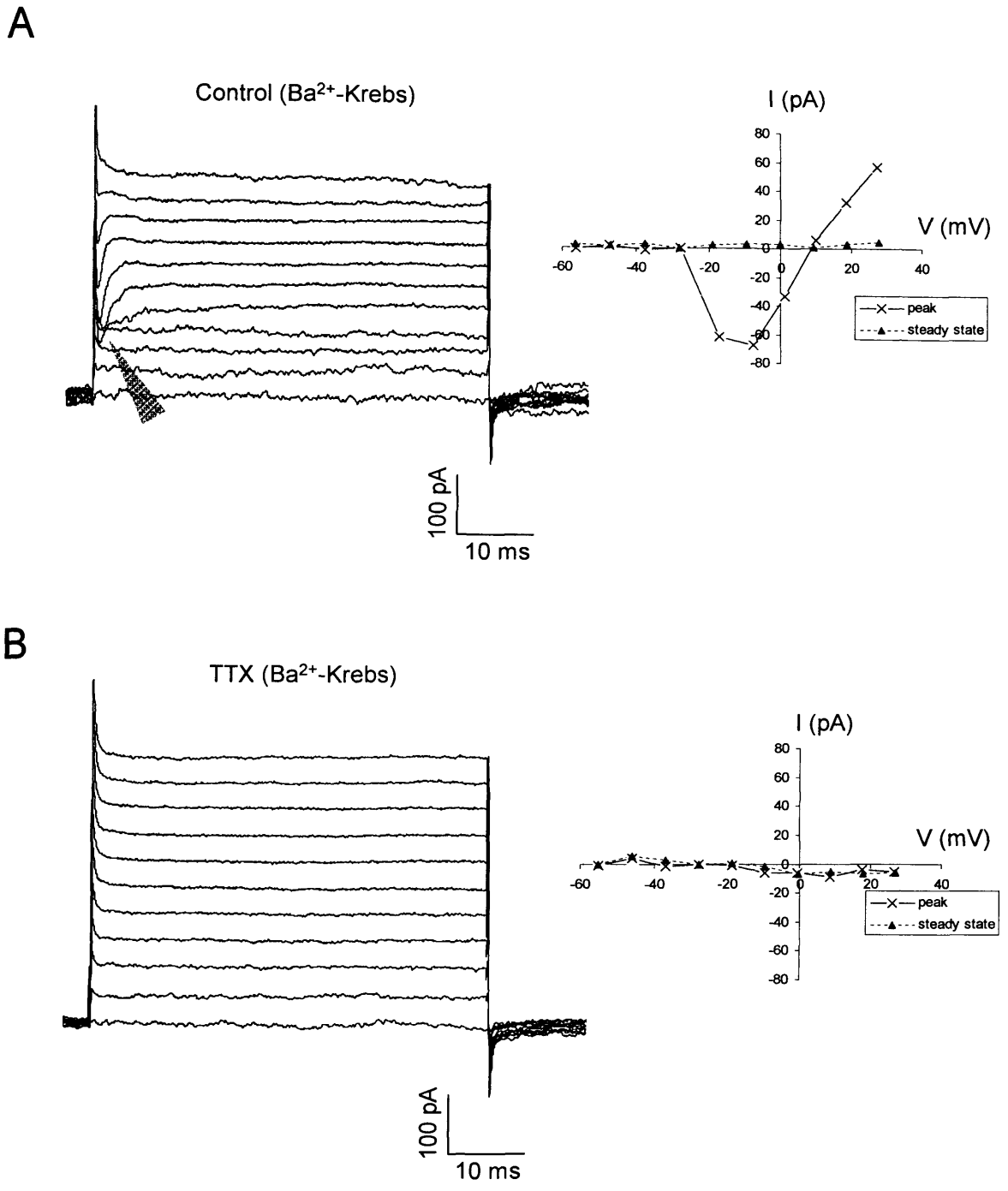

Figure 3.9 Some Type 2 cells show voltage-gated Na^+-current
In some Type 2 cells, when K^+-currents were blocked by the presence of Ba^{2+} in the external solution and Cs^+ in the internal solution, a small inward current was revealed. *A,* Left panel: Current response of a Type 2 cell to a series of depolarising voltage steps (10 mV increments) from a holding potential of -70 mV. Right panel: IV plot of the current-responses shown on the left, following leak-current subtraction and correction for voltage error, shows an inward current activating between -30 and -20 mV. *B,* The current shown in *A* was blocked by TTX (1 μM), identifying it as a Na^+-current.

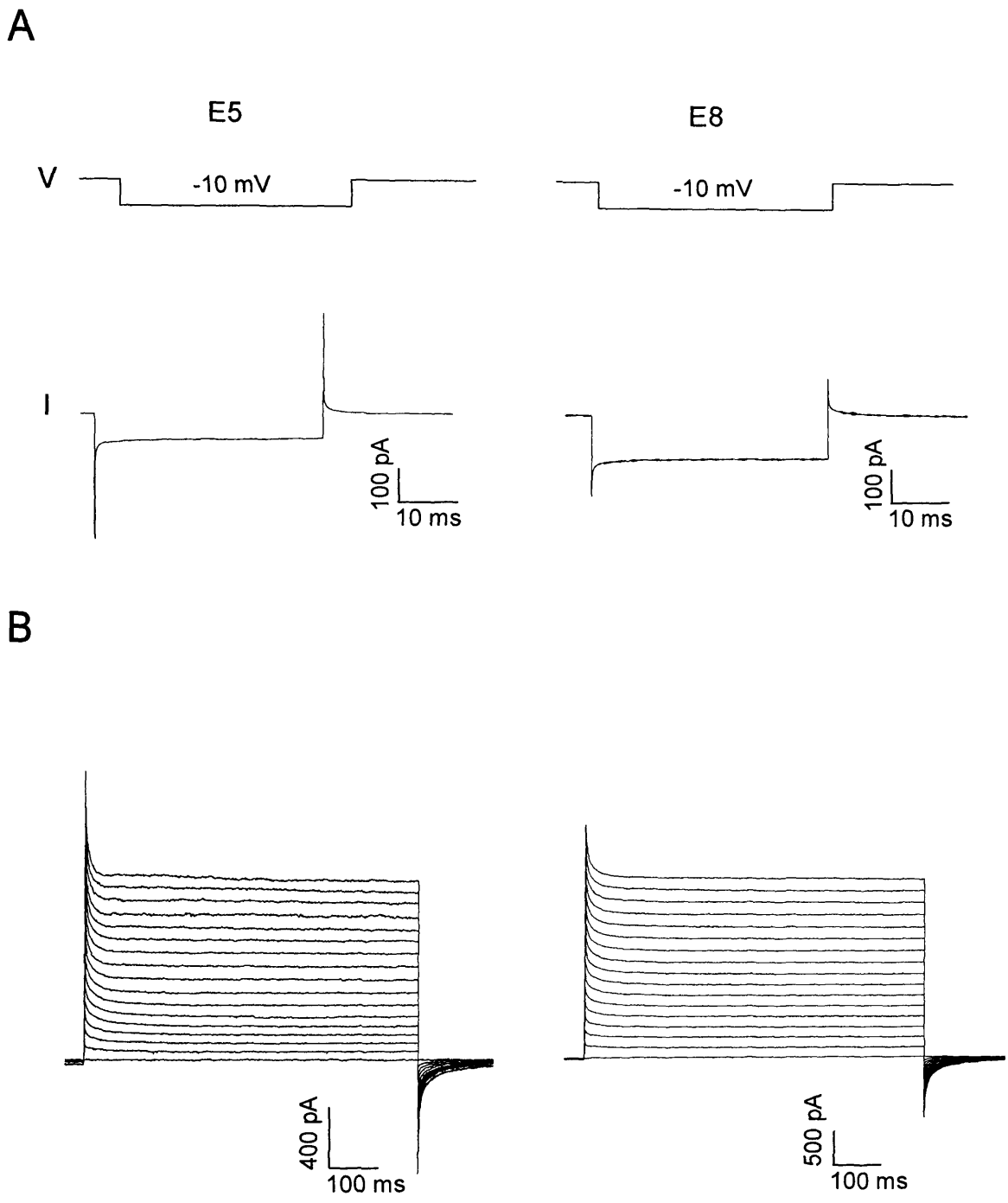

Figure 3.10 Cells found in the VZ at E8 are similar to Type 1 cells at E5
A, Current response (lower trace) to a -10 mV voltage step (upper trace) from a holding potential of -70 mV shows cells from E5 and E8 to have a low input resistance (E5 cell: 120MΩ, E8 cell: 47MΩ) *B*, Current response to a series of depolarising steps (10 mV increments) from a holding potential of -70 mV of the same two cells as shown in *A*. Both Type 1 E5 and E8 cells respond ohmically to depolarising voltage steps.

A

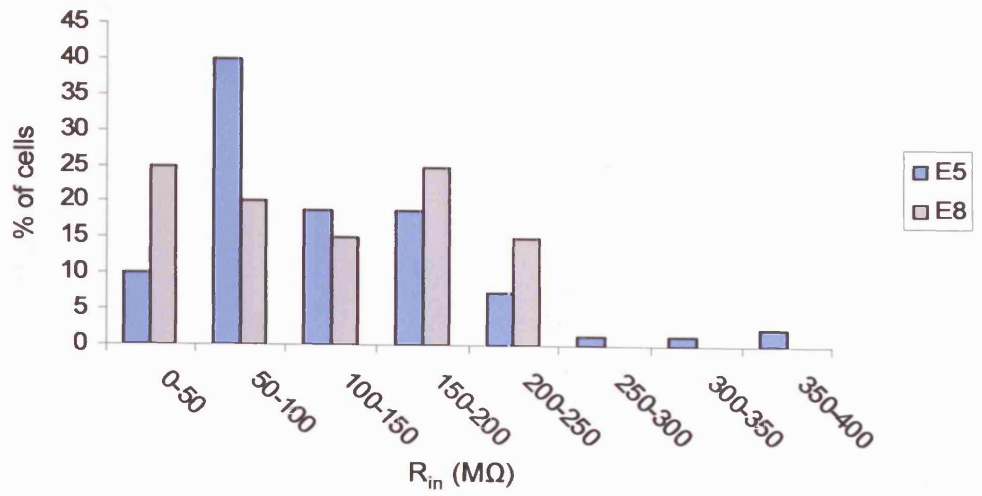

B

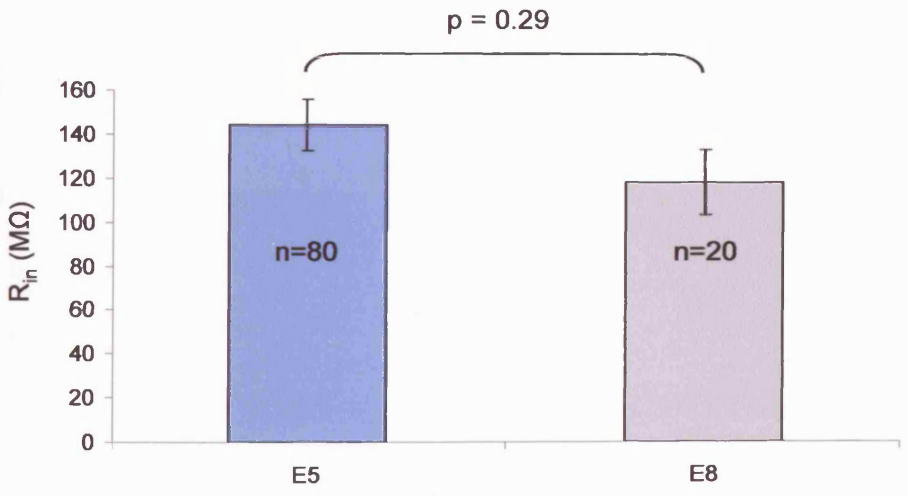

Figure 3.11 Input resistance of Type 1 cells at E5 and E8
A, Histogram showing the distribution of the input resistance (R_{in}) of Type 1 cells at E5 and E8. *B*, The mean R_{in} of Type 1 cells at E5 and E8 are not significantly different (E5, 145±12MΩ; E8, 119±15MΩ)

A

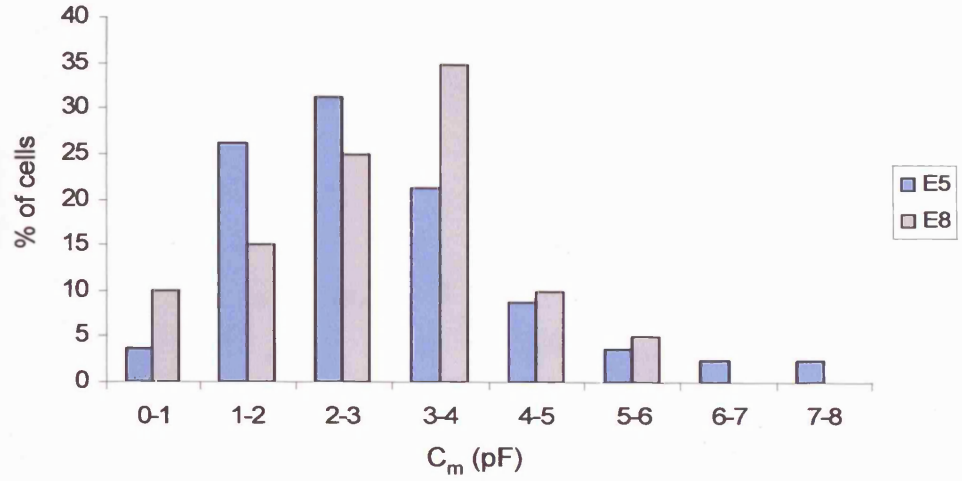

B

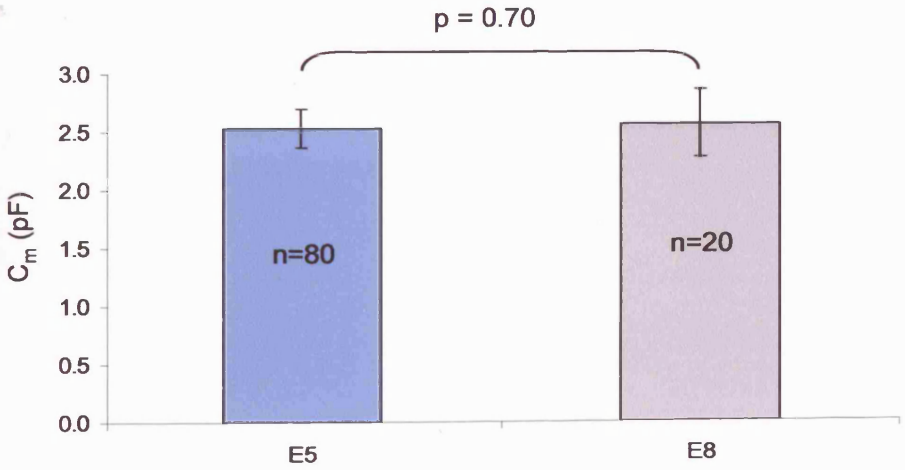

Figure 3.12 Membrane capacitance of Type 1 cells at E5 and E8
A, Histogram of the distribution of the membrane capacitance of Type 1 cells at E5 and E8
B, The mean membrane capacitance (C_m) of Type 1 cells at E5 is similar to that of Type 1 cells at E8 (E5, 2.5±0.17pF; E8, 2.6±0.29pF)

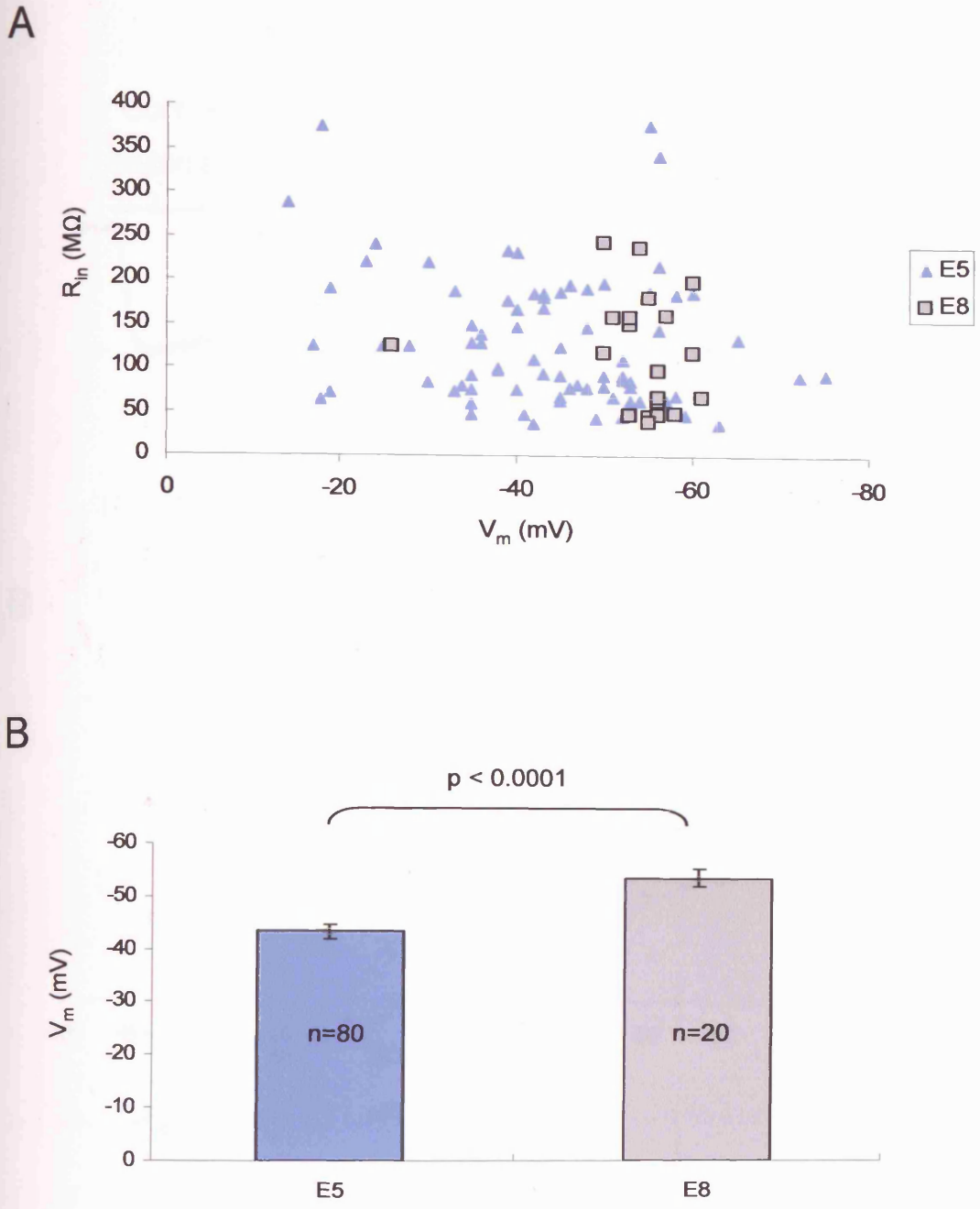

Figure 3.13 Resting potential of Type 1 cells at E5 and E8
A, Scatter plot of R_{in} and V_m of Type 1 cells at E5 and E8. The V_m values of E5 Type 1 cells range from -14 to -75 mV, whereas at E8, the V_m values cluster around -50 to -60 mV. *B*, The mean V_m of Type 1 cells at E5 is significantly more positive than the mean V_m at E8 (E5, -44±1.4mV; E8, -54±1.6mV)

A

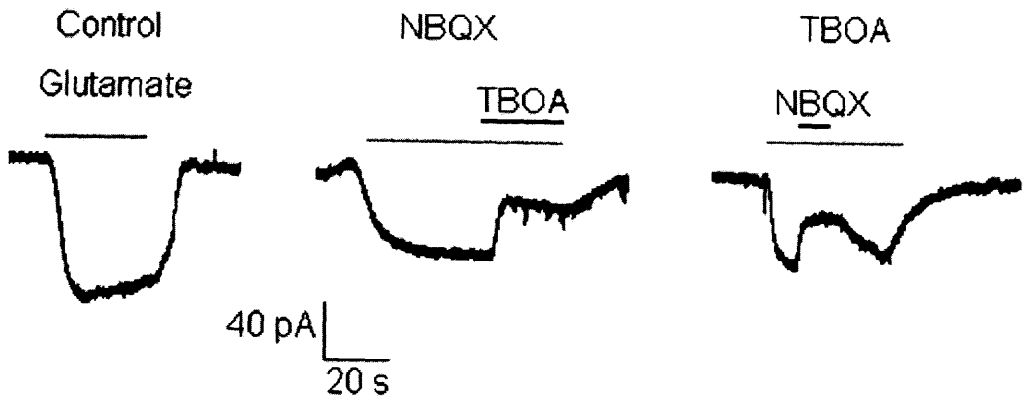

B

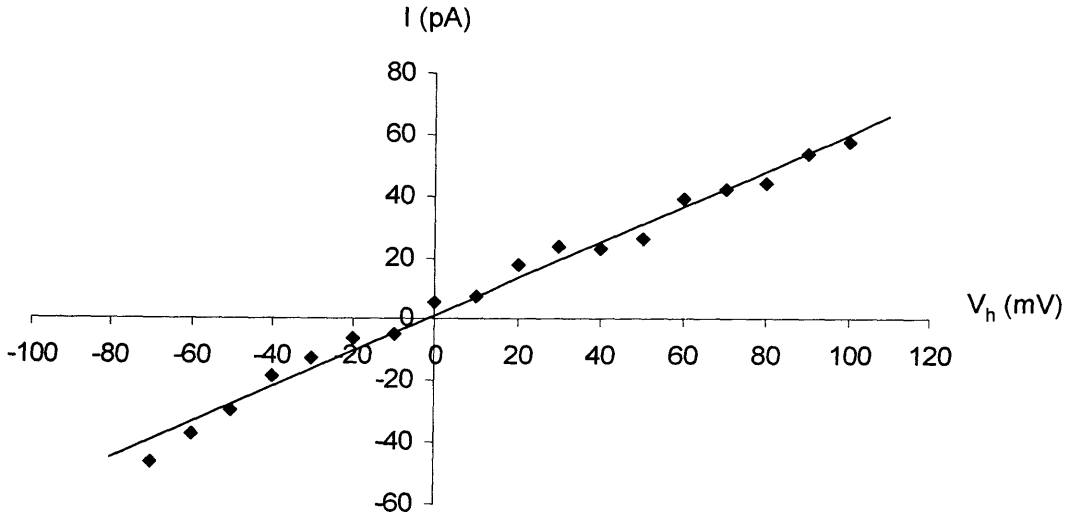

Figure 3.14 Type 1 cells respond to glutamate
A, The response to bath-application of glutamate in a typical Type 1 cell held at -70 mV is partially sensitive to both NBQX and TBOA (n=5). *B,* Reversal of the glutamate evoked current in the same cell as shown in *A* in the presence of TBOA. The plotted data was obtained by recording a rapid series of voltage-steps (10 mV increments) in the presence glutamate and TBOA, and subtracting the responses to the same protocol in control solution. The line represents a least squares linear fit (R-squared value = 0.99), and reverses at -2.6 mV.

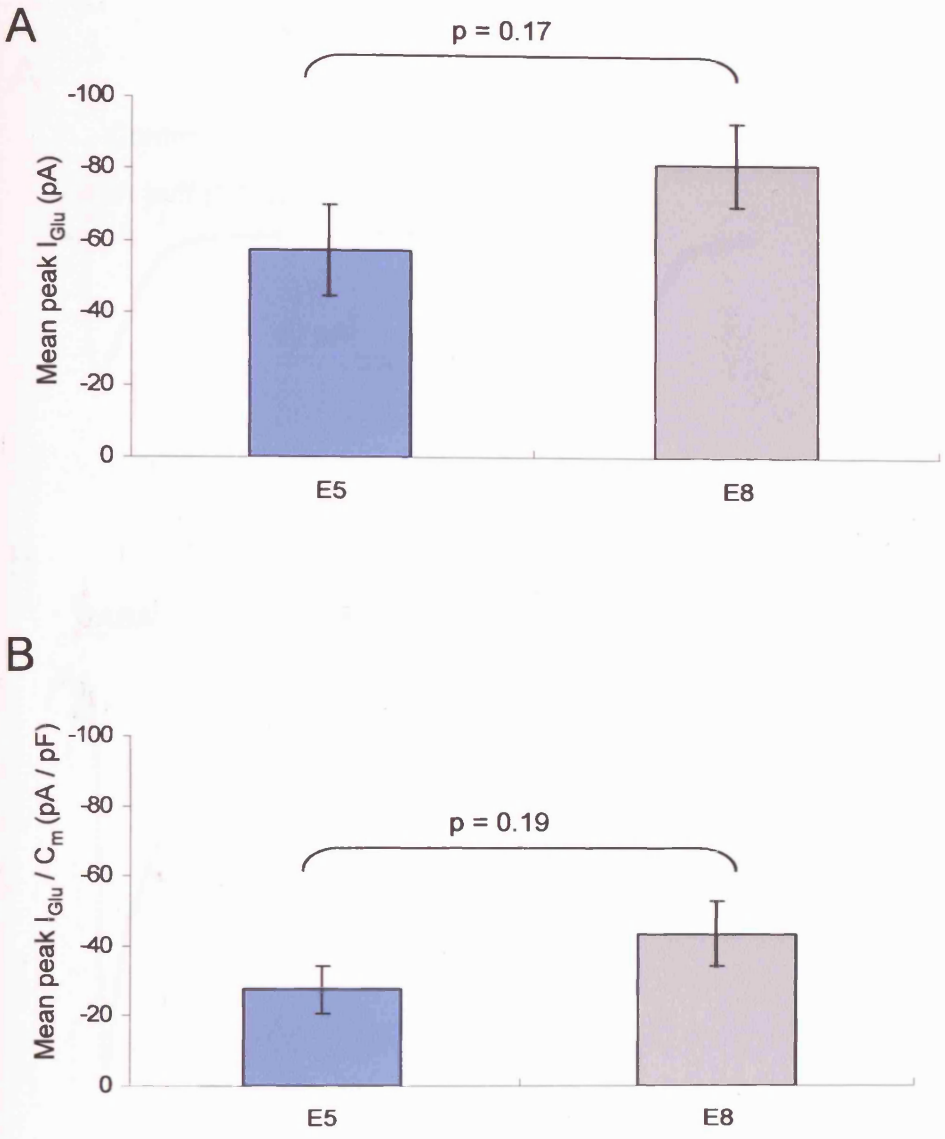

Figure 3.15 Glutamate responses at E5 and E8
A, The mean amplitude of the glutamate-evoked current in cells held at -70 mV was -57±13pA (n = 11) at E5 and -82±12pA (n = 13) at E8. *B,* The mean current density of the glutamate-evoked current was -28±7pA/pF (n=11) at E5 and -44±10pA/pF (n=13) at E8.

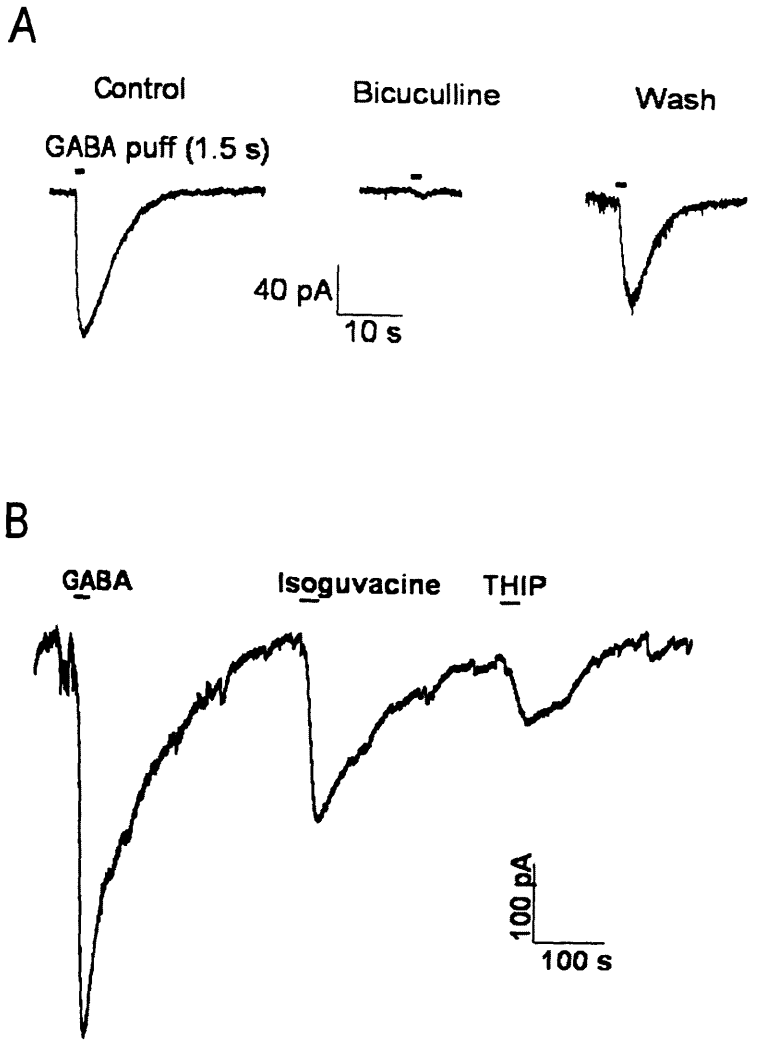

Figure 3.16 Type 1 cells respond to GABA
A, The response to puff-application of GABA (100 μM) in a typical Type 1 cell held at -70 mV could be reversibly blocked by bicuculline (50 μM). *B*, The $GABA_A$-receptor agonists, isoguvacine (300 μM) and THIP (500 μM) also evoked currents in this cell.

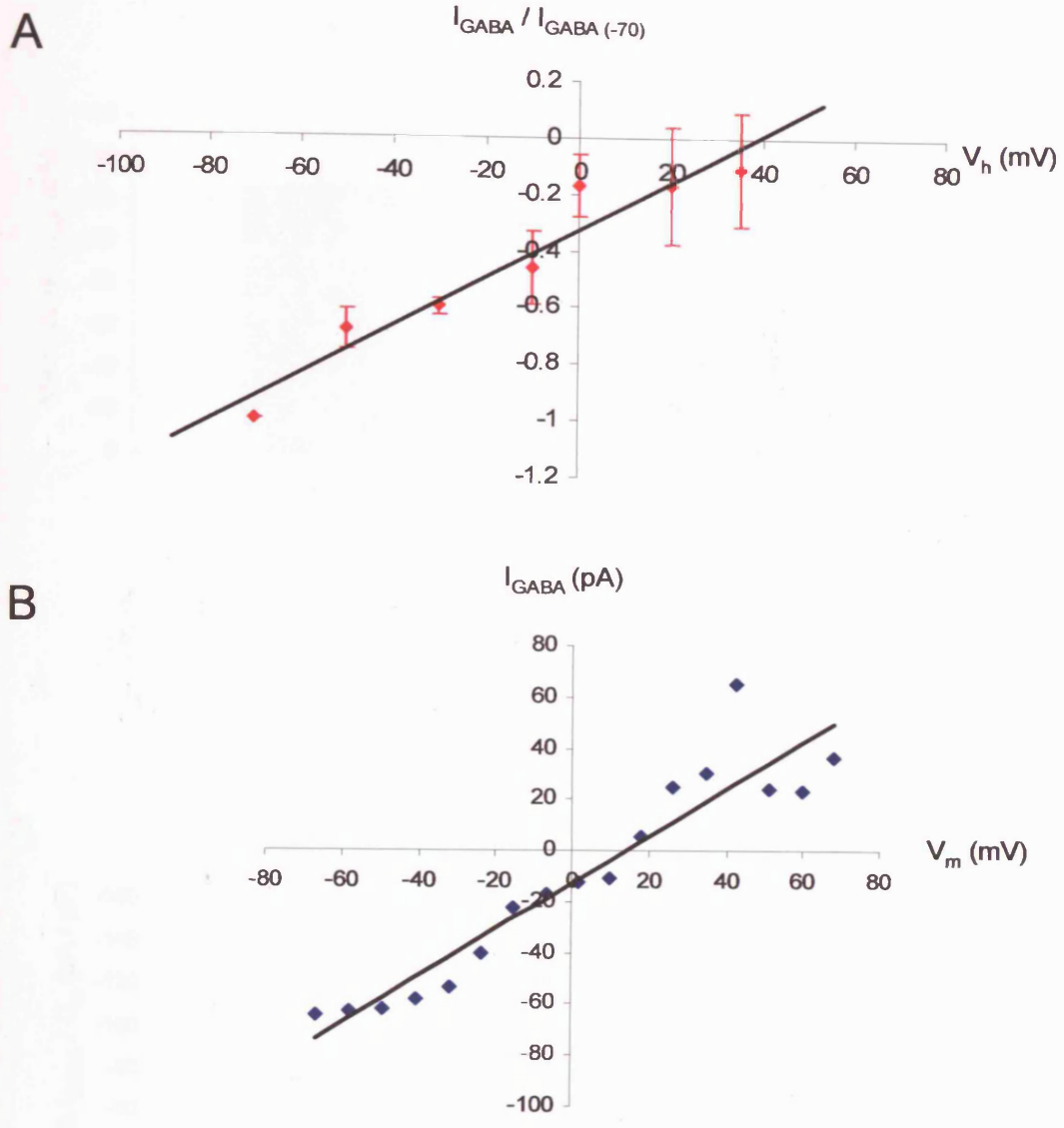

Figure 3.17 Voltage-dependence of GABA-evoked current
A, Voltage-dependence of the GABA-evoked current in E5 Type 1 cells. The peak responses to bath-applied GABA at different holding potentials were averaged for 8 cells ($n_{(-70)}$=8, $n_{(-50)}$=7, $n_{(-30)}$=4, $n_{(-10)}$=3, $n_{(0)}$=2, $n_{(+20)}$=2, $n_{(+35)}$=2). The response has been normalised to the peak response at V_{hold} = -70 mV for each cell. Error bars indicate s.e.m. for each data point.The line is a least squares fit, and predicts a reversal potential of +38.7mV. *B*, A potential problem with bath-applying the drug at different holding potentials is incomplete recovery from desensitization between each application. To overcome this, a rapid voltage-ladder (10 mV increments from -70mV) was applied in control solution, and in the presence of GABA, to see the current-responses at all membrane potentials within the first few seconds of the response. The GABA-evoked current plotted here was obtained by subtracting the current responses in control from those in the presence of GABA. The data has been corrected for R_s voltage error. The line represents a least squares fit. The GABA-evoked current reverses at +13.8 mV.

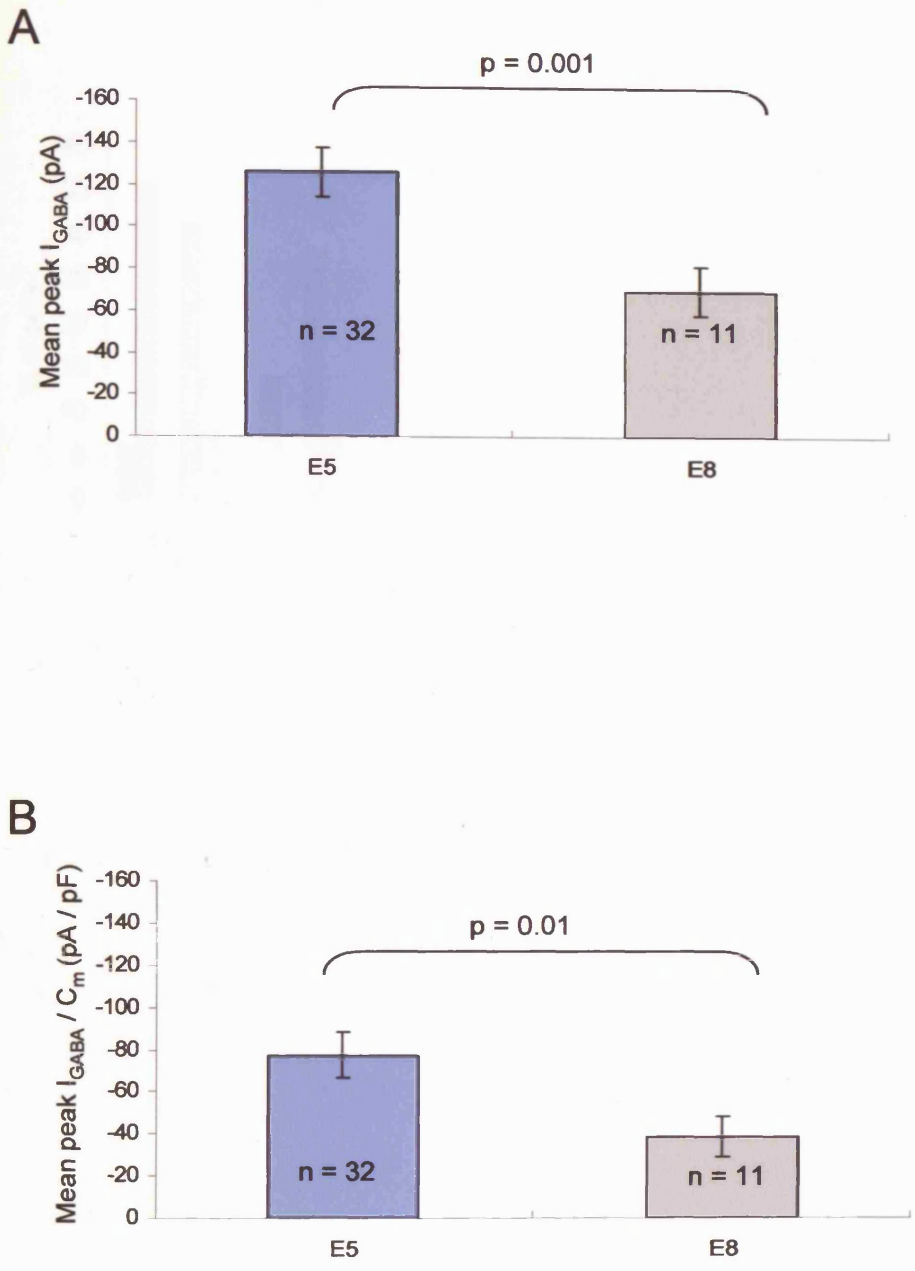

Figure 3.18 The mean GABA-evoked current is greater at E5 than at E8
A, The mean amplitude of the GABA-evoked current in cells held at -70 mV at E5 was -126±12pA and -70±11pA at E8. *B*, The mean current density of the GABA-evoked current in cells held at -70 mV was 78±11pA/pF at E5 and -38±10pA/pF at E8.

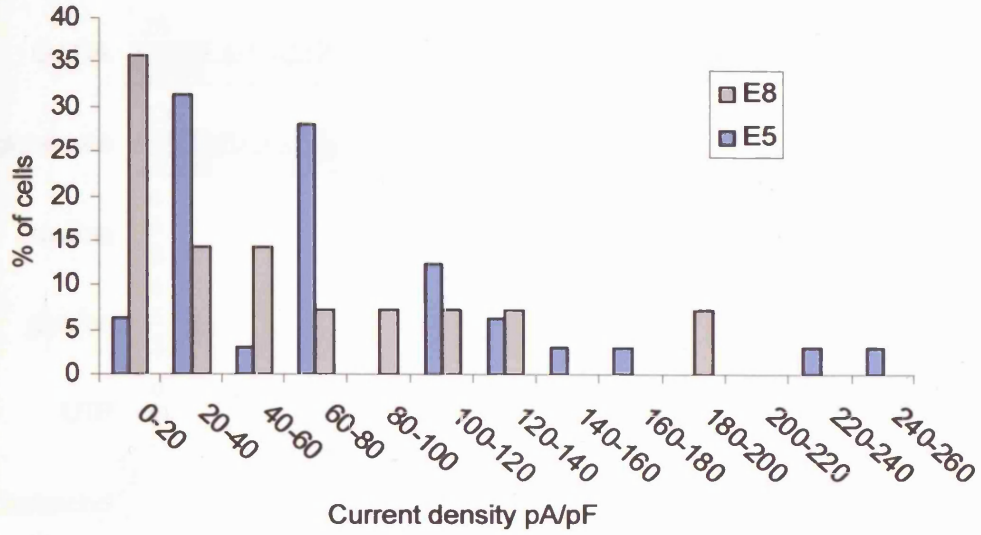

Figure 3.19 Distribution GABA-evoked current densities
The distribution of the GABA current density for Type 1 cells at -70mV. This ranges from -10pA/pF to -268pA/pF

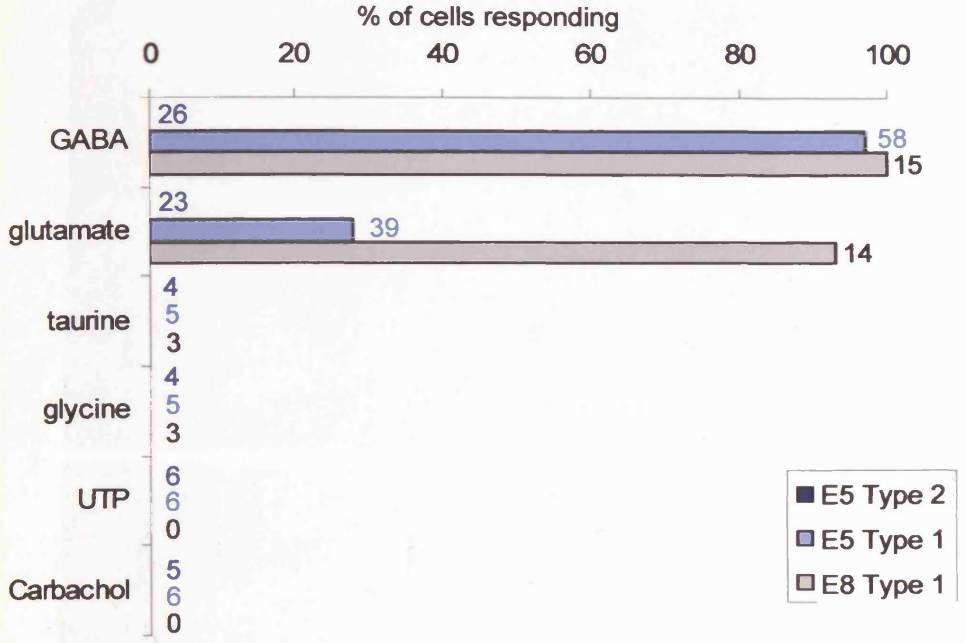

Figure 3.20 Current-responses to neurotransmitters during retinal development
Nearly all Type 1 cells respond to GABA at both E5 and E8, whereas responses to glutamate were observed in 28% of Type 1 cells at E5, increasing to 93% at E8. No responses were recorded at any time to taurine, glycine, UTP or carbachol in Type 1 cells. Type 2 cells did not respond to any of the transmitters tested. Bars represent % of cells that responded to ligand-application. Numbers shown at the end of each bar indicate the total number of cells tested for each transmitter.

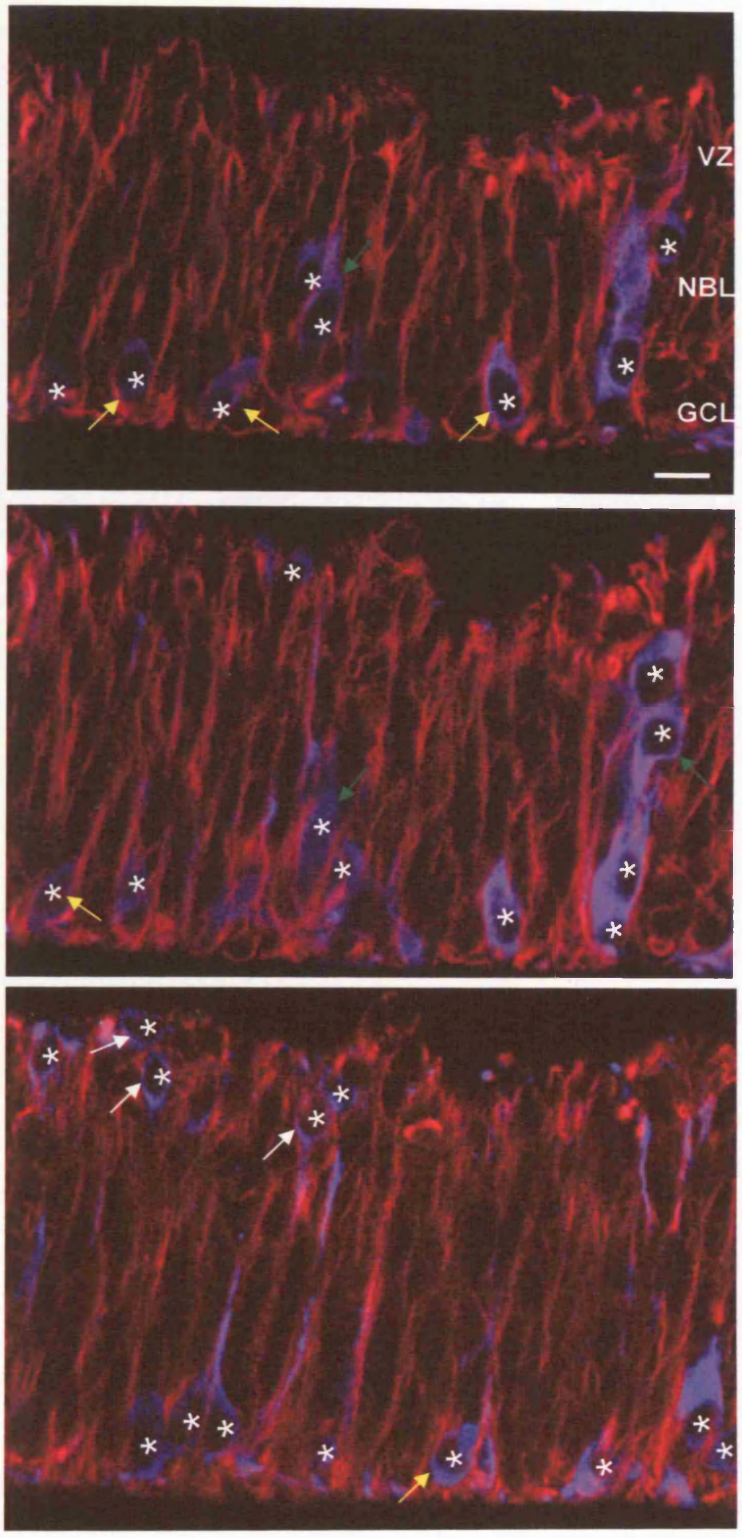

Figure 3.21 TuJ1 and vimentin expression at E5
Single confocal sections from 3 different levels in an E5 retinal slice labelled with antibodies for TuJ1 (blue) and vimentin (red). Most cells in the retina at this time express the progenitor cell marker vimentin. The majority of cells expressing TuJ1 (marked with an *) are located in the GCL (yellow arrows), but some are located in the VZ (white arrows) and in the neuroblastic layer (NBL, green arrows). The morphology of TuJ1$^+$ cells at this time is indistinguishable from that of vimentin$^+$ cells. Scale bar 10 um.

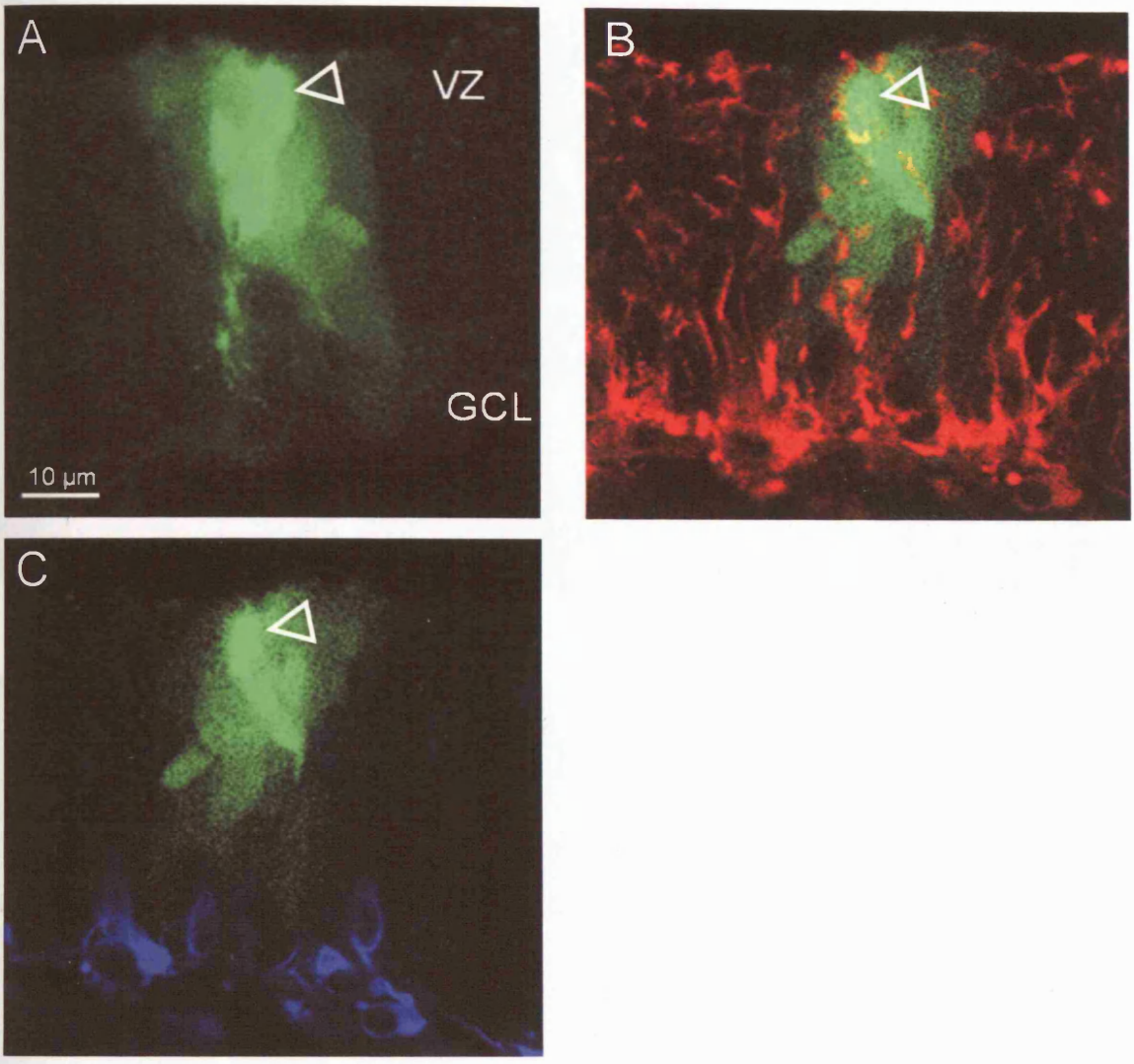

Figure 3.22 Vimentin and TuJ1 expression in a recorded E5 Type 1 cell
A recorded Type 1 cell in an E5 retinal slice was filled with Alexa 488 (green), and stained for vimentin (red) and TuJ1 (blue). The recorded cell was identified from a DIC image of the slice at the time of the recording, and is indicated here by an arrowhead. *A,* A projection through several confocal sections show that the cell is coupled to multiple neighbouring cells. *B,* A single confocal section of the Alexa 488 overlaid with the vimentin channel shows that the recorded cell and most of its coupled neighbours are vimentin$^+$. *C,* The same confocal section as shown in *B* of the Alexa 488 overlaid with the TuJ1 channel shows that none of the cells in the cluster express TuJ1.The recorded cell had an R_{in} of 48 MΩ, V_m of -40 mV, did not show any obvious voltage-gated currents, and responded to glutamate, GABA and isoguvacine.

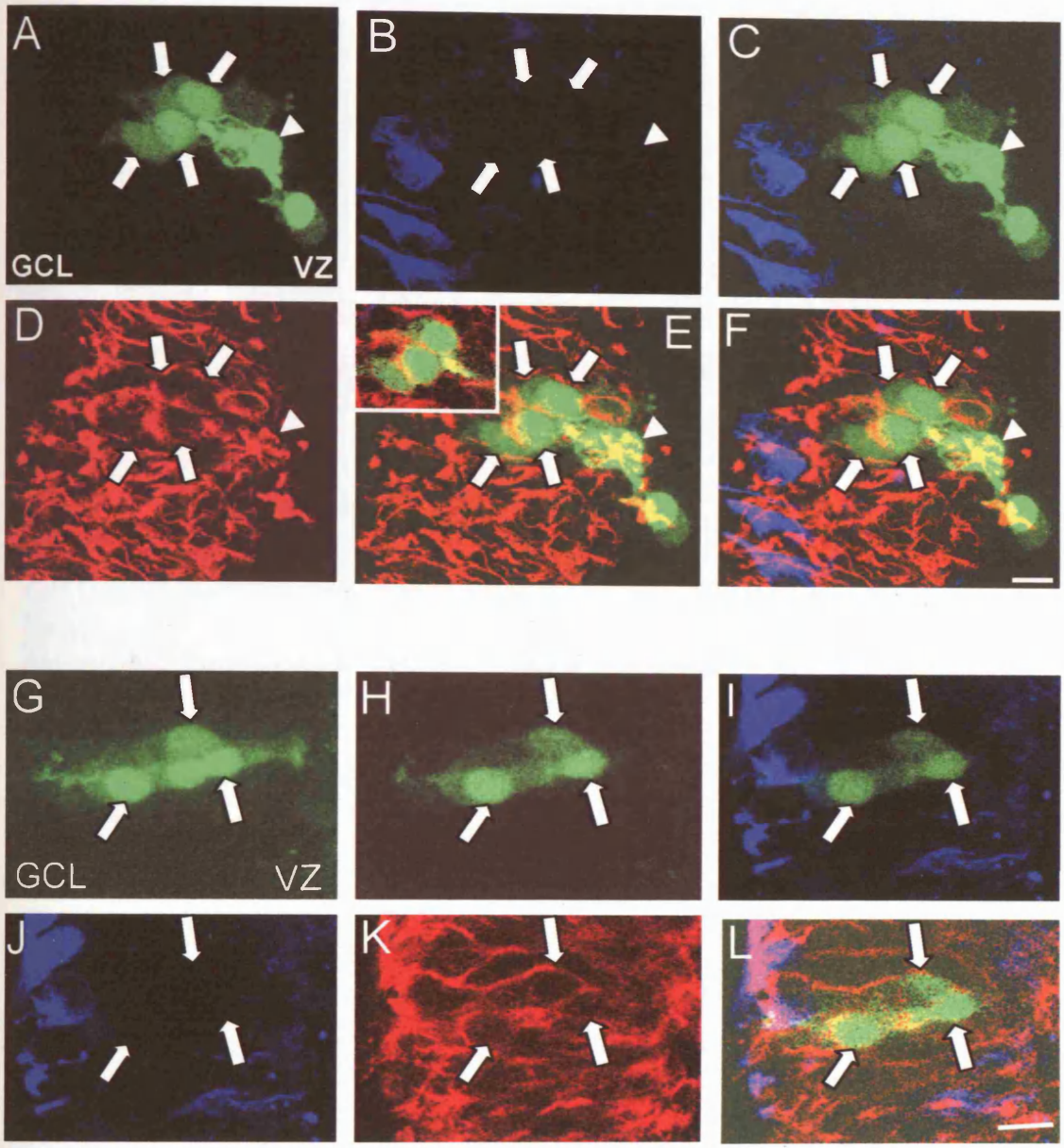

Figure 3.23 Two further examples of vimentin and TuJ1 expression in E5 Type 1 cells
Two Type 1 cells recorded in E5 retinal slices were filled with Alexa 488 (green), and stained for vimentin (red) and TuJ1 (blue). The first cell, shown in panels *A-F,* was identified from a DIC image at the time of the recording, and is indicated here by an arrowhead. *A,* a projection through several confocal sections shows that the cell is coupled to multiple neighbouring cells (indicated by white arrows). The same projection is shown in *B* for the TuJ1 channel (arrows indicate the location of the cells shown in *A*), and the two are overlaid in *C*, which shows that none of the coupled cells express TuJ1. *D-E* show the same projection for the vimentin channel, and shows extensive overlap between the vimentin expression and the Alexa-labelled cells. The inset in *E* shows a single confocal section, confirming the co-localisation. This cells had an R_{in} of 130 MΩ; V_m of -60 mV, no obvious voltage-gated currents, and responded to GABA but not to glutamate. The second cell is also coupled to several neighbouring cells (indicated by arrows), shown in the projection in *G*. The images in *H-L* are single confocal sections, showing that none of the cells in the cluster are TuJ1$^+$ (*I-J*), and all cells in the cluster are vimentin$^+$ (*K, L*). This cells had an R_{in} of 205 MΩ; V_m of -50 mV, no obvious voltage-gated currents, and responded to GABA but not to glutamate. Scalebars 10 uM.

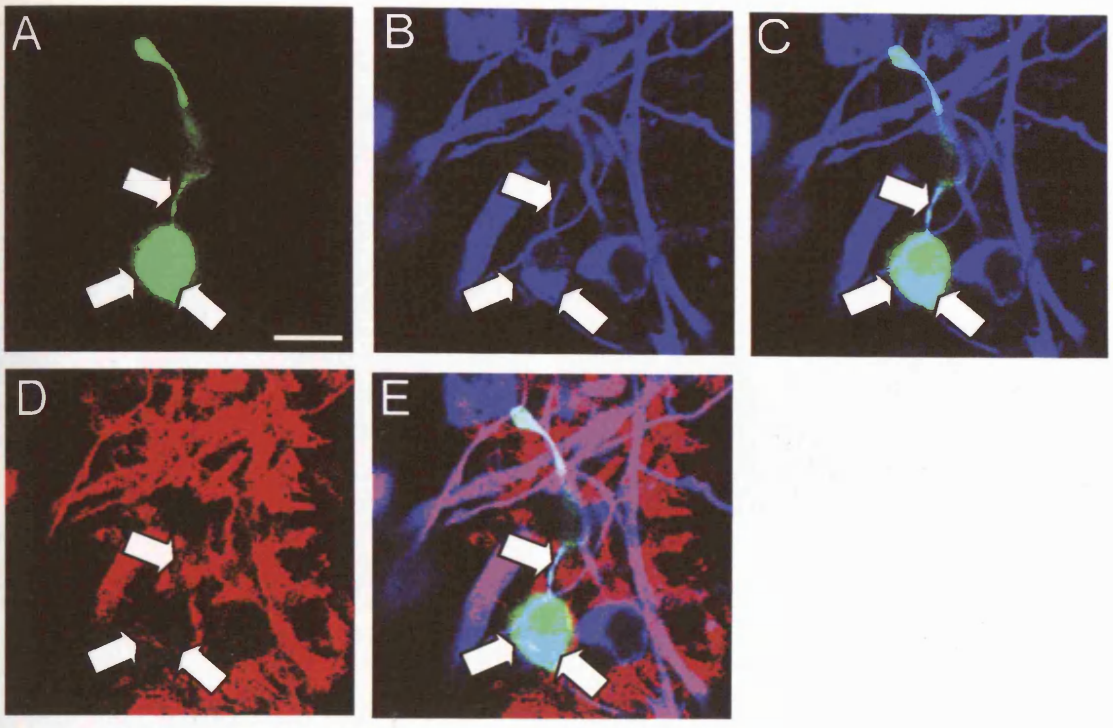

Figure 3.24 Vimentin and TuJ1 expression in a recorded E5 Type 2 cell
A Type 2 cell recorded in an E5 retinal slice was filled with Alexa 488 (green), and stained for vimentin (red) and TuJ1 (blue). *A,* A single confocal section of the Alexa 488 channel shows that the cell is not coupled to any neighbouring cells. *B*, The same confocal section shown in *A* for the TuJ1 channel (arrows indicate the location of the cell body and process, as in *A*) shows that the cell expresses TuJ1. *C,* Overlay of *A* and *B*. *D,* shows the same confocal section for the vimentin channel, and shows the cell is vimentin$^-$. *E,* Overlay of *A, B,* and *D*. This cell had an R_{in} of 1250 MΩ, V_m of -52 mV, and showed outward voltage-gated K^+-currents. Scalebar 10 uM.

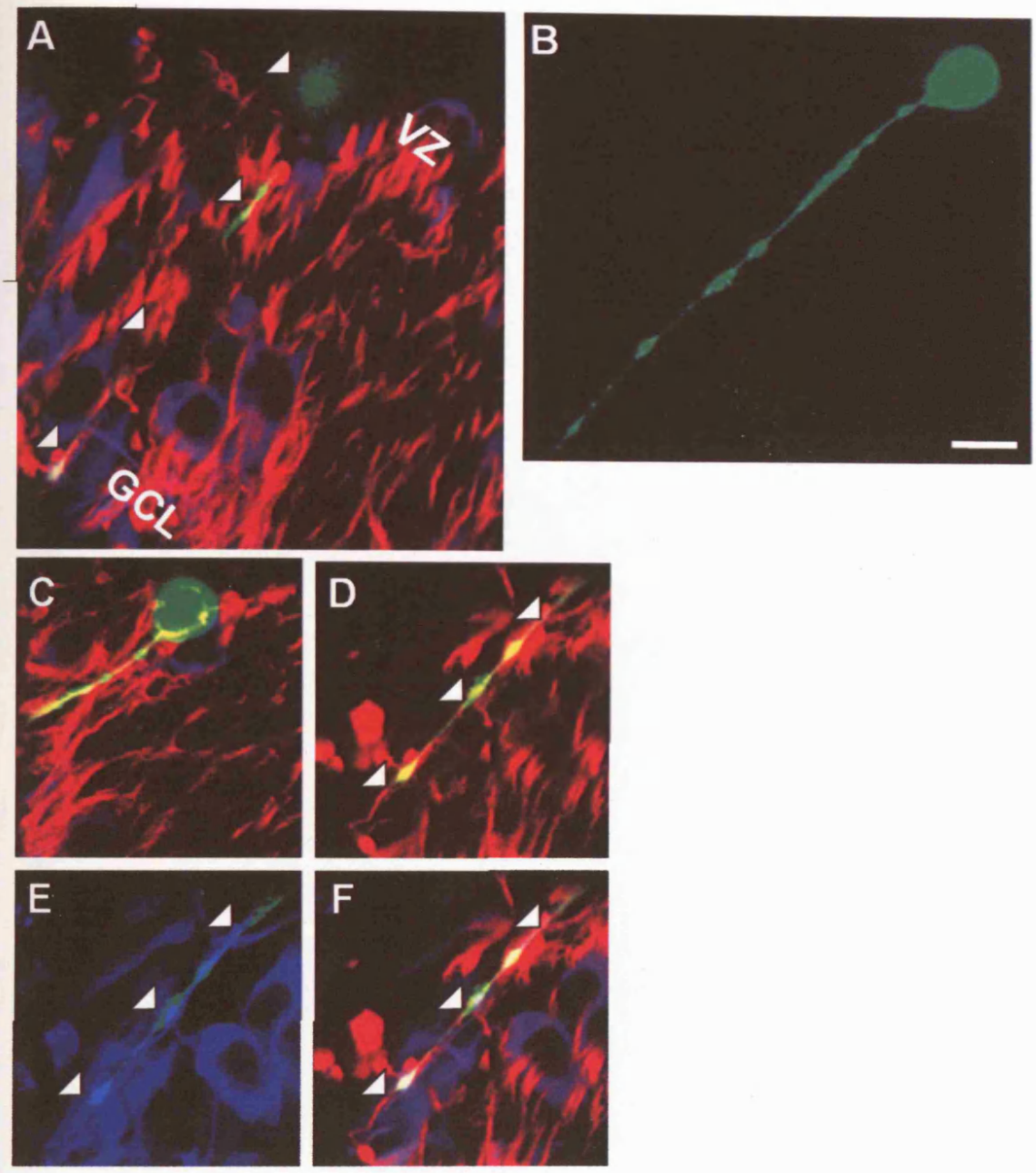

Figure 3.25 A further example of a Type 2 cell showing vimentin and TuJ1 expression at E5. A Type 2 cell recorded in an E5 retinal slice was filled with Alexa 488 (green), and stained for vimentin (red) and TuJ1 (blue). *A*, A single confocal section through the slice shows the location of the cell within the retina, and the distribution of TuJ1 (blue) and vimentin (red). Arrowheads outline the cell. *B*, A projection through the slice of the Alexa 488 (green) channel shows the full morphology of the cell, which extends over multiple confocal sections, and shows the cell is not coupled to any other cells. *C-F*, Single confocal sections show details of the vimentin-labelling along the process and in the cellbody. The cellbody, which is located in the VZ surface, is vimentin$^+$ (*C*), whereas the process is both vimentin$^+$ (*D,F*) and TuJ1$^+$ (*E,F*), suggesting this cell has just gone through terminal mitosis. This cell had an R_{in} of 500 MΩ, V_m of -60 mV, and showed outward, voltage-gated K^+- currents. Scalebar 10 µm.

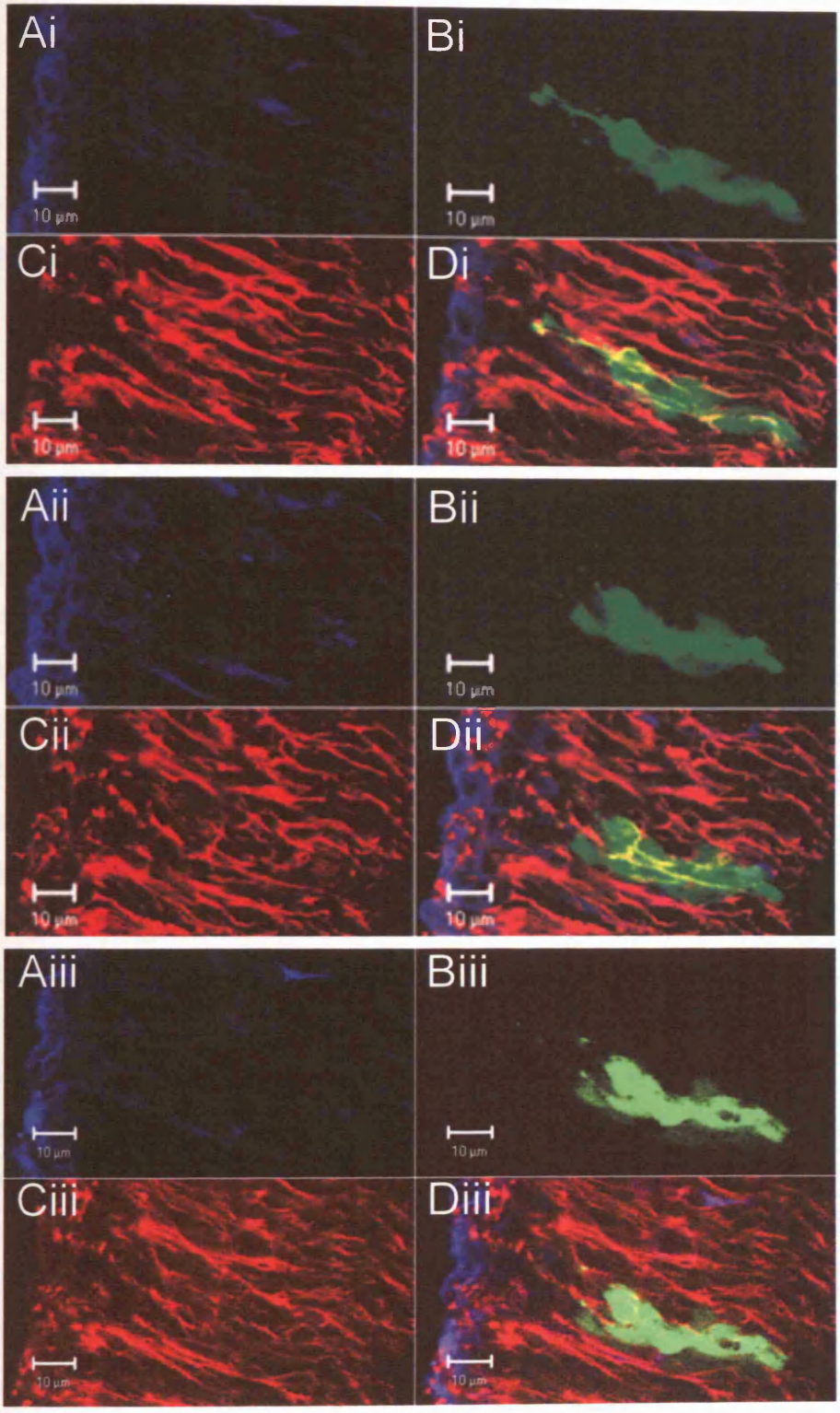

Figure 3.26 Vimentin and TuJ1 expression in a Type 1 cell recorded at E8
A Type 1 cell recorded in an E8 retinal slice was filled with Alexa 488 (green), and stained for vimentin (red) and TuJ1 (blue). Three confocal sections through the slice are shown (i, ii, iii), and for each one three channels (*A*, TuJ1; *B*, Alexa 488; *C*, vimentin) and the overlay of these (*D*), revealing an extensively coupled cluster of cells which express vimentin, but not TuJ1. The recorded cell had an R_{in} of 64 MΩ, V_m of -56 mV, no obvious voltage-gated currents, and responded to GABA.

Chapter 4

GAP JUNCTIONAL COUPLING OF PROGENITOR CELLS DURING EARLY DEVELOPMENT OF THE CHICK RETINA

4.1 Introduction

Gap junctions are a major pathway for intercellular communication in the CNS. In the adult retina, gap junctions play important roles in the processing of visual information by functioning as electrical synapses that are dynamically modulated by neurotransmitters and the level of ambient illumination, and mediate lateral connections between neurons (for review, see Sterling et al., 1986). During development, gap junctional communication is thought to be involved in a number of processes, including proliferation, cell death, differentiation and migration (for review, see Montoro & Yuste, 2004). Numerous studies have shown extensive coupling of progenitor cells in the developing cortex, dynamic regulation of connexin expression, and an overall decrease in coupling with maturation (LoTurco & Kriegstein, 1991; Nadarajah et al., 1996; Bittman et al., 1997; Nadarajah et al., 1997; Bittman et al., 2002). In the embryonic neocortex, Bittman and colleagues found that progenitor cells and radial glia form coupled clusters that extend radially through the ventricular zone (VZ), and exclude differentiated cells. They speculate that coupling between cells within these radial clusters serves to coordinate cell cycle events. Combined injection of biocytin and BrdU labelling showed dynamic modulation of gap junctional coupling related to the cell cycle, with maximal coupling in S and G2 phases and uncoupling in M phase. If the cell re-entered the cell cycle following M phase it either again became coupled to its neighbours in the next G1 or S phase, or remained uncoupled and began to migrate to the cortical plate (Bittman et al, 1997). Cortical progenitor cells from mouse (Cheng et al., 2004) and rat (Nadarajah et al., 1998) cultured in the presence of basic fibroblast growth factor (bFGF), which is present at high

levels in the developing cortical VZ (Weise et al., 1993), show an increase in Cx43 expression, which is mediated via a tyrosine kinase receptor and MAP kinase activation. Removing bFGF from the culture medium led to a reduction in gap junctional coupling, and caused progenitor cells to cease proliferating and differentiate into neurons. These studies show that gap junction channels provide a pathway for mediating responses to growth factors such as bFGF to regulate proliferation, and that gap junctional coupling is required to maintain progenitor cells in a proliferative state (Cheng et al., 2004).

In the developing chick retina, electron microscope studies showed an increase in gap junctions from E3 to E5-6, followed by a sharp decrease between E7.5 and E9, a timecourse that parallels the period of neurogenesis and differentiation (Fujisawa et al., 1976). Antisense oligodeoxynucleotide (asODN) treatment to Cx43, one of the first connexins to be expressed, in the E2-4 chick eye caused an overall reduction in eye size, which was not due to apoptotic cell death, but more likely due a decrease in the rate of proliferation (Becker & Mobbs, 1999).

Here, whole-cell patchclamping of cells in whole-mounts of embryonic chick retina was used to introduce a combination of dyes to investigate the extent and developmental profile of gap junctional coupling between retinal progenitor cells. This technique is combined with immunohistochemistry to test the identity of the coupled cells, and examine the pattern of expression of specific gap junction proteins, Cx43 and Cx36. Finally, the role of Cx43 in mediating cell coupling is tested using molecular approaches.

4.2 Methods

The methods employed are described in detail in section 2.3. Briefly, acutely dissected retinae were placed with the VZ facing upwards in a recording chamber. The retina was held flat with a nylon- and platinum harp, and transferred to the stage of an upright microscope, where the tissue was continuously superfused with Krebs' solution, and held at 36° C. The tissue was visualised using bright field illumination and DIC optics. The internal solution used to fill the patch pipette (Cs-Gluc, Table 2.2) contained 1% FITC dextran (MW 10000) and 1% Neurobiotin (MW 323), unless otherwise specified. High resistance seals (>1GΩ) were made onto processes at the ventricular surface, the membrane underneath the seal ruptured and cells kept in whole-cell mode for ~2mins before withdrawing the pipette to permit sufficient time for dye-diffusion. The low molecular weight Neurobiotin is free to diffuse through gap junctions from the recorded cell into any cells coupled to it, whereas the high molecular weight FITC-dextran remains trapped in the injected cell. Following dye-labelling of the cells, the tissue was fixed in PFA, and processed to reveal the Neurobiotin, and imaged on a confocal microscope. Expression of cell type specific markers and connexin proteins was examined using immunocytochemistry. Expression of Cx43 was modulated by transfection of individual cells with a dominant negative construct of Cx43 using electroporation, and by gel application of Cx43-specific antisense oligodeoxynucleotides.

Confocal images were acquired by taking XY-sections in the plane of the retina every 1-2 µm through the thickness of the tissue. These image stacks could subsequently be rotated to produce a side-view of the retina, called an XZ-section (a single pixel thick), or an XZ-projection (through the entire stack), or projected to produce a single image view through the entire stack in the XY-plane. Images were analysed in Zeiss LSM and Metamorph software. For details, see section 2.8. Results are presented as means ± standard error of the mean, where n is the number of observations, unless otherwise stated.

4.3 Results

4.3.1 The pattern of coupling in embryonic retinae can be assessed using whole-cell patchclamping to introduce dyes

The use of whole-cell patchclamping permitted cells to be filled with dyes via the thin processes which cover the ventricular surface. Cells could be held in the whole-cell configuration for several minutes, and dye-filling could be monitored using the FITC filter set of the epifluorescence microscope. More than 140 dye-fill experiments in whole-mounted E4-E9 retinae were carried out, and the pattern of dye-coupling imaged using confocal microscopy. The illustrations in this chapter are representative of the results obtained. Figure 4.1-4.2 show typical examples of cells filled in this way in E4-E9 retinae. The FITC is restricted to the injected cell (yellow), while the Neurobiotin (NB, red) spreads into many of the surrounding cells, forming a radial cluster of labelled cells through the retina. At all stages of development tested, the injected cell had a bipolar morphology, with processes extending to either surface of the retina. This morphology is characteristic of both retinal progenitor cells and newly postmitotic cells (Sauer, 1935; Seymour & Berry, 1975; Nagele & Lee, 1979).

4.3.2 Dye-coupling results from diffusion of Neurobiotin through gap junctions

The gap junction blocker carbenoxolone (CBX, 100 µM) abolished dye-coupling at all developmental stages examined, confirming that the spread of NB to cells surrounding the FITC-injected cell is due to the presence of gap junctional coupling. Figure 4.3 shows three cells injected with FITC/NB in the presence of CBX, at E5, E6 and E9. In each case, the extensive dye-coupling usually seen (see Figures 4.1 and 4.2) is abolished, and the spread of NB is largely restricted to the FITC-injected cell. The mean number of cells labeled with NB only in the presence of CBX was 0.47±0.22 (n=15, in retinae aged E5 to E9). The coupled

clusters revealed by NB comprise columns of cells that span the retina; within these columns, dark profiles of cells excluded from the coupling are clearly outlined by the stained cells that surround them (Figure 4.7E). The presence of these cells, and the effects of CBX in preventing dye spread, show that the spread of NB reflects specific cell-cell coupling, and does not result from dye leakage and non-specific uptake.

4.3.3 The extent of dye-coupling observed at early times is determined by the concentration of Neurobiotin

Further inspection of the images in Figure 4.1 shows that the NB labelling becomes increasingly faint with distance from the injected cell. In addition, in all four cases shown, the injected cell is positioned in the centre of the NB labelled cluster of cells. This suggests that the apparent extent of coupling in these preparations is determined by how far the NB diffuses before becoming too dilute to be visible, rather than by it reaching any anatomical boundary. In contrast, the pattern of NB spread at E8-E9, shown in Figure 4.2, is less diffuse; individual cells are more easily identified, and the cluster appears to have discrete limits. In he E9 retina shown in Figure 4.2, the FITC-labeled cell is positioned asymmetrically within the NB-coupled cluster, suggesting that it has a finite limit, determined by the extent of coupling rather than the extent of dye-diffusion. To examine if the pattern of coupling observed at earlier times was dependent on the NB-concentration, dye-filling experiments in which this was varied from 0.1% to 10% were carried out in E5 retinae. The results are shown in Figure 4.4. In young retinae (< E8), the coupled cluster was usually too dense to enable individual cells to be counted. As a result, the number of coupled cells was determined by measuring the radius of the cluster at the widest and narrowest point to determine its volume. This was then divided by the average volume of a single cell to give an estimate of the number of cells in the cluster (for further details of how this was done, see section 2.8.2 in the Methods). As illustrated in Figure 4.4,

use of a 10% NB concentration in the patch pipette led to a 10-fold increase in the extent of dye-coupling observed at E5, compared to use of 1% NB. Reducing the NB concentration to 0.1% did not have any effect on the extent of the dye-coupling observed, compared to 1% NB. This suggests that at early times, retinal cells are coupled into a continuous syncytium. On this basis, any comparisons of the observed extent of coupling should be restricted to experiments using identical labelling protocols. All subsequent experiments were carried out using 1% NB injections.

4.3.4 The extent of dye-coupling changes during development

As illustrated in Figure 4.5, the extent of dye-coupling changes through the period of retinal development studied. The number of coupled cells gradually increases from E4 to E6. Although the horizontal spread of dye-coupling is often greater at E4 than at E5-6 (Figure 4.5A), the increase in the thickness of the NBL during this time (see Figure 4.1) means that a greater number of cells are included in the coupled cluster at later times. Between E6 and E7, the extent of coupling is unchanged, but this is followed by a sharp drop in the extent of coupling seen at E8 and E9. The decrease in coupling between E7 and E8 was highly significant ($p=0.004$). In addition, the mean level of coupling observed during the period of development from E4-E7 (131±9 coupled cells, $n=42$) was significantly greater than that observed from E8-E9 (28±5, $n=24$, $p<0.0001$). The initial increase in coupling between E4 and E6, and the subsequent decrease observed between E7 and E8 closely mirrors that observed in earlier electron microscope studies of retinal sections, reported by Fujisawa et al., (1976), who found an increase in gap junctions from E3 to E5-6, followed by a sharp decrease between E7.5 and E9.

On occasion, more than one cell was injected with FITC and NB in a single patch-experiment. Typical examples of multiple cell labelling in retinae aged from E5 to E8 are shown in Figure 4.6. Up to 5 individual cells could be labelled in a

single patch-experiment, due to the close apposition of the cell processes on the ventricular surface, although simultaneous labelling 2 or 3 cells was more common. However, the mean number of coupled cells did not increase when several cells where injected with FITC/NB (Figure 4.6B), presumably because cells within close proximity of one another are part of the same coupled cluster. Therefore, injections where multiple cells were FITC labelled were not excluded from the data.

4.3.5 Cells at all levels of the neural retina are coupled at E4-E7, but not at E8-E9.

At early times in development (E4-E7), cells at all levels of the neural retina are coupled into clusters. Figure 4.7 shows a typical E7 retina injected with FITC and NB. Single XY-sections at the level of the VZ, the neuroblastic layer (NBL) and the GCL confirm the presence of NB^+-cells at all levels. Since retinal progenitor cells undergo INM as they progress through the cell cycle, the location of the cell body is indicative of their stage within the cell cycle (Figure 1.2). In the developing rodent neocortex, biocytin injections combined with BrdU revealed extensive coupling during S, G_2 and G_1, but clusters were not found to contain cells in M phase (Bittman et al., 1997). By contrast, in the studies described here, the cells in the VZ were extensively coupled (as seen in examples in Figures 4.1, 4.2, 4.6 and 4.7). In addition, the presence of mitotic profiles (distinguishable by the elongated bars of chromatin visible in metaphase) within the coupled cluster confirms that cells in M phase are often included in the coupling (Figures 4.7B and 4.8B).

At later times in development (E8-E9), the coupling was restricted to cells with their nuclei in the NBL and the VZ, and only the processes of NB^+ cells extended through the GCL (Figures 4.2, 4.6 and 4.11).

From E4 to E6, dye injections showed that the cell body of the injected cell could be located anywhere between the VZ and the GCL. Figure 4.8 shows typical examples of cells in E5 retinae where the nucleus is located in the VZ (Figure 4.8A-B), the NBL (Figure 4.8C) and the GCL (Figure 4.8D). In order to compare how the extent of coupling varied with the somal location of the injected cell at E5, the thickness of the retina was divided into three sections for the purpose of classifying the location of the nucleus. The VZ was defined as the upper quarter, the NBL as the middle half, and the GCL as the lower quarter of the retina (as indicated by dashed lines in Figure 4.8A). At E5, the extent of coupling was greater when the nucleus of the injected cell was located in the VZ than if in any other part of the retina, although the difference was not significant. There was no difference between the extent of coupling in retinae where the nucleus of the injected cell was located in the NBL and those where it was located in the GCL (Figure 4.8E).

The variation in the somal location was greatest at early times. At E4-E6, the nuclei of the injected cells were found at all levels of the retina (15% in the VZ, 56% in the NBL, 29% in the GCL). At E7-E9, the nuclei were most often found in the NBL (83%), and occasionally in the VZ (17%), but not in the GCL.

4.3.6 Coupled clusters exclude postmitotic cells

In their study of cortical progenitor cells, Bittman et al. (1997) found postmitotic neurons to be excluded from coupled clusters within the VZ, and cells in the intermediate zone and the cortical plate were also uncoupled. Figures 4.9, 4.10 and 4.11 show typical examples of E4, E6 and E8 retinae, processed for the neuronal marker β-tubulin (TuJ1) following FITC and NB injection. At E4, $Tuj1^+$ cells are seen at all levels in the retina (Figure 4.9A-E), and are mostly excluded from the coupled cluster. $TuJ1^+/NB^-$-cells are not restricted to regions outside the coupled cluster, as illustrated in Figure 4.9D, where an XZ-section shows a

TuJ1$^+$/NB$^-$-cell (white arrow) surrounded by coupled cells. In the GCL, most TuJ1$^+$ cells are also excluded from the coupling, although some TuJ1$^+$/NB$^+$-cells are seen (green arrows in Figure 4.9E). In addition, in Figure 4.9E a TuJ1$^+$/NB$^+$-cell can be seen outside the coupled cluster (yellow arrow), suggesting it may have migrated tangentially on reaching the GCL.

At E6, Tuj1$^+$ cells are mostly restricted to near or within the GCL (Figure 4.10A-D), and are largely excluded from the coupled cluster. For example, in Figure 4.10B-D, no TuJ1$^+$-cells are visible within the VZ, although the processes of TuJ1$^+$/NB$^-$-cells are seen within the coupled cluster as small blue dots (Figure 4.10B), whereas near or within the GCL, the majority of cells are either TuJ1$^+$/NB$^-$ or TuJ1$^-$/NB$^+$ (Figure 4.10C-D). A single TuJ1$^+$-cell is included in the coupled cluster (Figure 4.10C, green arrow).

At E8, the retina shows an increasingly distinct separation of NB$^+$ cells within the VZ and NBL, and TuJ1$^+$-cells in the GCL and the putative inner nuclear layer (INL, Figure 4.11A). For example, in Figure 4.11B-D, no TuJ1$^+$-cells are visible in the VZ (Figure 4.11B), and no NB$^+$-cells are visible within the GCL (Figure 4.11D). Processes of NB$^+$-cells span the thickness of the retina, projecting through the GCL (Figure 4.11D).

At early times, the chick retina comprises mainly progenitor cells and newly generated neurons, which express TuJ1. The vast majority of coupled cells are TuJ1$^-$, and thus are likely to be progenitors. Processing for the progenitor cell marker vimentin following FITC and NB labelling confirms the identity of the coupled cells as progenitor cells, showing that the majority of NB$^+$-cells are also vimentin$^+$ (Figure 4.12).

4.3.7 The expression of Cx43 and Cx36 mirrors the changes in dye-coupling during retinal development

In order to examine which connexin proteins mediate the coupling observed during this period of retinal development, the expression of two connexin proteins, Cx43 and Cx36, was investigated using immunohistochemistry. Cx43 has been widely implicated in gap junctional communication at early times in development. In the developing rat neocortex, Cx43 is expressed from E12 onwards (the earliest time tested), which corresponds to the onset of neurogenesis. The level of Cx43 expression increases until E16, then decreases during the period of late neurogenesis to birth (E18-P0; Nadarajah et al., 1997). Mouse cortical progenitor cells maintained *in vitro* require Cx43 expression to maintain a proliferative state (Cheng et al., 2004). In the developing chick eye, reducing Cx43 expression leads to an overall decrease in eye size, which is attributed to a decrease in proliferation (Becker & Mobbs, 1999). The role of Cx36 in development has received less attention. In the developing mouse neocortex, Cx36 is expressed at low levels from E12.5 onwards (Gulisano et al., 2000).

The expression of Cx43 and Cx36 in the retina from E4 to E8 is shown in Figures 4.13-4.17. Both connexin proteins could be detected at all times examined (Figure 4.13A, F; Figure 4.14A, E; Figure 4.15A, E; Figure 4.16A, E; and Figure 4.17A, E), and was not due to non-specific binding of secondary antibodies, as shown by negative controls where the primary antibodies were omitted (Figure 4.13B, G; Figure 4.14B, F; Figure 4.15B, F; Figure 4.16B, F; and Figure 4.17B, F).

The level of Cx43 expression shows a gradual increase from low levels at E4 (Figure 4.13A), an intermediate level at E5 (Figure 4.14A), and high levels of expression at E6 (Figure 4.15A), which is maintained at E7 (Figure 4.16A), and then shows a marked decrease in expression at E8 (Figure 4.17A). The changes in the levels of Cx43 expression mirror the pattern and timecourse of the changes

in the numbers of dye-coupled cells observed, as shown in Figure 4.5. At all times, the expression of Cx43 appears to be partly in TuJ1^{+}-cells, or their processes, and partly in TuJ1^{-}-cells or -processes (Figure 4.13C, D; Figure 4.14C, D; Figure 4.15C, D; Figure 4.16C; and Figure 4.17C, D), although at E8, the majority of Cx43 staining appears to be co-localised with TuJ1 (Figure 4.17D). In addition to staining in the VZ and NBL, Cx43-staining is seen in the fibre layer at all times (Figure 4.13E; Figure 4.14D; Figure 4.15A; Figure 4.16D; Figure 4.17A).

Cx36 is expressed at high levels throughout the retina from E4 to E6 (Figure 4.13F; Figure 4.14E; and Figure 4.15E). At E7, Cx36 expression is high within the VZ, and expressed at lower levels within the NBL, but is weak or absent from the GCL and fibre layer (Figure 4.16E, G-I). At E8, Cx36 expression shows further spatial restriction, with high levels of expression at the VZ surface, but a very low level of expression throughout the rest of the tissue, and is entirely absent from the GCL (Figure 4.17E, G-H). At all times, the pattern of Cx36 expression appears to outline the cell bodies and processes of TuJ1^{-}-cells (Figure 4.13H; Figure 4.14G-H; Figure 4.15G; Figure 4.16G; and Figure 4.17G), consistent with a role for this connexin in mediating the extensive dye-coupling between progenitor cells described above. Sparse co-localisation with TuJ1 is also evident at early times (Figure 4.13I; Figure 4.14G; Figure 4.15G; and Figure 4.16H), consistent with the occasional presence of a TuJ1-expressing cell within the dye-coupled cluster at E4-E6. The spatial separation between Cx36 and TuJ1 expression at E8 parallels that of NB-coupled cells and TuJ1 expression at this time (Figure 4.17E, G-H; and Figure 4.11).

Simultaneous labelling of Cx43 and Cx36 shows extensive overlap between these two connexin proteins (Figure 4.18), suggesting that they may combine to form heteromeric or heterotypic gap junctions (different connexins making up a single connexon, or different connexons combining to forming a gap junction, respectively).

4.3.8 Expression of a dominant negative Cx43 construct reduces dye-coupling

Electroporation was used to introduce a pIRES vector with a CMV promoter into cells to drive the expression of eGFP and a dominant-negative Cx43 construct (dnCx43), which interferes with gap junction formation. Due to their high sequence homology, this construct may affect other connexins in addition to Cx43. Electroporation led to expression of the construct in cells with bipolar, progenitor cell morphology, which could be readily identified by virtue of the eGFP (Figure 4.19A). These preparations could subsequently be injected with dyes as previously described. In order to distinguish between eGFP expression and cell labelling, FITC was replaced by Alexa 568 dextran (1%, MW 10000) in these experiments. The Alexa 568 could be viewed using an epifluorescence microscope equipped with a rhodamine filter-set. Injection of dyes into cells in dnCx43-expressing retinae led to extensive NB-coupling of non-eGFP expressing cells (Figure 4.19B-E), whereas most eGFP expressing cells were excluded from the coupling (Figure 4.19C-E).

Using the FITC filter set to view the eGFP expression during the dye-filling experiment, fluorescence-guided patching of eGFP-expressing cells was attempted. An example is shown in Figure 4.20. The cell body of the injected cell was located just below the VZ, and the cell had a bipolar morphology similar to that seen in previous experiments (Figure 4.20B). The NB is restricted to the injected cell, and no dye-coupling to neighbouring cells is visible (Figure 4.20B). Overlay of the Alexa 568 channel and the eGFP channel confirm the dnCx43 expression of the injected cell. Unfortunately the eGFP fluorescence was very low, making it difficult to accurately identify eGFP-expressing cells during the patch-clamp experiment. Due to the low levels of fluorescence, the eGFP-expressing cells could only be identified at the level of the soma, as the fluorescence from the thin processes was too faint to detect on the microscope used for the patch-clamp recordings. This meant that the target cell had to be identified by focusing up and down between the cell body and the ventricular

surface, and thus identify the process of the target cell, which proved to do be extremely difficult. For these reasons, only a small number of successful injections were made into eGFP-expressing cells. In these, the mean number of NB-coupled cells to an injected eGFP-expressing cell was 4.3±2.3 (n=3, all in E5 retinae).

4.3.9 Antisense oligodeoxynucleotides to Cx43 reduces dye-coupling

Cx43 protein expression can be transiently and specifically knocked down by Cx43 antisense oligodeoxynucleotides (asODN) (Becker and Mobbs, 1999; Becker et al., 1999; McGonnell et al., 2001), providing an alternative technique by which to test the specific role of Cx43 in mediating coupling of cells in the developing retina. Application of Cx43 antisense, using pluronic gel as a vehicle, reduces expression of Cx43 protein in the whole tissue, thus avoiding the problems encountered in targeting the dnCx43-expressing cells for dye-injection. The pluronic gel used as a vehicle for delivering the asODN to the tissue was used as a control treatment. The knockdown of Cx43 following asODN treatment was confirmed using antibody-labelling (Figure 4.22A).

Treatment with asODN prior to dye-labelling led to a reduction in the extent of dye-coupling, relative to 'gel only' controls, at all times examined (Figure 4.21 and Figure 4.22B). The reduction in dye-coupling following asODN treatment was significant at E5, E6 and E8.

4.4 Discussion

4.4.1 Injection of dyes into cells in the developing retina reveals gap junctional coupling

Introduction of a combination of gap-junction permeable and impermeable dyes using whole-cell patchclamping allows the profile and development of gap junction coupling in the developing chick retina to be investigated. Here, gap junctional coupling between retinal cells from E4 to E9 was examined. Injected cells at all ages had a bipolar morphology with processes spanning the retina, and showed coupling to neighbouring cells. Coupled cells formed a radial cluster through the retina, similar to those observed in the developing neocortex (Bittman et al., 1997). Coupling could be abolished by the gap junction blocker carbenoxolone. Furthermore, coupling was not promiscuous, with dark profiles representing uncoupled cells visible within the column of coupled cells. Together, these observations confirm that NB-labelling reflects gap junctional coupling between cells. At early times, the extent of coupling revealed by dye-injection was dependent on the concentration of dye, and a 10-fold increase in dye-concentration led to a 10-fold increase in the numbers of cells labeled with dye, suggesting that progenitor cells in the early embryonic retina are coupled into a continuous syncytium.

4.4.2 Gap junctional coupling changes during retinal development

The number of coupled cells gradually increases from E4 to E7, from a mean of 84±8 at E4 to peak of 155±10 at E6-E7. From E7 to E8, there is an 81% drop in the mean number of coupled cells, to 29±5 at E8, which remains low at E9 (18±5), the latest time point studied. This pattern of development of gap junctional coupling is similar to that observed by Fujisawa et al. (1976) in electron microscopy studies of thin retinal sections. These authors found an increase in

gap junctions from E3 to E5-6, followed by a sharp decrease between E7.5 and E9. This timecourse parallels the period of progenitor cell proliferation and neurogenesis. In a study using [^{3}H]thymidine incorporation, Dütting et al. (1983) found that self-renewal of progenitor cells in the chick retina drops below 50%, implying a transition from increase to depletion of the absolute number of progenitor cells in the tissue, around day 7.5. In cultured progenitor cells from the developing mouse neocortex, a reduction in gap junction expression and dye-coupling resulted in premature withdrawal of progenitor cells from the cell cycle and subsequent neuronal differentiation (Cheng et al., 2004). Progenitors in the developing neocortex are also coupled via gap junctions, and show a similar pattern of decreasing coupling as neurogenesis proceeds (LoTurco & Kriegstein, 1991). Pharmacological uncoupling of cortical progenitors at early times combined with BrdU labelling showed a decrease in the numbers of cells entering S phase (Bittman et al., 1997). These findings suggest that gap junctional coupling of cortical progenitor cells is required to maintain a proliferative state. The findings described in the present study show that gap junctional coupling between progenitor cells in the developing retina could play a similar role.

4.4.3 Cell cycle and cell coupling

At early times in retinal development (E4-E7), cells at all level of the neural retina are coupled into clusters. In studies of cortical progenitors, cells were found to be coupled during S, G_2 and G_1, but not during M phase (Bittman et al., 1997). In contrast, in the studies described here, the cells in the VZ were extensively coupled, and the presence of mitotic profiles in NB-labeled cells confirms that gap junctional coupling to neighbouring cells is retained during M phase. At early times (E4-E7), FITC/NB labelled cells were located anywhere within or between the VZ and the GCL, showing that cells at all stages of the cell cycle are coupled. The nuclei of coupled progenitor cells at later times (E8-E9) were not observed within the GCL. At this time, the majority of GCs have been born, and the INL and

IPL are emerging. This suggests that at later times, the nuclear translocation of retinal progenitors is restricted to proliferating layers, although the processes of coupled cells project through the GCL to the fibre layer.

4.4.4 Coupled clusters exclude postmitotic cells

Immunostaining for β-tubulin, which is expressed by postmitotic neurons, and vimentin, a progenitor cell marker, confirmed that coupled cells are vimentin-expressing progenitors, whereas postmitotic cells were excluded from the coupled clusters. The exclusion of TuJ1-expressing cells was not restricted to cells in the GCL or to cells remote from the cluster, as uncoupled, TuJ1-expressing cells were observed in the middle of coupled column, and at all levels of the retina, suggesting that cells are specifically uncoupled upon cell cycle exit. This is consistent with the findings presented in Chapter 3 of this thesis: progenitor cells (Type 1) were characteristically coupled to neighbouring cells, whereas postmitotic cells (Type 2) showed little or no coupling. A similar distinction between progenitor cells and postmitotic neurons was observed in the cortex (LoTurco & Kriegstein, 1991), where progenitors are extensively coupled, but postmitotic neurons are uncoupled. In addition, Cheng and colleagues (2004) show that cortical progenitors maintained *in vitro* are induced to differentiate upon uncoupling by a reduction in gap junction expression. Together, these findings suggest that during neurogenesis, gap junctional coupling is a feature of progenitor cells, but not of postmitotic cells.

4.4.5 Gap junctional coupling and expression of connexins in retinal development

The expression of Cx36 and Cx43 was found to be consistent with a role for these connexin proteins in mediating the gap junctional coupling described during this period of retinal development. Both connexins were detectable at all times,

and in the case of Cx43, the level of expression followed a similar pattern and timecourse to the changes in numbers of coupled cells. Cx36 was widely expressed at early times, and became increasingly restricted to non-TuJ1 expressing areas at later times, consistent with the increasing separation between NB-coupled cells and TuJ1-expressing cells seen at E8-E9. The involvement of Cx36 in neuronal development has not received much attention to date. In the developing mouse neocortex, Cx36 is expressed at low levels from E12.5 onwards, which corresponds to the onset of neurogenesis (Gulisano et al., 2000). In the NT2/D1 cells, a human teratocarcinoma progenitor cell line, which can be induced to differentiate into functional neurons by retinoic acid treatment, both Cx36 and Cx43 are expressed and mediate functional gap junctions, but their expression is reduced upon neuronal differentiation (Boucher & Bennett, 2003). In the adult retina, Cx36 is expressed in amacrine and bipolar cells (Mills et al., 2001), ganglion cells (Hidaka et al., 2002), and cone photoreceptors (Feigenspan et al., 2004). The findings described here demonstrate that, in addition to the roles of Cx36 in mediating coupling in the adult retina, this connexin may also play a role during retinal development.

The involvement of Cx43 in neuronal development has been shown in several previous studies (Nadarajah et al., 1997, Nadarajah et al., 1998; Becker & Mobbs, 1999; Cheng et al., 2004). The expression of Cx43 in developing rat cortex shows a similar pattern to that described here, gradually increasing from E12 to E16, which is the main period of neurogenesis, and then decreasing from E18 to birth (Nadarajah et al., 1997). In mouse (Cheng et al., 2004) and rat (Nadarajah et al., 1998) cortical progenitor cells maintained *in vitro,* the expression of Cx43 is increased in response to bFGF, a growth factor abundant in the developing cortex (Weise et al., 1993). Withdrawal of bFGF from the culture medium leads to a reduction in Cx43 expression and gap junctional coupling, which results in premature exit from the cell cycle. Furthermore, pharmacological uncoupling of cultured cortical progenitors had profound effects on cell survival, and this effect was more pronounced in cells from earlier stages

of neurogenesis, where most cell divisions are proliferative (Cheng et al., 2004). Scemes et al., (2003) found neural progenitor cells derived from the striatum of a mutant Cx43 null mouse to show altered proliferation and migration when they were maintained *in vitro* as neurospheres. Here, the role of Cx43 in retinal development was confirmed in progenitor cells *in situ*, rather than in culture. Dye-injection into cells expressing eGFP with a dominant negative Cx43 (dnCx43) showed dramatically reduced the gap junctional coupling to neighbouring cells. Labelling of non-transfected cells in a retina containing dnCx43-expressing cells showed extensive coupling of the non-transfected cell to their neighbours, with most dnCx43-expressing cells excluded from the coupled cluster. Similar results were obtained by specific knockdown of Cx43 using application of antisense ODNs. In recent studies, E5-E6 retinal progenitor cells expressing dnCx43 over 24 hours (a longer time period than in the studies described here) were observed to cluster in the VZ and differentiate prematurely into a neuronal phenotype, characterized by TuJ1-expression and neurite extension, which normally only occurs once postmitotic cells have reached their final destination (D Becker, personal communication). Similar results were found by culturing embryonic retinae in the presence of pharmacological gap junction blockers, or by prolonged Cx43 knockdown using antisense ODNs to Cx43. Application of Cx43 antisense ODNs at earlier times in embryonic development (E2-E4) leads to an overall reduction in eye size, an effect which was not due to apoptotic cell death, but more likely due a decrease in the rate of proliferation (Becker & Mobbs, 1999). Taken together, these findings demonstrate that Cx43 mediated gap junctional coupling between retinal progenitor cells plays a critical role in maintaining a proliferative state.

4.5 Further studies

The results described in this chapter extend previous findings relating to the role of gap junctional coupling between progenitors, and show that a similar pattern to that observed in the developing cortex is present in the developing retina, suggesting that gap junctional coupling of progenitors is a conserved strategy during neurogenesis. This raises interesting questions about nature of the signals that pass through gap junctions to maintain progenitor cell proliferation. Because gap junctions provide a direct conduit for the transfer of molecules between coupled cells, it is possible that survival factors or mitogens induced by bFGF or other growth factors pass through the gap junction to promote the survival of progenitor cells and keep them in a proliferative state. Signals that stimulate Ca^{2+} influx or release from intracellular stores have been shown to stimulate retinal and cortical progenitor cell proliferation (Pearson et al., 2002; Ma et al., 2000), and Ca^{2+}-signals have been shown to occur in both cortical and retinal progenitors, both in individual cells and as coordinated wave-activity which is blocked by pharmacological gap junction blockers (Owens & Kriegstein, 1998; Pearson et al., 2004). The identification of the signals that pass through gap junction channels and maintain progenitor cells in a proliferative state will be an important area for future investigation.

It would be interesting to investigate how specific connexins, other than Cx43, contribute to the pattern of gap junctional coupling described. The expression pattern of Cx36 is consistent with a role for this connexin in mediating the observed coupling. Cx36 has not previously been shown to be developmentally regulated, and it would be interesting to probe the role of this connexin in development. Guldenagel et al. (2001) generated a homozygous Cx36 null mutant mouse, which had a normally developed retina. However, it is possible that upregulation of different connexins compensated for the absence of Cx36 in the knockout mouse during development, or that subtle effects on early development were not detected in the adult. The use of antisense ODNs and

electroporation to express dominant negative connexins provides powerful tools to further examine the role of individual connexins.

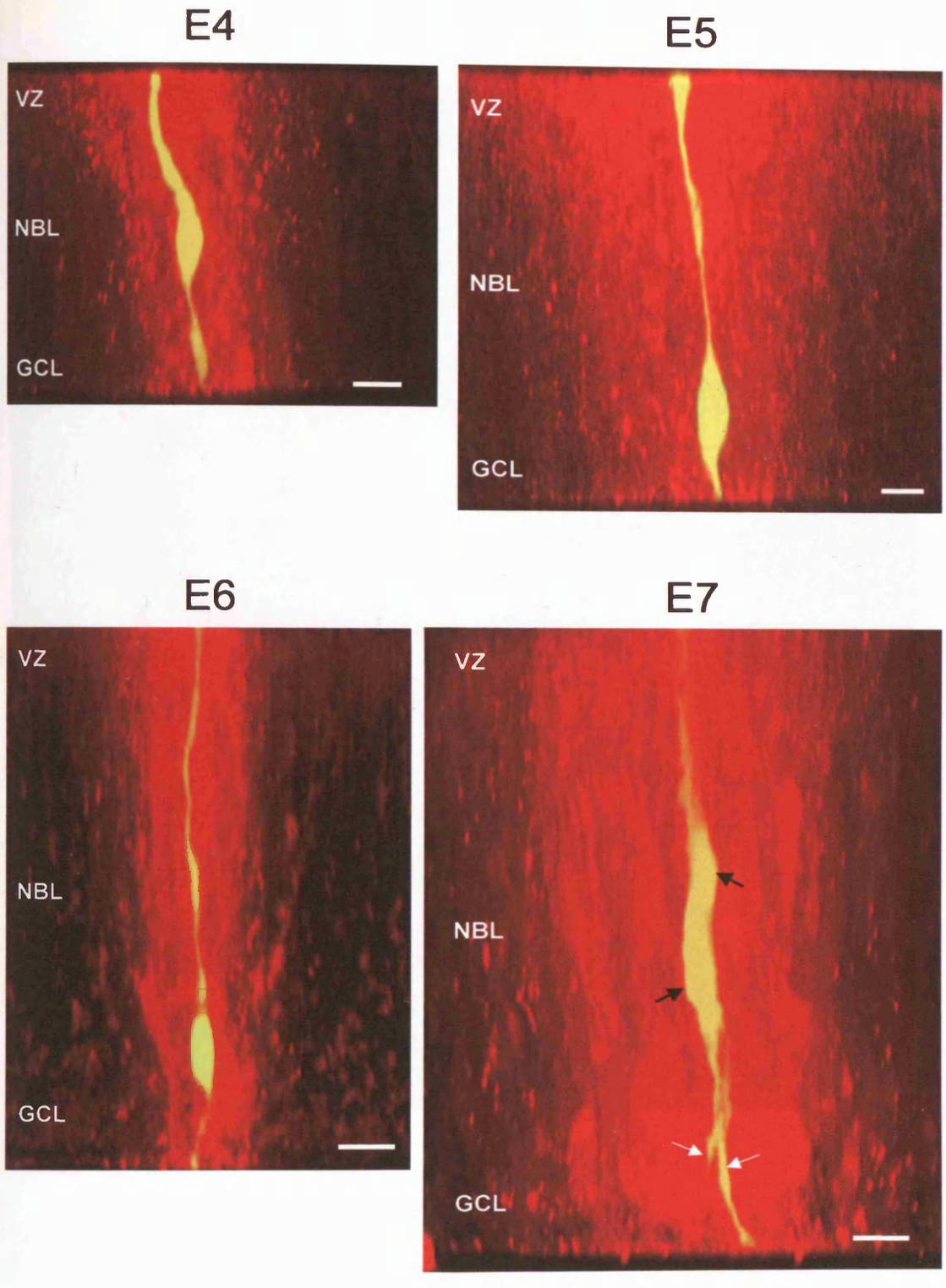

Figure 4.1 Cell coupling in the neural retina can be revealed by FITC and Neurobiotin injection. Cells in retinae from E4 to E7 have been labelled, and following imaging on a confocal microscope, the image stack rotated to produce an XZ-projection. The FITC injected cells are shown in yellow, whereas the Neurobiotin-coupled cells are shown in red. Cells are extensively coupled at all times. In the E7 retina shown, the processes of two cells were captured by the patch pipette. The two cell bodies are indicated by the black arrows, and the two separate processes are indicated by the white arrows.
VZ – ventricular zone; NBL – neuroblastic layer; GCL – ganglion cell layer.
Scalebars 10 µm.

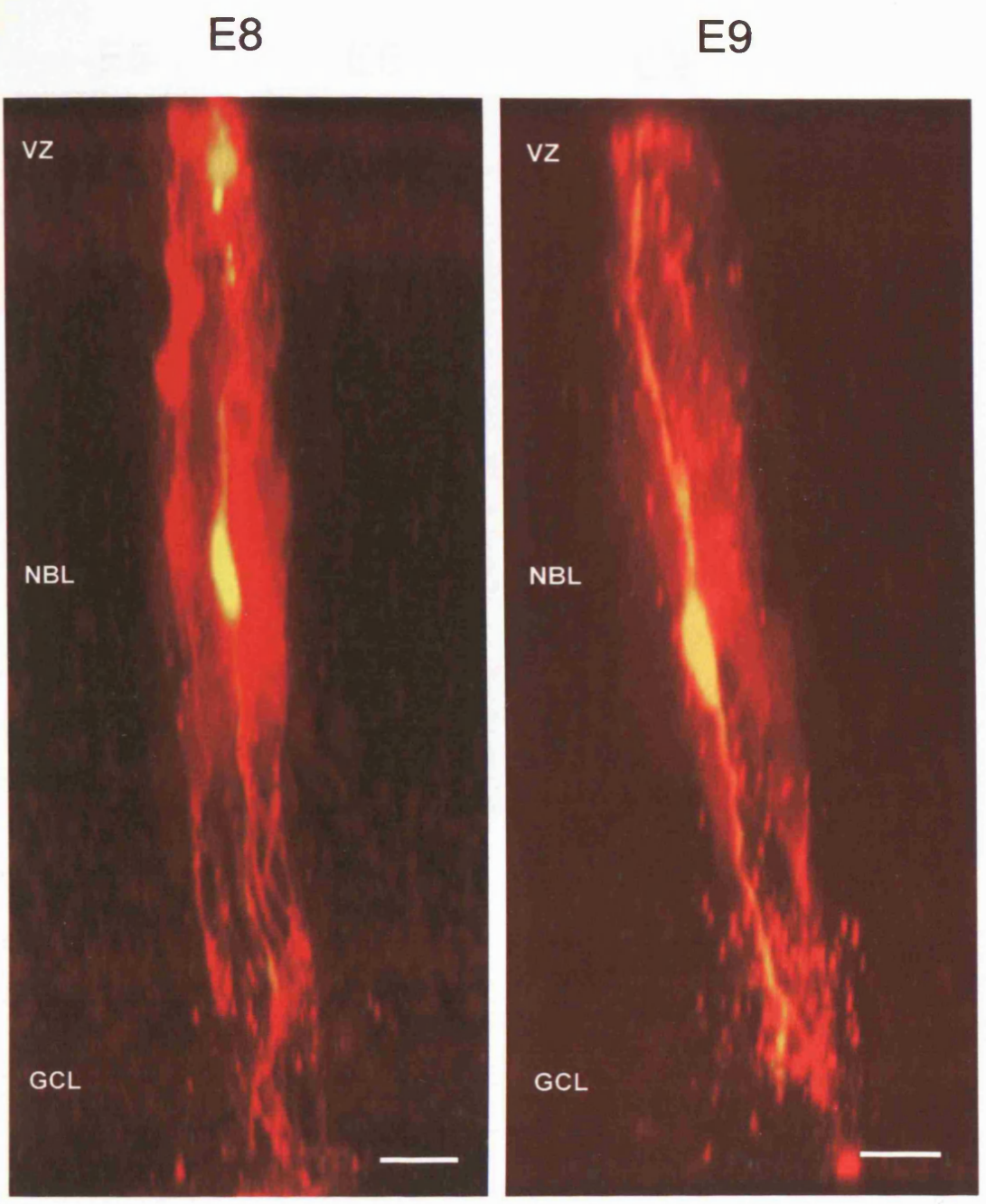

Figure 4.2 Cell coupling in the neural retina at E8-E9. Cells in E8 and E9 retinae labelled with FITC and NB, as described in the previous figure. In both preparations, the FITC injected cell (yellow) is surrounded by cells coupled to it, revealed by NB (red). All labelled cells have a bipolar morphology, extending processes from the ventricular surface through the GCL to the fibre layer. Scalebars 10 μm.

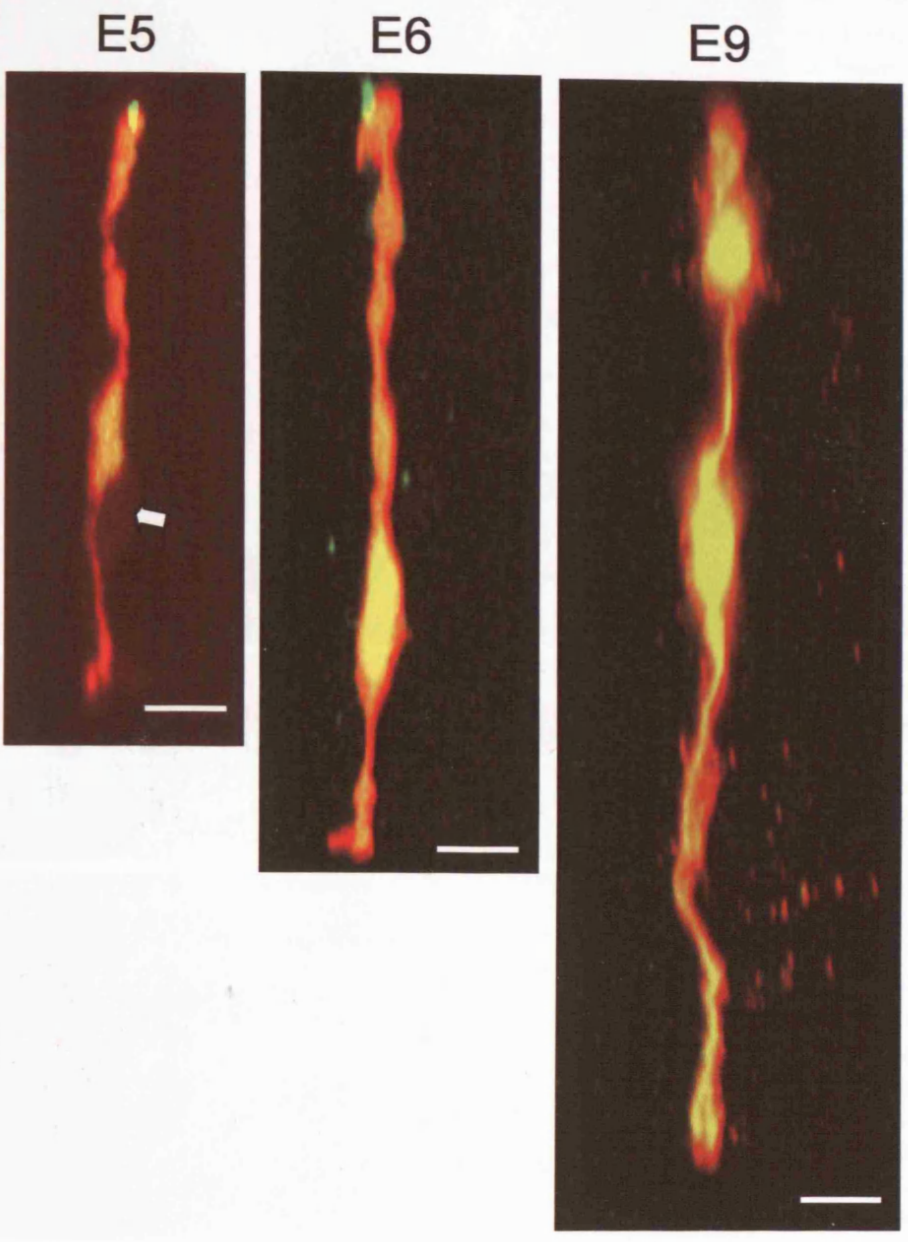

Figure 4.3 Dye-coupling is blocked by carbenoxolone.
CBX (100 μM) abolishes dye-coupling at all ages examined. In the E5 retina shown here, a single cell has been injected with FITC and NB in the presence of CBX (yellow cell body and processes). The white arrow indicates a single coupled cell that is faintly labelled with NB. In the E6 and E9 retinae shown, single cells have been labelled in the presence of CBX, and are not coupled to any other cells. Scale bars 10 μm.

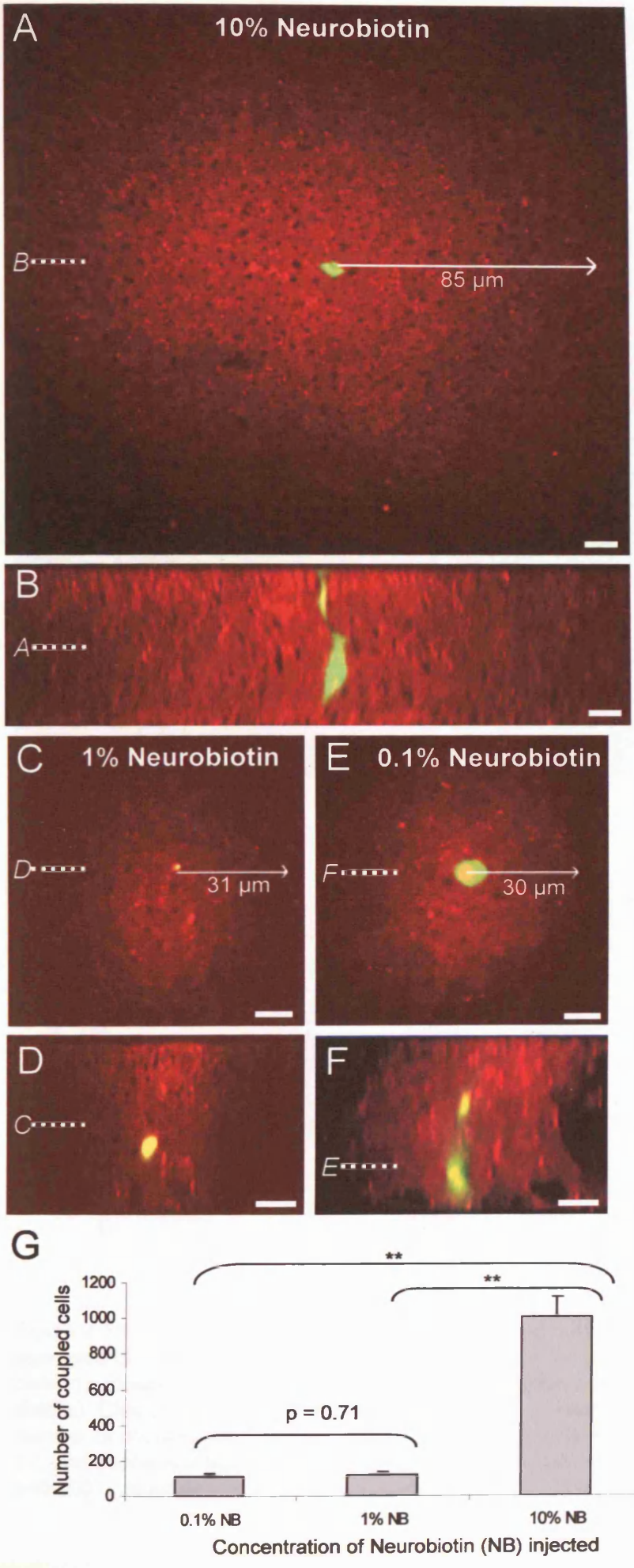

Figure 4.4 The extent of coupling revealed by injection of Neurobiotin is dependent on dye concentration. *A, C, E,* Single confocal XY-sections through clusters of coupled cells in E5 retinae, with 10%, 1% or 0.1% NB, respectively, in the patch pipette solution. *B, D, F,* Single XZ-sections of the same cells shown in *A, C, E.* The number of cells in a cluster was calculated by measuring the radius of the cluster as shown (see section 2.8.2 for further details). The levels of each section are shown by dashed lines and the letters in italics on each image. *G,* Histogram showing the mean number of coupled cells as a function of NB concentration. There is no difference in the number of coupled cells revealed by 0.1% (n=4) and 1% (n=14) NB, whereas injection of 10% NB (n=4) leads to a 10-fold increase in the extent of cell coupling revealed. Scale bars 10µm, ** $p<0.01$.

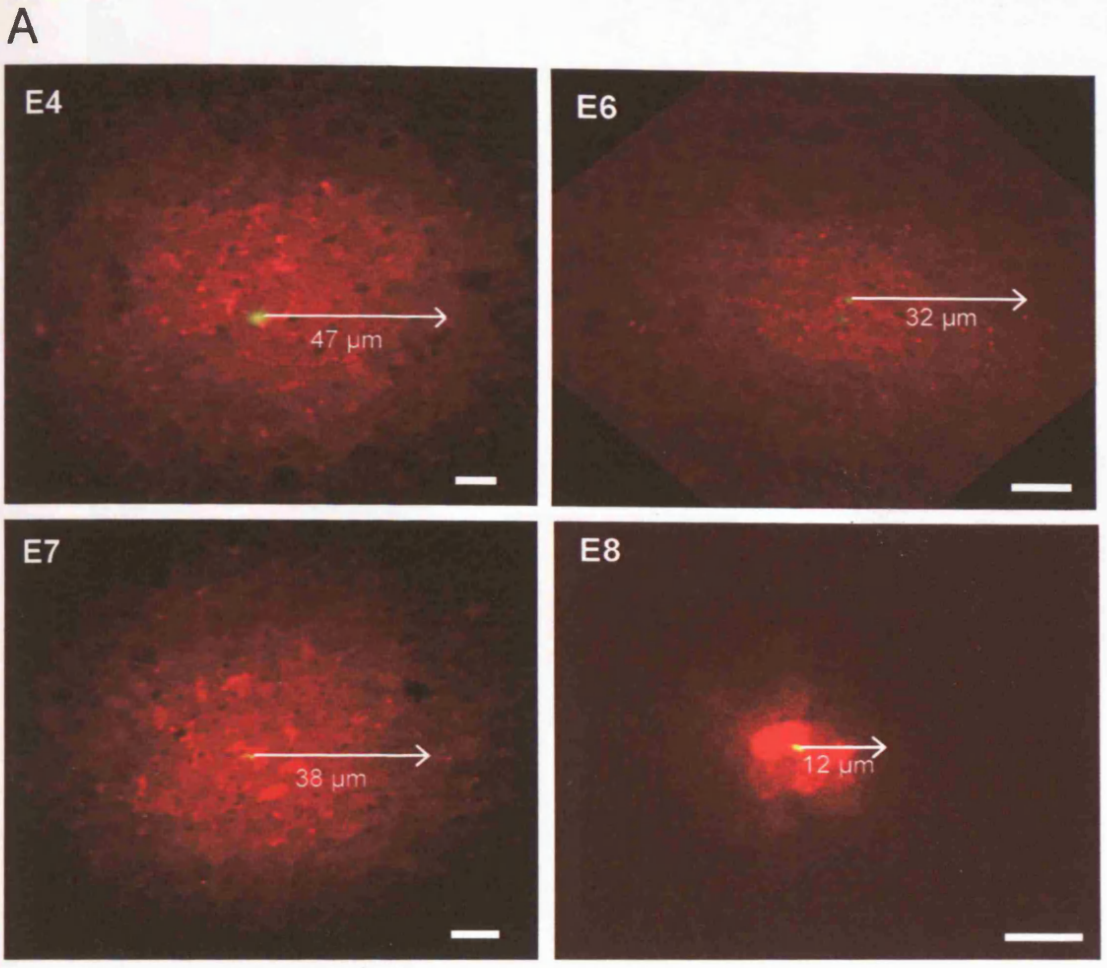

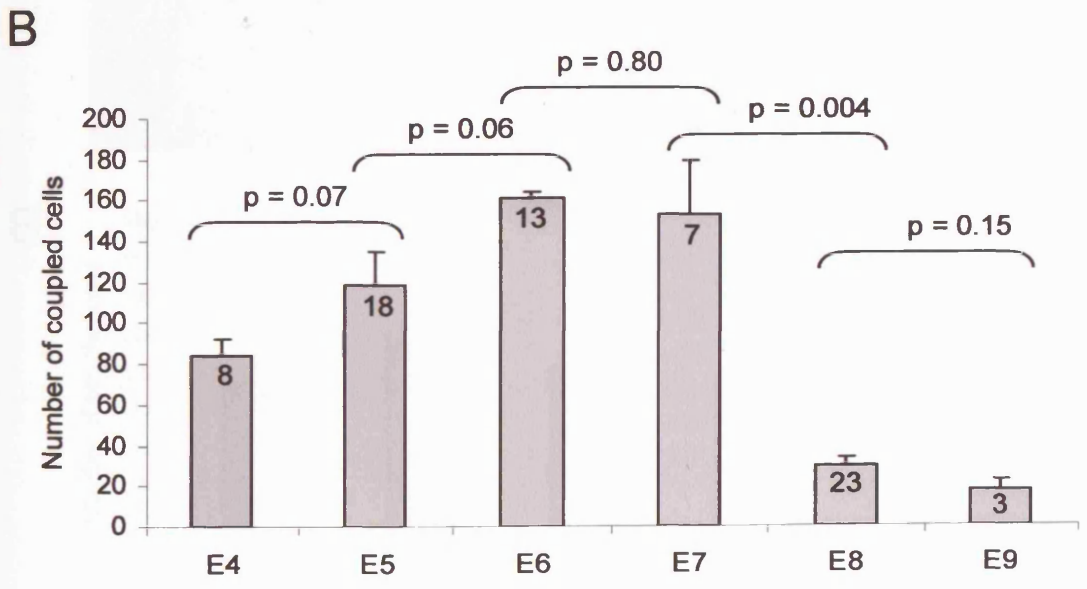

Figure 4.5 The extent of dye-coupling changes during retinal development. Typical examples of dye-spread at different times in development are shown in *A*. The number of cells in a cluster was calculated by measuring its radius (see section 2.8.2 for further details). Cluster radius is as shown on each image. *B*, Histogram showing the mean number of coupled cells from E4 to E9. The number of coupled cells increases from E4 to E7, and decreases significantly at E8-9 (E4-7 combined, compared to E8-9 combined, $p<0.0001$). Numbers on each bar indicate number of observations. Scale bars 10µm.

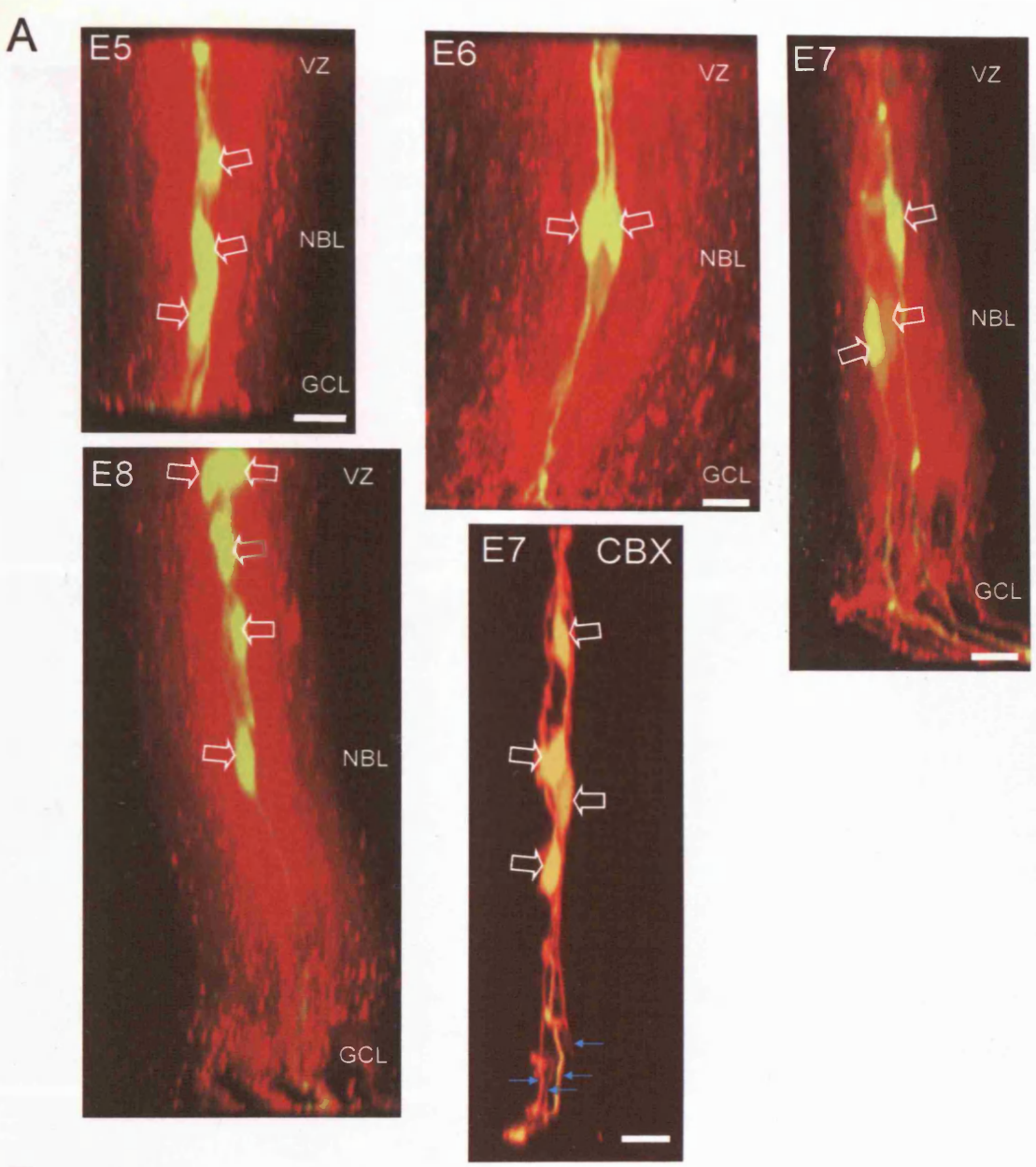

Figure 4.6 On occasion, more than one cell was injected with FITC and NB in a single patch-experiment. A, Typical examples of multiple cell labelling in retinae aged from E5 to E8 are shown. White arrows indicate the cell bodies in each image. An example of multiple labelling in the presence of CBX, where the individual cell processes (blue arrows) are more easily distinguishable, is shown. *B*, As illustrated in the histogram, the mean number of coupled cells did not increase when several cells were injected with FITC and NB. The number of observations in each case is indicated on the bars. Scale bars 10μm.

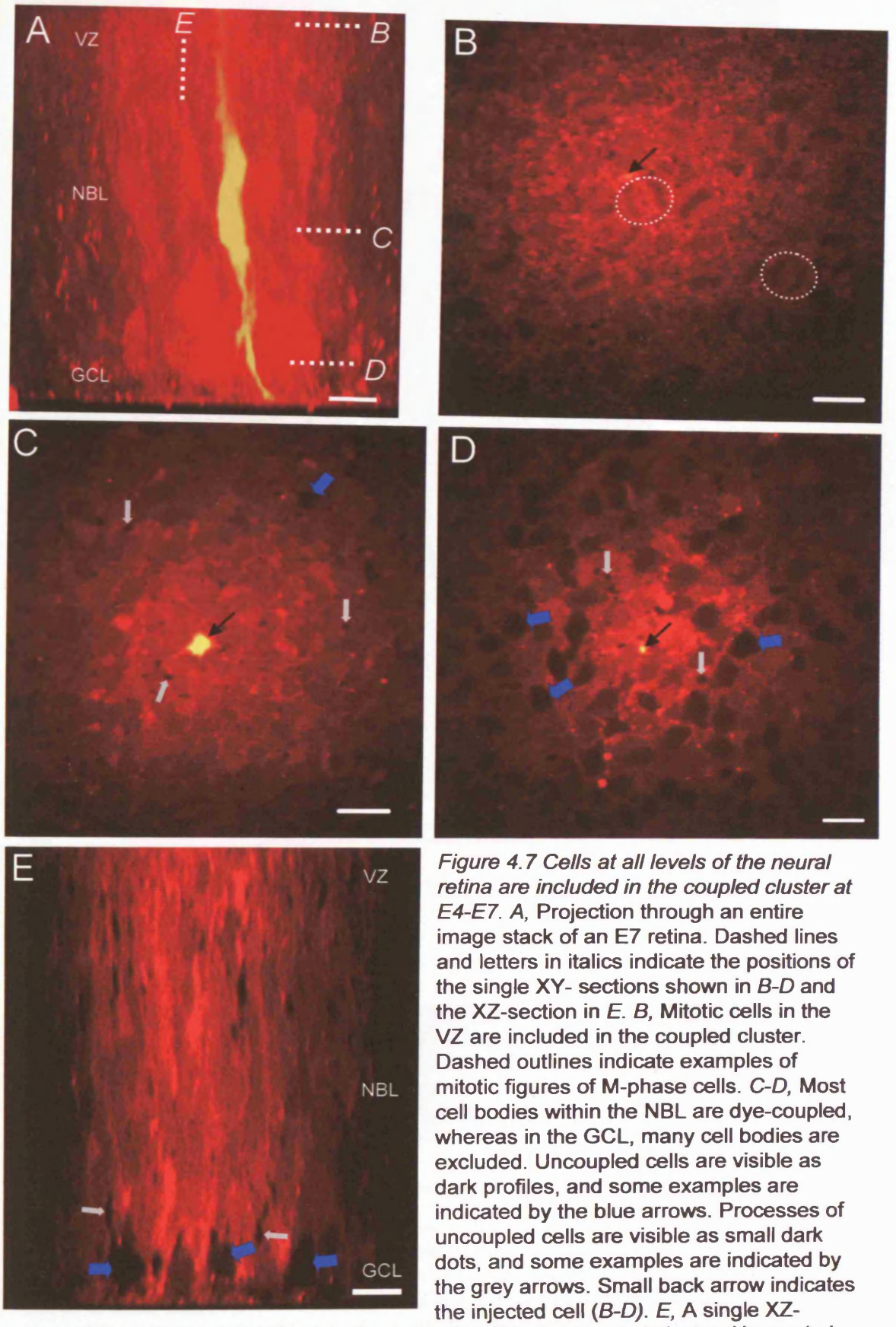

Figure 4.7 Cells at all levels of the neural retina are included in the coupled cluster at E4-E7. A, Projection through an entire image stack of an E7 retina. Dashed lines and letters in italics indicate the positions of the single XY- sections shown in *B-D* and the XZ-section in *E. B,* Mitotic cells in the VZ are included in the coupled cluster. Dashed outlines indicate examples of mitotic figures of M-phase cells. *C-D,* Most cell bodies within the NBL are dye-coupled, whereas in the GCL, many cell bodies are excluded. Uncoupled cells are visible as dark profiles, and some examples are indicated by the blue arrows. Processes of uncoupled cells are visible as small dark dots, and some examples are indicated by the grey arrows. Small back arrow indicates the injected cell (*B-D*). *E,* A single XZ-section illustrates the bipolar morphology of cells within the coupled cluster. Uncoupled cell bodies (blue arrows) are visible in the GCL. Some of the processes of these cells are indicated by grey arrows. Scale bars 10 µm.

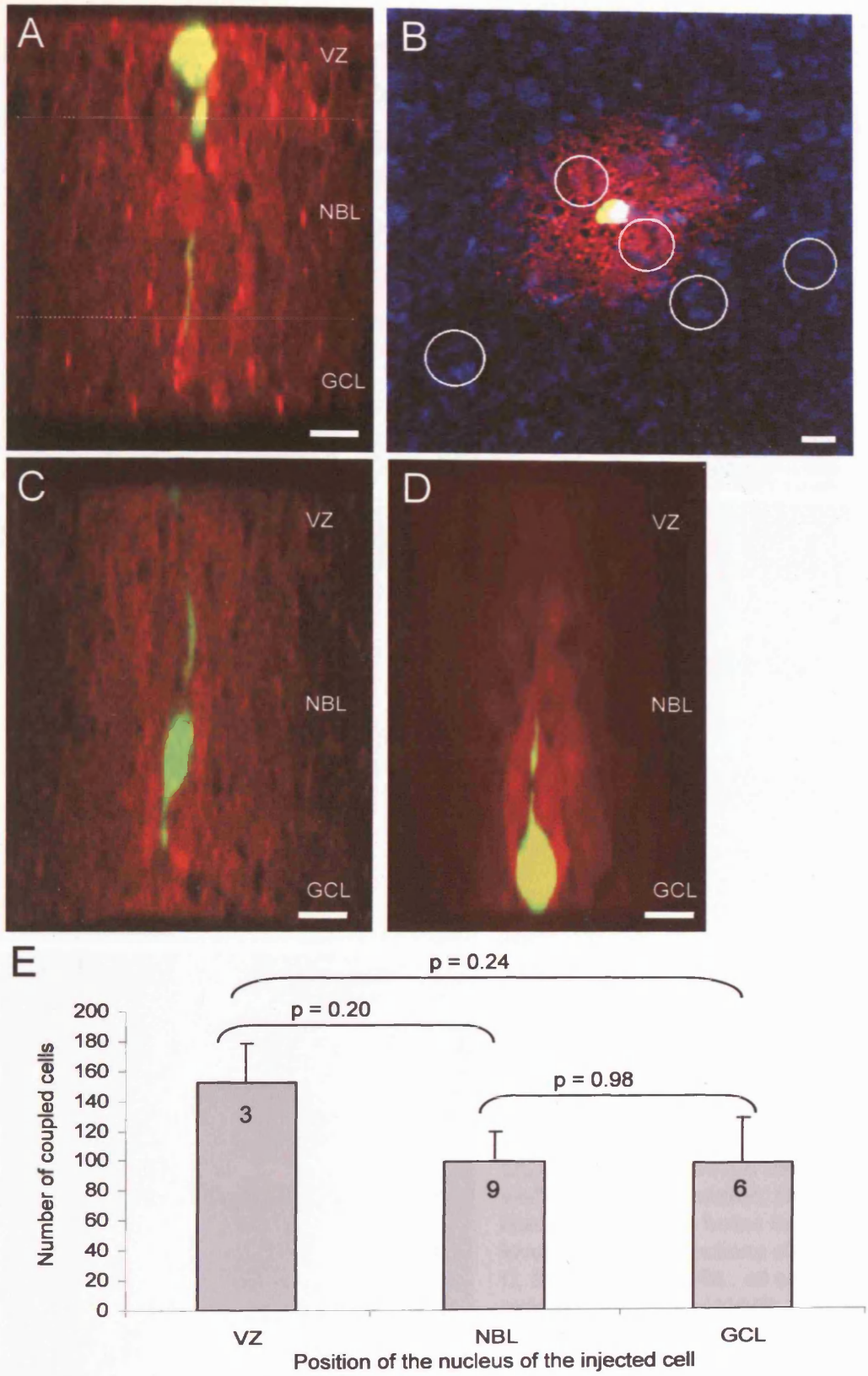

Figure 4.8 The extent of cell coupling varies with cell cycle stage. A-D, Typical examples of cells in E5 retinae, with the nucleus of the injected cell in the VZ (*A-B*), in the NBL (*C*), and in the GCL (*D*). *B,* a single XY-section of the cell shown in *A*, labelled with Hoechst 33243 to show mitotic profiles (examples are circled), confirming the location of the cell body of the injected cell within the VZ. *E,* Histogram showing the mean numbers of coupled cells for each nuclear location at E5. This number is greater for cells with their nuclei in the VZ than in other locations, although the difference is not significant. The dashed lines in *A* indicate how the retina was divided into sections for the classifications used in *E*. Numbers on each bar indicate number of observations. Scale bars 10 μm.

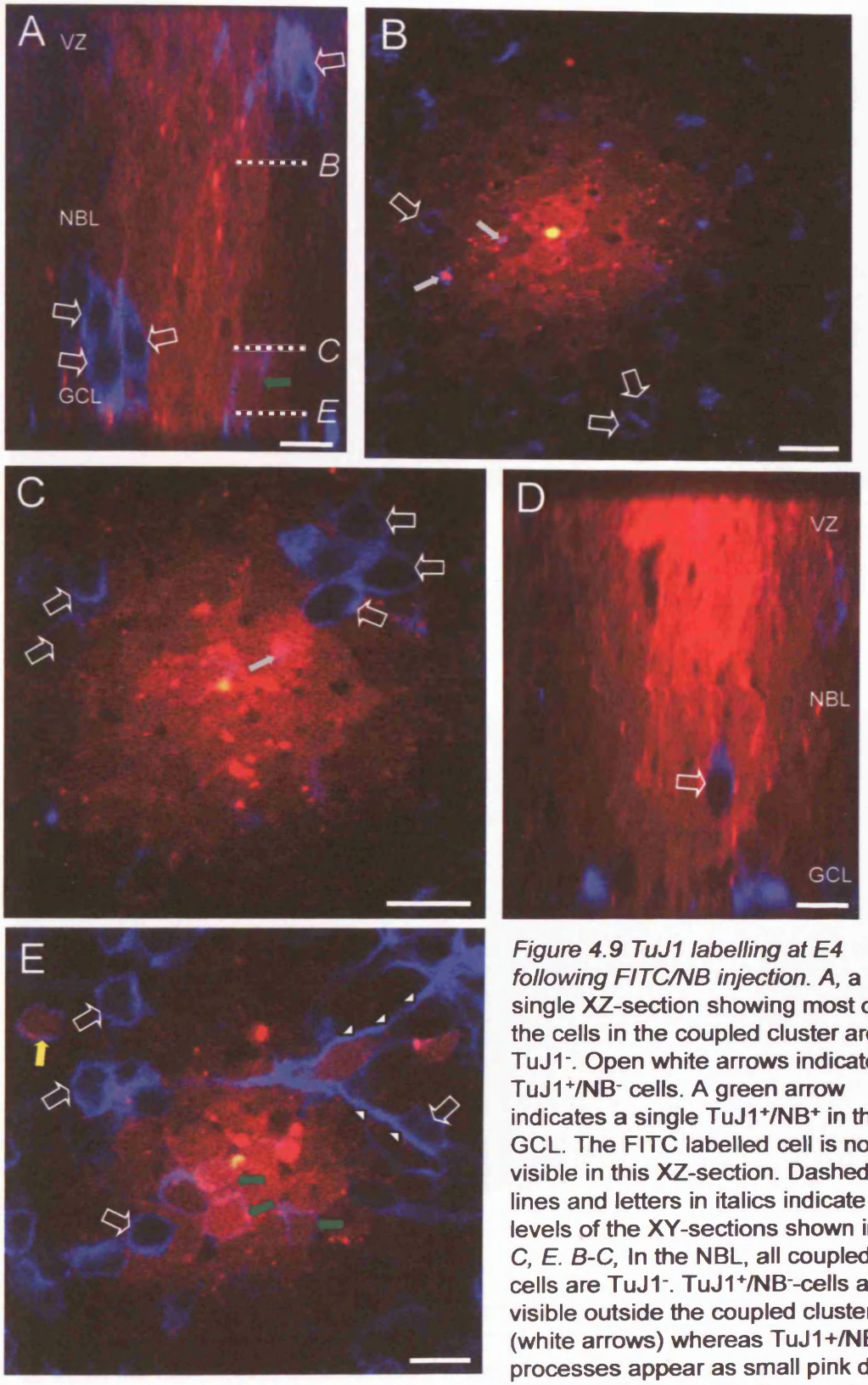

Figure 4.9 TuJ1 labelling at E4 following FITC/NB injection. A, a single XZ-section showing most of the cells in the coupled cluster are TuJ1$^-$. Open white arrows indicate TuJ1$^+$/NB$^-$ cells. A green arrow indicates a single TuJ1$^+$/NB$^+$ in the GCL. The FITC labelled cell is not visible in this XZ-section. Dashed lines and letters in italics indicate the levels of the XY-sections shown in *B, C, E. B-C,* In the NBL, all coupled cells are TuJ1$^-$. TuJ1$^+$/NB$^-$-cells are visible outside the coupled cluster (white arrows) whereas TuJ1+/NB+ processes appear as small pink dots (grey arrows). *D,* TuJ1$^+$/NB$^-$-cells are not restricted to regions outside the coupled cluster. This XZ-section shows a TuJ1$^+$/NB$^-$-cell (white arrow) surrounded by coupled cells. *E,* In the GCL, multiple TuJ1$^+$/NB$^-$ are visible (white arrows), and several cells within the coupled cluster are also TuJ1$^+$ (green arrows). In addition, a Tuj1$^+$ cell outside the coupled cluster is also NB$^+$ (yellow arrow). White arrowheads indicate GC axons. Scale bars 10 µm.

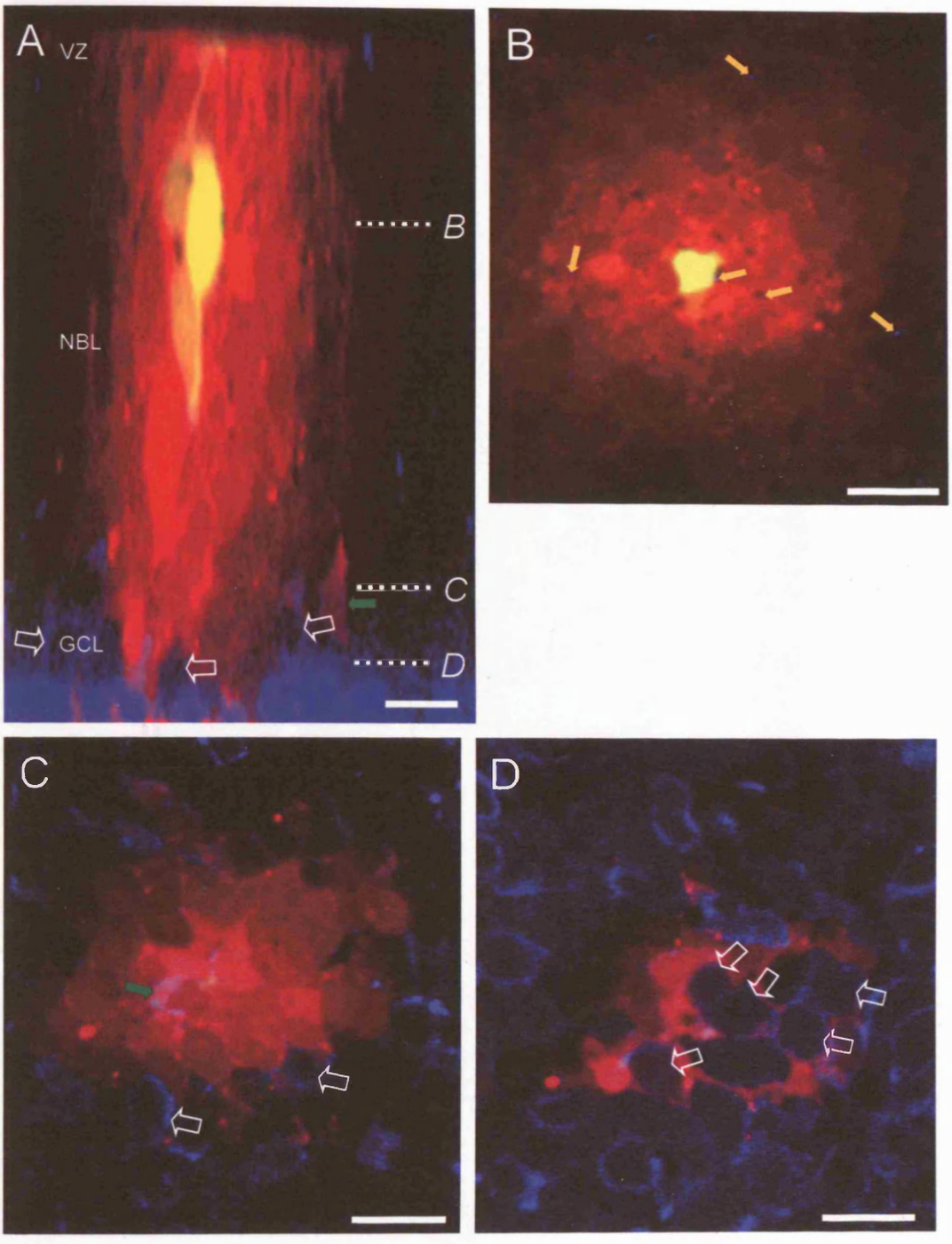

Figure 4.10 TuJ1 labelling at E6 following FITC/NB injection. A, a single XZ-section shows the cells in the coupled cluster to be TuJ1$^-$, and TuJ1$^+$-cells are restricted to near or within the GCL. Open white arrows indicate TuJ1$^+$/NB$^-$ cells. A green arrow indicates a single TuJ1$^+$/NB$^+$ cell near the GCL. Dashed lines and letters in italics indicate the levels of the XY-sections shown in *B-D. B,* In the NBL, all coupled cells are TuJ1$^-$, and no TuJ1$^+$-cells are visible at this stage in the NBL. Processes of TuJ1$^+$-cells appear as small blue dots (gold arrows), which are not NB-coupled. *C,* Near the GCL, TuJ1$^+$/NB$^-$ are visible outside the cluster (white arrows), and a single cell within the coupled cluster is also TuJ1$^+$ (green arrow). *D,* Tuj1$^+$ cells within the GCL are excluded from the NB coupling (white arrows). Scale bars 10 µm.

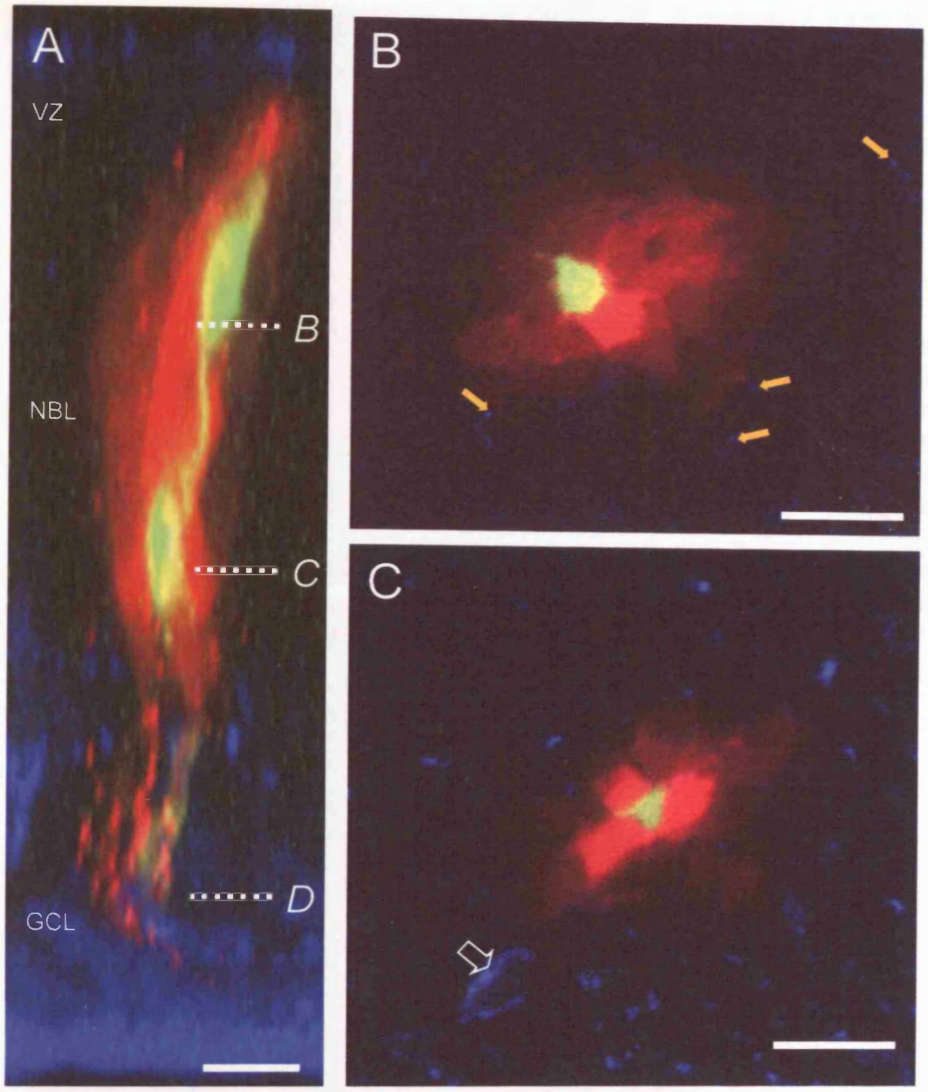

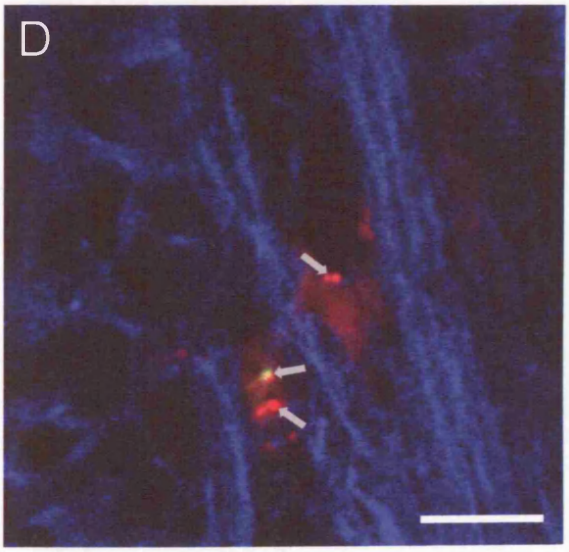

Figure 4.11 TuJ1 labelling at E8 following FITC/NB injection. A, a projection of ten XZ-sections shows the cells in the coupled cluster to be separated from the TuJ1+ cells in the putative INL and GCL. Dashed lines and letters in italics indicate the levels of the XY-sections shown in *B-D. B,* In the NBL, all coupled cells are $TuJ1^-$, and no $TuJ1^+$-cells are visible at this stage in the NBL. Processes of $TuJ1^+$-cells appear as small blue dots (gold arrows), which are not dye-coupled. *C,* A $TuJ1^+/NB^-$ cell is visible outside the cluster (white arrow). None of the dye-coupled cells are TuJ1+. *D,* Within the GCL, no NB-containing cell bodies are visible, although some NB^+ processes extend through the GCL (grey arrows). Scale bars 10 µm.

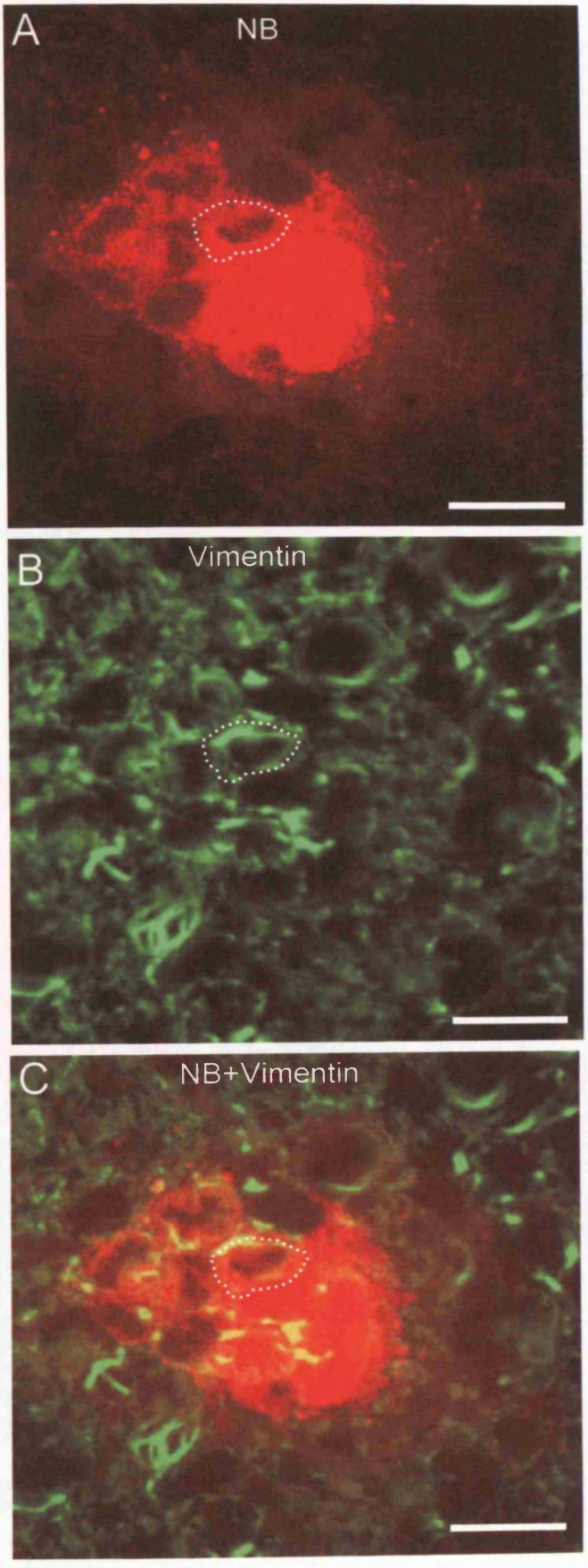

Figure 4.12 Vimentin labelling at E5 following FITC/NB injection. A-C, Images show the same single XY-section at the level of the VZ through the dye-coupled cluster of cells. *A,* NB-only image. Several cells are labeled with NB (red), and a single cell body is outlined (white dashed line). *B,* Vimentin-only image of the same confocal plane shown in *A*. The majority of cells in the VZ are vimentin$^+$ (green). *C,* Overlay of the red (NB) and green (vimentin) channels. Cells filled with NB also stain for vimentin (yellow), identifying them as progenitor cells. Scale bars 10 µm.

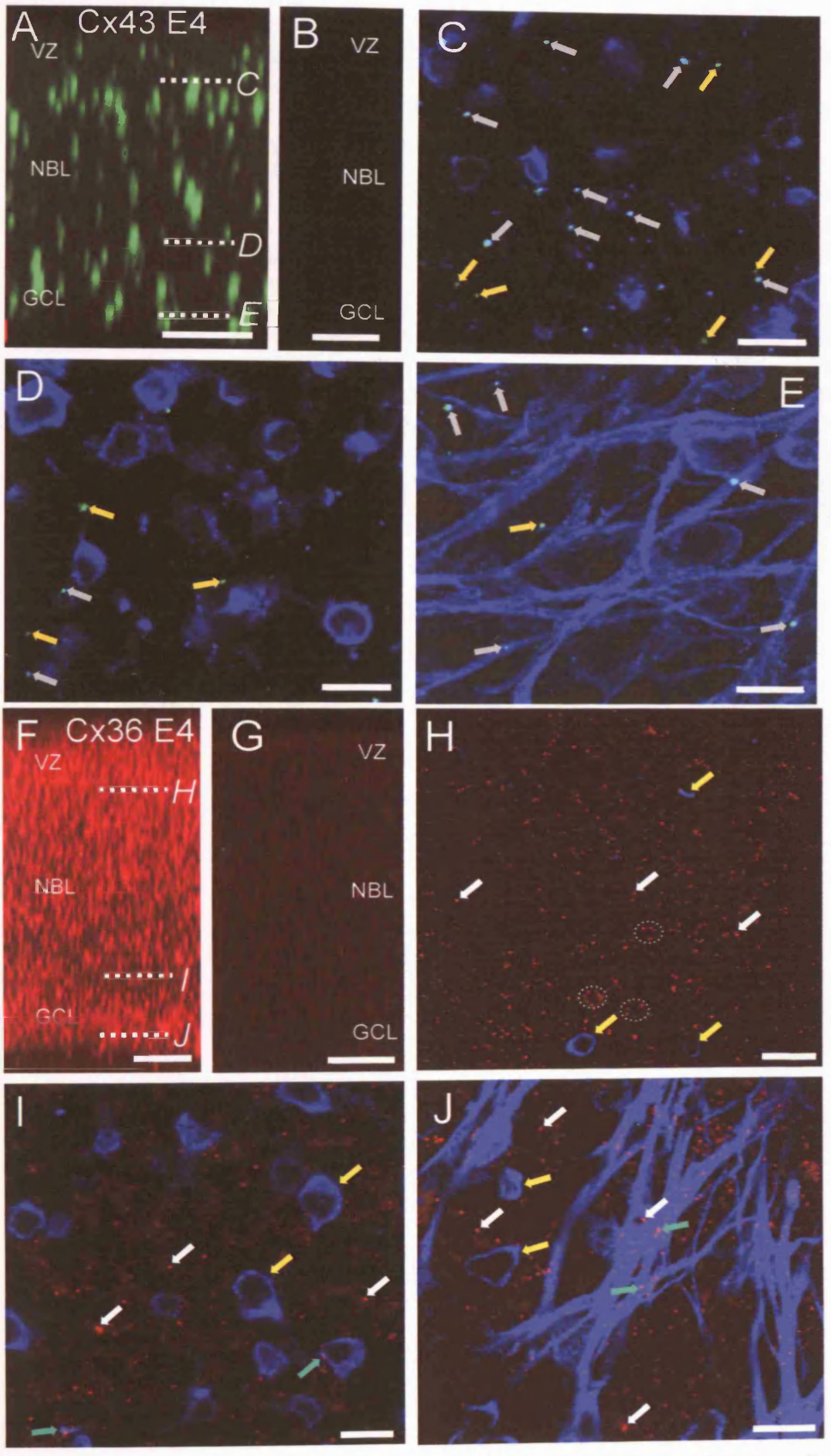

Figure 4.13. Double-labelling of Cx43 (green) / TuJ1 (blue), and Cx36 (red) / TuJ1(blue) in E4 retina (see figure legend on the following page).

Figure 4.13. Double-labelling of Cx43 (green) / TuJ1 (blue), and Cx36 (red) / TuJ1 (blue) in E4 retina.
A, An XZ-projection through the retina shows low levels of staining of large plaques of Cx43 throughout the E4 retina. *B,* Negative control, in which the primary antibody was omitted. *C,* Single XY-section at the level of the VZ shows puncta of Cx43 staining (gold arrows), some of which appear to be co-localised with TuJ1 (grey arrows). A similar pattern of staining is observed near the GCL (*D*) and in the fibre layer (*E*). *F,* An XZ-projection through the retina shows a high level of staining of small puncta of Cx36 throughout the E4 retina. *G,* Negative control, in which the primary antibody was omitted. *H,* Single XY-section just below the the level of the VZ shows small puncta of Cx36 staining (white arrows), and processes of $TuJ1^+$ cells (yellow arrows) which do not express Cx36. The pattern of Cx36 staining appears to outline the profiles of $TuJ1^-$-processes (dashed outlines). A similar pattern of staining is observed near the GCL (*I*) and in the fibre layer (*J*). In addition, some $TuJ1^+$ cells (*I*) and GC fibres (*J*) also express Cx36 (green arrows).Dashed lines and letters in italics in *A* and *F* indicate the levels of the XY-sections shown in *C-E* and *H-J*, respectively. Scale bars 10 µm.

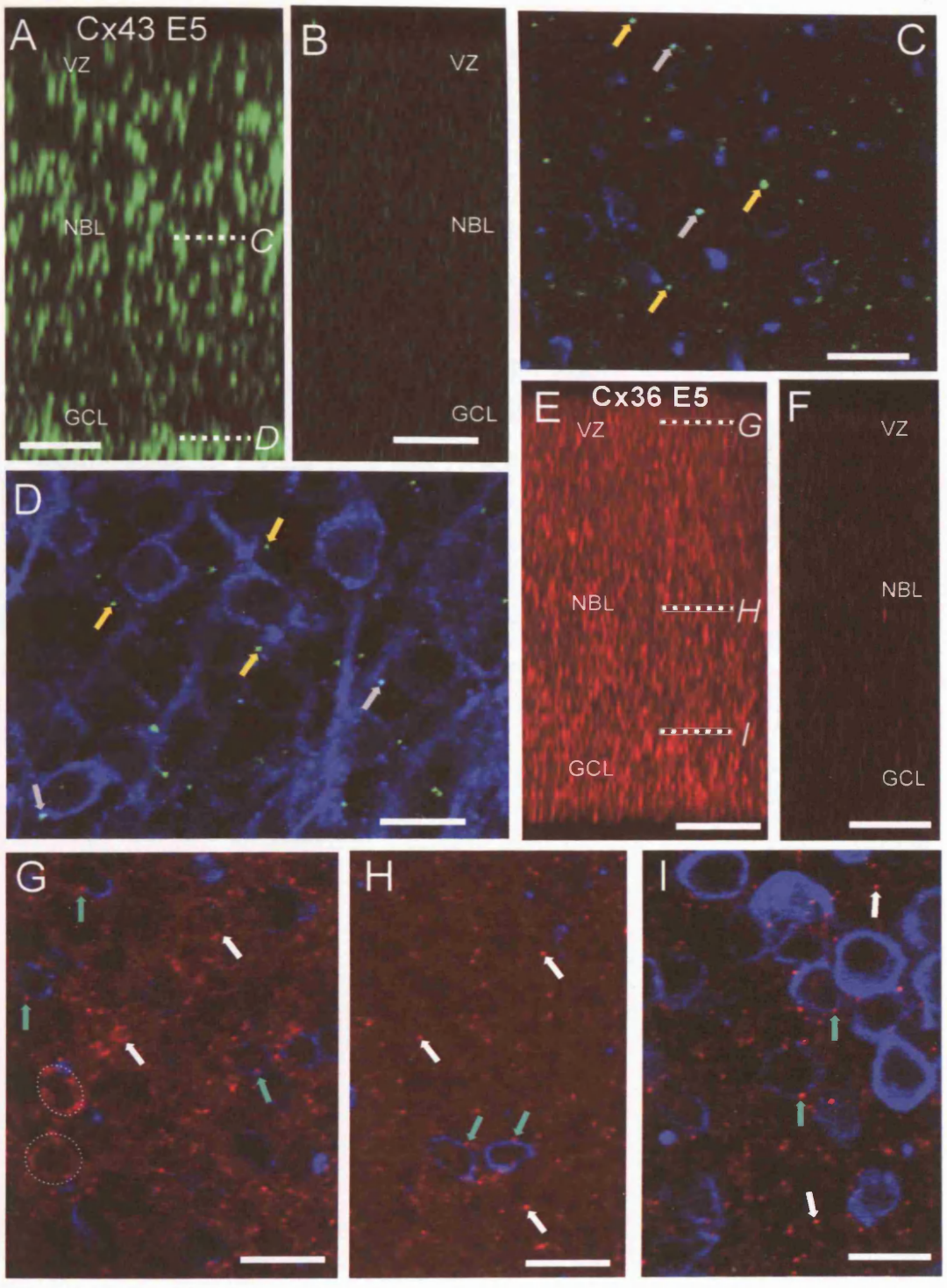

Figure 4.14. Double-labelling of Cx43 (green) / TuJ1 (blue), and Cx36 (red) / TuJ1 (blue) in E5 retina. A, An XZ-projection through the retina shows a moderate level staining of large plaques of Cx43 throughout the E5 retina. *B,* Negative control, in which the primary antibody was omitted. *C,* Single XY-section at the level of the NBL shows puncta of Cx43 staining (gold arrows), some of which are co-localised with TuJ1 (grey arrows). A similar pattern of staining is observed in the GCL (*D*). *E,* An XZ-projection through the retina shows a high level of staining of small puncta of Cx36 throughout the E5 retina. *F,* Negative control, in which the primary antibody was omitted. *G,* Single XY-section near the surface of the VZ shows small puncta of Cx36 staining (white arrows), which outline cell bodies and processes of both TuJ1$^+$ (green arrows) and TuJ1$^-$ cells (white arrows, dashed outline). A similar pattern of staining is observed in the NBL (*H*) and near the GCL (*I*). Dashed lines and letters in italics in *A* and *E* indicate the levels of the XY-sections shown in *C-D* and *G-I*, respectively. Scale bars 10 µm.

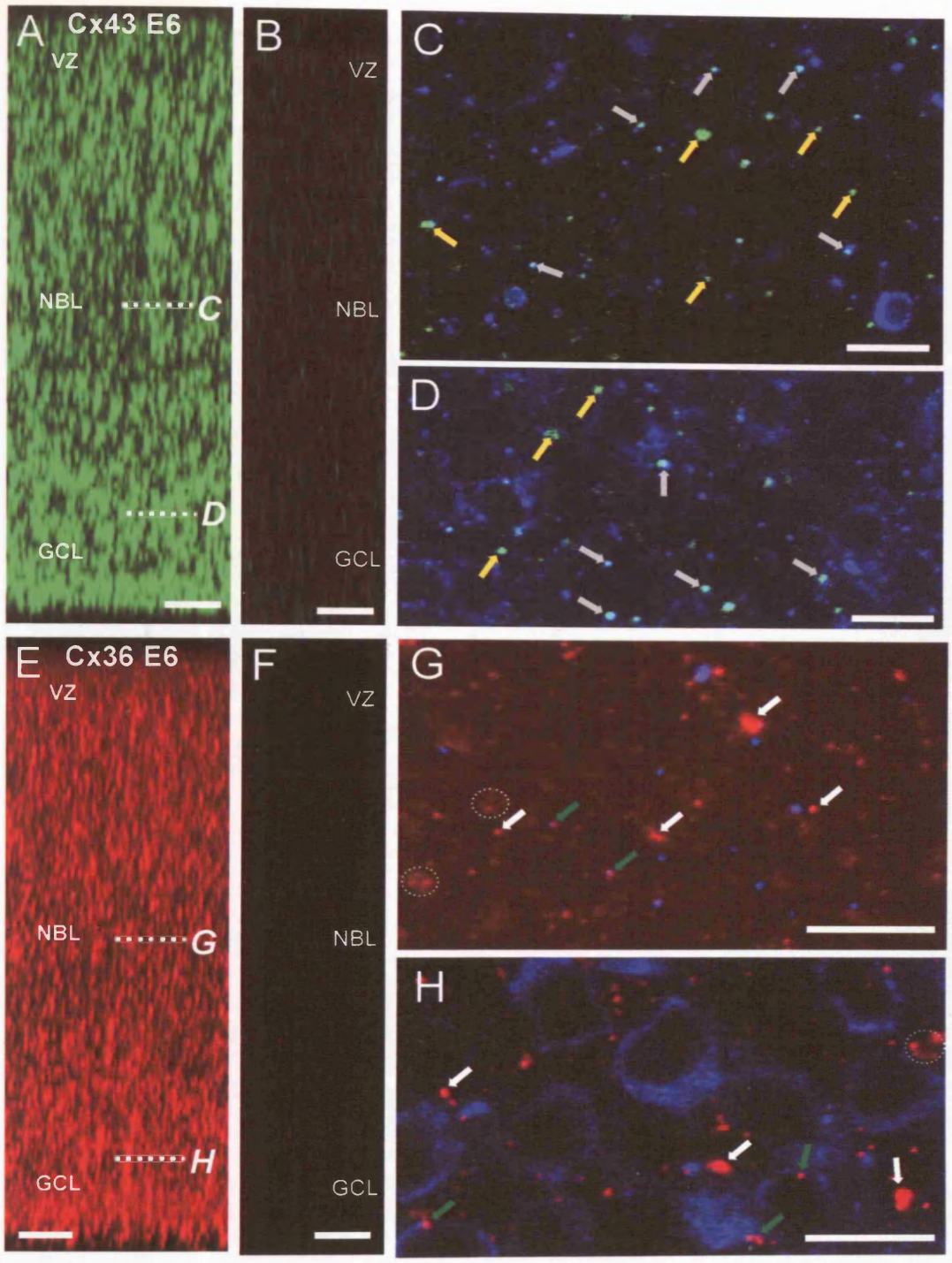

Figure 4.15. Double-labelling of Cx43 (green) / TuJ1 (blue), and Cx36 (red) / TuJ1 (blue) in E6 retina. A, An XZ-projection through the retina shows a high level of punctate staining of Cx43 throughout the E6 retina. *B,* Negative control, in which the primary antibody was omitted. *C,* Single XY-section at the level of the NBL shows puncta of Cx43 staining (gold arrows), some of which are co-localised with TuJ1 (grey arrows). A similar pattern of staining is observed in the GCL (*D*). *E,* An XZ-projection through the retina shows a high level of staining of small puncta of Cx36 throughout the E6 retina. *F,* Negative control, in which the primary antibody was omitted. *G,* Single XY-section at the level of the NBL shows small puncta of Cx36 staining (white arrows), some of which appear to outline cell processes (dashed outline), and some of which are co-localised with TuJ1 (green arrows). A similar pattern of staining is observed in the GCL (*H*). Dashed lines and letters in italics in *A* and *E* indicate the levels of the XY-sections shown in *C-D* and *G-H*, respectively. Scale bars 10 µm.

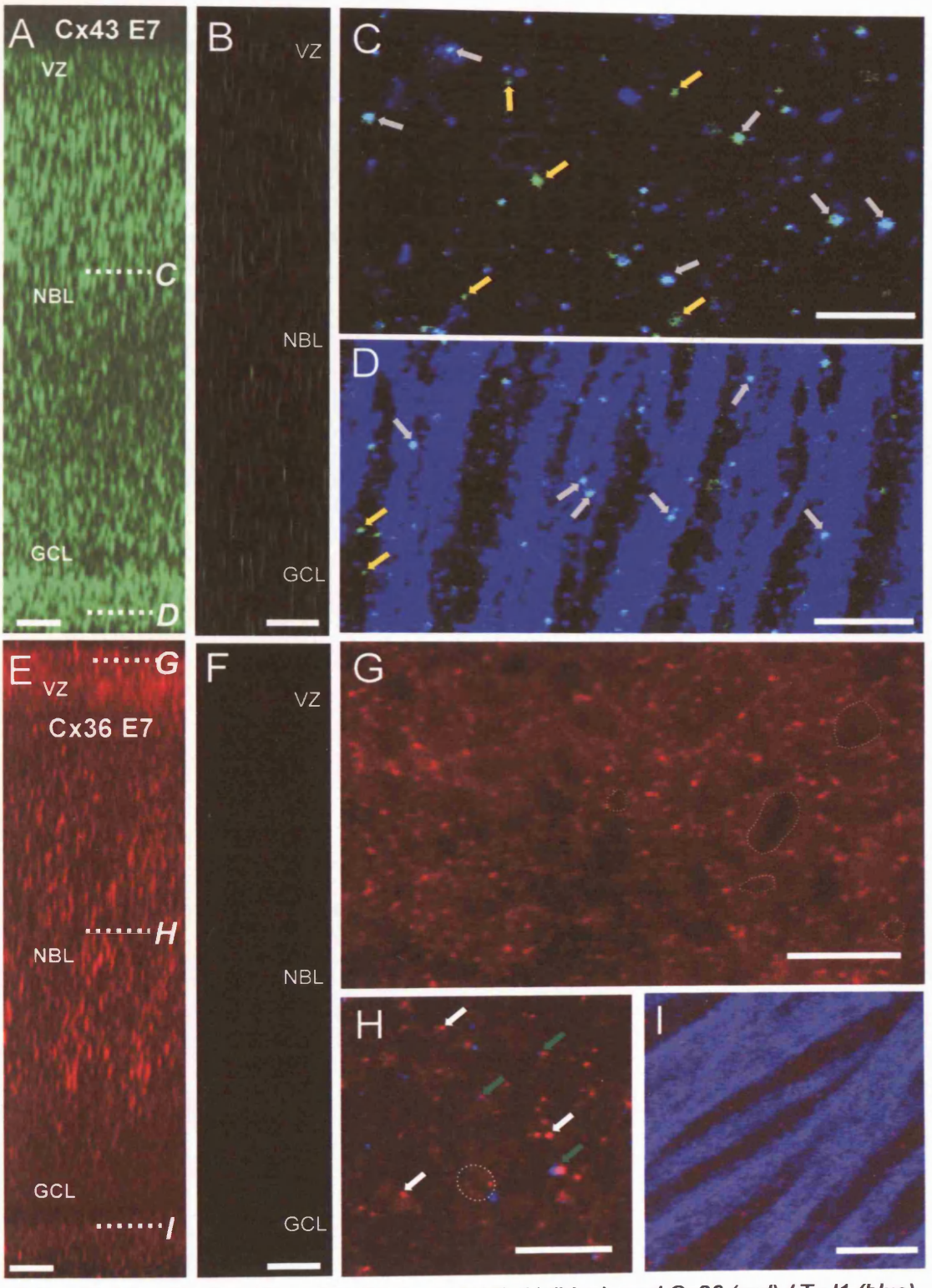

Figure 4.16 Double-labelling of Cx43 (green) / TuJ1 (blue), and Cx36 (red) / TuJ1 (blue) in E7 retina (see figure legend on the following page).

Figure 4.16 Double-labelling of Cx43 (green) / TuJ1 (blue), and Cx36 (red) / TuJ1 (blue) in E7 retina.
A, An XZ-projection through the retina shows a high level of punctate staining of Cx43 throughout the VZ and the upper half of the NBL at E7. Expression is reduced in the lower half of the NBL and the GCL, but high in the fibre layer. *B,* Negative control, in which the primary antibody was omitted. *C,* Single XY-section at the level of the NBL shows puncta of Cx43 staining (gold arrows), some of which appear to be co-localised with TuJ1 (grey arrows). A similar pattern of staining is observed in the fibre layer (*D*). *E,* An XZ-projection through the retina shows a moderate level of staining of small puncta of Cx36 in the VZ and NBL of the E7 retina, and low levels of staining in the GCL and fibre layer. *F,* Negative control, in which the primary antibody was omitted. *G,* Single XY-section at the level of the ventricular surface shows small puncta of Cx36 staining which appear to outline cell bodies and processes (dashed outlines). TuJ1 expression is absent from the ventricular surface at this time. *H,* In the NBL small puncta of Cx36 are stained (white arrows), some of which appear to outline cell processes (dashed outline), and some of which appear to be co-localised with TuJ1 (green arrows). *I,* Cx36 staining is absent from the GC fibre layer. Dashed lines and letters in italics in *A* and *E* indicate the levels of the XY-sections shown in *C-D* and *G-I*, respectively.
Scale bars 10 μm.

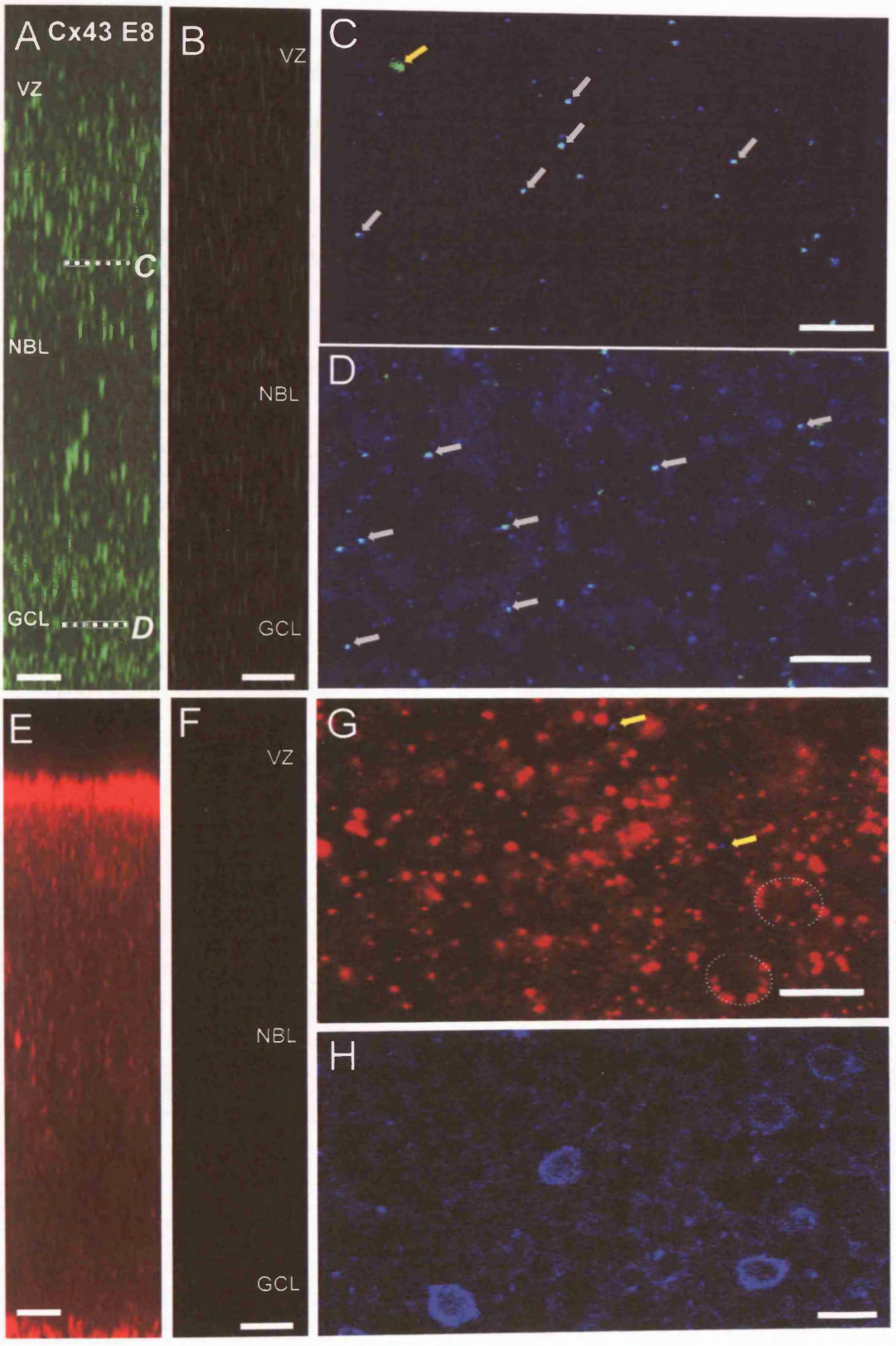

Figure 4.17 Double-labelling of Cx43 (green) / TuJ1(blue), and Cx36 (red) / TuJ1 (blue) in E8 retina (see figure legend on the following page).

Figure 4.17 Double-labelling of Cx43 (green) / TuJ1(blue), and Cx36 (red) / TuJ1 (blue) in E8 retina.
A, An XZ-projection through the retina shows a moderate level of staining of Cx43 throughout most of the E8 retina, except the lower part of the NBL, where expression is low. *B,* Negative control, in which the primary antibody was omitted. *C,* Single XY-section at the level of the NBL shows puncta of Cx43 staining co-localised with TuJ1 (grey arrows), and a single plaque of Cx43 which does not overlap with TuJ1 expression (gold arrow). *D,* In the GCL, all CX43 puncta appear co-localised with TuJ1 (grey arrows).
E, An XZ-projection through the retina shows a high level of Cx36 staining restricted to the VZ of the E8 retina, and a low level of staining in the NBL. *F,* Negative control, in which the primary antibody was omitted. *G,* Single XY-section at the level of the ventricular surface shows large plaques of Cx36 staining, some of which appear to outline cell bodies and processes (dashed outlines). Sparse TuJ1-expressing processes are visible (yellow arrows) which do not express Cx36. Cx36 staining is absent from the GCL at this time(*H*). Dashed lines and letters in italics in *A* and *E* indicate the levels of the XY-sections shown in *C-D* and *G-H*, respectively. Scale bars 10 µm.

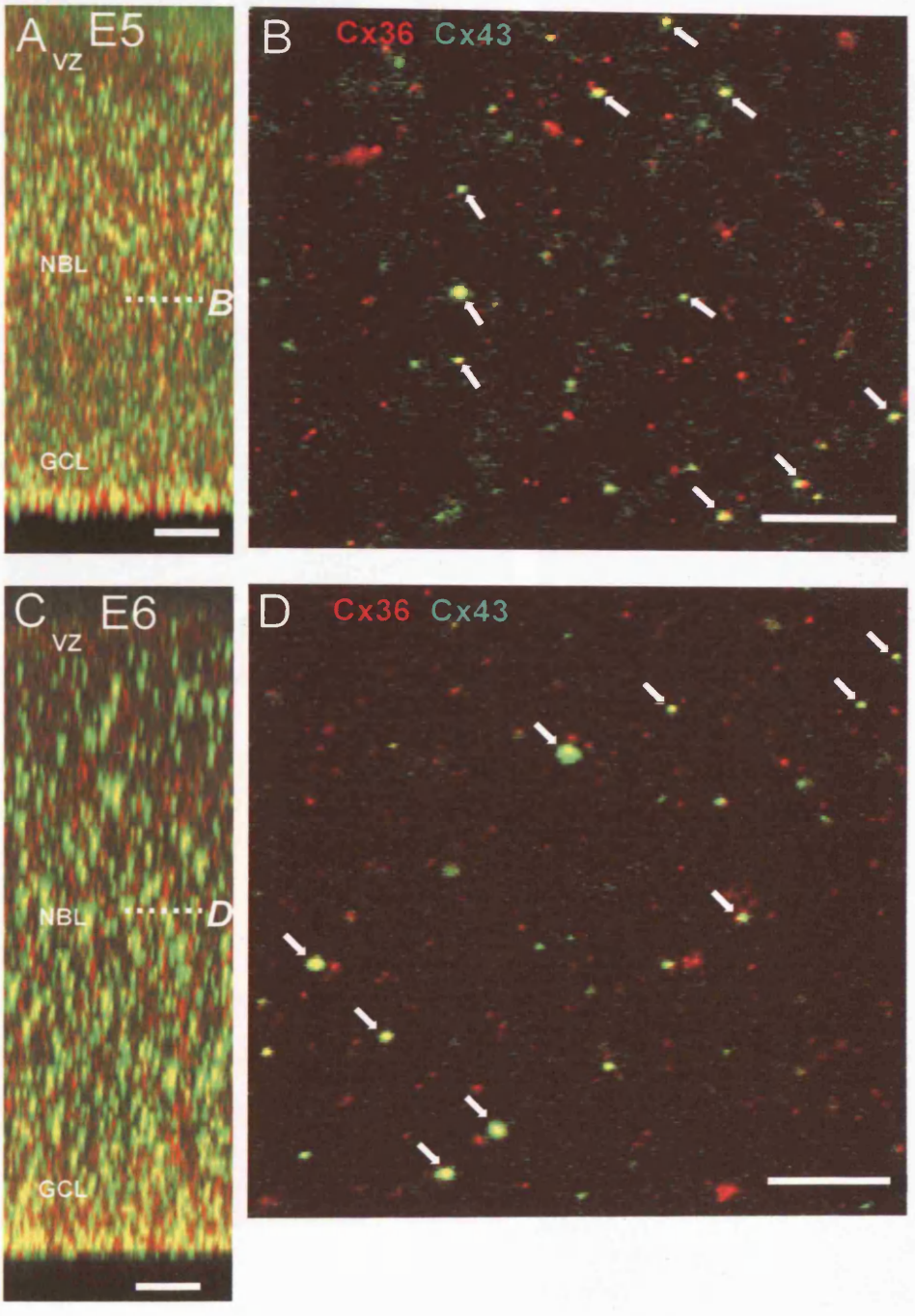

Figure 4.18 Double-labelling of Cx43 (green) and Cx36 (red) in E5 and E6 retina. Simultaneous labelling of Cx43 and Cx36 shows extensive overlap between the expression of these connexins. *A,* Projection through an E5 retina. *B,* single XY-section at the level of the NBL, as indicated in *A*. *C,* Projection through an E6 retina. *D,* single XY-section at the level of the NBL, as indicated in *C*. White arrows indicate examples of co-localised expression of Cx36 and Cx43, suggesting formation of heteromeric or heterotypic gap junctions. Scale bars 10 μm.

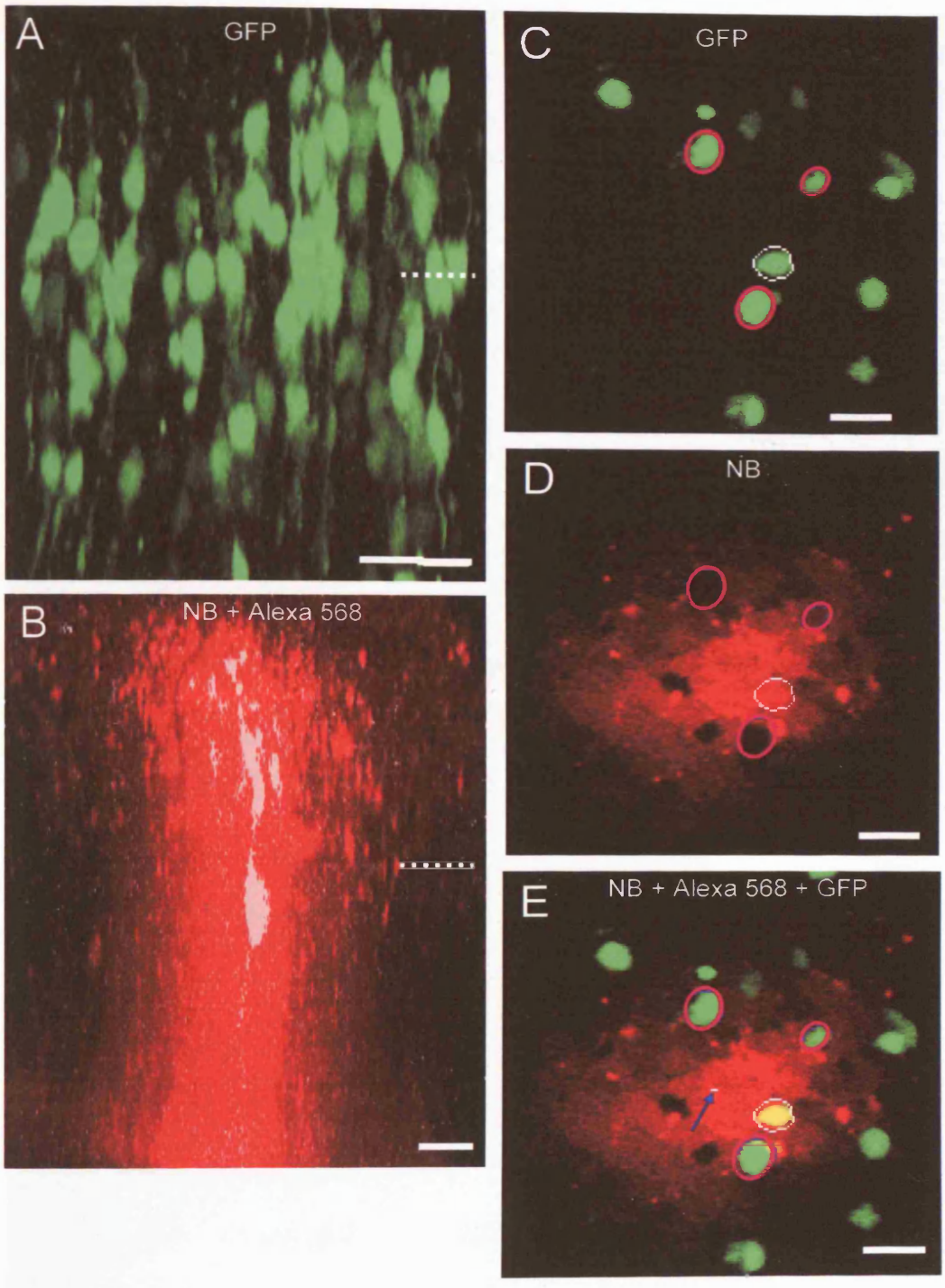

Figure 4.19 Dye-coupling in dnCx43-expressing retina. *A*, Electroporation with dnCx43 in E5 retina leads to its expression along with GFP in cells with bipolar, progenitor morphology. *B*, Injection with NB and Alexa 568 in the retina shown in *A* shows a coupled cluster similar to those seen in control preparations. Dashed lines in *A* and *B* indicate the level of the XY-sections shown in *C-E*. *C-E*, Most GFP^+ cells adjacent to dye-coupled cells are excluded from the coupling (circled in violet), although one GFP^+ cell is also NB^+ (circled in white). Blue arrow in *E* indicates the Alexa-labelled process of the injected cell.

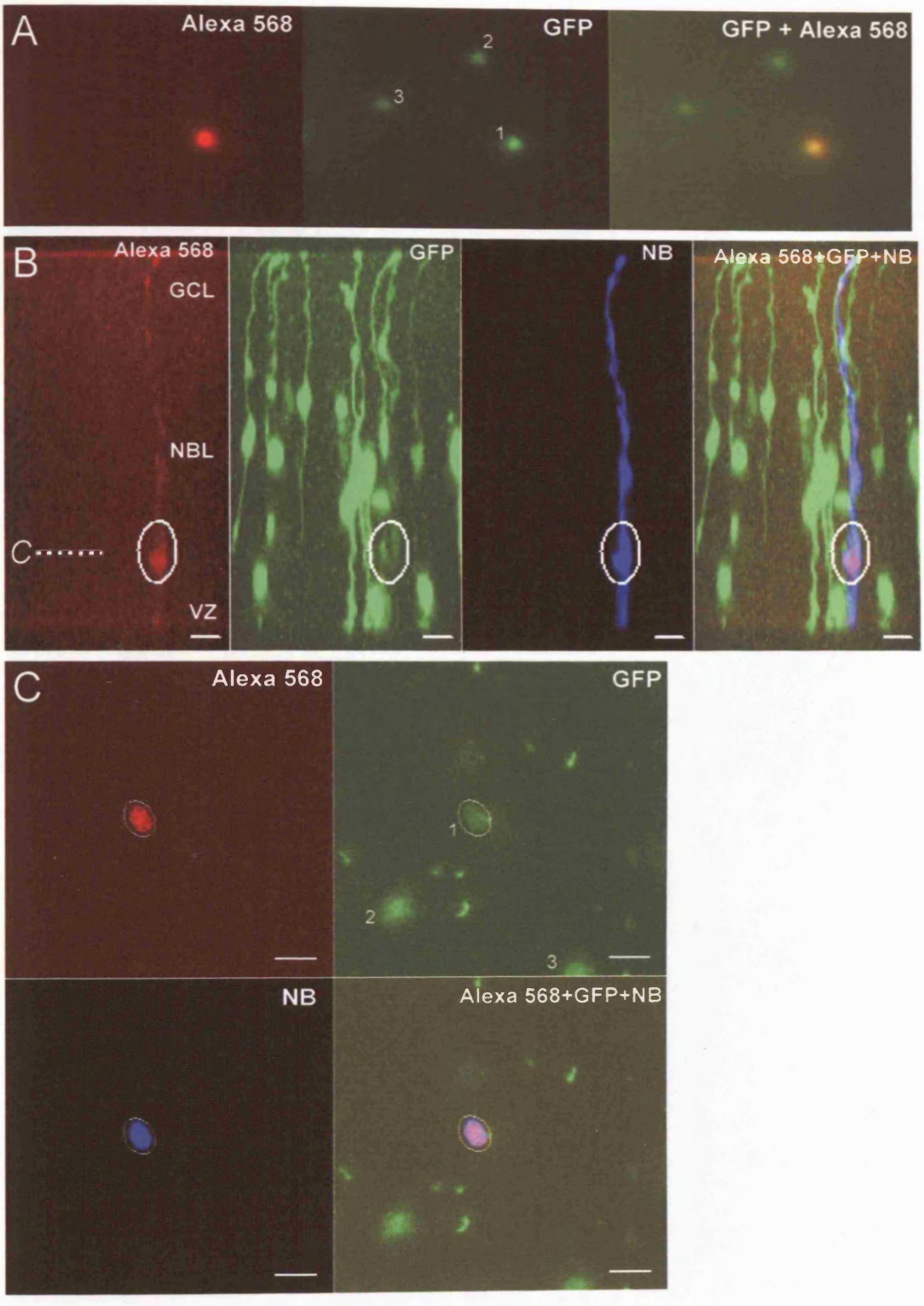

Figure 4.20 Fluorescence-guided patching of dnCx43-expressing cells. A, Using GFP expression for fluorescence-guided patchclamping, a dnCx43-expressing cell was injected with NB and Alexa 568 dextran. The images in *A* were captured using a CCD-camera on the microscope at the time of the experiment. *B,* Confocal XZ-projection images of the cell shown in *A* shows an absence of coupling to any neighbouring cells. *C,* single confocal XY-sections of each channel confirm the overlap between the Alexa 568, GFP and NB. The injected cell body is outlined, and the adjacent GFP^+/NB^--cells are numbered to show how they correspond to those seen in *A*. Scale bars 10 µm.

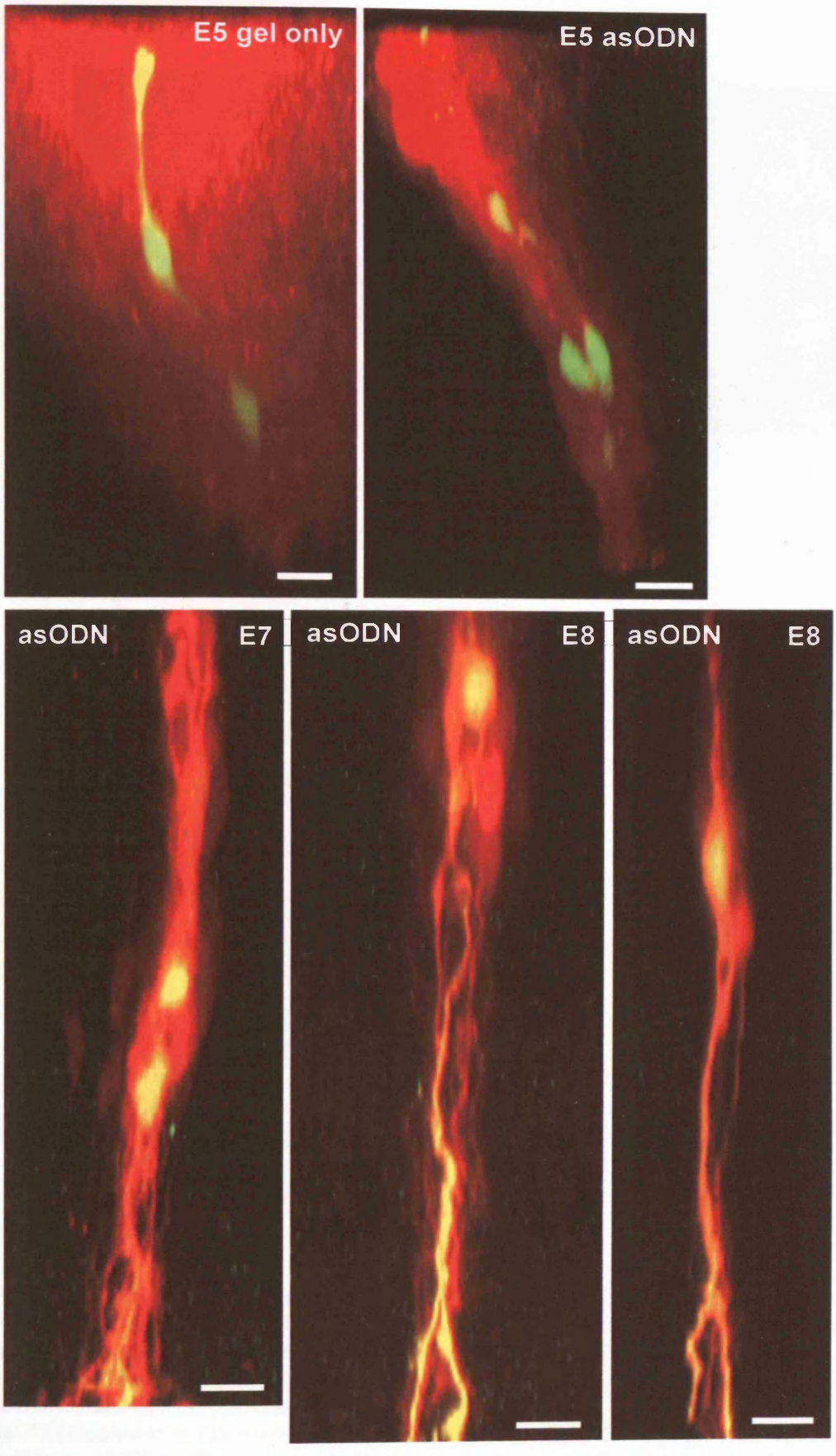

Figure 4.21. Dye-coupling in antisense Cx43 ODN treated retinae. Antisense Cx43 ODN treatment (asODN) reduced the extent of dye-coupling, compared to controls treated with pluronic gel only (the vehicle employed for application of asODN) at all ages examined. Scale bars 10 μm.

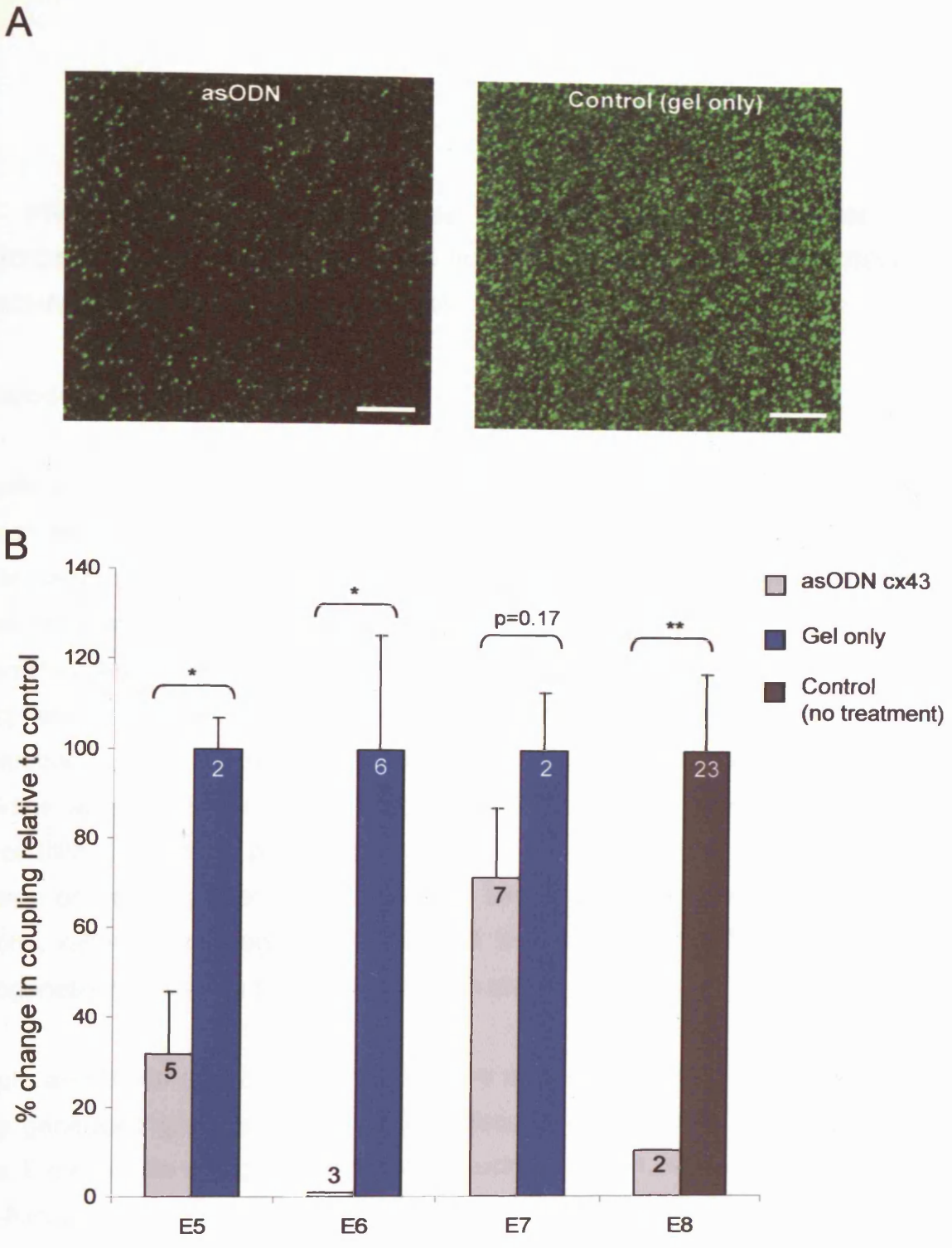

Figure 4.22 Reduction in Cx43 expression and dye-coupling following antisense treatment. A, Antibody-labelling of Cx43 following asODN treatment in an E6 retina confirms the reduction in Cx43 expression compared to 'gel only' control. Images show an XY-projection through the entire retina. *B,* Histogram showing the effect of asODN-treatment on dye-coupling at E5-E8. The reduction in coupling following asODN treatment is normalised to the levels in control (for E8, no 'gel only' data is available, and the effect of asODN-treatment is compared to controls). At all ages examined, asODN treatment led to a reduction in the extent of coupling. Numbers on each bar indicate the number of observations. Scale bars 10 μm; * $p<0.05$; ** $p<0.01$

Chapter 5

THE PROPERTIES OF INTERKINETIC NUCLEAR MIGRATION IN EMBRYONIC CHICK RETINA AND ITS MODULATION BY GAP JUNCTIONS, HEMICHANNELS AND NEUROTRANSMITTERS

5.1 Introduction

At early times in the developing neural retina (E4-E6), progenitor cell nuclei undergo interkinetic nuclear migration (INM), moving from the ventricular zone (VZ) to the vitreal surface in G1 of the cell cycle, before replicating their DNA in S phase, returning to the VZ in G2 and undergoing mitosis (Fig. 1.2B). After terminal division, newly differentiated cells migrate from the VZ to a location appropriate to their fate. This pattern of movement accompanying cell proliferation was first described by Sidman et al. (1959) in a study using [^{3}H]-thymidine labelling. Since mitosis only occurs within the VZ, factors affecting the rate of INM also affect proliferation. Despite the implications for proliferation, research on cell migration in development has focused on newly differentiated neurons, rather than progenitor cells, and the role and regulation of INM in neurogenesis to date has not received much attention.

Komuro and Rakic (1992; 1995; 1998) have studied the migratory behaviour of newly generated granule cells, using confocal microscopy in acute cerebellar slices. Experiments using Ca^{2+} indicators, such as Fluo-4, to monitor intracellular Ca^{2+}-fluctuations, show a correlation between dynamic changes in $[Ca^{2+}]_i$ and movement of the cell body (Komuro and Rakic, 1996). Physiological and pharmacological approaches have revealed that the activity of voltage-gated ion channels and neurotransmitter receptors regulate migration. Glutamate has been shown to regulate migration of newborn cerebellar granule cells (Komuro & Rakic, 1993, 1998; Rossi & Slater, 1993; Farrant et al., 1994), and migration of newborn cortical neurons is modulated by GABA (Behar et al., 1999).

As shown in the previous chapter, gap junctions couple progenitor cells into networks that largely exclude differentiated neurons. It has been suggested that the Ca^{2+}-waves that propagate between gap junction-coupled progenitor cells in early development may serve to coordinate cell cycle events (Owens & Kriegstein, 1998; Pearson et al., 2002; Weissman et al., 2004). Previous studies suggest that gap-junctional coupling is positively correlated with cell proliferation. In neural crest cells, blocking gap junctions pharmacologically was associated with an increase in cell death via apoptosis, as indicated by TUNEL labelling (Bannerman et al., 2000). In the developing chick, suppression of Cx43 expression, the first gap junction protein to be expressed in the embryonic chick eye (Becker et al., 2002), reduces progenitor cell proliferation and results in small eyes (Becker and Mobbs, 1999). The extent of gap junction-coupling and the rate of cell migration are positively correlated in neural crest cells. Neural crest cells from transgenic mice overexpressing Cx43 show increased rates of migration, whereas cells from transgenic mice expressing a dominant negative Cx43 show decreased rates of migration, and this could be mimicked in cells from nontransgenic animals using pharmacological gap junction blockers (Huang et al., 1998).

Here, the nature and rate of INM in the chick retina are investigated in real time using live confocal imaging of cells labelled with lipophilic carbocyanine dye. In addition, the roles of gap junctions, hemichannels and neurotransmitters in the regulation of INM are examined.

5.2 Methods

The methods employed are described in detail in section 2.6. Briefly, cells in acutely dissected retinae from E5 embryos were labelled using one of two methods: the biolistic technique described by Gan et al. (2000) or by bath immersion of retinal preparations in Krebs' solution containing DiI. Retinae were transferred to a gas-, humidity- and temperature-controlled (36°C) closed chamber on the stage of a confocal microscope (LSM 510, Zeiss, UK or SP2, Leica, Milton Keynes, UK) with the VZ facing the objective and held flat with a 'harp' consisting of nylon strands glued to a platinum frame. Stacks of XY images in the plane of the retinal surface were taken at 1 μm steps, throughout the depth of the retina and ~5 μm on either side, and repeated at regular time intervals. These image-stacks were analysed offline, rotated to give an XZ view over time, and the movements of the labelled cells measured relative to the ventricular surface. In studies using pharmacological agents, one eye from each embryo was used to study the effects of the drug and the opposite eye used as a paired control. Expression of Cx43 was modulated by transfection of individual cells with a dominant negative construct of Cx43 using electroporation, and by gel application of Cx43-specific antisense oligodeoxynucleotides, as described in section 2.4.

Results are presented as means ± standard error of the mean, where N=number of retinae and n=number of cells. Statistical significance was tested using an unpaired Student's t-test, and the results were considered significant at two levels, $p<0.05$, marked by *, or $p<0.01$, marked by **.

5.3 Results

5.3.1 Migratory behaviour of embryonic retinal cells

The characteristics of INM in retinal progenitor cells were followed in acutely dissected, intact retinae in real time, using time-lapse confocal microscopy. Cells undergoing INM had a bipolar shape, with an elongate cell body and processes extending to the ventricular and vitreal surfaces (Figure 5.1). The process of labelling the cells with dye did not appear to impair cell function, since mitosis proceeded normally (Figure 5.2). It was not possible to distinguish between progenitor and newly postmitotic cells on the basis of morphology alone. However, since postmitotic cells are born in the VZ and migrate away to other levels in the retina, it is generally assumed that cells moving *towards* this region are progenitors in G_2 of the cell cycle (Figure 1.2A). The population of cells moving *away* from the VZ contains both progenitor cells in G_1 and postmitotic cells. Recently, newborn horizontal cells, which in the adult occupy the region immediately below the photoreceptor layer, have been shown to migrate bidirectionally, first moving towards the immature ganglion cell layer but subsequently return to a region just below the VZ (Edqvist and Hallbook, 2004). However, this behaviour was only observed from E7, significantly later than the period under observation in this study (E5). The cell types born at E5 (ganglion and amacrine cells) reside at the vitreal surface of the retina and migrate directly from the VZ to the vitreal side of the retina following exit from the cell cycle. Thus, the population of cells moving towards the VZ in embryos of the age used in these experiments is comprised solely of progenitor cells.

INM is characterized by phases of movement in either direction, interspersed by periods in which cells move only slowly or are stationary (Figure 5.1). Figure 5.3A shows three typical DiI-labelled progenitor cells undergoing INM, imaged at 15min intervals over a ~3h period (see also Supplementary Movie). At the start of the recording cells 1 and 3 were located approximately halfway between the

ventricular and vitreal surfaces of the retina. During the time period of the recording, cell 1 moved rapidly, and cell 3 more slowly, towards the VZ before dividing. Details of the movement of cell 3 are shown in Figure 5.3B-C, illustrating the saltatory nature of the migratory movement. Cell 2 moved at a slower rate in the direction of the VZ, moving a total of 20μm during the period shown. Progenitor cells moving in this direction only moved radially; no tangential movement was observed.

On approach to the VZ, the progenitor cell nuclei lost their elongated shape and rounded up (see cells 1 and 3, Fig. 5.3A and Fig 5.3D). Nuclei located between 20 and 80 μm from the VZ had an average length/width ratio of 3.2 (range 1.6-4.3). For those located in the VZ, and up to 20 μm away, this ratio was 1.1±0.1 (range 0.8-1.8).

Previous evidence suggested that the vitreal process of a progenitor cell was lost during cell division (Hinds & Ruffett 1971; Seymour & Berry 1975; Chenn and McConnell, 1995; Fukushima et al., 2000). However, more recent work has provided evidence that this process is retained through mitosis and inherited by one of the daughter cells (Miyata et al. 2001; Noctor et al., 2004; Saito et al., 2003). In this study, retention of the vitreal contact throughout cell division was observed on several occasions. In the example shown in Figure 5.3A, Cell 1 retained its contact with the vitreal surface throughout mitosis (*arrow heads*) and the two daughter cells remained in close physical contact following mitosis. Another example of this is shown in Figure 5.4, which clearly shows retention of the vitreal process during the cytokinesis phase of mitosis. In their study, using cultured retinal slices, Saito et al. (2003) suggest that while the process is retained throughout mitosis, it becomes increasingly thinned as the soma approaches the apical surface and initiates mitosis. A similar morphological change was observed in this study, as illustrated in Figure 5.5. During the first half hour of imaging, the basal process is 2-3 μm in diameter. However, as the cell body approaches the VZ and rounds up (Figure 5.5, t 45 and t 60) the

process thins to a fraction of a micron and becomes nearly invisible. Following mitosis, the process becomes thicker again.

However, on a number of occasions, retraction of the vitreal process was observed as the nucleus approached the VZ (Figure 5.6). This suggests that the maintenance of contact with the vitreal surface is not an absolute requirement for division. However, the longest period over which it was possible to image in cases where process retraction was observed to occur were too short to encompass mitosis, and it is thus not possible to draw firm conclusions.

Nuclear movements during INM are not linear (see Fig. 5.1, 5.3A-B). To examine the dynamics of INM in more detail, images were acquired at a frequency of 0.025 Hz for shorter periods of time. At this more rapid sampling frequency, the movements of progenitor cell nuclei could be seen to be comprised of frequent short stationary phases that alternated with periods of movement in a forward or backward direction. An example of this movement is shown for two cells in Figure 5.7. The cell shown in Figure 5.7A-B moved at a mean rate of 12.2 μm/h during a the 20 min period shown, moving in a step-wise manner towards the VZ; it spent a total of 9min 20s making movements towards the VZ, interspersed with movements in the opposite direction (a total of 3min 20s) and periods during which it remained stationary (totalling 7min 20s). The cell shown in Figure 5.7C-D moved more rapidly towards the VZ, at a mean rate of 33.3μm/h during the 20min period shown. During this time, the cell spent a total of 12min making movements towards the VZ, 3min moving in the opposite direction, and 3min remaining stationary.

The migratory behaviour of cells moving towards the vitreal surface was similar to that of cells moving towards the VZ. Figure 5.8A shows a recording of two cells moving in the vitread direction. During the period of observation (120min) the nuclei made saltatory movements towards the vitread surface (Figure 5.8B-C). Although the nuclei change shape during INM, there is no rounding up as they

reach the vitread surface, as shown in the lower panels of Figure 5.8B-C. As with cells moving toward the VZ, only radial, and no tangential, movements were observed.

5.3.2 Speed of nuclear translocation during INM

At E5, the average speed of INM was 20.7±0.5μm/h (N=53, n=389). The speed of movement of nuclei moving towards the VZ (progenitor cells in G_2) was 20.5±0.7μm/h (range 2.5-68.6μm/h; n=213), whilst those moving in the vitreal direction (mixed population of progenitor cells and postmitotic cells) did so at 21.0±0.8μm/h (range 4.5-64.2μm/h; n=176). The distributions of speeds of INM in either direction are shown in Figure 5.9. The number of proliferative divisions is high at E5, but neurons are also born at this time (Prada et al., 1991; Snow and Robson, 1994; Adler & Belecky-Adams, 1999). Thus, the population of cells moving away from the VZ likely includes postmitotic cells. Chenn and McConnell (1995) proposed that, in the cortex, these two populations migrate at different speeds, with immature neurons migrating at velocities ~10-fold greater than progenitor cells. However, the distribution of velocities for the population of retinal cells moving away from the VZ is almost identical to that seen for the population moving towards it; both are unimodal with a single peak at 16-20μm/h (Fig. 5.9A, B), and median values of 19.1 and 18.5μm/h, respectively. There was no statistical difference between the distributions or mean speeds (p=0.617) of INM in cells moving towards or away from the VZ.

5.3.3 Coordinated movement during INM

As shown in Chapter 4, retinal progenitor cells form gap junction-coupled clusters, which largely exclude newly differentiated cells. Previous studies show that gap junction-dependent Ca^{2+}-waves occur that reflect this pattern of dye-

coupling (Figure 5.10C-D, Pearson et al., 2004). It is possible that gap junction-mediated signals, such as Ca^{2+}-waves, may represent a mechanism for neighbouring cells to coordinate events within the cell cycle and/or INM (Pearson et al., 2004; Weissman et al., 2004). DiI labelling provides some evidence for coordinated movements; particles often labelled groups of neighbouring cells and cells within these clusters were frequently observed to move in synchrony, as shown in the two examples in Figure 5.10A-B. Such synchrony of movement was observed in cells moving towards and away from the VZ.

In the enclosed supplementary movie, DiI labelled cells imaged over a period of 5.5 hours are shown. The movie illustrates the behaviours described above, including saltatory movement, rounding up of the nucleus on approach to the VZ, retention of the basal process during mitosis, and coordinated movement of neighbouring cells.

5.3.4 Pharmacological gap junction blockers slow the rate of INM

In order to investigate the role of gap junction mediated communication on INM, a panel of pharmacological gap junction blockers was used [carbenoxolone (CBX), 100μM; 18-α-glycerrhetinic acid (18-α-GA), 50μM and retinoic acid (RA), 25μM]. Application of each of the three blockers significantly impaired INM (Figure 5.11). Following the application of CBX, the speed of INM was reduced by 50%, from 14±1μm/h in control to 7±1μm/h in CBX ($p<0.0001$, Figure 5.11A). Populations of cells moving towards (14±1μm/h in control, 6±1μm/h in CBX, $p<0.0001$) and away (13±2μm/h in control, 8±1μm/h in CBX, $p=0.03$) from the VZ were similarly affected. Application of 18-α-GA slowed migration by 69%, from 20±2μm/h in control to 6±1μm/h in 18-α-GA ($p<0.0001$, Figure 5.11B. Populations of cells moving towards (21±2μm/h in control, 7±1μm/h in 18-α-GA, $p<0.0001$) and away (19±3μm/h in control, 5±1μm/h in 18-α-GA, $p<0.0001$) from the VZ were similarly affected. Similar effects were seen following application of RA; cells moved at

10±1μm/h in RA, compared to 22±2μm/h in control, a reduction of 53% ($p<0.0001$, Figure 5.11C). Populations of cells moving towards (23±2μm/h in control, 11±2μm/h in RA, $p<0.0001$) and away (17±3μm/h in control, 9±1μm/h in RA, $p=0.03$) from the VZ were similarly affected. Figure 5.12 illustrates the effect of all three gap junction blockers on the distribution of speed of INM. The distribution of INM speed in CBX and 18-alpha-GA show a sharp shift to the left, indicating that these agents have a profound effect on the rate of INM, causing most cells to move at a very slow rate or not at all, compared to controls. Retinoic acid, while also significantly slowing the rate of INM, shows a less marked clustering of cells in the slowest category. The effects of all three blockers on the distribution of speed of INM were similar for cells moving towards and away from the VZ. The uniform effect of the panel of gap junction blockers employed makes it unlikely that these were due to any non-specific actions of these drugs. Thus, pharmacological uncoupling of gap junctions significantly impairs progenitor cell INM.

5.3.5 Interfering with gap junction channel formation slows INM

Connexin 43 (Cx43) is the first gap junction protein to be expressed in the eyecup (Becker et al., 2002; Becker and Mobbs, 1999) and suppressing the expression of this protein causes a reduction in retinal proliferation resulting in small eyes (Becker and Mobbs, 1999). Cx43 is likely to mediate the gap junction coupling seen between retinal (Pearson et al., 2004) and cortical (Bittman and LoTurco, 1999) progenitor cells in early development. The effect of interfering with the formation of functional gap junction channels on INM was examined. Electroporation was used to introduce a pIRES vector with a CMV promoter into cells to drive the expression of eGFP and a dominant negative form of Cx43 (dnCx43), eGFP and wild type Cx43, or eGFP alone (see Becker et al., 2001). Control eGFP cells made saltatory movements, migrating at an average of 12±1μm/h, and moved at similar speeds both towards (13±2μm/h) and away

(9±1μm/h; p=0.123) from the VZ. The average speed of INM recorded in eGFP preparations was slower than in those labelled with DiI (see above). However, the DiI-labelled preparations described above were observed immediately following acute dissection and labelling, whilst eGFP preparations were held in an incubator for 8-10 hours in order to establish GFP expression. The rate of INM was reduced by 62% in cells transfected with the dnCx43 construct, compared to eGFP controls, to 5±1μm/h ($p<0.0001$; Fig. 5.13A). Populations of cells moving towards (13±1μm/h with control eGFP, 6±1μm/h with dnCx43, $p<0.0001$) and away (10±2μm/h with control eGFP, 2±0.5μm/h with dnCx43, $p<0.0001$) from the VZ were similarly affected. Transfection with the wild-type Cx43 (WT) did not significantly alter the rate of INM, compared to eGFP controls (total cell population, 16±2 μm/h WT, 12±1μm/h eGFP, p=0.08; cells moving towards VZ, 16±1μm/h WT, 13±1μm/h eGFP, p=0.21; cells moving away from VZ, 15±2μm/h WT, 10±2μm/h eGFP, p=0.12). The distribution of the velocities of INM following transfection with these constructs is shown in Figure 5.13B. While the cells transfected with eGFP or WT show INM across a range of velocities, the rates of INM of cells transfected with dnCx43 are clustered in the lowest category.

The dnCx43 construct interferes with gap junction channel formation and, due to the high degree of homology between different connexins, potentially affects other connexins. However, Cx43 protein expression can be transiently and specifically knocked down by Cx43 antisense oligodeoxynucleotides (asODN) (Becker and Mobbs, 1999; Becker et al., 1999; McGonnell et al., 2001), providing an alternative technique by which to test the specific role of Cx43 in INM. Further, whilst the pIRES dnCx43 constructs only affect communication in the eGFP-expressing transfected cells, application of Cx43 antisense reduces expression of Cx43 protein in the whole tissue (Figure 5.14C). In order to monitor the extent of knockdown that results from asODN treatment, immunohistochemical labelling of Cx43 expression was carried out. A pair of retinae was processed, one following treatment with asODN, and the other after exposure to pluronic gel, the vehicle employed to deliver the asODN to the tissue. These were fixed and labelled with

an antibody for Cx43 and imaged on a confocal microscope. Projections of stacks of images of these immunolabelled preparations show a marked reduction of Cx43 expression in retinae treated with asODNs compared to controls treated with pluronic gel alone (Figure 5.14C). The effects of asODN treatment on INM are shown in Figure 5.14A-B. Control cells treated with pluronic gel moved at an average of 13±1μm/h. The slower rate of movement in control may be attributable to the incubation period between dissection and imaging, to allow the effect of the asODN to be established, as was observed for the eGFP transfected cells. Application of asODN caused a 56% reduction in the speed of INM, to an average of 5±1μm/h ($p<0.0001$). Cells moving towards (13±2μm/h in control, 6±1μm/h with asODN, $p=0.001$) and away (12±1μm/h in control, 4±1μm/h with asODN, $p<0.0001$) from the VZ were similarly affected. The distribution of INM speed following asODN treatment is shown in Figure 5.14B. While the cells treated with gel only show INM across a range of speeds, the velocities of INM in cells treated with asODN are clustered in the lowest category.

5.3.6 The role of gap junction hemichannels in INM

In whole gap junctions, each of the coupled cells contributes a hemichannel (or connexon), a hexamer of connexin proteins. There is increasing evidence of a role for unopposed hemichannels in intercellular signalling (Bennett et al., 2003). In the developing retina, hemichannels, located at the border of the RPE and the neural retina, are spontaneously active, and their opening results in the release of ATP. ATP has a profound stimulatory effect on the rate of mitosis of progenitor cells in the underlying neural retina, as well as initiating Ca^{2+} waves that spread between RPE cells (Pearson et al., 2005a). Similarly, in the developing cortex, hemichannel-mediated release of ATP from radial glial cells is involved in generating calcium-waves in the VZ, which in turn regulate proliferation (Weissman et al., 2004). The pharmacological and molecular approaches used here to test the role of gap junctions affect both coupled and uncoupled

hemichannels, so the effects described above may arise in part from an action at unopposed hemichannels. Here, the presence of functional hemichannels in the developing neural retina was investigated, and their role in the regulation of INM was examined.

The presence of gap junction hemichannels in the developing neural retina was investigated using an antibody, Gap 7M, which binds to a region on the first external loop of the connexin, which is only exposed on unopposed gap junction hemichannels and so does not bind to complete gap junctions (D Becker, personal communication). Labelling revealed sparse punctate immunoreactivity distributed throughout the neural retina (Figure 5.15A). Staining was absent from controls in which the primary antibody was omitted (Figure 5.15B).

In isolated cells, a reduction in extracellular Ca^{2+} can cause hemichannels to open (Bennett et al., 2003), and open hemichannels can pass small dye molecules (Hofer & Dermietzel, 1998; Weissman et al., 2004). To test if functional hemichannels are present in the embryonic neural retina, a technique of monitoring the rate of dye-efflux in varying external Ca^{2+}-concentrations was employed. This method was used by Pearson et al. (2005a) to probe the presence of functional hemichannels in the retinal pigment epithelium (RPE). An example of a retina loaded with Alexa 488, and counterstained with Hoechst 33342, is shown in Figure 5.16A. A single confocal section through the VZ shows uptake of Alexa 488 (green) in groups of cells. The confocal section shown in *A* was imaged for ~25 minutes in the presence of varying concentrations of Ca^{2+}. If the rate of dye efflux is controlled by hemichannels, varying the $[Ca^{2+}]$ in the perfusate should produce a corresponding variation in the rate of dye loss. The normalised change in fluorescence (from Alexa 488 only) is shown in Figure 5.16B, and the changes in Ca^{2+} concentration of the perfusate are indicated. The rate of fluorescence decay was not correlated with the Ca^{2+} concentration, but rather appeared to relate to photobleaching. Despite numerous attempts, no consistent pattern of change in fluorescence was found with this method. It

appears that either the rate of dye-efflux does not correlate with the Ca^{2+} concentration of the perfusate, or alternatively, the photobleaching of the Alexa dye obscures any effects of varying the Ca^{2+} concentration on the rate of dye loss.

In order to overcome the problems associated with the dye-efflux experiments, the uptake of Neurobiotin in varying Ca^{2+} concentrations or gap junction and hemichannel blockers was assessed. This methods has been described previously to asses the presence of hemichannels (Hofer & Dermietzel, 1998; Weissman et al., 2004). Acutely dissected retinae were incubated in Ca^{2+}-free solution for ~30 min with Neurobiotin, and subsequently fixed and processed to reveal the Neurobiotin, and imaged on a confocal microscope. The majority of cells showed uptake of dye, except within the GCL (Figure 5.17A). The amount of dye uptake could be reduced by CBX (Figure 5.17B) and by substituting the Ca^{2+}-free solution for one containing 2mM Ca^{2+} (Figure 5.17C). In addition to CBX, which affects both hemichannels and gap junctions, a connexin mimetic peptide, Gap26, was used. Gap26 blocks hemichannels by mimicking a 13 amino acid sequence (VCYDKSFPISHVR) on the first extracellular loop of Cx43. A study on endothelial cell lines found Gap26 to act on hemichannels alone, without affecting coupled gap junctions (Braet et al., 2003). Here, on some occasions (N=2 out of 4), Neurobiotin uptake was reduced by Gap26 (Figure 5.17E), but not by a scrambled version of the peptide, used as a control. The number of experiments possible was limited by the high cost of the reagents.

Taken together, the evidence suggests that functional hemichannels are present in the embryonic neural retina. Gap26 and the scrambled control peptide were used to specifically target the role of hemichannels in regulating INM, without affecting intact coupled gap junctions. To rule out any effect on intact gap junctions, the dye-coupling technique utilised in Chapter 4 was employed. Figure 5.18 shows three cells filled with Neurobiotin and FITC in control solution, Gap26 or CBX. The extensive coupling, seen in control, is prevented by CBX, but not by

Gap26, which was incubated with the retina for 2 hours prior to the dye-filling. This confirms that Gap26 does not interfere with intact gap junctions over this time course (2 hours).

The effects of Gap26 on INM are shown in Figure 5.19. Following incubation in Gap26, the speed of INM was reduced by 25%, to 13±1μm/h, compared to 18±1μm/h in scrambled control ($p<0.0001$). The effect of Gap26 in slowing the migration of cells toward the VZ was more marked (20±1μm/h in scrambled control, 14±1μm/h in Gap26, $p=0.001$) than for cells moving away (14±1μm/h in scrambled control, 13±1μm/h in Gap26, $p=0.067$). The range of velocities of INM in the presence of Gap26 and in scrambled controls is shown in Figure 5.19B. For the population of cells moving towards the VZ, Gap26 causes a marked shift in the speed of the movement of the nuclei towards the lower end of the range, compared to the scrambled controls. For the population of cells moving away from the VZ, this is much less pronounced. The reasons for this difference are unclear.

5.3.7 Effect of purinergic signalling on INM

In the embryonic neocortex, ATP mediates Ca^{2+}-waves, and purinergic antagonists cause a decrease in the extent of wave-propagation and BrdU uptake (Weissman et al., 2004). Studies using Ca^{2+}-imaging in the developing chick retina has shown large Ca^{2+} response to purinergic stimulation from E3 onwards, which declined towards E8 and decreased further until E11-13, suggesting that the Ca^{2+} mobilisation via purinoceptors is characteristic of early embryonic retinal cells, and may be involved in modulating proliferation (Sugioka et al., 1996, Sakaki et al., 1996). Pearson et al. (2002) reported profound effects of purinergic signalling on proliferation of cells in the retinal VZ: UTP generates $[Ca^{2+}]_i$ transients among the cells of the VZ, and acts as an accelerator on proliferation, speeding mitosis by reducing the time it takes for the chromosomes

to separate. These effects do not seem to be compensated for at later stages, as shown by long-term exposure of the developing embryo to receptor agonists and antagonists *in ovo*, where UTP causes an increase in overall eye size and the number of mitotic cells. Here, the role of purinergic signalling in the regulation of INM was investigated.

The effects of UTP and the purinergic antagonist PPADS on INM are shown in Figure 5.20. Application of UTP caused a 20% reduction in the speed of INM, from 22±1μm/h in control to 17±1μm/hr in UTP ($p=0.01$). This effect is greater for cells moving away from the VZ (23±2μm/h in control, 17±2μm/h in UTP, $p=0.032$) than for cells moving towards it (21±2μm/h in control, 18±1μm/h in UTP, $p=0.20$). Application of the purinergic antagonist PPADS, to block endogenous purinergic signalling, had the opposite effect of UTP. The speed of INM in PPADS was increased by 26% compared to control, from 18±1μm/h in control to 22±1μm/h in PPADS ($p<0.001$). Again, this effect is greater for cells moving away from the VZ (18±1μm/h in control, 24±2μm/h in PPADS, $p<0.001$), than for cells moving towards it (18±1μm/h in control, 19±2μm/hr in PPADS, $p=0.537$). Figure 5.21 shows the distribution of the speed of INM in UTP and PPADS. The effect of UTP in comparison to control was similar for cells moving towards or away from the VZ, and did not appear to preferentially affect fast- or slow-moving cells. The distribution of rates of INM in PPADS and control suggests that PPADS causes an increased number of cells to move through INM at a fast rate (> 30μm/h).

5.3.8 Effect of muscarinic signalling on INM

Muscarinic AChRs are widely expressed during development, and the expression of different receptor subtypes is dynamically regulated (Nadler et al., 1999). Pearson et al. (2002) reported profound effects of muscarinic signalling on proliferation of cells in the retinal VZ. These authors show that carbachol generates $[Ca^{2+}]_i$ transients among the cells of the VZ, and acts to slow mitosis

by increasing the time it takes for the chromosomes to separate. These effects do not seem to be compensated for at later stages, as shown by long-term exposure of the developing embryo to receptor agonists and antagonists *in ovo*, where carbachol causes a decrease in overall eye size and the number of mitotic cells. Thus, Pearson et al. suggest that mACh receptor activation acts as a brake on mitosis and opposes the effects of P2Y receptor activation, which accelerate proliferation. Here, the role of muscarinic signalling in regulation of INM was investigated.

The effects of carbachol and pirenzepine on INM are shown in Figure 5.22. Application of carbachol produced a 20% increase in the rate of INM, from 15±1μm/h in control to 18±1μm/h in carbachol ($p=0.03$). The rate of INM in carbachol was greater than in control for cells moving in either direction, but this effect was only significant for the total population of cells (cells moving towards the VZ, 15±1μm/h in control, 18±1μm/h in carbachol, $p=0.11$; cells moving away from the VZ, 15±2μm/h in control, 19±1μm/h in carbachol, $p=0.18$). Application of the muscarinic antagonist pirenzepine, to block endogenous muscarinic stimulation, did not significantly affect the speed of INM (18±1μm/h in control, 17±1μm/h in pirenzepine, $p=0.37$). The effect of carbachol and pirenzepine on the distribution of speed of INM is shown in Figure 5.23. For both of these agents, the INM velocities of cells in drug and control span a similar range.

5.3.9 Effect of glutamatergic signalling on INM

Glutamate has been shown to have profound effects on the migration of newborn neurons. NMDA-receptor activation regulates the migration of newborn cerebellar granule cells (Komuro & Rakic, 1993, 1998; Rossi & Slater, 1993; Farrant et al., 1994), and newborn cortical neurons (Behar et al., 1999). Pearson et al. (2002) reported that glutamate can generate Ca^{2+}-transients in cells within the VZ of the embryonic retina. The patch clamp experiments described in Chapter 3 of this

thesis show that at E5, a subset of progenitor cells respond to glutamate, and that this response is mediated in part by AMPA-receptors, and in part by a TBOA-sensitive glutamate transporter. Here, the role of glutamatergic signalling in INM was examined.

The effects of glutamate, NBQX and TBOA on the speed of INM are shown in Figure 5.24. Application of glutamate did not significantly affect the speed of INM for the total population of cells (14±0.5μm in control, 15±0.5μm/h in glutamate, p=0.14). However, for the population of cells moving towards the VZ, glutamate produced a 20% increase in the speed of INM, from 13±1μm/h in control to 16±1μm/h in glutamate (p=0.009). In contrast, the mean speed of INM of cells moving away from the VZ was unaffected by glutamate (14±0.5μm/h in control, 14±0.5μm/h in glutamate, p=0.88). Application of NBQX, to block endogenous glutamatergic signalling via AMPA/kainate receptors, also did not affect the speed of INM for the total population of cells (15±0.5μm/h in control, 14±0.5μm/h in NBQX, p=0.23). However, for the population of cells moving away from the VZ, NBQX produced a 13% decrease in the speed of INM, from 15±1μm/h in control to 13±0. μm/h in NBQX (p=0.004). For the population of cells moving towards the VZ, NBQX had no effect (14±1μm/h in control, 15±1μm/h in NBQX, p=0.29). Application of TBOA, to block endogenous activation of glutamate transporters, caused a 16% decrease in the rate of INM, from 19±1μm/h in control to 16±1μm/h in TBOA (p=0.01). The mean rate of INM in TBOA was lower than in control for both populations of cells, but these differences were not statistically significant (for cells moving towards the VZ, 19±1μm/h in control, 17±1μm/h in TBOA, p=0.08; for cells moving away from the VZ, 19±1μm/h in control, 16±1μm/h in TBOA, p=0.07). The distribution of the speed of INM of cells in glutamate, NBQX and TBOA are shown in Figure 5.25. While glutamate did not affect the mean speed of INM of cells moving away from the VZ, compared to control, the distribution of the velocities of INM shows a different picture. While the majority of cells in both control and glutamate undergo INM at rates of 10-

15μm/h, ~35% of cells in glutamate move at rates >20μm/h, compared to less than 10% in control.

5.3.10 Effect of GABAergic signalling on INM

GABA can stimulate migration of cortical neurones during rat cortical histogenesis, where dynamic expression of GABA-receptors modulates the migratory responses to GABA (Behar et al., 1998; 2000). Cells in the VZ of the embryonic cortex show depolarizing responses to GABA (LoTurco et al., 1995). The findings presented in Chapter 3 show that at E5, most chick retinal cells show depolarizing responses GABA, which are sensitive to bicuculline. Pearson et al. (2002) showed that GABA can elicit Ca^{2+}-reponses within the VZ at this time. Here, the role of GABAergic signalling in INM was examined.

The effects of GABA and bicuculline on the speed of INM are shown in Figure 5.26. Application of GABA did not affect the rate of INM. The mean velocity of INM in GABA for the total population of cells, as well as the subpopulations moving towards and away from the VZ, were very similar to those in control (total cell population, 20±1μm/h in control, 19±1μm/h in GABA, p=0.46; cells moving towards the VZ, 18+1μm/h in control, 20±1μm/h in GABA, p=0.29; cells moving away from the VZ, 21±2μm/h in control, 18±1μm/h in GABA, p=0.16). Application of bicuculline, to block endogenous GABAergic signalling, had no effect on the population of cells moving towards the VZ (14±1μm/h in control, 16±1μm/h in bicuculline, p=0.34) but significantly slowed INM in cells moving away from the VZ compared to controls (14±1μm/h in control, 13±0.5μm/h in bicuculline, p=0.009), although the effect was small, ~12%. The effect of bicuculline was not significant for the total population (14±1μm/h in control, 13±0.5μm/h in bicuculline, p=0.07). The distribution of the speed of INM of cells in GABA and bicuculline are shown in Figure 5.27. The INM velocities span a similar range in the presence of both agents, compared to control.

5.4 Discussion

5.4.1 Live imaging of INM of DiI labelled cells

Labelling of retinal cells with DiI labelled cells at all stages of the proliferative cycle, enabling the nuclei of individual cells, seen at all depths throughout the thickness of the retina, to be followed in real time. Labelling using the biolistic technique, compared to immersion labelling, produced similar results, with no difference in cell morphology, or rate and nature of INM, suggesting that bombardment with biolistic particles does not cause significant damage to the tissue. The labelling process does not appear to impair normal cell function, since mitosis could be observed in labelled cells (see Figures 5.2, 5.3A, 5.4 and 5.5). Long periods of illumination of fluorescently labelled cells with laser light can result in phototoxic damage. In order to minimise these effects, laser intensity and the frequency of image acquisition were reduced to the minimum necessary to obtain clear images and adequate resolution of the movement of cells. Using low acquisition frequencies (usually a stack was acquired every 15 minutes) and low laser power, preparations could often be imaged continuously for several hours. The limiting factor determining the duration of the recordings was usually the physical stability of the preparation rather than its viability. Any drift in the XY-plane made it difficult to follow the movements of individual cells. Using a combination of long-term recordings over several hours to observe INM and mitosis, and shorter recordings at higher image frequencies, it was possible to gain detailed information about the nature and rate of INM, the changes in morphology of progenitor cells as they pass through the cells cycle, and the effects of a range of agents acting on gap junctions, hemichannels and neurotransmitter receptors.

5.4.2 Properties of INM in the retina

Retinal cells undergoing INM display characteristic changes in morphology. Progenitor cells are of bipolar morphology with an elongated cell body and processes that extend to either side of the retina (see Figure 5.1). In time lapse imaging experiments the cell nucleus can be seen to translocate within the processes, the cell body rounding up on approach to the VZ and elongating on exit. This behaviour is similar to that reported in early anatomical studies of retinal and cortical progenitor cell cycling (Sauer, 1935; Sidman et al., 1959; Seymour and Berry, 1975; Nagele and Lee, 1979). In the retina, INM is characterized by the frequent alternation of periods of movement with phases in which the cell nucleus is stationary or moves at a much reduced rate. Similar patterns of movement were observed regardless of the direction in which the cell was travelling. These saltatory movements resemble those seen in migrating post-mitotic neurons in acute cerebellar (Komuro and Rakic, 1995) and cortical (Nadarajah et al., 2001) slice preparations.

Previous evidence suggested that the vitreal process of a progenitor cell was lost during cell division (Hinds & Ruffett 1971; Seymour & Berry 1975; Chenn and McConnell, 1995; Fukushima et al., 2000). However, in this study, retention of the vitreal contact throughout cell division was observed on several occasions. This observation adds to several other recent reports of process retention through mitosis, and suggests that this may be a conserved mechanism. Process retention through mitosis has been described in the developing retina of mouse (Saito et al., 2003), rat (Cayouette & Raff, 2003), zebrafish (Das et al., 2003), and here in the chick. In addition, it has also recently been described in other areas of the developing nervous system, including the cortex (Miyata et al. 2001; Noctor et al., 2004;), tectum, cerebellum and spinal cord (Saito et al., 2003). In their study, using cultured retinal slices from mouse embryos, Saito et al. (2003) report that while the process is retained throughout mitosis, it becomes increasingly thinned as the soma approaches the apical surface and initiates mitosis. A similar

phenomenon was observed in the cortex (Miyata et al. 2001). This change in morphology of the process during mitosis was also observed in the present study. However, on a number of occasions, retraction of the vitreal process was observed as the nucleus approached the VZ (Figure 5.6). Halfter et al. (2001) used collagenase injections into the embryonic chick eye at E5-7 to study the effect of temporary destruction of the basal lamina on development, and found that this led to retraction of the progenitor cell processes, and abnormal development and organisation of the GCL. Similar abnormalities in migration and organisation were observed in a mutant mouse where the pial basement membrane was disrupted during cortical development (Halfter et al., 2002). In both the chick retina and the mouse cortex, disruption of the basement membrane did not appear to affect cell division (Halfter et al., 2001; 2002). These findings, coupled with the observations of process retraction in the present study, suggest that the maintenance of contact with the vitreal surface is not an absolute requirement for division, but plays an essential role in maintaining the ordered organisation of the developing tissue. The retention of the basal process and inheritance by one of the daughter cells may explain how radial progenitors are able to combine the dual functions of progenitor cells, dividing and giving rise to new neuronal progeny, with the traditionally ascribed role of acting as guides during neuronal migration (reviewed in Hatten, 1990).

It is still unknown whether retention of the basal process plays a role in the subsequent behaviour and fate choice of the cell. Process retention has been observed in both symmetric divisions that give rise to two progenitor cells, and asymmetric divisions that give rise to one progenitor and one neuronal daughter cell (Saito et al., 2003). Saito et al. speculate that the daughter cell that inherits the process, and which leaves the VZ more rapidly, can do so because it can insert its nucleus into an existing process. However, due to the difficulty in following identified cells for long enough periods to observe subsequent fate choices, no further links between process inheritance and fate have been established. The problem of tissue movement, which was an obstacle in the

studies described here, appears also to have limited the duration of observation of cell movement in the studies described above. The zebrafish embryo, which allows the retina to be imaged *in vivo,* may provide a better model in which to study cell movement. The transparency of the tissue and sparse labelling with GFP permits the same cells, and their progeny, to be more easily followed over extended periods of time (Das et al., 2003). Further, the zebrafish embryo can be immobilized in low density agarose, providing good mechanical stability, a technique which does not work with a thin sheet of tissue such as the chick retina.

The speed of INM in control retinae was similar for cells moving towards and away from the VZ (~20 μm/h). At the velocities measured, the nucleus of a progenitor cell would complete a whole cycle of INM, from the VZ to the GCL and back, a distance of approximately 160 μm at E5, in an average time of around 8 hours. At this age, mitosis takes ~30 minutes (Pearson, 2003). These estimates fit well with the range of cell cycle times in embryonic chick retina measured by others at this stage (6-10 hours, Morris and Cowan, 1995). The velocities recorded lie within the range of speeds observed for cerebellar (Komuro and Rakic, 1998) and cortical (Nadarajah et al., 2001; Takahashi et al., 1996) neuronal migration, and are similar to those of progenitor cells in the VZ of the ferret cortex (~18μm/h, Chenn and McConnell, 1995). However, Chenn and McConnell proposed that, in the ferret cortex, progenitor cells and immature neurons move away from the VZ at markedly different speeds. They proposed that the daughter cells resulting from the symmetric division of a progenitor cell moved away from the VZ at like rates, and at a speed much slower than that seen during G_2, when cells are moving in the opposite direction. Conversely, they suggest that, following an asymmetric division, which produces a postmitotic cell and a progenitor cell, the daughter cell nearest the cortical surface (the presumed progenitor cell) moves away slowly (~1 μm/h), whilst the more distal of the daughters moves at a rate 10-fold faster. The findings presented here do not support this proposition. In the early embryonic retina, the population of cells

moving away from the VZ, which includes a number of immature neurons (Prada et al., 1991; Snow and Robson, 1994), migrates at the same rate as progenitor cells moving towards it. There was no evidence to suggest that within the population of cells moving away from the VZ, there is one group that moves faster than another. Further, in the retina, the same wide range of velocities of INM was observed for both the progenitor cell-only population (moving towards the VZ), and the mixed population of progenitor cells and postmitotic cells (moving away from the VZ).

Postmitotic cortical and retinal neurons can undergo both radial and tangential dispersion (Fekete et al., 1994; Komuro et al., 2001; O'Rourke et al., 1997) but whether progenitor cells undergo tangential dispersion is unclear. Reid et al. (1995) suggested that, in the embryonic cortex, progenitor cells move tangentially through the VZ, pausing periodically to generate subclones. However, in this study in E5 chick retina, all movements of cells occurred within the radial plane with no evidence of tangential migration, suggesting that tangential dispersion may only occur after postmitotic cells reach the layer appropriate to their fate. This notion is supported by studies of transgenic mosaic mouse retinae, in which tangential migration was found to be a property of postmitotic cells (Reese and Tan, 1998), and by live imaging of progenitor cells in the ferret cortex, which showed that these cells moved only radially and not tangentially (Chenn and McConnell, 1995).

5.4.3 Gap junctions modulate INM

Gap junctional communication is a common feature of both cortical (Bittman et al., 1997; LoTurco and Kriegstein, 1991) and retinal (Becker et al., 2002; Pearson et al., 2004, Chapter 4 of this thesis) progenitor cells and is an essential requirement for maintaining cultures of mouse cortical neural stem cells in a proliferative state (Cheng et al., 2004). The pharmacological and molecular tools

employed here provide evidence to show that gap junction coupling is essential for the maintenance of normal progenitor cell INM. Although the pharmacological blockers employed have been shown to have effects other than those on gap junctions (Vessey et al., 2004), the similar actions of a variety of blockers on INM makes a non-gap junction-mediated effect highly unlikely. Specifically targeting Cx43, using asODN or expression of a dominant negative Cx43, similarly disrupted INM, confirming a critical role of gap junction communication in maintenance of normal rates of INM. Given that, in the retina, the VZ (the equivalent of the outer region of the VZ in the cortex) is the only location in which cells can divide, it is possible that gap junctions regulate the proliferative cycle by modulating the rate at which cells undergo INM and thus reach a region permissive for cell division. Similarly, in the cortex, the nuclei of proliferating radial glial must migrate between the outer and inner edges of the cortical VZ. Mathematical models have demonstrated the need for INM in maintaining proliferation (Murciano et al., 2002), based on evidence that local cell-cell interactions and lateral inhibition by Notch and Delta are important in determining whether cells remain proliferative or differentiate (reviewed in Lewis, 1998). Where INM was excluded from a model of proliferation, an enhanced rate of neurogenesis was predicted due to a greater physical interaction between proliferating and differentiating cells. This enhancement of neurogenesis led to the diminished growth of the neuroepithelium and a reduction in the later production of neurons. In keeping with this, short-term pharmacological block of INM, using the actin polymerization inhibitor cytochalasin B, which disrupts contractile microfilaments, results in an initial overproduction of retinal ganglion cells (Murciano et al., 2002). Consistent with these observations, suppressing the expression of Cx43, shown here to slow INM, causes a reduction in progenitor cell proliferation and leads to small eyes (Becker and Mobbs, 1999). Similarly, in the developing cortex, gap junction uncoupling reagents such as halothane and octanol decrease the number of cells in S phase (Bittman et al., 1997). Thus, the findings described here, that gap junction communication is necessary for maintaining normal rates of progenitor cell INM, which in turn is a determinant of

the rate of proliferation, are consistent with the role of gap junctions described in previous studies of increasing proliferation.

In the cortex, many of the cells that form coupled clusters in the VZ are clonally related (Cai et al., 1997b). Gap junction coupling may provide a means by which local groups of progenitor cells can exchange developmentally relevant signals, and could facilitate synchronized entry into the different phases of the cell cycle. The difference in cell cycle times between cortical progenitor cells of the same age is remarkably small, showing less than 8% variation (Cai et al., 1997a); clonal descendents progress through the cell cycle in synchrony and form tight clusters (Cai et al., 1997a, b). In the retina, as in the cortex, clonal descendants form columns (Reese and Tan, 1998). In this study, adjacent retinal progenitor cells were shown to move in synchrony. Gap junctions may thus act to locally coordinate the cell cycle via INM; $[Ca^{2+}]_i$-waves passing between progenitor cells via this route may represent one such synchronizing signal.

5.4.4 Hemichannels in the retina and their role in modulating INM

The presence of functional hemichannels in the embryonic neural retina was assessed using a variety of methods. Antibody staining with Gap 7M, which binds to a region on the first external loop of the connexin, which is only exposed on unopposed gap junction hemichannels and so does not bind to complete gap junctions, revealed sparse punctate immunoreactivity distributed throughout the neural retina. Pearson et al. (2005a) used the rate of dye-efflux in varying external Ca^{2+}-concentrations to probe the presence of functional hemichannels in the RPE. The rate of dye-efflux, indicated by the decrease in fluorescence, could be altered by changing the external Ca^{2+}-concentration, consistent with the presence of functional hemichannels in the developing RPE (Pearson et al., 2005a). However, despite numerous attempts, no correlation between rate of dye-efflux and change in external Ca^{2+}-concentrations was found in the neural

retina. A possible explanation for the divergent results obtained from this method and immunohistochemical labelling is that the density of hemichannels in the RPE is much greater than in the neural retina, allowing greater uptake and efflux of dye, resulting in more readily measurable changes in fluorescence.

Assessment of hemichannel expression by dye-uptake, as described by Weissman et al. (2004), showed that most cells in the E5 neural retina, but excluding cells in GCL, took up dye during a 30 minute incubation period, and this could be substantially reduced by incubation in high Ca^{2+} or CBX, consistent with a hemichannel-mediated uptake mechanism. Incubation in Gap26, a connexin-mimetic peptide used as a specific hemichannel blocker, reduced dye-uptake in 2 out of 4 preparations. Possible explanations for the inconsistent results of Gap26 incubation include firstly, that there is a nonlinear relationship between dye-uptake and fluorescence, due to the amplification-step in the revelation of Neurobiotin, and secondly, hemichannels formed by connexins other than Cx43 would not be blocked by Gap26. Since these cells are extensively coupled, a small amount of dye uptake from any residual hemichannels would spread to other cells within the coupled cluster. The consistency with which proliferating cells were loaded with dye, and the non-uniformity of the dye-uptake, excluding cells within the GCL, makes it unlikely that the observed pattern of dye-uptake results from damage caused during dissection or from a lack of membrane integrity. Given the effects of incubation in high Ca^{2+} or CBX, it is unlikely that the dye-uptake is mediated via a mechanism unrelated to gap junction proteins. Despite the lack of success with the dye-efflux experiments, and the equivocal results of the dye-loading experiments with Gap26, the observed pattern of dye-loading and its reduction by high Ca^{2+} or CBX, coupled with the immunohistochemical labelling, suggest that functional hemichannels are present in the neural retina.

The presence of Gap26 caused a small, but significant reduction in the speed of INM. While the effect was smaller than that caused by pharmacological gap

junction block or gap junction down regulation, the results suggest that, in addition to intact gap junctions, unopposed hemichannels may play a role in regulating INM. Weissman et al. (2004) recently reported that hemichannels in progenitors in the VZ of the developing cortex are involved in initiation of VZ Ca^{2+}-waves, possibly via the release of ATP, and that both the frequency and extent of these Ca^{2+}-waves increase as neurogenesis proceeds. While the actions of purinergic agents on INM do not support a similar role for ATP-release via hemichannels in the neural retina (see below), it is possible that hemichannel opening leads to release of other signalling molecules, which are involved in the regulation of INM, and/or have other direct or indirect effects on proliferation. The results presented here do not shed any light on how opening of hemichannels affects INM, and this requires further investigation.

5.4.5 The role of neurotransmitters in modulation of INM

Neurotransmitters are intimately involved in the regulation of neuronal migration. In the developing cortex, NMDA-receptor activation regulates migration of newborn cerebellar granule cells (Komuro & Rakic, 1993, 1998; Rossi & Slater, 1993; Farrant et al., 1994), and newborn cortical neurons (Behar et al., 1999). GABA can stimulate migration of cortical neurons during rat cortical histogenesis, where dynamic expression of GABA-receptors modulates the migratory responses to GABA (Behar et al., 1998; 2000). During neuronal migration, the cell moves via mechanisms that involve microtubules and their associated motor proteins (Rakic et al., 1996). $[Ca^{2+}]_i$ transients are involved in the regulation of the dynamic assembly and disassembly of these cytoskeletal elements. Given the central role of Ca^{2+}-signalling in regulating migration of postmitotic cells, and the similarities between the mode of migration of immature neurons, and INM in retinal PCs, signalling molecules that affect $[Ca^{2+}]_i$ are likely to play pivotal roles in the regulation of INM. In the developing retina, GABA, glutamate, UTP and carbachol have all been shown to generate $[Ca^{2+}]_i$ transients among the cells of

the VZ, and, in the case of UTP and carbachol, exert profound effects on proliferation (Pearson et al., 2002; Pearson, 2003). It was therefore surprising that these neurotransmitters exert only limited effects on the rate of INM in the retina. While, as described below, some significant effects were observed within each paired drug/control group, the magnitude of the effects were small, and the range of INM velocities observed spanned a similar range in controls and in retinae treated with neurotransmitters and their antagonists.

Purinergic stimulation caused a small reduction in the rate of movement of cells away from the VZ, whilst the antagonist PPADS had the opposite effect of increasing the rate of movement from the VZ. In both cases, there was no effect on cells moving towards the VZ, i.e. progenitors in G_2. Given the positive modulatory effects of purinergic signalling on Ca^{2+}-transients, both in individual cells (Sugioka et al., 1996; Pearson et al., 2002) and as coordinated wave activity (Weissman et al., 2004), and the positive correlation between the amplitude and frequency of Ca^{2+} fluctuations with migration, for example in cerebellar granule cells (Komuro & Rakic, 1996), these findings are unexpected. Firstly, it is puzzling that no effects are seen in the population of cells moving towards the VZ, given the extensive evidence of robust purinergic Ca^{2+}-responses in progenitor cells from the earliest times examined in the chick retina. Secondly, it is surprising that UTP decreases rate of INM, whereas PPADS causes an increase, given the positive effects of purinergic agonists, and negative effects of purinergic antagonist, on overall eye size and mitotic cells when present *in ovo* (Pearson et al. 2002).

Carbachol caused a small but significant increase in the rate of INM, compared to control. The muscarinic antagonist pirenzepine had no effect on the rate of INM. Pearson et al. (2002) reported that, within the VZ of E4-6 retinae, nearly all cells respond to carbachol with an increase in $[Ca^{2+}]_i$, and at E6, pirenzepine (25 μM, the same concentration used here) caused a 70-80% decrease in the number of spontaneous $[Ca^{2+}]_i$ transients. Given the dramatic effects of muscarinic signalling

on $[Ca^{2+}]_i$, it is perhaps surprising that that these agents have little or no effect on the rate of INM at E5.

Glutamate caused a small but significant increase in the rate of INM of cells moving towards the VZ. While there was no increase in the mean rate of cells moving away from the VZ, a closer examination of the distribution of INM speeds in this population suggests there may be also be an increase in the velocities of INM in a sub-population of cells moving away from the VZ in the presence of glutamate. Unfortunately, amongst the cells moving away from the VZ, it is not possible to distinguish between progenitors in G_1 and postmitotic cells, to assess if glutamate affects these two populations differently. Several previous studies have shown that glutamate can affect the migration of postmitotic neurons (Komuro & Rakic, 1993, 1998; Rossi & Slater, 1993; Farrant et al., 1994; Behar et al., 1999). However, the results presented in Chapter 3 show that newly differentiated cells in the retina do not express ionotropic glutamate receptors at this time, and only a subset of progenitors at E5 respond to glutamate. NBQX caused a small but significant decrease in the speed of INM of cells moving away from the VZ. The glutamate transport inhibitor, TBOA, also caused a small decrease in the rate of INM of both populations. The effect of both NBQX and TBOA on the speed of INM suggests that endogenous glutamate does play a role in the regulation of INM, potentially mediated via calcium influx following depolarisation. The role of glutamate transport in retinal progenitor cells at this time is intriguing: blocking glutamate uptake with TBOA resulted in an effect similar to, rather than opposing, the effect of NBQX; one might expect that any actions of glutamate mediated by an NBQX-sensitive receptor would be enhanced by blocking glutamate uptake, rather than reduced. This requires further investigation. It would be interesting to test the combined effect of NBQX and TBOA, to see if their effects are additive.

The application of GABA had no effect on the speed of INM. This is surprising, given the findings presented in Chapter 3 that nearly all progenitor cells at this

time respond to GABA with depolarisation, which may result in Ca^{2+} influx through voltage-gated calcium-channels. The presence of bicuculline resulted in a small decrease in the rate of movement of cells moving away from the VZ, indicating that endogenously released GABA may play a role in regulating INM. The absence of any effect of exogenously applied GABA highlights a potential problem with the present study, namely that all transmitters were bath-applied, resulting in a constant elevated agonist concentration, which may lead to receptor desensitisation. In particular, the effects of GABA- and glutamatergic blockers were not mirrored by the effects of the receptor agonists, signifying that although endogenous signalling takes place through these receptors, this is not increased by exogenous agonist application. Interfering with the uptake or breakdown of these transmitters may be a better way to study their role in INM.

In summary, the large variation in the range of movement velocities seen in the control population, and the small magnitude of the effects of neurotransmitter agonists and antagonist makes it difficult to assess if the observed effects reflect genuine physiological phenomena or experimental artefacts. However, the observation that the antagonists PPADS, NBQX and bicuculline, and the glutamate transport inhibitor, TBOA, exerted effects in the absence of exogenously applied agonists, suggests that endogenous release of agonists for these receptors may affect INM. Potentially, multiple signalling pathways act in concert to regulate INM. If this is so, perhaps the role of neurotransmitters in the regulation of INM can be more clearly evaluated by blocking several signalling pathways simultaneously. However, given the extensive evidence of neurotransmitter responses in progenitor cells, and the robust effects of transmitters on $[Ca^{2+}]_i$ in these cells, it is surprising that these transmitters did not have more marked effects on the speed on INM.

5.5 Further studies

In order to unravel the effects of neurotransmitters on $[Ca^{2+}]_i$ and the effects of $[Ca^{2+}]_i$ in regulating INM, numerous attempts were made to image $[Ca^{2+}]_i$ in migrating cells. However, the need to image at sufficiently high time resolution to see any meaningful changes in $[Ca^{2+}]_i$ was confounded by the rapid bleaching of the $[Ca^{2+}]_i$-indicators employed during the ~20-minute period needed to reliably measure migration. Further work is required to develop a method to measure the changes in $[Ca^{2+}]_i$ in migrating cells with a high temporal resolution. The use of two-photon microscopy may facilitate this, by reducing the bleaching of the $[Ca^{2+}]_i$-indicator. It would also have the advantage of reducing phototoxic damage.

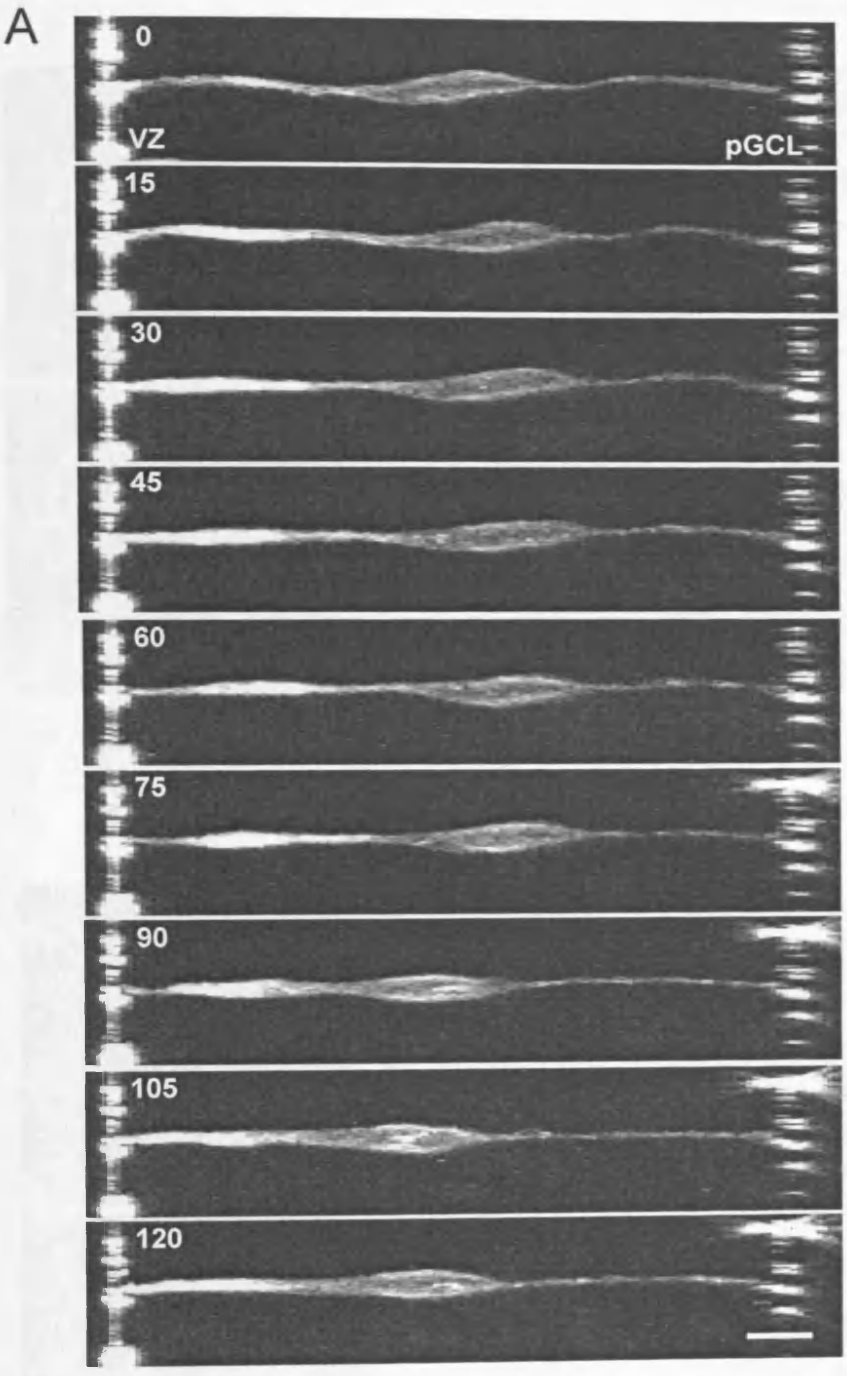

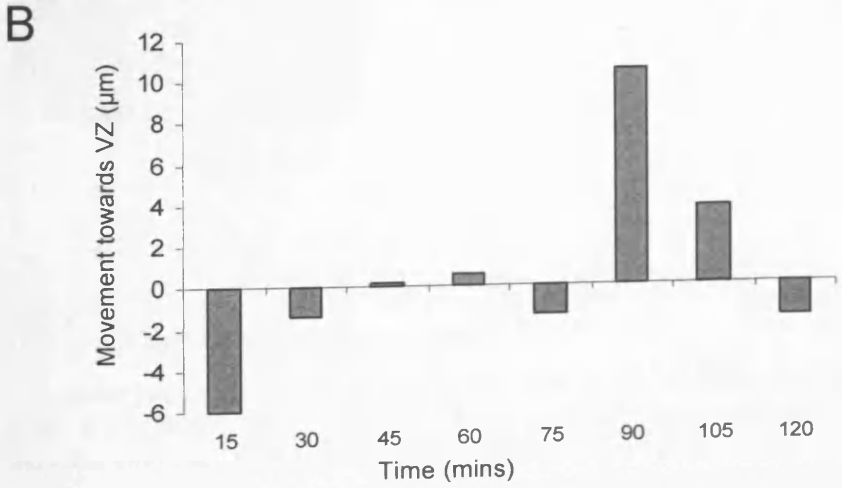

Figure 5.1 Interkinetic nuclear migration in the retina. A, DiI labelling of retinal cells at E5 reveals a bipolar cell morphology, with processes extending to either surface of the tissue. The ventricular process is thicker than the vitreal process.The cell makes movements in both directions, with net movement towards the VZ, at an average speed of 12.8 µm/h. *B,* The movement of the cell body for each time interval is illustrated, with movements away from the VZ shown as negative. This illustrates the saltatory nature of the movement, with rapid movements in either direction interspersed with periods of little or no progress.

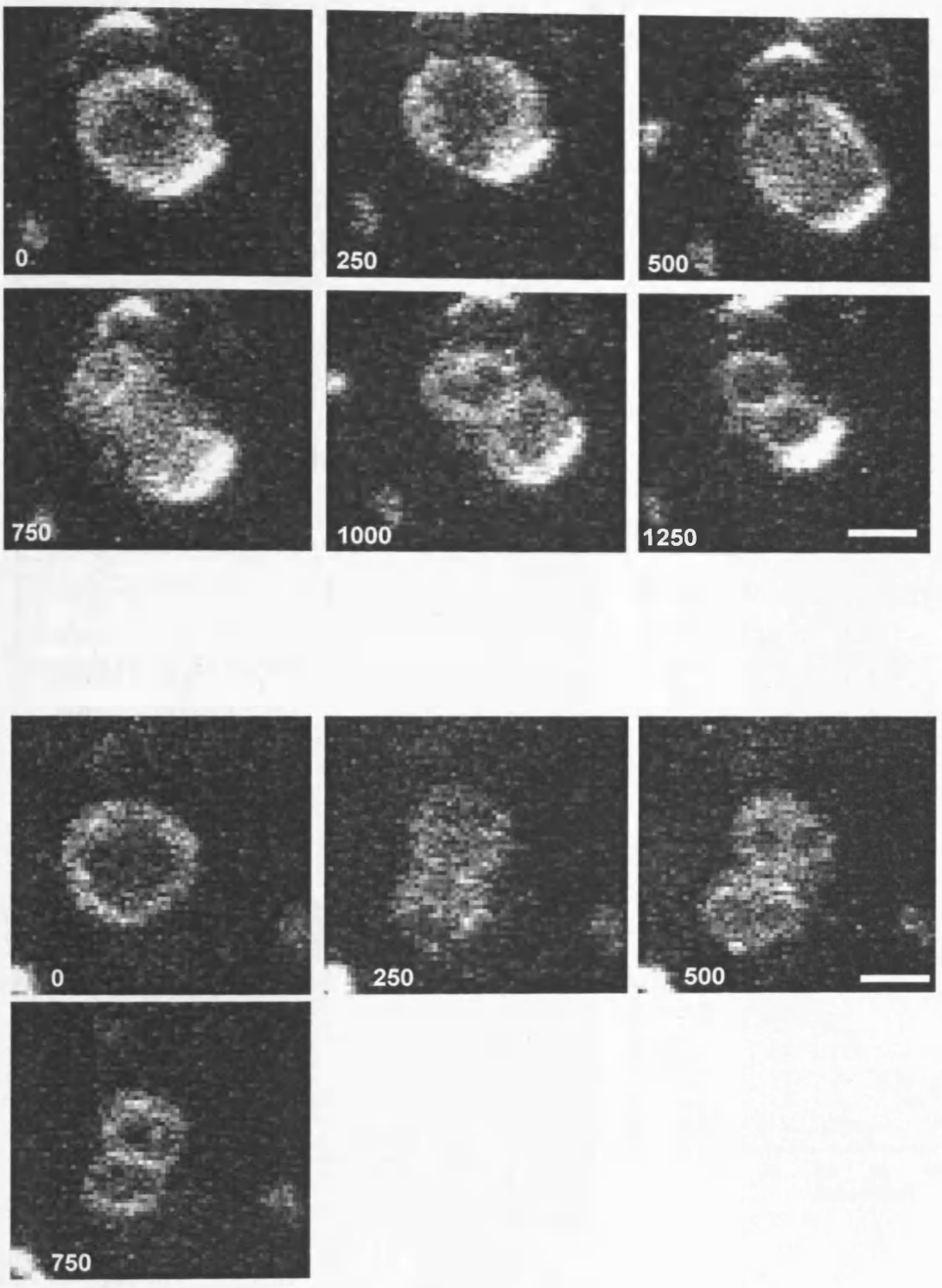

Figure 5.2 Mitosis in DiI-labelled cells

Two examples of DiI-labelled progenitor cells in an E5 retina undergoing mitosis. Images show a single confocal section through the VZ. Numbers in lower left hand corner indicate time (seconds). Scale bars 5 μm.

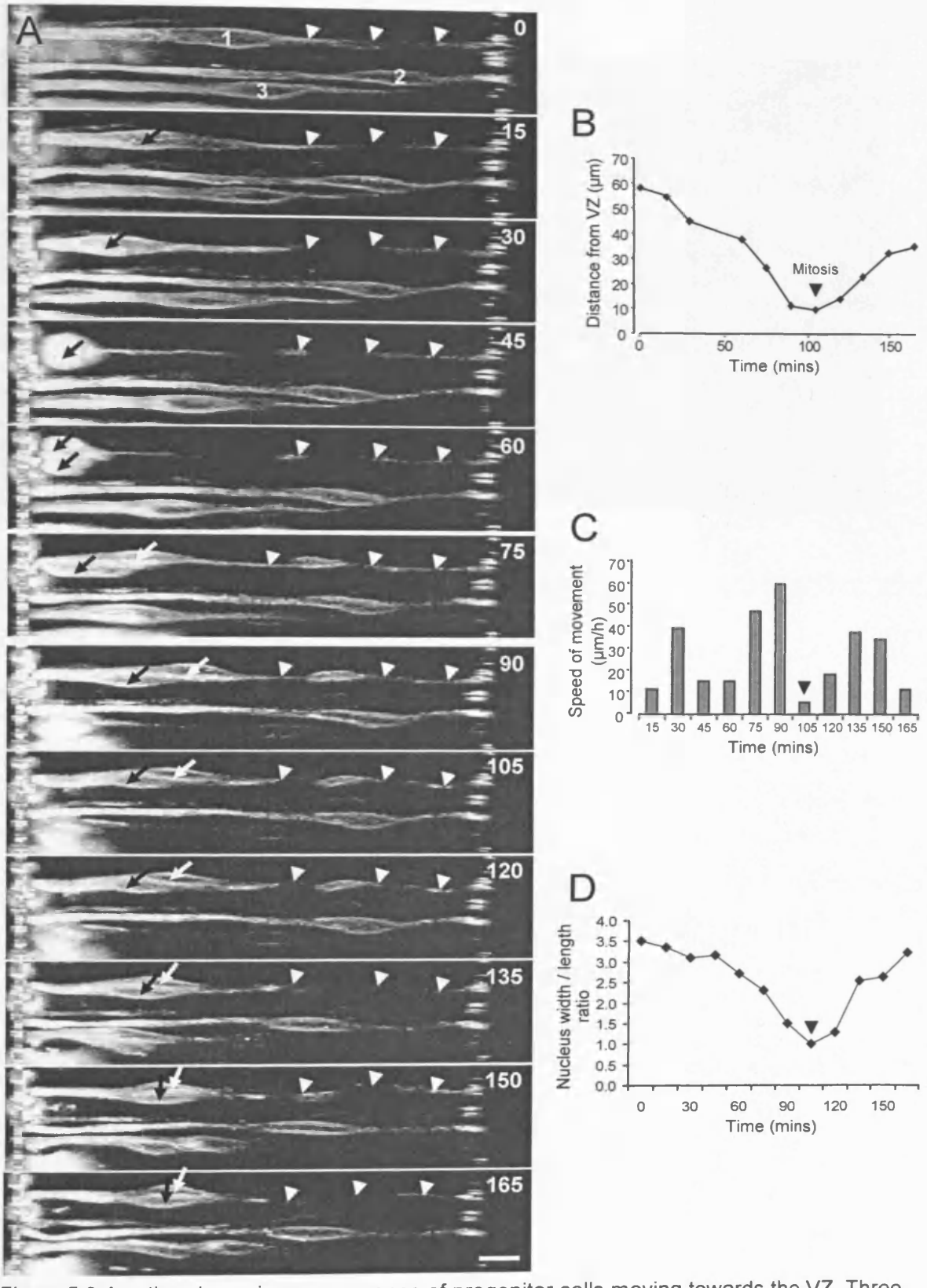

Figure 5.3 A, a time-lapse image sequence of progenitor cells moving towards the VZ. Three cells are shown (1-3). Cells 1 and 3 make saltatory movements towards the VZ. The cell bodies round up prior to division. Cell 1 retains its contact with the vitreal surface throughout division (*arrowheads*). Following division, the daughter cells remain in close contact as they move away from the VZ (*arrows*, cell 1). Scale bar 10 µm. *B-D*, details of the movements of cell 3. *B*, The distance traveled, *C*, the speed of movement and *D*, the length/width ratio of the cell body are each shown as a function of time. Mitosis occurs between 90 and 105mins (indicated by arrowheads). After this time, measurements are shown for the daughter cell nearest the VZ.

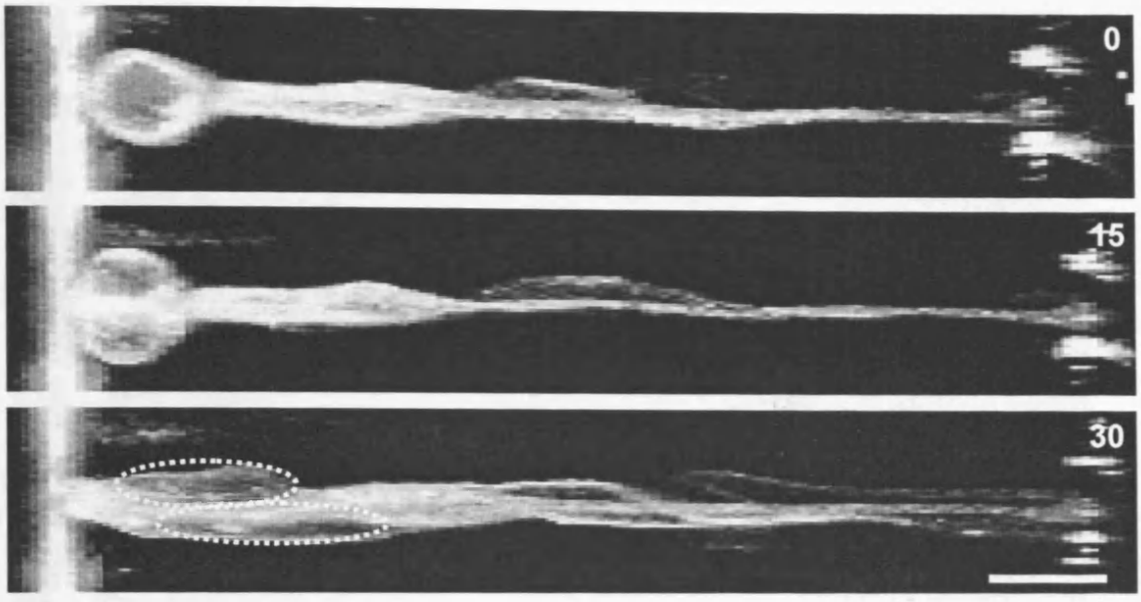

Figure 5.4 Maintained process during mitosis
A time-lapse image sequence of cell division. Numbers in the top right hand corner of each frame indicate the time (mins) of imaging. In the first frame (t 0), the nucleus is juxtaposed to the ventricular surface and rounded up. At t 15, the cell is going through mitosis, with the vitreal process clearly maintained. At t 30, the two daughter cells (cell bodies are outlined) start to move away from the VZ. Scale bar 10 μm.

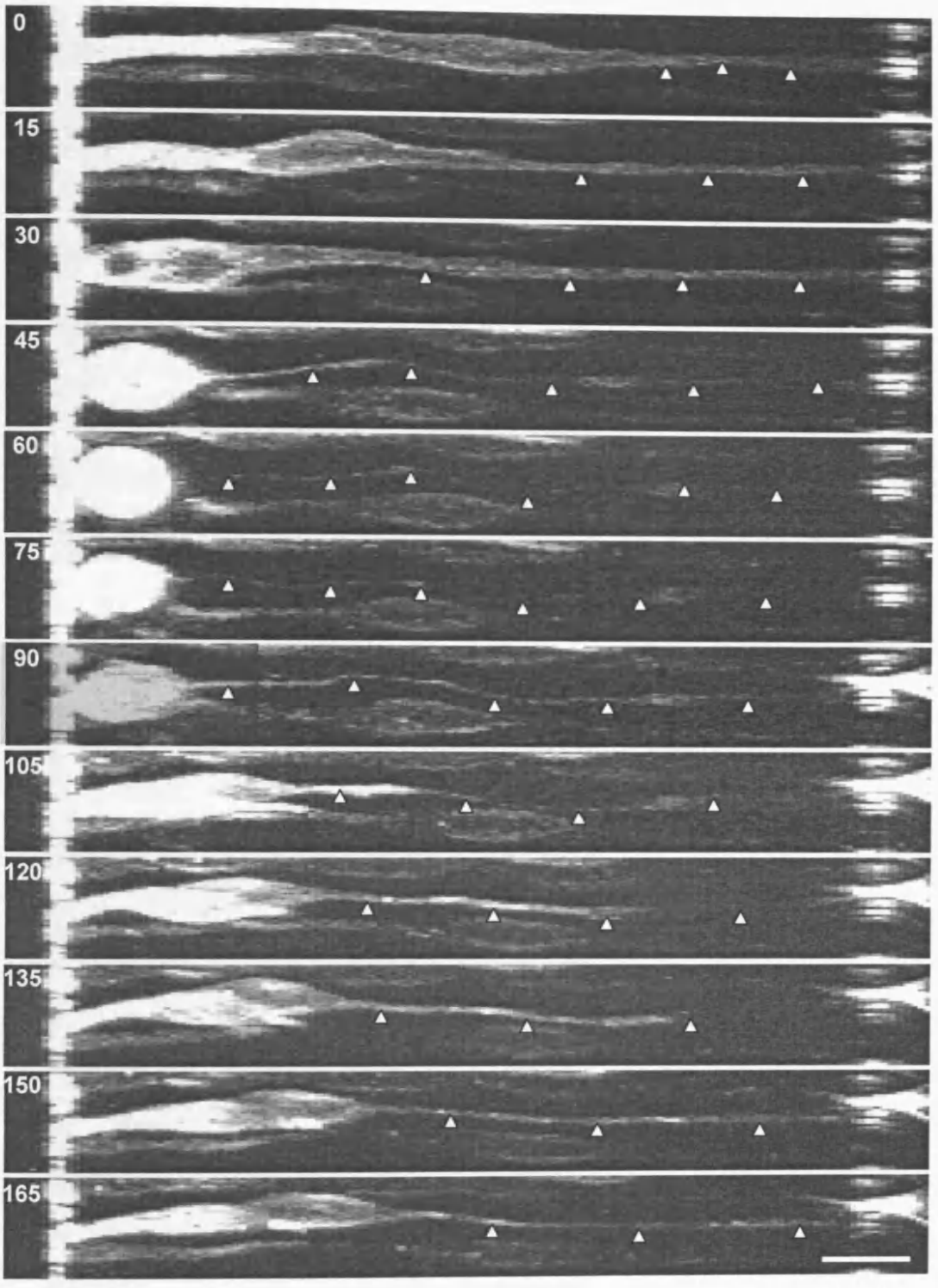

Figure 5.5 Process thinning during mitosis
A time-lapse image sequence of cell division. Numbers in the top left hand corner of each frame indicate the time (mins) of imaging. At timepoints 0-30, the vitreal process is several µm thick and clearly visible. As the nucleus rounds up on approach to the VZ (t 45), and goes through mitosis (t 60-75), the process thins to a fraction of a micron and becomes nearly invisible. Following mitosis, the vitreal process thickens again (t 90 onwards). The process is highlighted by white arrowheads in each frame. Scale bar 10 µm

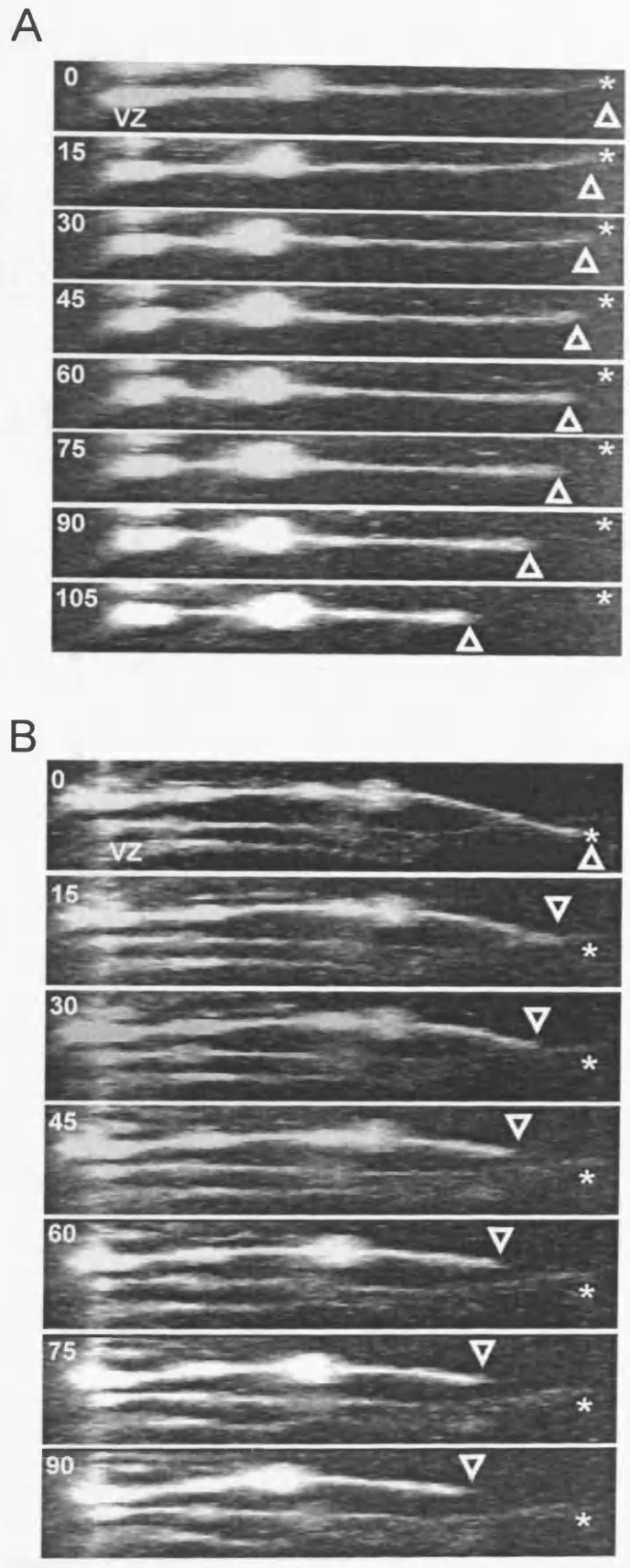

Figure 5.6 Process retraction as the nucleus moves towards the VZ
A-B, Two examples of cells showing retraction of the vitreal process as the nuclues makes saltatory movements towards the VZ. In each frame, the number in the top left corner indicates time of imaging (mins), the asterisk marks the position of the tip of the vitreal process at t_0, whereas the open arrowhead marks the current position.

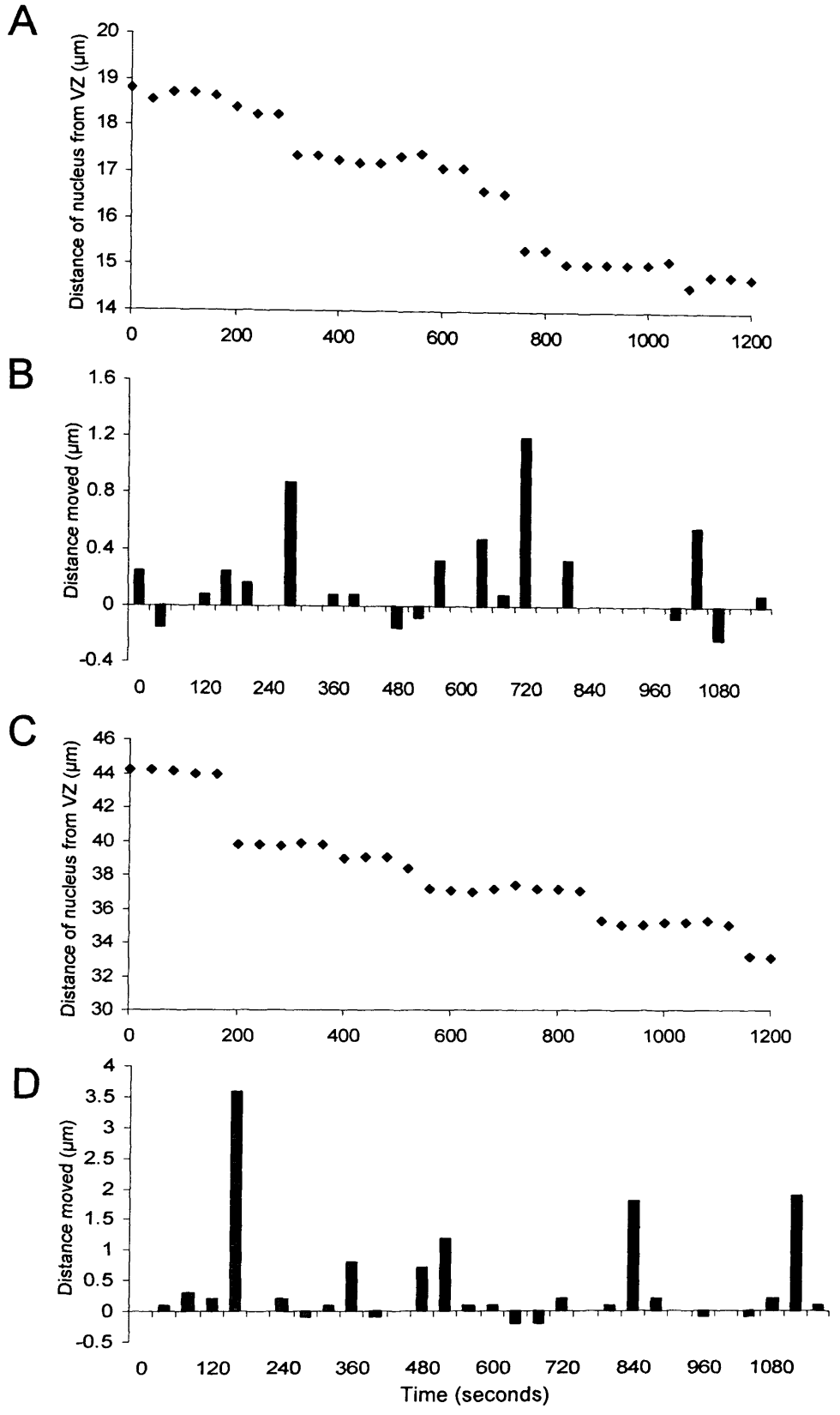

Figure 5.7 Imaging of INM at higher frequencies of a slow and a fast moving progenitor cell. *A*, The distance of the nucleus from the VZ as a function of time, and *B*, the distance moved at each timepoint of a cell moving at a mean rate of 12.2 µm/h. *C*, The distance of the nucleus from the VZ as a function of time, and *D*, the distance moved at each timepoint for a cell moving at a mean rate of 33.3 µm/h. In *B* and *D*, positive values represent movement towards the VZ, whereas negative values represent movement towards the putative GCL.

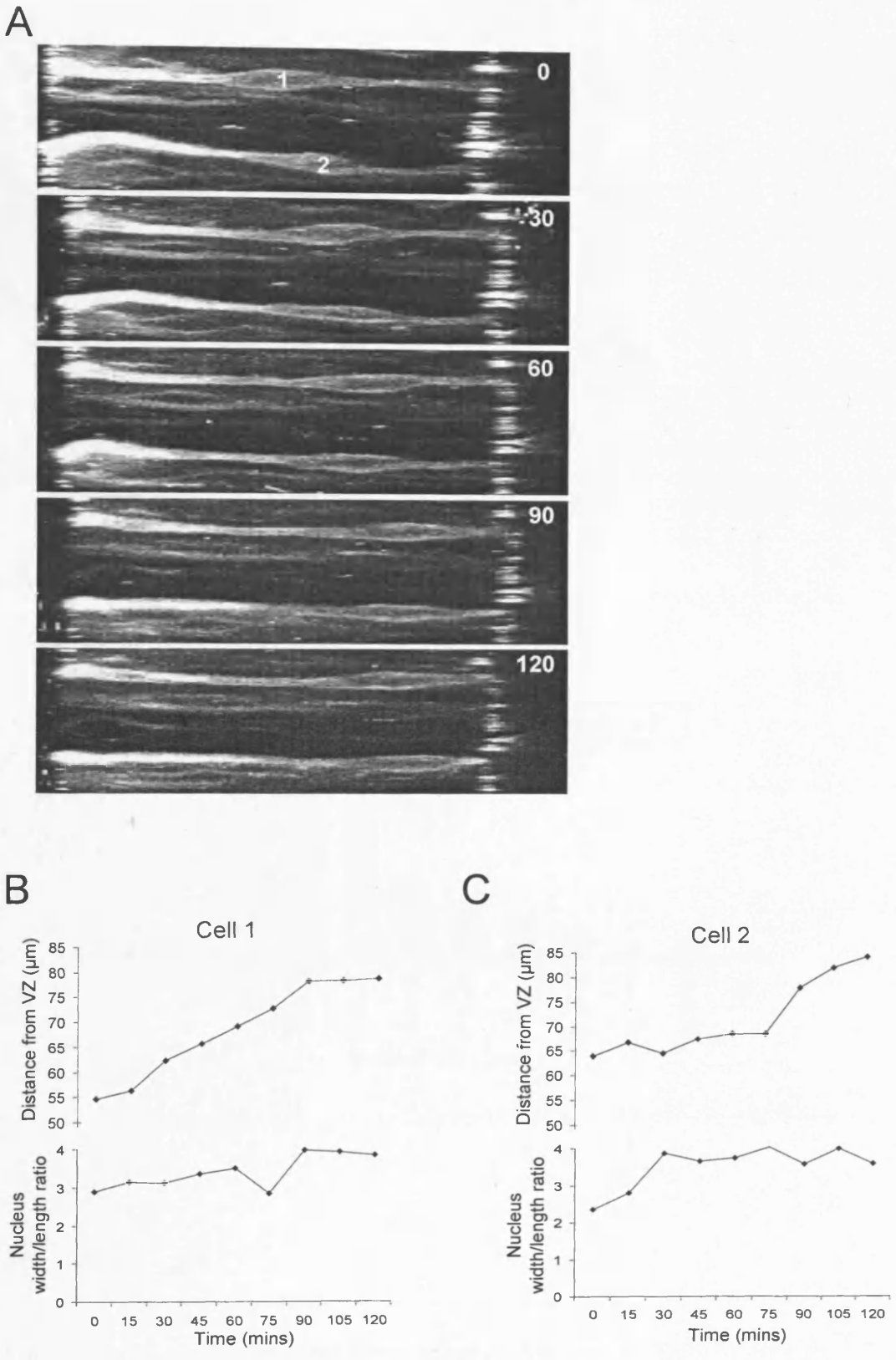

Figure 5.8 A, Timelapse images of two DiI-labelled cells moving away from the VZ. Numbers in the top right corner of each frame indicate time of imaging (mins). *B-C*, Details of cells 1 and 2, respectively, showing the distance from the VZ and the width/length ratio of the nucleus over time. The average rates of movement was 12.1 µm/hr for cell 1 and 12.3 µm/hr for cell 2.

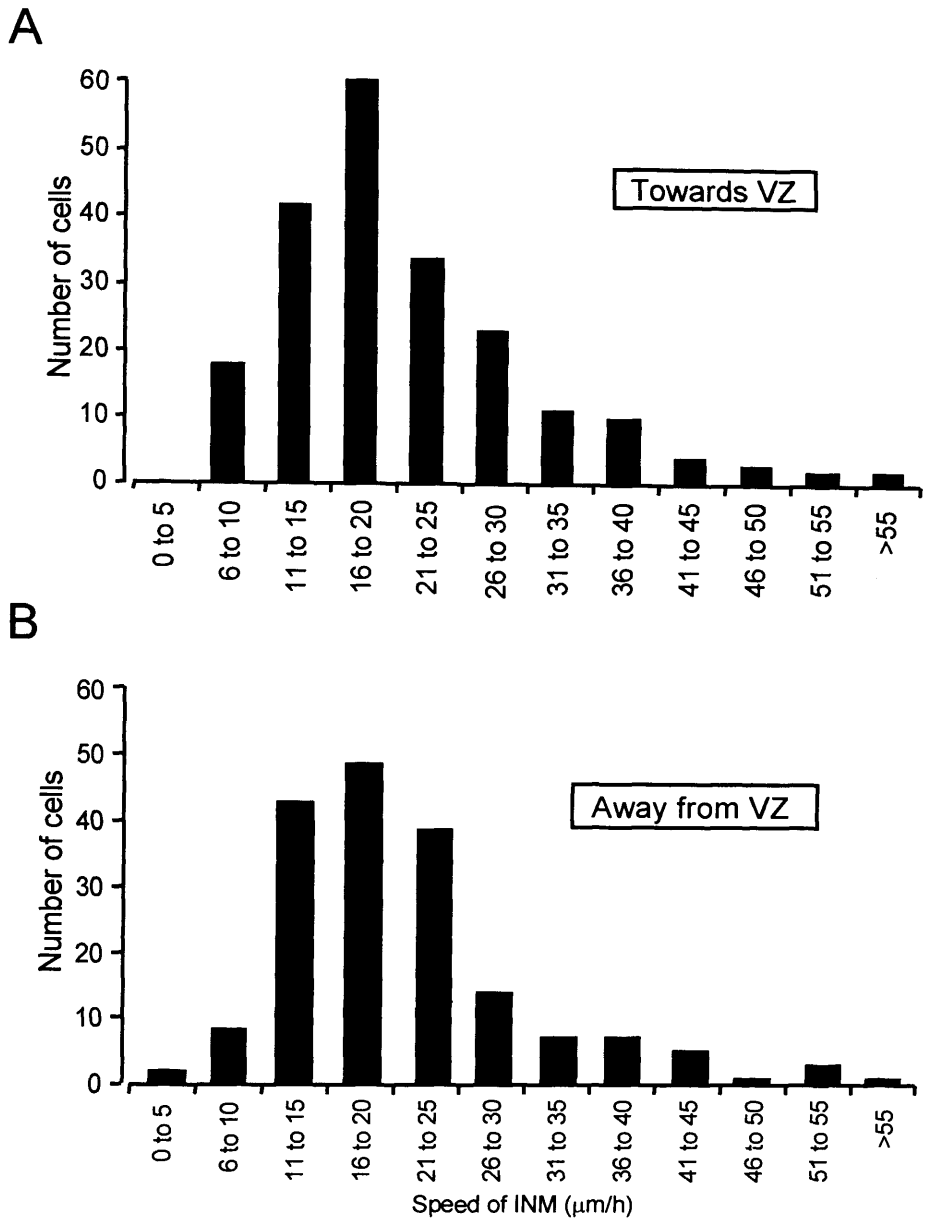

Figure 5.9 The distribution of the mean speed of INM
At E5, the average speed of INM is 20.7±0.5μm/h (N=53, n=389). *A,* The rate of movement of nuclei moving towards the VZ (progenitor cells in G2) was 20.5±0.7μm/h (range 2.5-68.6μm/h; n=213). *B,* The rate of movement of nuclei moving away from the VZ (mixed population of progenitor cells and postmitotic cells) was 21.0±0.8μm/h (range 4.5-64.2μm/h; n=176; Fig. 3b). There is no statistical difference between the mean speeds (p=0.617) of INM in cells moving towards or away from the VZ.

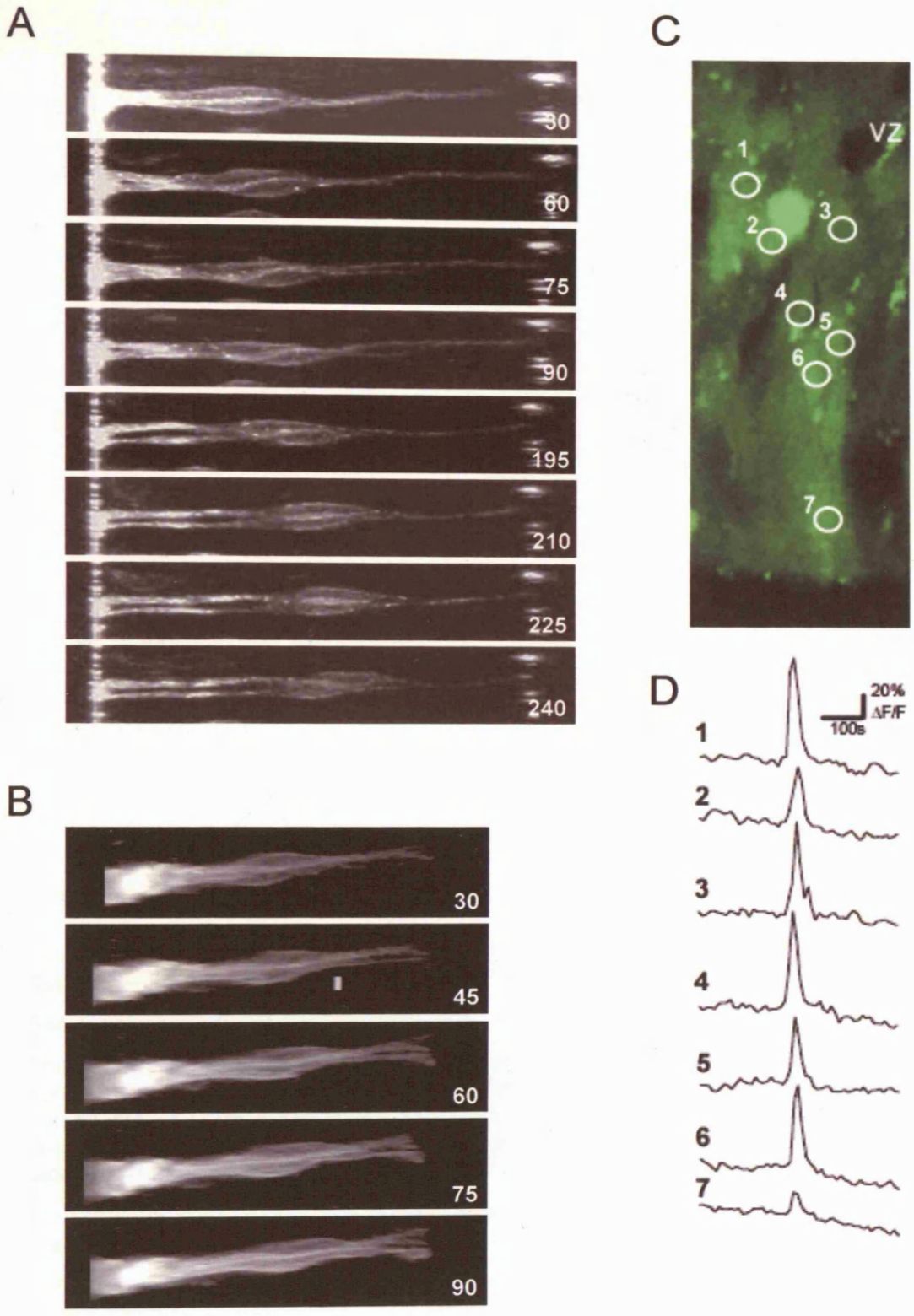

Figure 5.10 The coordinated movement of neighbouring cells
A-B, Examples of coordinated movement in pairs of neighbouring cells. Numbers in the lower right corner of each frame indicate time of imaging (mins). *C*, Ca^{2+}-imaging through the thickness of a retina loaded with Fluo-4 shows a column of cells undergoing a spontaneous coordinated [Ca2+]i-wave. Image provided by RA Pearson. *D*, traces showing fluorescence changes in cells 1-7 depicted in *C*.

See CD bound in on back cover

Supplementary movie of interkinetic nuclear migration.

See supplementary movie on enclosed CD

The preparation was labelled with DiI using immersion labelling and imaged using confocal microscopy. Z-stacks through the thickness of the retina were acquired at 15 minute intervals over a period of 5.5h. The resulting 3D stacks were rotated through 90 degrees to give a side-on projection view; this was repeated for each time point and assembled to produce a time-lapse movie.

Four cells (or pairs of cells) are highlighted by numbers (left). In each case, an asterisk marks the position of the nucleus in the first frame.

The nucleus of **cell 1** undergoes saltatory movements in both directions at an average rate of 15μm/hour, and rounds up on approach to the VZ, towards the end of the time-series. The nucleus moves a total of 42μm towards the VZ from first to last frame.

The nucleus of **cell 2** makes saltatory movements and moves towards the vitreal surface, at an average rate of 11μm/hour.

The nucleus of **cell 3** moves rapidly towards the VZ during the first 6 frames (average rate of 45μm/hour), rounding up as it does so, and undergoes mitosis during frames 7-10. The cell maintained its vitreal process throughout division. From frame 11 onwards, two separate daughter cells can be seen moving away from the VZ.

Cell pair 4 also undergoes saltatory movements, moving a total of 34μm away from the VZ during the period imaged, the two nuclei maintaining close proximity throughout.

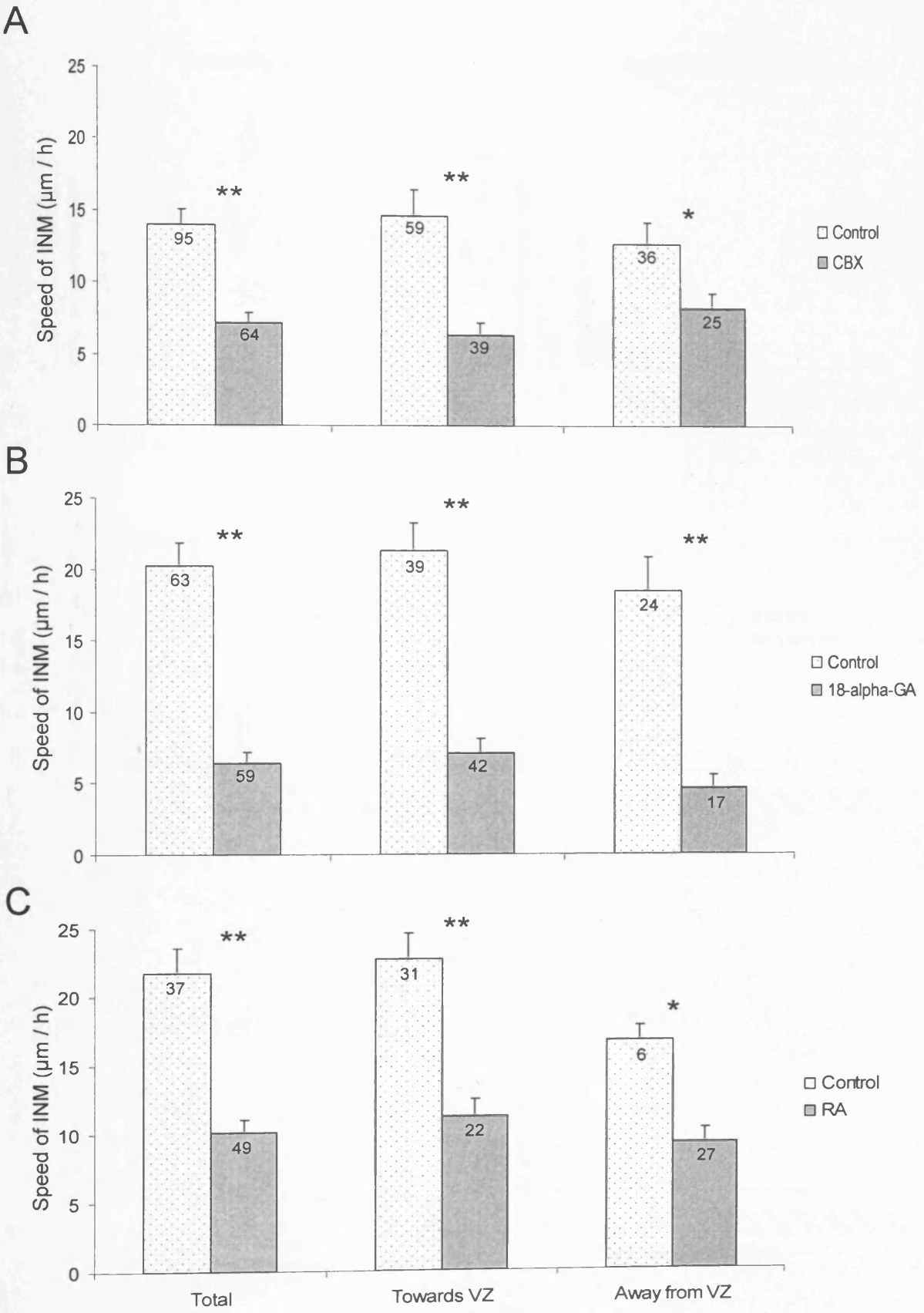

Figure 5.11 The effect of gap junction blockers on the speed of INM All three gap junction blockers tested cause a significant decrease in the rate of INM, for cells moving both towards and away from the VZ. *A*, CBX (N=6), *B*, 18-α-GA (N=6), *C*, retinoic acid (N=4).

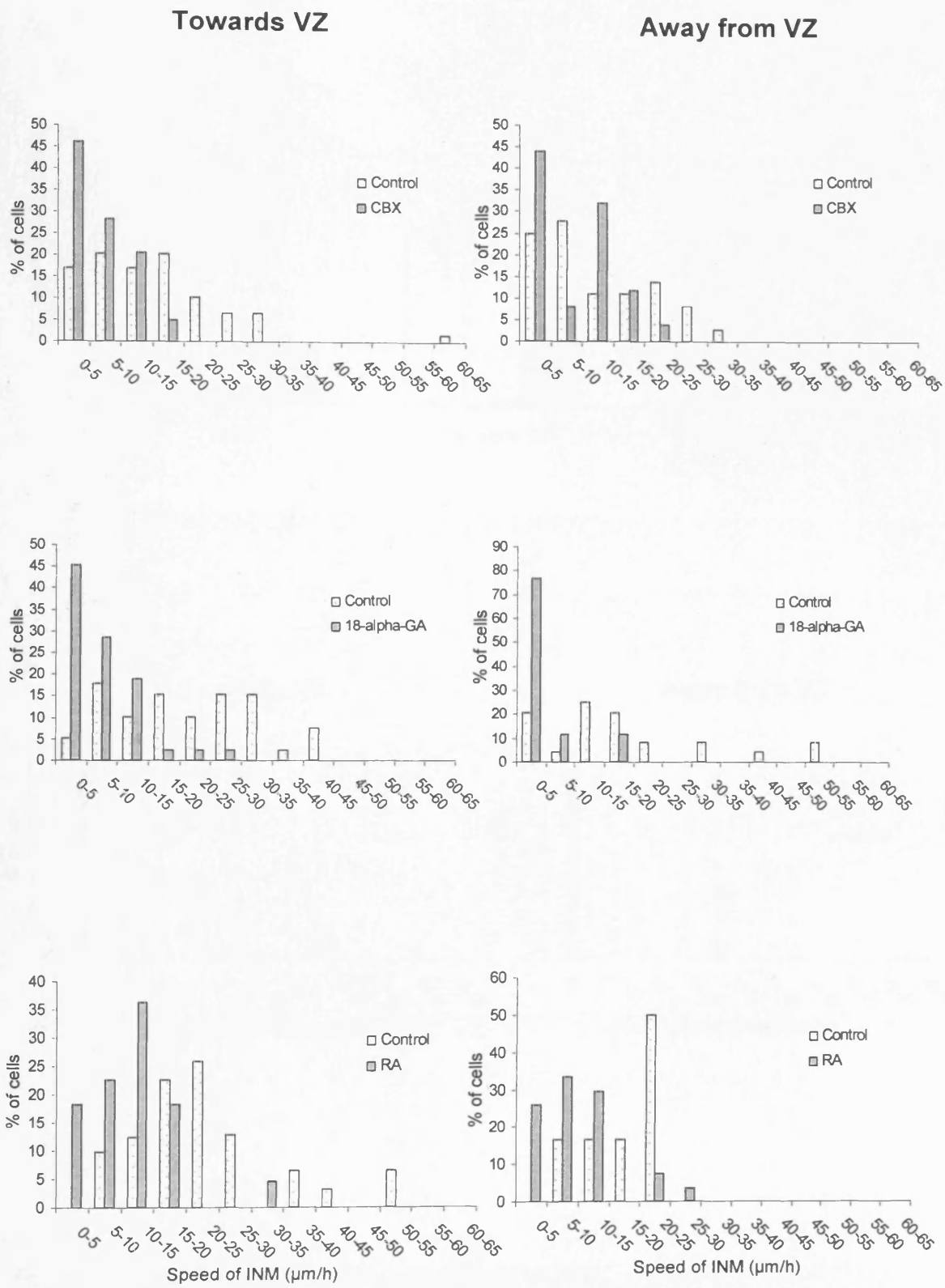

Figure 5.12 The effect of gap junction blockers on the distribution of the speed of INM
The distribution of the speed of INM in control and CBX (*A*), 18-alpha-GA (*B*), and retinoic acid (*C*). See previous figure for numbers of cells in each category.

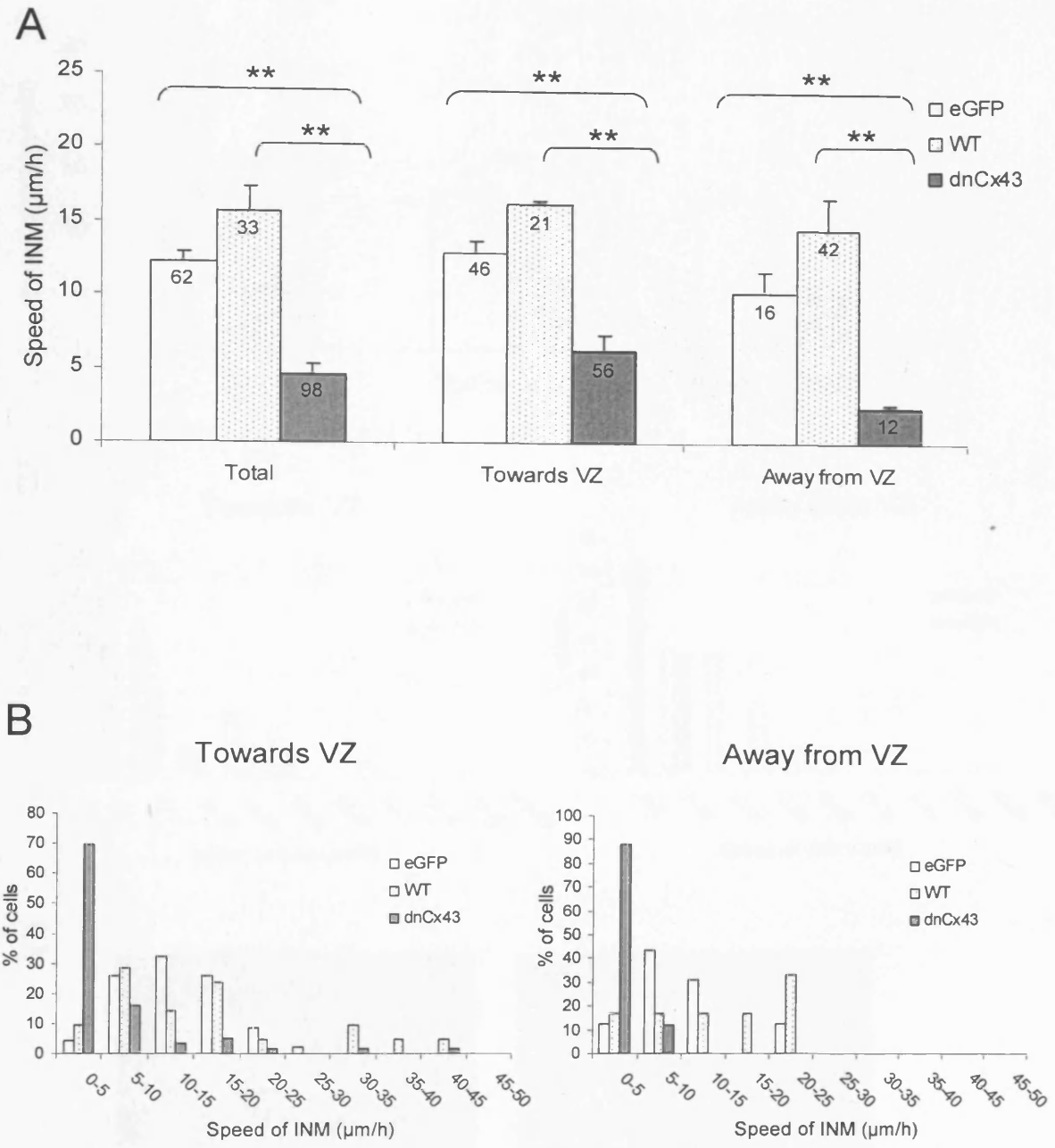

Figure 5.13 The effect of transfection with dnCx43 on INM
A, Graph showing the effects of dnCx43 (N=5) and wildtype (WT) Cx43 (N=2), compared to eGFP (N=5) control, on the mean speed of INM. Transfection with wildtype Cx43 does not significantly alter mean rate of INM, compared to eGFP control (p=0.08, total cell population; p=0.21, toward VZ; p=0.12, away from VZ). *B*, Distribution of the speed of INM in cells transfected with eGFP, WT or dnCX43. The effect of the dnCx43 is similar for cells moving towards or away from the VZ.

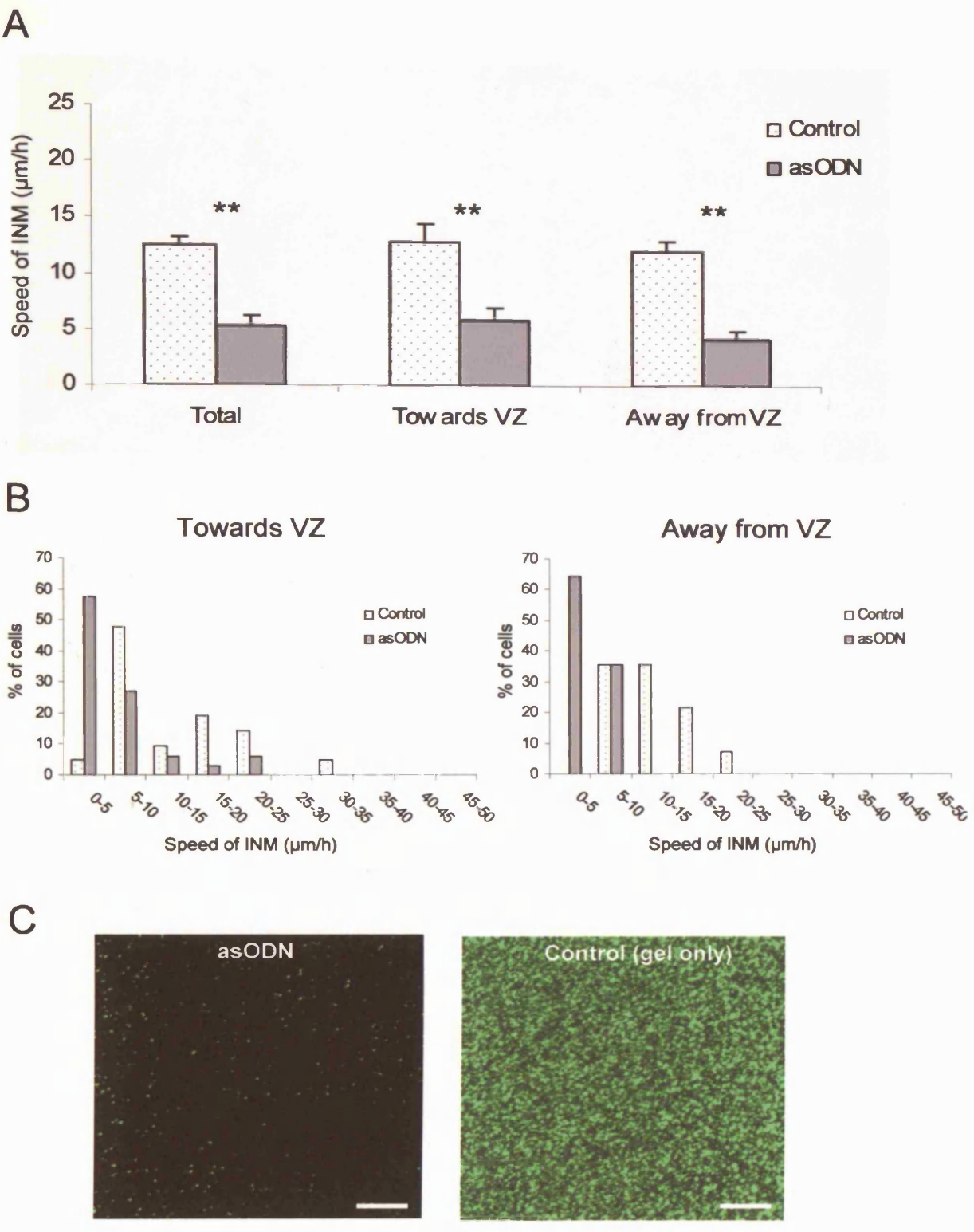

Figure 5.14 The effect of Cx43asODNs on INM
A, Graph showing the effects of Cx43asODNs on the mean speed of INM compared to control (N=4). *B*, Distribution of speed of INM in cells following application of Cx43asODNs compared to control. The effect of the Cx43asODN is similar for cells moving towards or away from the VZ. *C*, Projections of confocal image stacks through the entire retina labelled with an antibody for Cx43, showing the extent of Cx43 expression after treatment with asODN or with pluronic gel. Scale bar 10 µm.

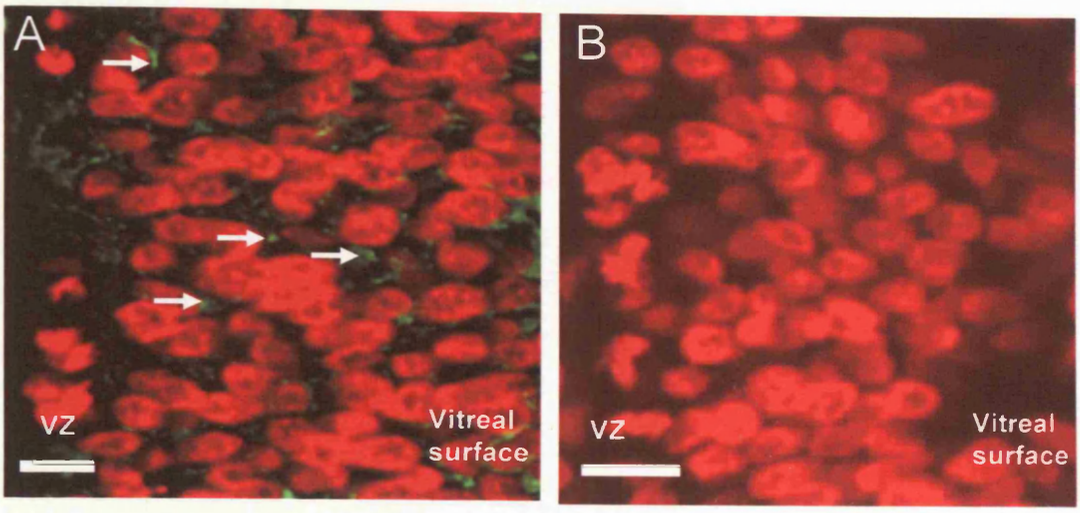

Figure 5.15 Antibody staining confirms the presence of hemichannels in the neural retina. A, Projection of 5 confocal sections taken at 1μm intervals of an E5 retina which has been labeled with Hoechst 33342 (red) and Alexa-488-tagged Gap 7M (green), which labels connexin hemichannels. Sparse punctate staining is seen throughout the neural retina (*arrows*). *B,* Control staining in which the primary antibody was omitted. Scale bars 10 μm.

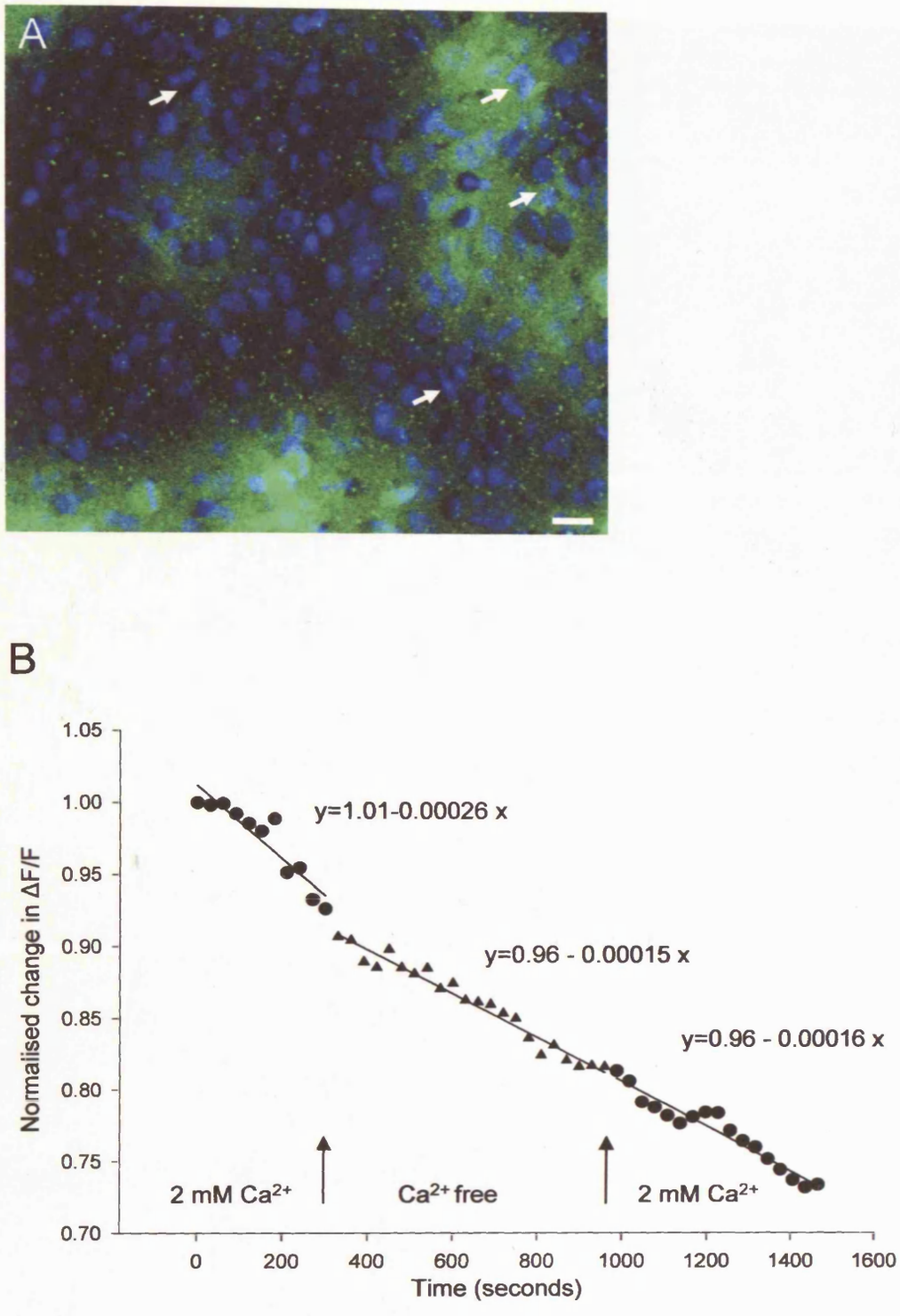

Figure 5.16 Assessment of hemichannels by imaging Alexa efflux
A, a single confocal section through the VZ shows uptake of Alexa 488 (green) in groups of cells. Simultaneous imaging of Hoechst 33342 (blue) was used to localise the VZ, and examples of mitotic profiles of cells, some including and some excluding Alexa 488, are indicated (arrows). *B*, The confocal section shown in *A* was imaged for 25 minutes in the presence of varying concentrations of Ca^{2+}, and the normalised change in fluorescence (from Alexa 488 only) is shown over time. The changes in Ca^{2+} concentration of the perfusate are indicated. Least squares lines are fitted to the data, and the equations shown. Scale bar 10 μm.

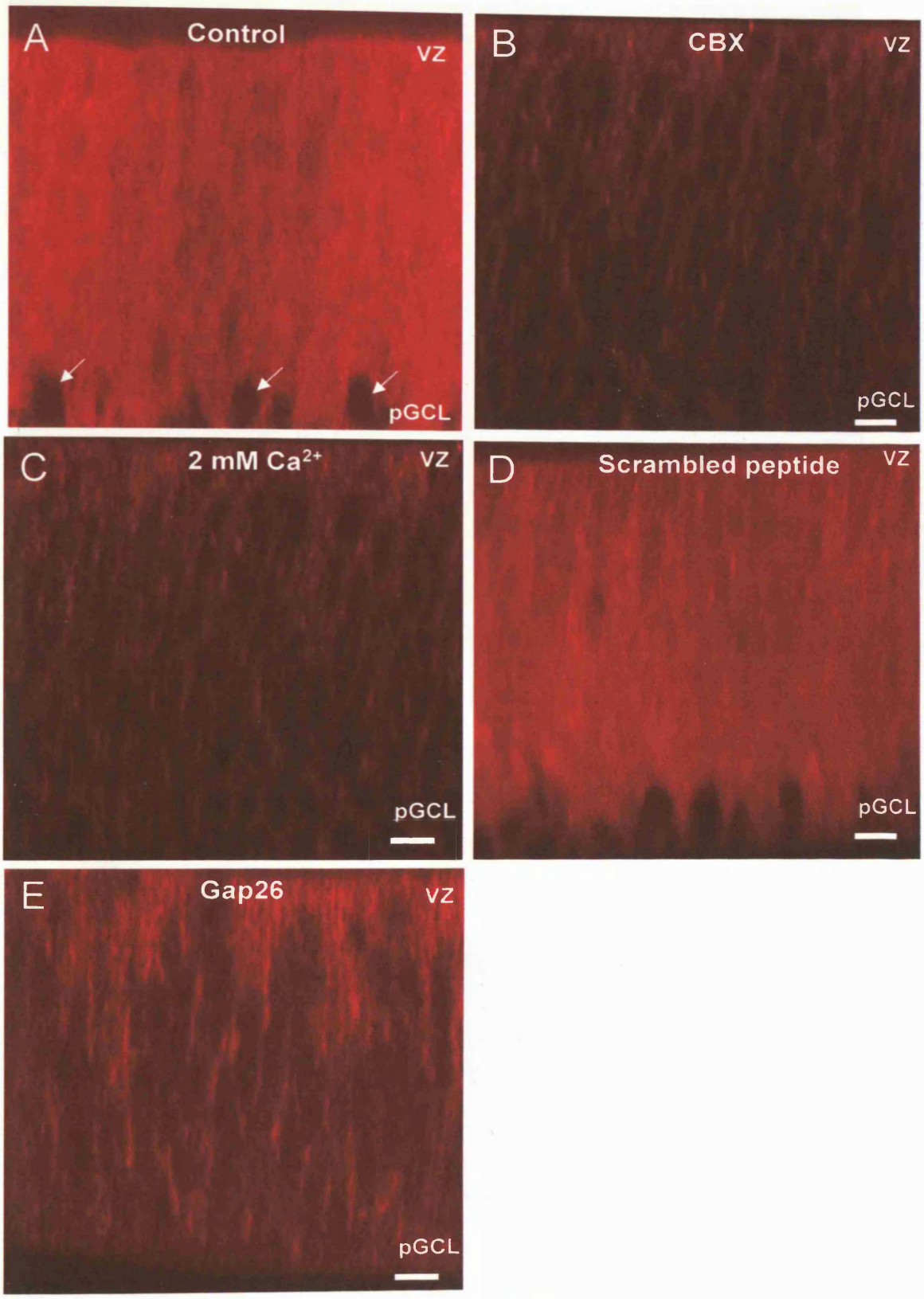

Figure 5.17 Assessment of hemichannels by Neurobiotin uptake
During a 30 min incubation period with 1mM Neurobiotin, acutely dissected E5 retinae show uptake of dye in the majority of cells *(A)*, except within the GCL (arrows). The amount of dye uptake could be reduced by CBX (*B*) and high Ca^{2+} *(C)*. The connexin mimetic peptide, Gap26, partly reduced uptake of Neurobiotin *(E)*, but the scrambled control peptide had no effect *(D)*. Scale bars 10 µm

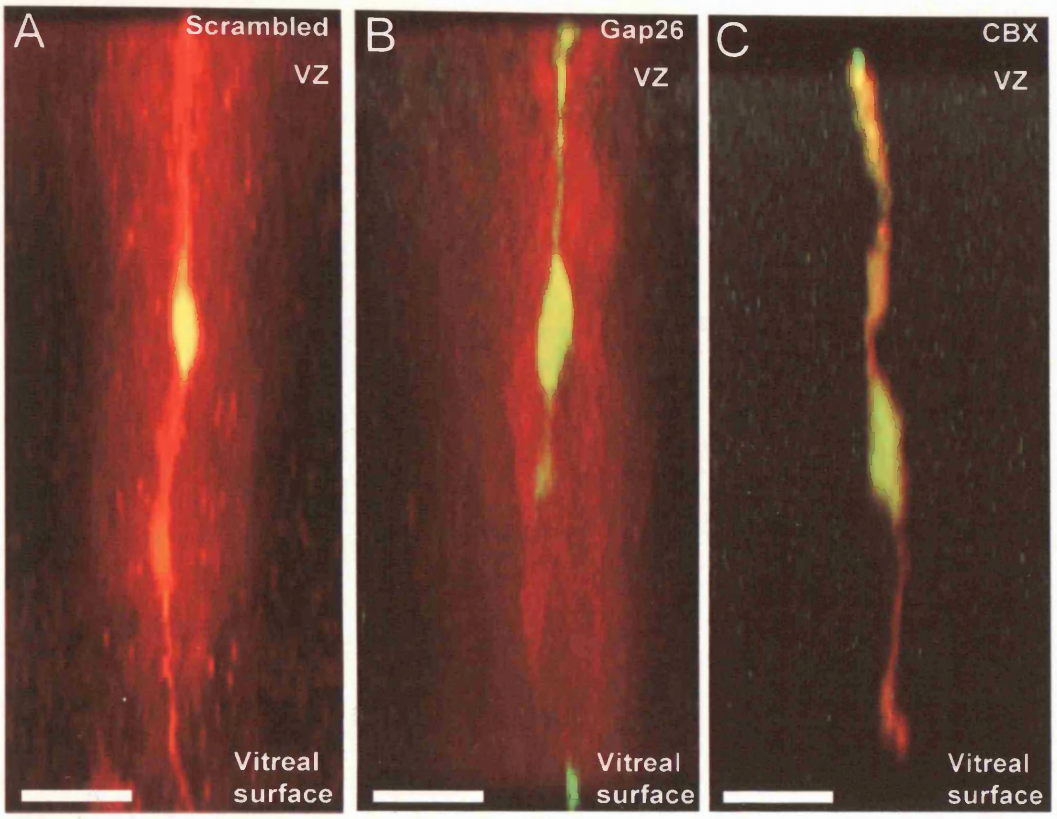

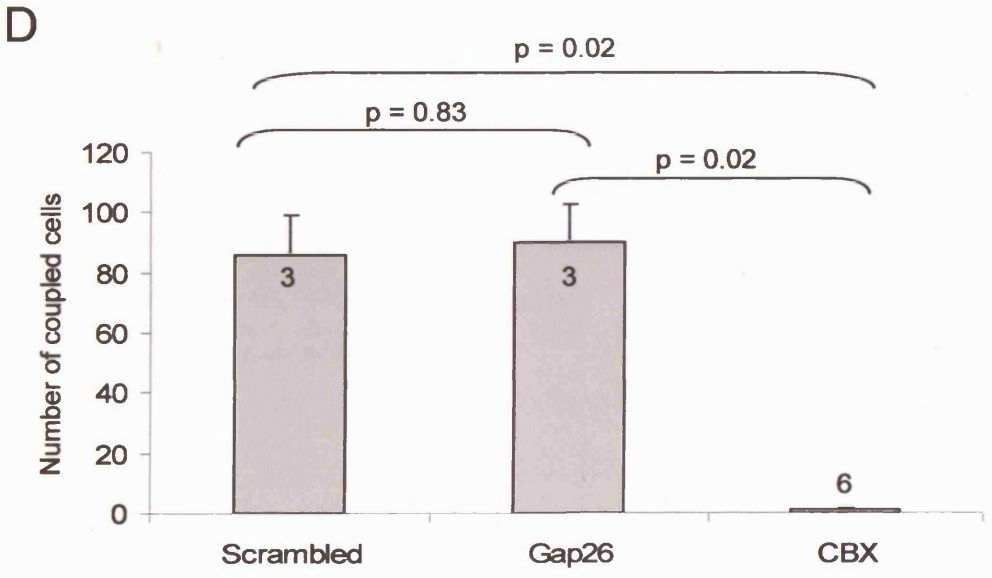

Figure 5.18 The effect of Gap26 on intact gap junctions
Cells in the neural retina filled with the gap junction-impermeant marker FITC-dextran and the gap junction-permeant tracer Neurobiotin (*yellow*) are dye-coupled to a large number of adjacent cells (*red*) in controls (*A*). Coupling is prevented by CBX (*C*) but not by Gap26 (*B*). *D,* The mean number of coupled cells in scrambled control is similar to that in Gap26, whereas CBX results in a significant reduction in the extent of coupling in E5 retinae. Scale bars 10 µm.

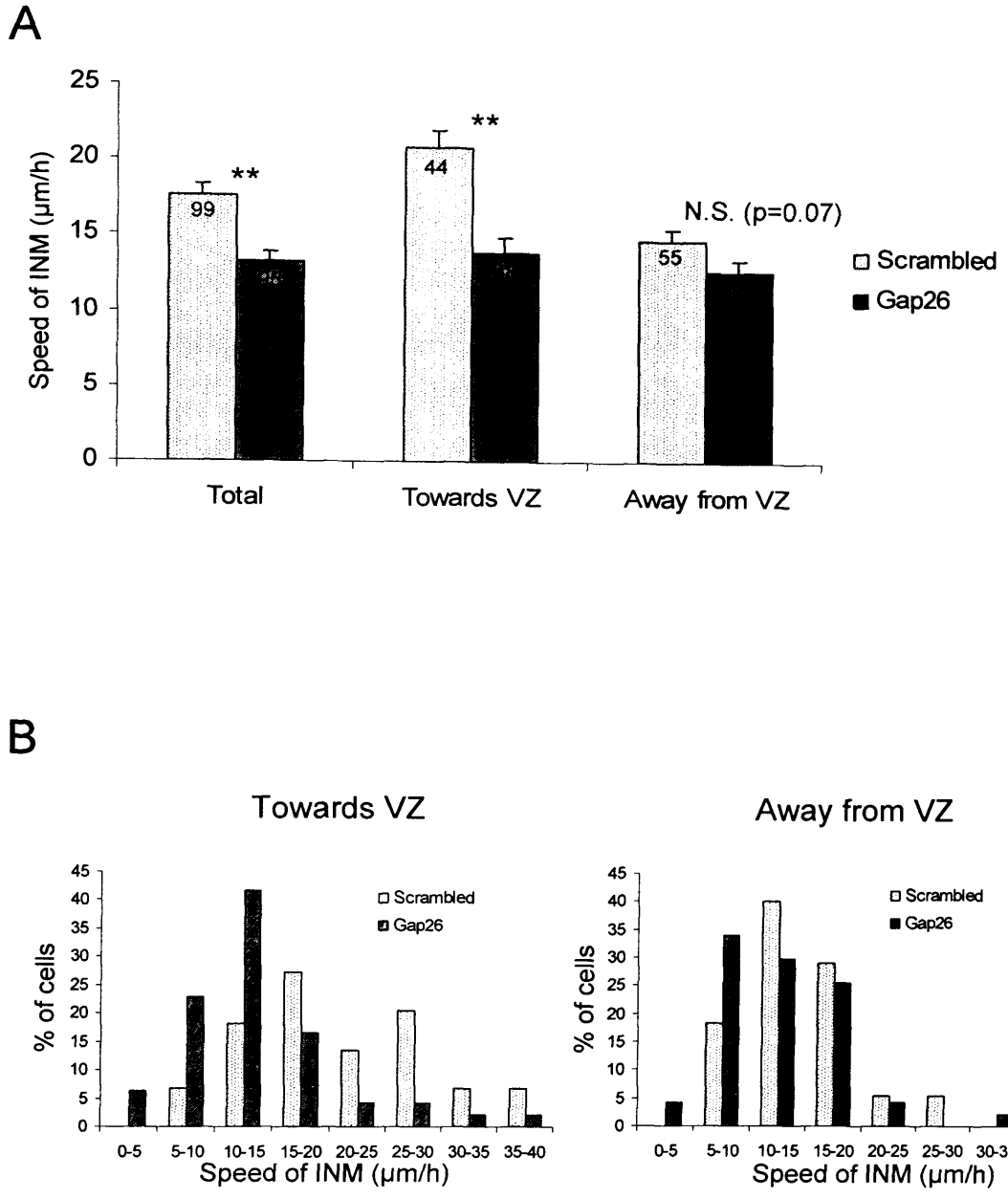

Figure 5.19 The effect of Gap26 on the speed of INM
A, The mean speed of INM is significantly reduced by Gap26, compared to the scrambled control peptide. The effect is highly significant for the total population of cells, and for the subgroup moving towards the VZ. For cells moving away from the VZ, the mean speed of INM is also reduced in Gap26 compared to scrambled control, although this is not statistically significant (p=0.07). *B,* The distribution of the speed of INM in Gap26 compared to scrambled control. Gap26 causes a slight shift to the left, but does not appear to affect fast-moving or slow-moving cells differentially.

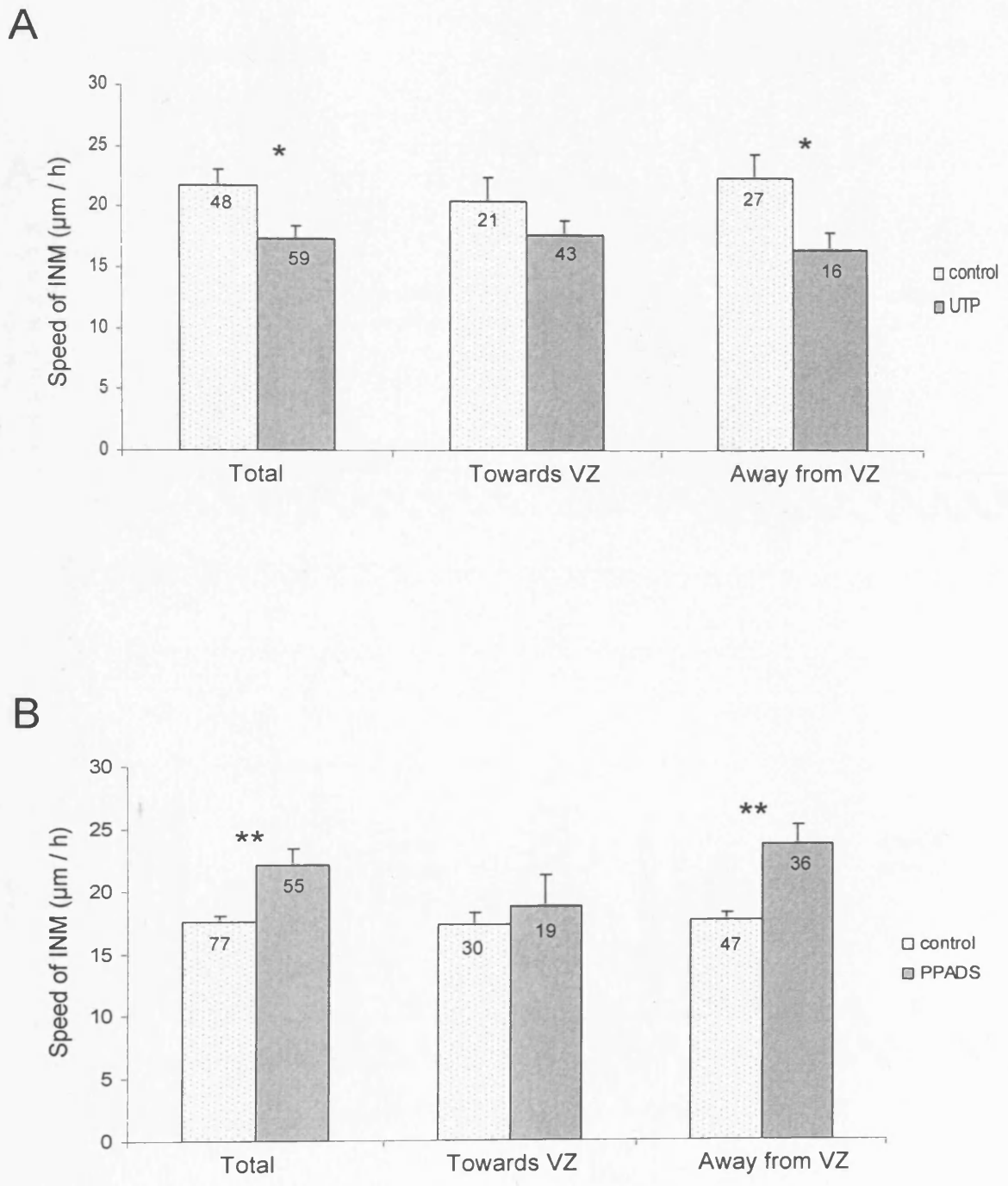

Figure 5.20 The effect of purinergic signalling on the speed of INM
A, Exogenous purinergic stimulation causes cells to progress through INM at a slower rate than in control solution (N=6). *B*, Blocking purinergic receptors with PPADS increases the rate of INM (N=6). This effect is significant for cells moving away from the VZ, but not for cells moving towards the VZ.

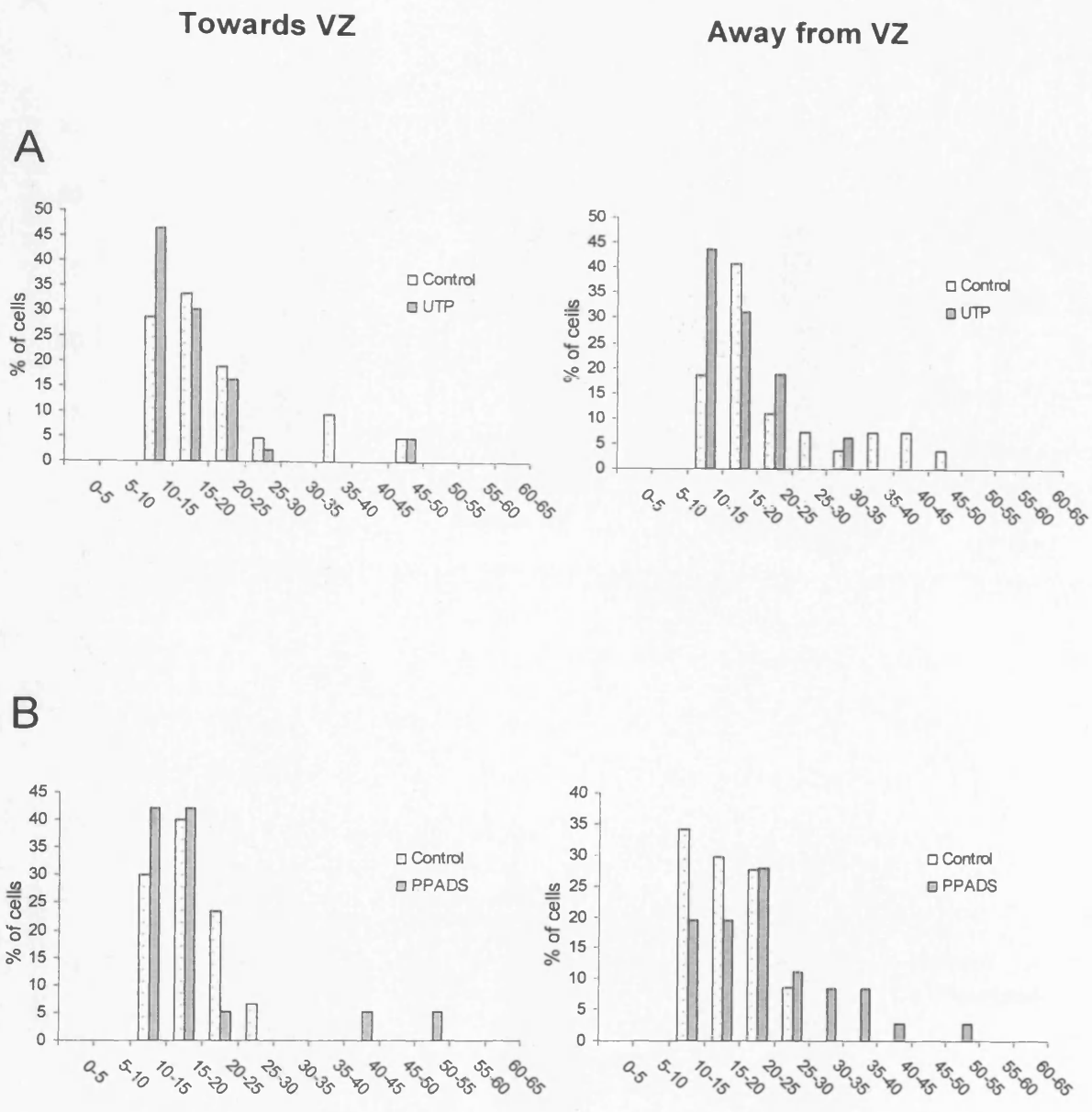

Figure 5.21 The effect of purinergic signalling on the distribution of the speed of INM
A, The effect of UTP in comparison to control is similar for cells moving towards or away from the VZ, and does not appear to affect fast- or slow-moving cells preferentially. *B*, The effect of PPADS is greater for cells moving away from the VZ than for cells moving towards it. The distribution of the rates of INM in PPADS and control suggests that PPADS causes an increased number of cells to move through INM at fast rates (> 30μm/h).

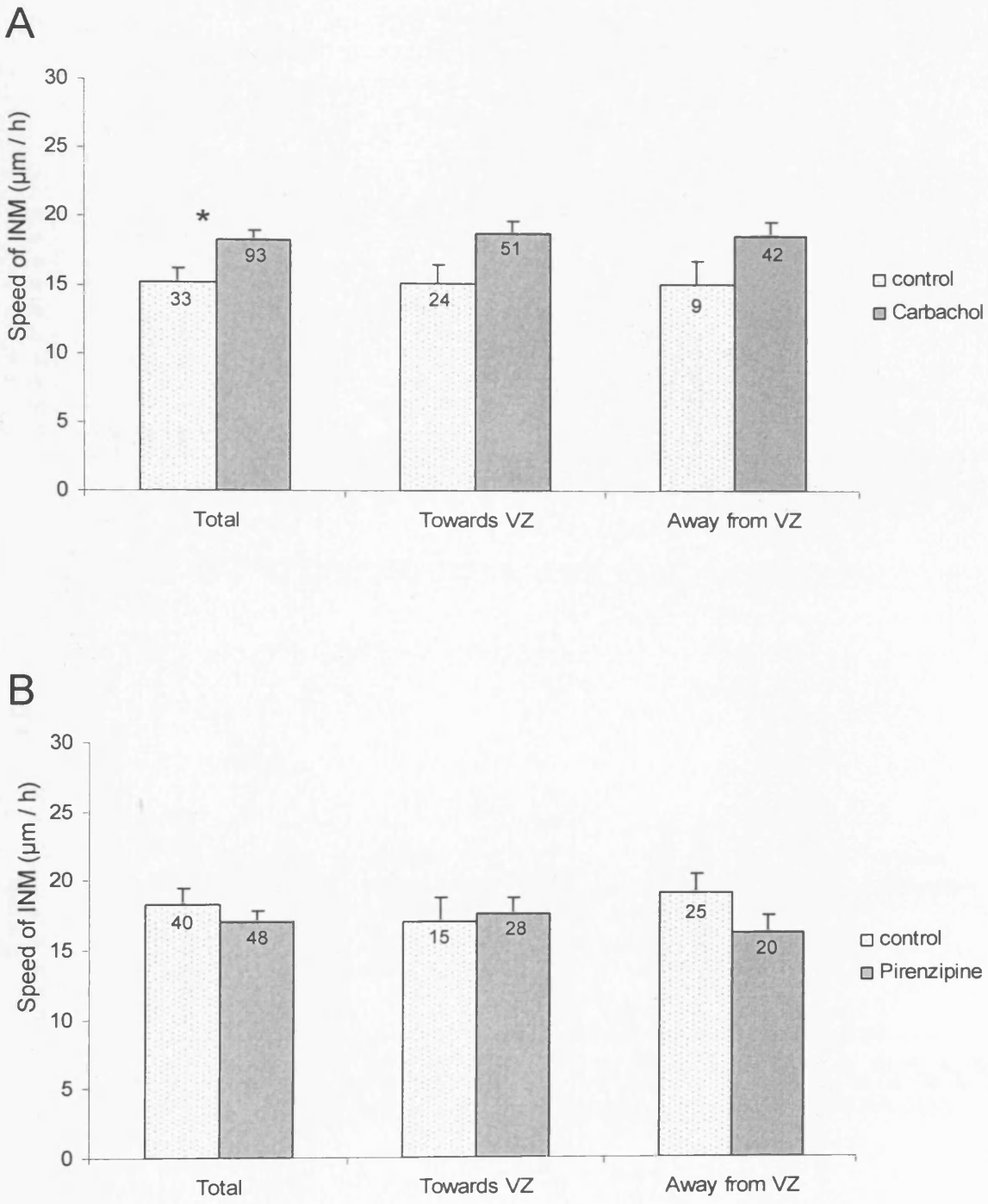

Figure 5.22 The effect of muscarinic signalling on the speed of INM
A, Exogenous muscarinic stimulation causes a significant increase in the rate of INM (N=4). *B*, Pirenzipine causes a slight decrease in the rate of INM. However, this is not statistically significant (N=4).

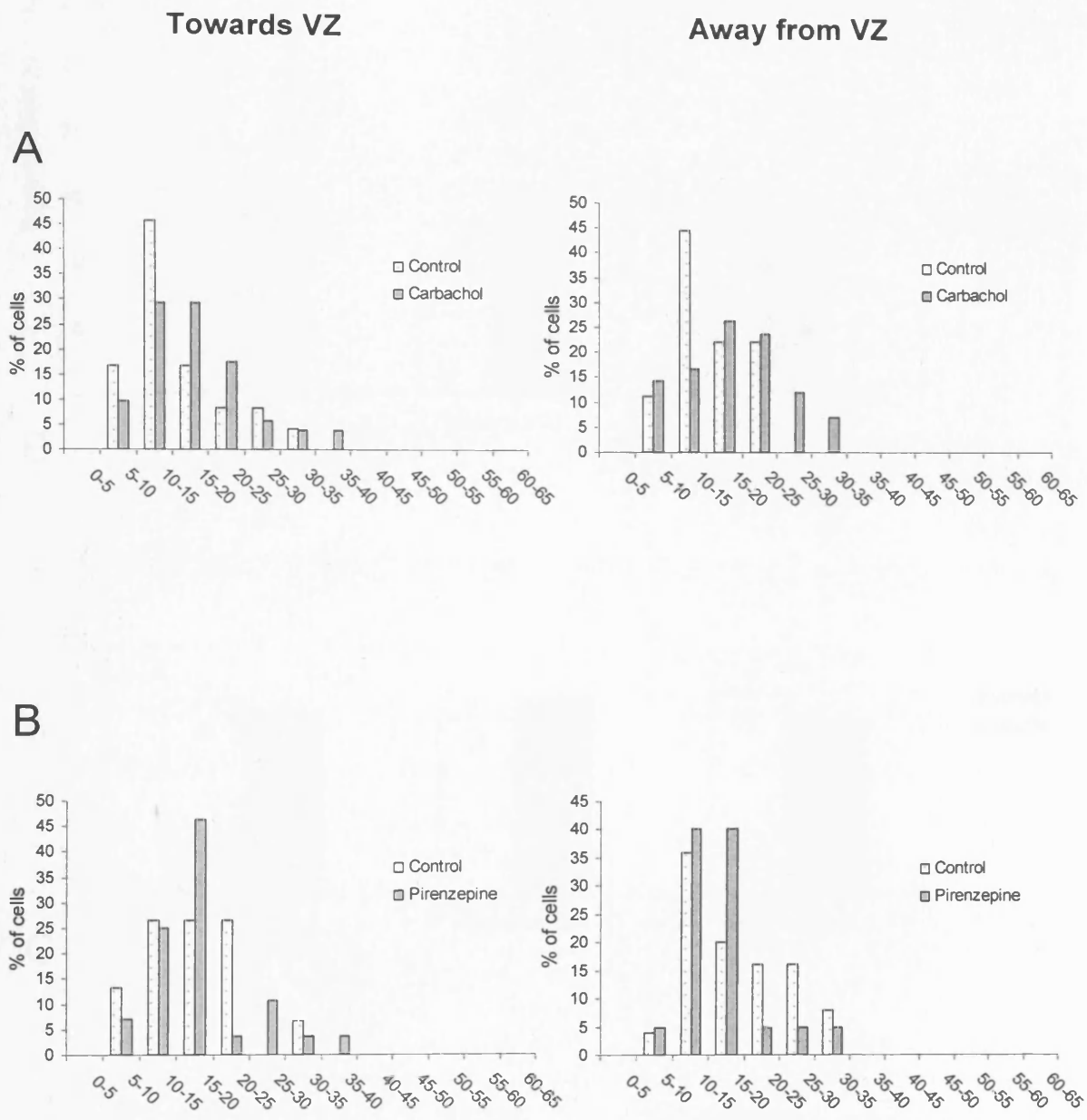

Figure 5.23 The effect of muscarinic signalling on the distribution of the speed of INM
A, Distribution of the speed of INM in carbachol compared to control. *B*, Distribution of the speed of INM in pirenzepine compared to control

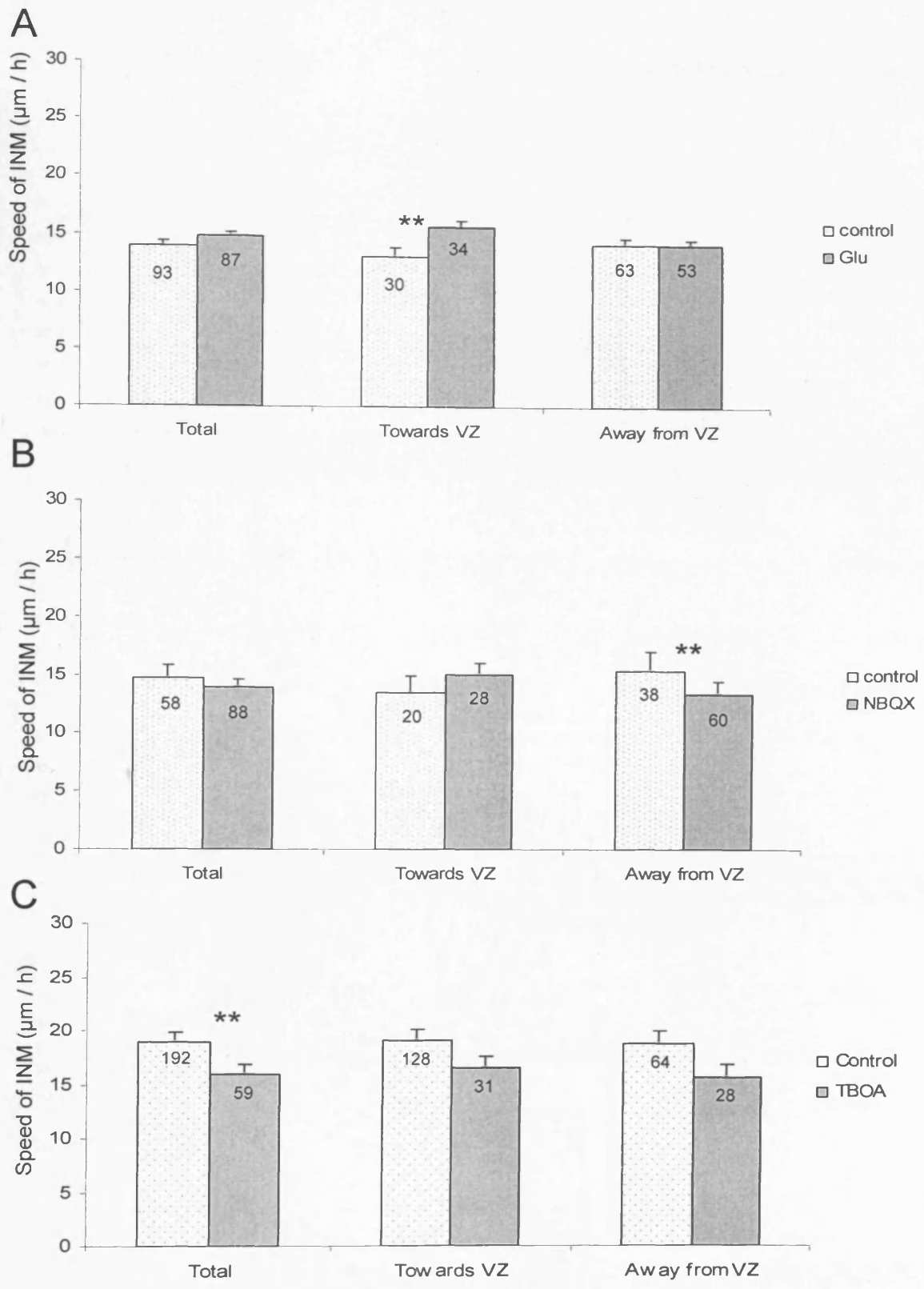

Figure 5.24 The effect of glutamatergic signalling on the speed of INM
A, Glutamate does not affect the rate of INM of cells moving towards the GCL, but significantly increases the rate of INM of progenitors moving towards the VZ (N=4). *B*, NBQX significantly decreases the rate of INM of cells moving away from the VZ, but not cells moving towards it (N=4). *C*, TBOA decreases the rate of INM, and appears to have similar effects on cells moving towards or away from the VZ. The effect of TBOA is significant for the total cell population, but not for either 'towards' or 'away' sub-population (N=3).

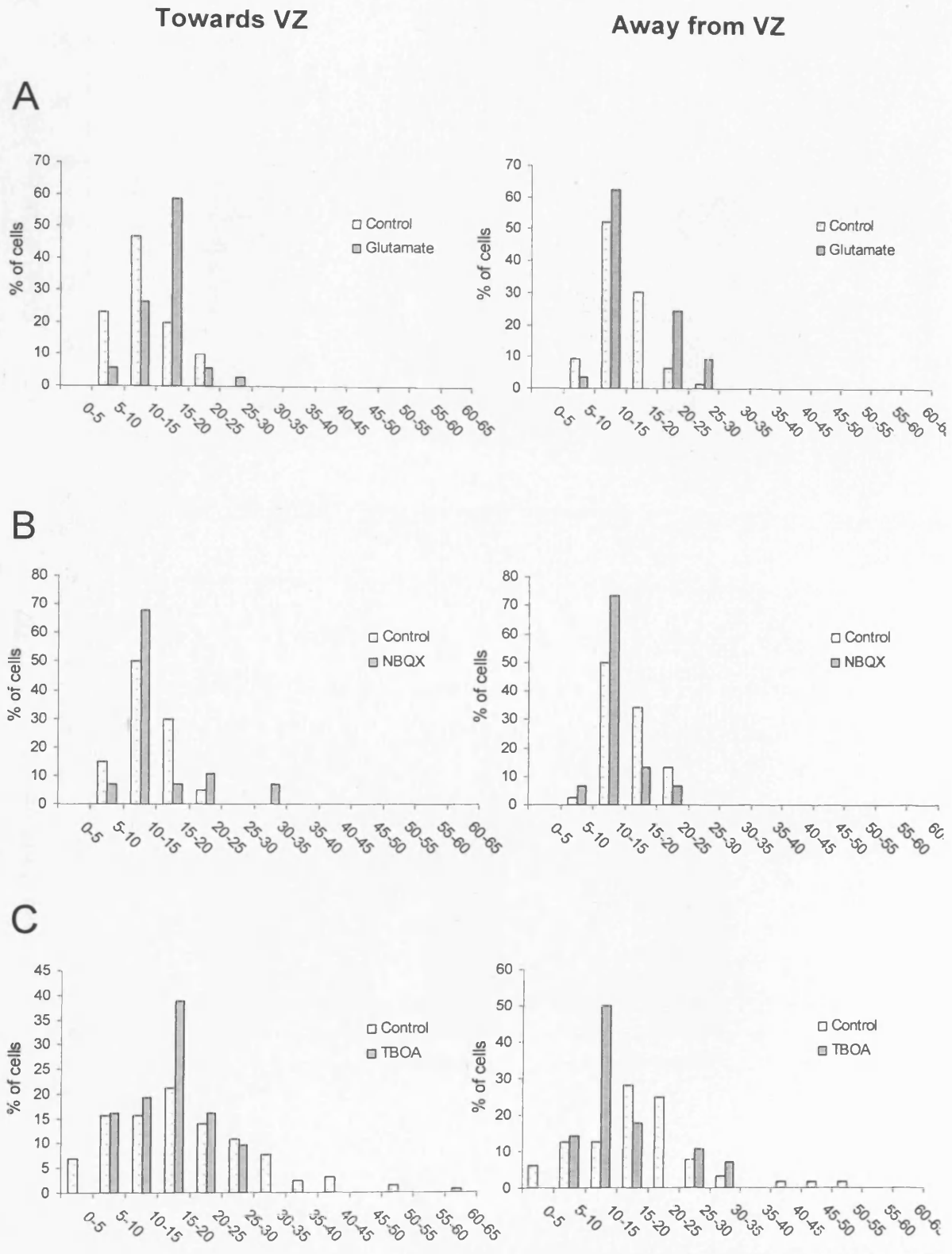

Figure 5.25 The effect of glutamatergic signalling on the distribution of the speed of INM *A*, Distribution of the speed of INM in glutamate compared to control. *B*, Distribution of the speed of INM in NBQX compared to control. *C*, Distribution of the speed of INM in TBOA compared to control

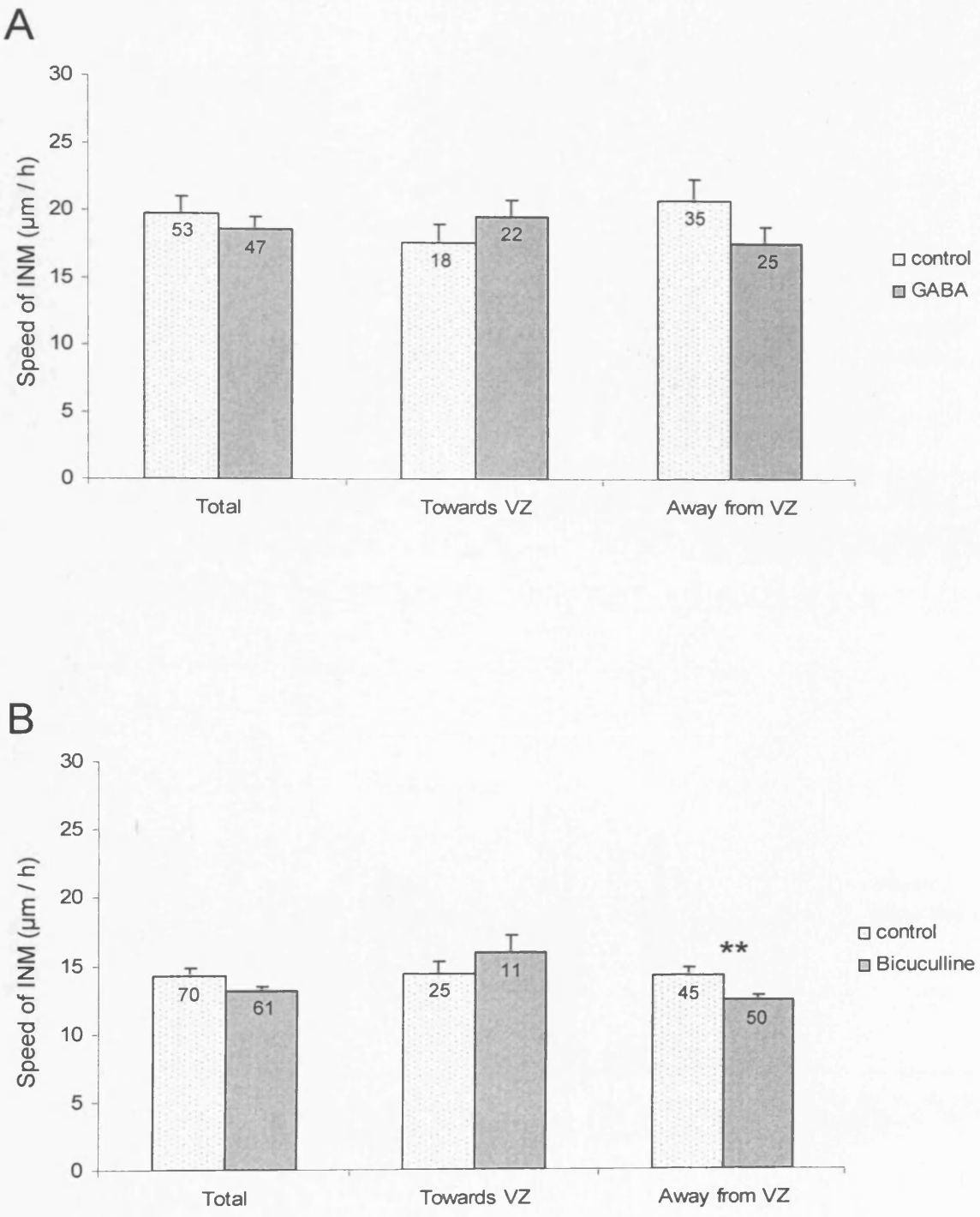

Figure 5.26 The effect of GABAergic signalling on the speed of INM
A, GABA has no effect on the speed of INM (N=4). *B*, Bicuculline causes a significant decrease in the rate of movement of cells moving away from the VZ (N=4).

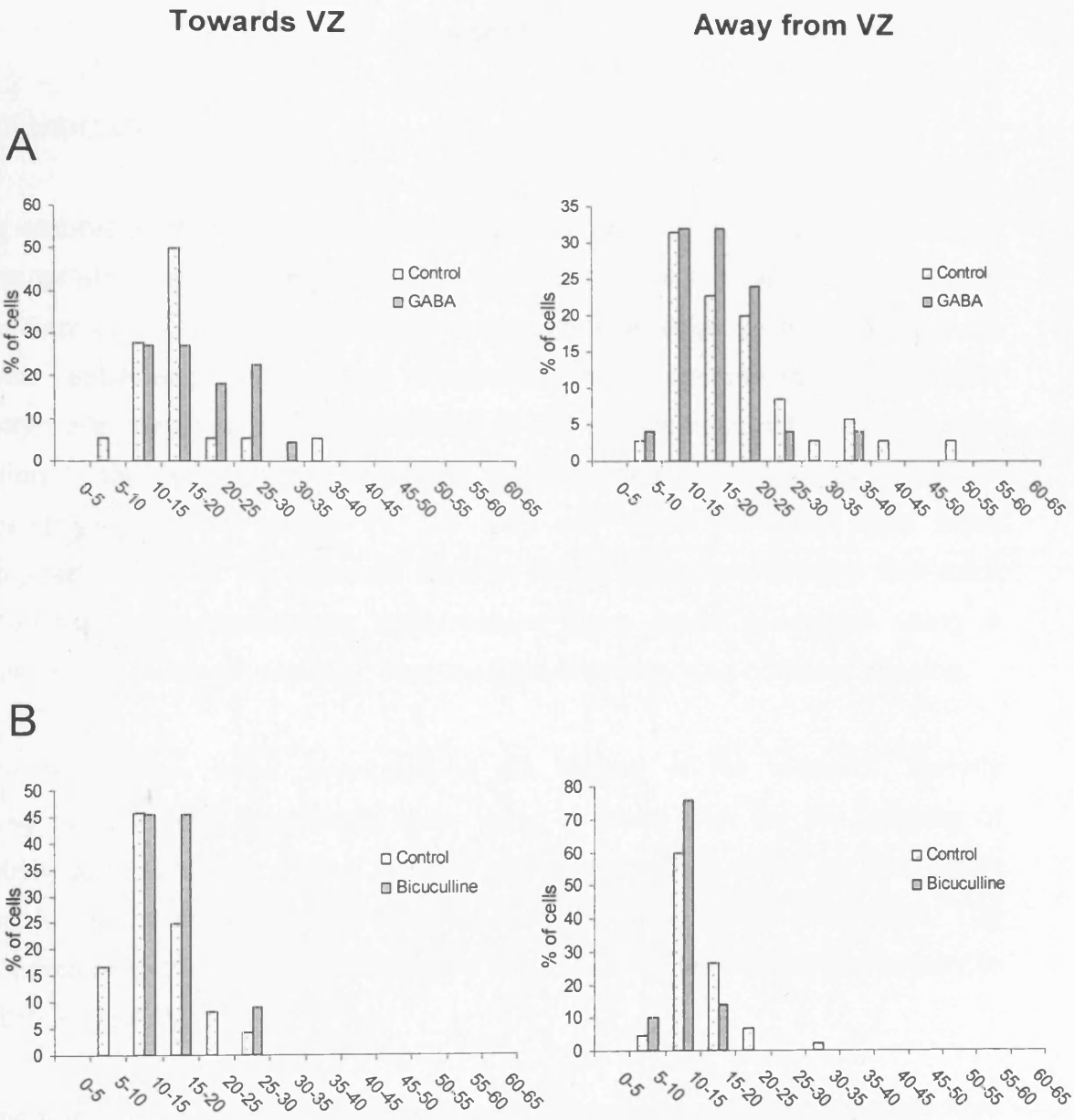

Figure 5.27 The effect of GABAergic signalling on the distribution of the speed of INM
A, Distribution of the speed of INM in GABA compared to control. *B*, Distribution of the speed of INM in bicuculline compared to control

Chapter 6

CONCLUSIONS

During embryonic development it is essential that neurons and glia are generated in appropriate numbers and assume the correct cell types, locations and connectivity to establish the function of the adult nervous system. Interactions between extracellular signalling molecules and intracellular transduction pathways are involved in the regulation of cell proliferation, differentiation and migration. In the studies presented here, the properties and behaviour of cells in the developing neural retina of 3-9 day old chick embryos have been investigated. Some of the potential ways in which cells communicate with each other during early embryonic development have been examined using a combination of electrophysiology, immunohistochemistry and confocal imaging.

Several techniques were developed in the course of the research, namely labelling of cells with membrane dyes using a Gene Gun for live imaging of migration, and guillotine slicing of very young embryonic retina to give better access to the membranes of progenitor cells for patch clamp recordings. The slices containing the recorded cells were then used for immunohistochemistry to establish the cell type.

The membrane properties of progenitor cells were found to differ markedly from newborn neurons. Progenitor cells did not show any obvious voltage-gated currents at the times investigated (E5-E8), but responded with an inward current to both GABA and glutamate. In contrast, newborn neurons were rarely coupled to other cells, did not respond to GABA or glutamate, and showed both inward and outward voltage-gated currents. The differences between these two cell types are similar to those described for early and late neural progenitors in the adult hippocampus (Fukuda et al., 2003).

Progenitor cells were characterized by extensive gap junctional coupling, which decreased over time towards the end of neurogenesis. Postmitotic cells were largely excluded from gap junction coupled clusters. The expression of Cx43 and Cx36 was consistent with a role for these connexin proteins in mediating the coupling between proliferating cells, and interference with Cx43 expression resulted in a reduction in gap junction coupling. These findings are consistent with early electron microscopy studies of gap junctions in the developing retina (Fujisawa et al., 1976), and show that gap junctional coupling in the retina follows a similar pattern to that described in the cortex during embryonic development (Bittman et al., 1998).

The interkinetic nuclear migration and division of progenitor cells was followed in real time using confocal microscopy, to reveal the rate and nature of this process, which was found to have many similarities with the migration of newborn neurons. The movement of progenitor cells was characterized by stationary phases interspersed with rapid movements in both directions, to produce an average rate of movement of around 20μm per hour. The maintenance of normal rates of migration was dependent on intact gap junctional communication. If this was perturbed using either pharmacological or molecular agents to interfere with gap junction formation, migration was significantly slowed, often by more 60-70% compared to control. Potentially, unapposed gap junction hemichannels may also be involved in maintaining migration, although the evidence for this is less extensive. The effect of neurotransmitters on interkinetic nuclear migration was also investigated, examining the effects of agonists and antagonists for GABA-, glutamate-, ACh-, and purine-receptors. Although some agents produced statistically significant effects, the effects of gap junctional blockers were more marked, suggesting that the neurotransmitter receptors investigated play only a minor role in maintaining normal migration.

Together, the findings presented here show that retinal progenitor cells have distinct properties to those of postmitotic cells; that progenitor cells can respond to neurotransmitters at early times; and that gap junction communication between progenitor cells is likely to play a critical role in maintaining normal progenitor cell proliferation.

PUBLICATIONS

Pearson, R.A., Catsicas, M., Becker, D.L., Bayley, P., Lüneborg, N.L. and Mobbs, P. (2004) Ca(2+) signalling and gap junction coupling within and between pigment epithelium and neural retina in the developing chick. *Eur J Neurosci* **19**, 2435-45.

Pearson, R.A.*, Lüneborg, N.L.*, Becker, D.L. and Mobbs, P. (2005) Gap junctions modulate interkinetic nuclear migration in retinal progenitor cells. *J Neurosci* (In Press) * Joint first authors

Lüneborg, N.L., Becker, D.L. and Mobbs, P. Progenitor cell proliferation and gap junction coupling in developing neural retina. (In preparation)

ABSTRACTS

Lüneborg, N., and Mobbs, P. Membrane properties of E5 chick retinal ventricular zone cells. Society for Neuroscience Abstract 2003; 29.5

Lüneborg, N., Pearson, R., Becker, D. and Mobbs, P. Purinergic and muscarinic signalling affect cell movements in the E5 embryonic chick retina. Physiological Society Abstract 2003; 547P DC2

References

Adler, R. and Belecky-Adams, T. (1999) Cell Fate Determination in the Chick Embryo Retina. In: Moody, S.A., (Ed.) *Cell lineage and fate determination*, San Diego, Calif. ; London : Academic Press

Allcorn, S., Catsicas, M. and Mobbs, P. (1996) Developmental expression and self-regulation of Ca2+ entry via AMPA/KA receptors in the embryonic chick retina. *Eur J Neurosci* **8**, 2499-510.

Altshuler, D., Lo Turco, J.J., Rush, J. and Cepko, C. (1993) Taurine promotes the differentiation of a vertebrate retinal cell type in vitro. *Development* **119**, 1317-28.

Anthony, T.E., Klein, C., Fishell, G. and Heintz, N. (2004) Radial glia serve as neuronal progenitors in all regions of the central nervous system. *Neuron* **41**, 881-90.

Austin, C.P., Feldman, D.E., Ida, J.A. Jr and Cepko, C.L. (1995) Vertebrate retinal ganglion cells are selected from competent progenitors by the action of Notch. *Development* **121**, 3637-50.

Bannerman, P., Nichols, W., Puhalla, S., Oliver, T., Berman, M. and Pleasure, D. (2000) Early migratory rat neural crest cells express functional gap junctions: evidence that neural crest cell survival requires gap junction function. *J Neurosci Res* **61**, 605-15.

Beazley, L.D., Perry, V.H., Baker, B. and Darby, J.E. (1987) An investigation into the role of ganglion cells in the regulation of division and death of other retinal cells. *Brain Res* **430**, 169-84.

Beck, H., Ficker, E. and Heinemann, U. (1992) Properties of two voltage-activated potassium currents in acutely isolated juvenile rat dentate gyrus granule cells. *J Neurophysiol* **68**, 2086-99.

Becker, D., Bonness, V. and Mobbs, P. (1998) Cell coupling in the retina: patterns and purpose. *Cell Biol Int* **22**, 781-92.

Becker, D., Ciantar, D., Catsicas, M., Pearson, R. and Mobbs, P. (2001) Use of pIRES vectors to express EGFP and connexin constructs in studies of the role of gap junctional communication in the early development of the chick retina and brain. *Cell Commun Adhes* **8**, 355-9.

Becker, D.L., Bonness, V., Catsicas, M. and Mobbs, P. (2002) Changing patterns of ganglion cell coupling and connexin expression during chick retinal development. *J Neurobiol* **52**, 280-93.

Becker, D.L., Evans, W.H., Green, C.R. and Warner, A. (1995) Functional analysis of amino acid sequences in connexin43 involved in intercellular communication through gap junctions. *J Cell Sci* **108 (Pt 4)**, 1455-67.

Becker, D.L., McGonnell, I., Makarenkova, H.P., Patel, K., Tickle, C., Lorimer, J. and Green, C.R. (1999) Roles for alpha 1 connexin in morphogenesis of chick embryos revealed using a novel antisense approach. *Dev Genet* **24**, 33-42.

Becker, D.L. and Mobbs, P. (1999) Connexin alpha1 and cell proliferation in the developing chick retina. *Exp Neurol* **156**, 326-32.

Behar, T.N., Schaffner, A.E., Scott, C.A., Greene, C.L. and Barker, J.L. (2000) GABA receptor antagonists modulate postmitotic cell migration in slice cultures of embryonic rat cortex. *Cereb Cortex* **10**, 899-909.

Behar, T.N., Schaffner, A.E., Scott, C.A., O'Connell, C. and Barker, J.L. (1998) Differential response of cortical plate and ventricular zone cells to GABA as a migration stimulus. *J Neurosci* **18**, 6378-87.

Behar, T.N., Scott, C.A., Greene, C.L., Wen, X., Smith, S.V., Maric, D., Liu, Q.Y., Colton, C.A. and Barker, J.L. (1999) Glutamate acting at NMDA receptors stimulates embryonic cortical neuronal migration. *J Neurosci* **19**, 4449-61.

Belliveau, M.J. and Cepko, C.L. (1999) Extrinsic and intrinsic factors control the genesis of amacrine and cone cells in the rat retina. *Development* **126**, 555-66.

Belliveau, M.J., Young, T.L. and Cepko, C.L. (2000) Late retinal progenitor cells show intrinsic limitations in the production of cell types and the kinetics of opsin synthesis. *J Neurosci* **20**, 2247-54.

Belmonte, K.E., McKinnon, L.A. and Nathanson, N.M. (2000) Developmental expression of muscarinic acetylcholine receptors in chick retina: selective induction of M2 muscarinic receptor expression in ovo by a factor secreted by muller glial cells. *J Neurosci* **20**, 8417-25.

Ben-Ari, Y. (2002) Excitatory actions of gaba during development: the nature of the nurture. *Nat Rev Neurosci* **3**, 728-39.

Benke, D., Michel, C. and Mohler, H. (2002) Structure of GABAB receptors in rat retina. *J Recept Signal Transduct Res* **22**, 253-66.

Bennett, M.V., Contreras, J.E., Bukauskas, F.F. and Saez, J.C. (2003) New roles for astrocytes: gap junction hemichannels have something to communicate. *Trends Neurosci* **26**, 610-7.

Bergmann, M., Grabs, D. and Rager, G. (2000) Expression of presynaptic proteins is closely correlated with the chronotopic pattern of axons in the retinotectal system of the chick. *J Comp Neurol* **418**, 361-72.

Biedermann, B., Bringmann, A. and Reichenbach, A. (2002) High-affinity GABA uptake in retinal glial (Muller) cells of the guinea pig: electrophysiological characterization, immunohistochemical localization, and modeling of efficiency. *Glia* **39**, 217-28.

Billinton, A., Ige, A.O., Bolam, J.P., White, J.H., Marshall, F.H. and Emson, P.C. (2001) Advances in the molecular understanding of GABA(B) receptors. *Trends Neurosci* **24**, 277-82.

Billups, D. (2002) Modulation of synaptic transmission by interacting proteins and transporters. University College London.
Ph.D. Thesis

Bittman, K., Becker, D.L., Cicirata, F. and Parnavelas, J.G. (2002) Connexin expression in homotypic and heterotypic cell coupling in the developing cerebral cortex. *J Comp Neurol* **443**, 201-12.

Bittman, K., Owens, D.F., Kriegstein, A.R. and LoTurco, J.J. (1997) Cell coupling and uncoupling in the ventricular zone of developing neocortex. *J Neurosci* **17**, 7037-44.

Bittman, K.S. and LoTurco, J.J. (1999) Differential regulation of connexin 26 and 43 in murine neocortical precursors. *Cereb Cortex* **9**, 188-95.

Blackshaw, S., Harpavat, S., Trimarchi, J., Cai, L., Huang, H., Kuo, W.P., Weber, G., Lee, K., Fraioli, R.E., Cho, S.H., Yung, R., Asch, E., Ohno-Machado, L., Wong, W.H. and Cepko, C.L. (2004) Genomic analysis of mouse retinal development. *PLoS Biol* **2**, E247

Bonness, V. (1999) The appearance of amino acid transmitters, their receptors and GAP junctions in the developing chick retina. University of London.
Thesis (Ph.D.)

Bormann, J. (2000) The 'ABC' of GABA receptors. *Trends Pharmacol Sci* **21**, 16-9.

Borodinsky, L.N., O'Leary, D., Neale, J.H., Vicini, S., Coso, O.A. and Fiszman, M.L. (2003) GABA-induced neurite outgrowth of cerebellar granule cells is mediated by GABA(A) receptor activation, calcium influx and CaMKII and erk1/2 pathways. *J Neurochem* **84**, 1411-20.

Borodinsky, L.N., Root, C.M., Cronin, J.A., Sann, S.B., Gu, X. and Spitzer, N.C. (2004) Activity-dependent homeostatic specification of transmitter expression in embryonic neurons. *Nature* **429**, 523-30.

Boucher, S. and Bennett, S.A. (2003) Differential connexin expression, gap junction intercellular coupling, and hemichannel formation in NT2/D1 human neural progenitors and terminally differentiated hNT neurons. *J Neurosci Res* **72**, 393-404.

Braet, K., Vandamme, W., Martin, P.E., Evans, W.H. and Leybaert, L. (2003) Photoliberating inositol-1,4,5-trisphosphate triggers ATP release that is blocked by the connexin mimetic peptide gap 26. *Cell Calcium* **33**, 37-48.

Brauner-Osborne, H. and Krogsgaard-Larsen, P. (1999) Functional pharmacology of cloned heterodimeric GABAB receptors expressed in mammalian cells. *Br J Pharmacol* **128**, 1370-4.

Brazel, C.Y., Nunez, J.L., Yang, Z. and Levison, S.W. (2005) Glutamate enhances survival and proliferation of neural progenitors derived from the subventricular zone. *Neuroscience* **131**, 55-65.

Brecha, N.C. and Weigmann, C. (1994) Expression of GAT-1, a high-affinity gamma-aminobutyric acid plasma membrane transporter in the rat retina. *J Comp Neurol* **345**, 602-11.

Burnstock, G. and Williams, M. (2000) P2 purinergic receptors: modulation of cell function and therapeutic potential. *J Pharmacol Exp Ther* **295**, 862-9.

Cai, L., Hayes, N.L. and Nowakowski, R.S. (1997a) Local homogeneity of cell cycle length in developing mouse cortex. *J Neurosci* **17**, 2079-87.

Cai, L., Hayes, N.L. and Nowakowski, R.S. (1997b) Synchrony of clonal cell proliferation and contiguity of clonally related cells: production of mosaicism in the ventricular zone of developing mouse neocortex. *J Neurosci* **17**, 2088-100.

Catsicas, M., Allcorn, S. and Mobbs, P. (2001) Early activation of Ca(2+)-permeable AMPA receptors reduces neurite outgrowth in embryonic chick retinal neurons. *J Neurobiol* **49**, 200-11.

Catsicas, M., Bonness, V., Becker, D. and Mobbs, P. (1998) Spontaneous Ca2+ transients and their transmission in the developing chick retina. *Curr Biol* **8**, 283-6.

Catsicas, M. and Mobbs, P. (2001) GABAb receptors regulate chick retinal calcium waves. *J Neurosci* **21**, 897-910.

Caviness, V.S. Jr, Takahashi, T. and Nowakowski, R.S. (1995) Numbers, time and neocortical neuronogenesis: a general developmental and evolutionary model. *Trends Neurosci* **18**, 379-83.

Cayouette, M. and Raff, M. (2003) The orientation of cell division influences cell-fate choice in the developing mammalian retina. *Development* **130**, 2329-39.

Cepko, C.L., Austin, C.P., Yang, X., Alexiades, M. and Ezzeddine, D. (1996) Cell fate determination in the vertebrate retina. *Proc Natl Acad Sci U S A* **93**, 589-95.

Chebib, M. (2004) GABAC receptor ion channels. *Clin Exp Pharmacol Physiol* **31**, 800-4.

Cheng, A., Tang, H., Cai, J., Zhu, M., Zhang, X., Rao, M. and Mattson, M.P. (2004) Gap junctional communication is required to maintain mouse cortical neural progenitor cells in a proliferative state. *Dev Biol* **272**, 203-16.

Chenn, A. and McConnell, S.K. (1995) Cleavage orientation and the asymmetric inheritance of Notch1 immunoreactivity in mammalian neurogenesis. *Cell* **82** , 631-41.

Cheung, K.K. and Burnstock, G. (2002) Localization of P2X3 receptors and coexpression with P2X2 receptors during rat embryonic neurogenesis. *J Comp Neurol* **443**, 368-82.

Collingridge, G.L. and Lester, R.A. (1989) Excitatory amino acid receptors in the vertebrate central nervous system. *Pharmacol Rev* **41**, 143-210.

Cook, B., Portera-Cailliau, C. and Adler, R. (1998) Developmental neuronal death is not a universal phenomenon among cell types in the chick embryo retina. *J Comp Neurol* **396**, 12-9.

Cook, J.E. and Becker, D.L. (1995) Gap junctions in the vertebrate retina. *Microsc Res Tech* **31**, 408-19.

Coulombre, J.L. and Coulombre, A.J. (1965) Regeneration of neural retina from the pigmented epithelium in the chick embryo. *Dev Biol* **12**, 79-92.

Cusato, K., Bosco, A., Rozental, R., Guimaraes, C.A., Reese, B.E., Linden, R. and Spray, D.C. (2003) Gap junctions mediate bystander cell death in developing retina. *J Neurosci* **23**, 6413-22.

da Costa Calaza, K., Hokoc, J.N. and Gardino, P.F. (2000) Neurogenesis of GABAergic cells in the chick retina. *Int J Dev Neurosci* **18**, 721-6.

Dajas-Bailador, F. and Wonnacott, S. (2004) Nicotinic acetylcholine receptors and the regulation of neuronal signalling. *Trends Pharmacol Sci* **25**, 317-24.

Das, T., Payer, B., Cayouette, M. and Harris, W.A. (2003) In vivo time-lapse imaging of cell divisions during neurogenesis in the developing zebrafish retina. *Neuron* **37**, 597-609.

Desarmenien, M.G., Clendening, B. and Spitzer, N.C. (1993) In vivo development of voltage-dependent ionic currents in embryonic Xenopus spinal neurons. *J Neurosci* **13**, 2575-81.

DeVries, S.H. and Schwartz, E.A. (1992) Hemi-gap-junction channels in solitary horizontal cells of the catfish retina. *J Physiol* **445**, 201-30.

Duarte, C.B., Santos, P.F., Sanchez-Prieto, J. and Carvalho, A.P. (1996) Glutamate release evoked by glutamate receptor agonists in cultured chick retina cells: modulation by arachidonic acid. *J Neurosci Res* **44**, 363-73.

Dutting, D., Gierer, A. and Hansmann, G. (1983) Self-renewal of stem cells and differentiation of nerve cells in the developing chick retina. *Brain Res* **312**, 21-32.

Edqvist, P.H. and Hallbook, F. (2004) Newborn horizontal cells migrate bi-directionally across the neuroepithelium during retinal development. *Development* **131**, 1343-51.

Farrant, M., Feldmeyer, D., Takahashi, T. and Cull-Candy, S.G. (1994) NMDA-receptor channel diversity in the developing cerebellum. *Nature* **368**, 335-9.

Fatima-Shad, K. and Barry, P.H. (1993) Anion permeation in GABA- and glycine-gated channels of mammalian cultured hippocampal neurons. *Proc R Soc Lond B Biol Sci* **253**, 69-75.

Feigenspan, A., Janssen-Bienhold, U., Hormuzdi, S., Monyer, H., Degen, J., Sohl, G., Willecke, K., Ammermuller, J. and Weiler, R. (2004) Expression of connexin36 in cone pedicles and OFF-cone bipolar cells of the mouse retina. *J Neurosci* **24**, 3325-34.

Fekete, D.M., Perez-Miguelsanz, J., Ryder, E.F. and Cepko, C.L. (1994) Clonal analysis in the chicken retina reveals tangential dispersion of clonally related cells. *Dev Biol* **166**, 666-82.

Fischer, A.J., McKinnon, L.A., Nathanson, N.M. and Stell, W.K. (1998) Identification and localization of muscarinic acetylcholine receptors in the ocular tissues of the chick. *J Comp Neurol* **392**, 273-84.

Fischer, A.J. and Reh, T.A. (2001) Muller glia are a potential source of neural regeneration in the postnatal chicken retina. *Nat Neurosci* **4**, 247-52.

Frade, J.M., Bovolenta, P., Martinez-Morales, J.R., Arribas, A., Barbas, J.A. and Rodriguez-Tebar, A. (1997) Control of early cell death by BDNF in the chick retina. *Development* **124**, 3313-20.

Fujisawa, H., Morioka, H., Watanabe, K. and Nakamura, H. (1976) A decay of gap junctions in association with cell differentiation of neural retina in chick embryonic development. *J Cell Sci* **22**, 585-96.

Fukuda, S., Kato, F., Tozuka, Y., Yamaguchi, M., Miyamoto, Y. and Hisatsune, T. (2003) Two distinct subpopulations of nestin-positive cells in adult mouse dentate gyrus. *J Neurosci* **23**, 9357-66.

Fushiki, S., Perez Velazquez, J.L., Zhang, L., Bechberger, J.F., Carlen, P.L. and Naus, C.C. (2003) Changes in neuronal migration in neocortex of connexin43 null mutant mice. *J Neuropathol Exp Neurol* **62**, 304-14.

Gan, W.B., Grutzendler, J., Wong, W.T., Wong, R.O. and Lichtman, J.W. (2000) Multicolor "DiOlistic" labeling of the nervous system using lipophilic dye combinations. *Neuron* **27**, 219-25.

Giepmans, B.N., Verlaan, I., Hengeveld, T., Janssen, H., Calafat, J., Falk, M.M. and Moolenaar, W.H. (2001) Gap junction protein connexin-43 interacts directly with microtubules. *Curr Biol* **11**, 1364-8.

Goldman, S. (2003) Glia as neural progenitor cells. *Trends Neurosci* **26**, 590-6.

Gomes, A.R., Cunha, P., Nuriya, M., Faro, C.J., Huganir, R.L., Pires, E.V., Carvalho, A.L. and Duarte, C.B. (2004) Metabotropic glutamate and dopamine receptors co-regulate AMPA receptor activity through PKA in cultured chick retinal neurones: effect on GluR4 phosphorylation and surface expression. *J Neurochem* **90**, 673-82.

Gomez, T.M. and Spitzer, N.C. (1999) In vivo regulation of axon extension and pathfinding by growth-cone calcium transients. *Nature* **397**, 350-5.

Goodenough, D.A. and Paul, D.L. (2003) Beyond the gap: functions of unpaired connexon channels. *Nat Rev Mol Cell Biol* **4**, 285-94.

Greka, A., Lipton, S.A. and Zhang, D. (2000) Expression of GABA(C) receptor rho1 and rho2 subunits during development of the mouse retina. *Eur J Neurosci* **12**, 3575-82.

Gridley, T. (1997) Notch signaling in vertebrate development and disease. *Mol Cell Neurosci* **9**, 103-8.

Gu, X. and Spitzer, N.C. (1995) Distinct aspects of neuronal differentiation encoded by frequency of spontaneous Ca2+ transients. *Nature* **375**, 784-7.

Guldenagel, M., Ammermuller, J., Feigenspan, A., Teubner, B., Degen, J., Sohl, G., Willecke, K. and Weiler, R. (2001) Visual transmission deficits in mice with targeted disruption of the gap junction gene connexin36. *J Neurosci* **21** , 6036-44.

Gulisano, M., Parenti, R., Spinella, F. and Cicirata, F. (2000) Cx36 is dynamically expressed during early development of mouse brain and nervous system. *Neuroreport* **11**, 3823-8.

Halfter, W., Dong, S., Balasubramani, M. and Bier, M.E. (2001) Temporary disruption of the retinal basal lamina and its effect on retinal histogenesis. *Dev Biol* **238**, 79-96.

Halfter, W., Dong, S., Yip, Y.P., Willem, M. and Mayer, U. (2002) A critical function of the pial basement membrane in cortical histogenesis. *J Neurosci* **22**, 6029-40.

Hamburger, V. and Hamilton, H.L. (1992) A series of normal stages in the development of the chick embryo. 1951. *Dev Dyn* **195**, 231-72.

Haque, S., Haruna, Y., Saito, K., Nalesnik, M.A., Atillasoy, E., Thung, S.N. and Gerber, M.A. (1996) Identification of bipotential progenitor cells in human liver regeneration. *Lab Invest* **75**, 699-705.

Harris, A.L. (2001) Emerging issues of connexin channels: biophysics fills the gap. *Q Rev Biophys* **34**, 325-472.

Hatten, M.E. (1990) Riding the glial monorail: a common mechanism for glial-guided neuronal migration in different regions of the developing mammalian brain. *Trends Neurosci* **13**, 179-84.

Haydar, T.F., Wang, F., Schwartz, M.L. and Rakic, P. (2000) Differential modulation of proliferation in the neocortical ventricular and subventricular zones. *J Neurosci* **20**, 5764-74.

Hidaka, S., Kato, T. and Miyachi, E. (2002) Expression of gap junction connexin36 in adult rat retinal ganglion cells. *J Integr Neurosci* **1**, 3-22.

Hille, B. (2001) *Ion Channels of Excitable Membranes*, Third edn. Sunderland, Massachusetts, USA: Sinauer Associates Incorporated.

Hofer, A. and Dermietzel, R. (1998) Visualization and functional blocking of gap junction hemichannels (connexons) with antibodies against external loop domains in astrocytes. *Glia* **24**, 141-54.

Hollmann, M. and Heinemann, S. (1994) Cloned glutamate receptors. *Annu Rev Neurosci* **17**, 31-108.

Hollyfield, J.G. and Witkovsky, P. (1974) Pigmented retinal epithelium involvement in photoreceptor development and function. *J Exp Zool* **189**, 357-78.

Honig, M.G. and Hume, R.I. (1986) Fluorescent carbocyanine dyes allow living neurons of identified origin to be studied in long-term cultures. *J Cell Biol* **103**, 171-87.

Hu, M., Bruun, A. and Ehinger, B. (1999a) Expression of GABA transporter subtypes (GAT1, GAT3) in the adult rabbit retina. *Acta Ophthalmol Scand* **77**, 255-60.

Hu, M., Bruun, A. and Ehinger, B. (1999b) Expression of GABA transporter subtypes (GAT1, GAT3) in the developing rabbit retina. *Acta Ophthalmol Scand* **77**, 261-5.

Huang, G.Y., Cooper, E.S., Waldo, K., Kirby, M.L., Gilula, N.B. and Lo, C.W. (1998) Gap junction-mediated cell-cell communication modulates mouse neural crest migration. *J Cell Biol* **143**, 1725-34.

Hughes, W.F. and McLoon, S.C. (1979) Ganglion cell death during normal retinal development in the chick: comparisons with cell death induced by early target field destruction. *Exp Neurol* **66**, 587-601.

Im, W.B., Binder, J.A., Dillon, G.H., Pregenzer, J.F., Im, H.K. and Altman, R.A. (1995) Acceleration of GABA-dependent desensitization by mutating threonine 266 to alanine of the alpha 6 subunit of rat GABAA receptors. *Neurosci Lett* **186**, 203-7.

Imaki, H., Moretz, R.C., Wisniewski, H.M. and Sturman, J.A. (1986) Feline maternal taurine deficiency: effects on retina and tapetum of the offspring. *Dev Neurosci* **8**, 160-81.

Jabs, R., Guenther, E., Marquordt, K. and Wheeler-Schilling, T.H. (2000) Evidence for P2X(3), P2X(4), P2X(5) but not for P2X(7) containing purinergic receptors in Muller cells of the rat retina. *Brain Res Mol Brain Res* **76**, 205-10.

Kahn, A.J. (1974) An autoradiographic analysis of the time of appearance of neurons in the developing chick neural retina. *Dev Biol* **38**, 30-40.

Kanner, B.I. (1994) Sodium-coupled neurotransmitter transport: structure, function and regulation. *J Exp Biol* **196**, 237-49.

Keyser, K.T., Hughes, T.E., Whiting, P.J., Lindstrom, J.M. and Karten, H.J. (1988) Cholinoceptive neurons in the retina of the chick: an immunohistochemical study of the nicotinic acetylcholine receptors. *Vis Neurosci* **1**, 349-66.

Komuro, H. and Rakic, P. (1998) Distinct modes of neuronal migration in different domains of developing cerebellar cortex. *J Neurosci* **18**, 1478-90.

Komuro, H. and Rakic, P. (1995) Dynamics of granule cell migration: a confocal microscopic study in acute cerebellar slice preparations. *J Neurosci* **15** , 1110-20.

Komuro, H. and Rakic, P. (1996) Intracellular Ca2+ fluctuations modulate the rate of neuronal migration. *Neuron* **17**, 275-85.

Komuro, H. and Rakic, P. (1993) Modulation of neuronal migration by NMDA receptors. *Science* **260**, 95-7.

Komuro, H. and Rakic, P. (1998) Orchestration of neuronal migration by activity of ion channels, neurotransmitter receptors, and intracellular Ca2+ fluctuations. *J Neurobiol* **37**, 110-30.

Komuro, H. and Rakic, P. (1992) Selective role of N-type calcium channels in neuronal migration. *Science* **257**, 806-9.

Komuro, H., Yacubova, E., Yacubova, E. and Rakic, P. (2001) Mode and tempo of tangential cell migration in the cerebellar external granular layer. *J Neurosci* **21**, 527-40.

Kugler, P. and Beyer, A. (2003) Expression of glutamate transporters in human and rat retina and rat optic nerve. *Histochem Cell Biol* **120**, 199-212.

Kuriyama, K., Hirouchi, M. and Kimura, H. (2000) Neurochemical and molecular pharmacological aspects of the GABA(B) receptor. *Neurochem Res* **25**, 1233-9.

Laasberg, T. (1990) Ca2(+)-mobilizing receptors of gastrulating chick embryo. *Comp Biochem Physiol C* **97**, 9-12.

Layer, P.G. and Sporns, O. (1987) Spatiotemporal relationship of embryonic cholinesterases with cell proliferation in chicken brain and eye. *Proc Natl Acad Sci U S A* **84**, 284-8.

Lewis, J. (1998) Notch signalling and the control of cell fate choices in vertebrates. *Semin Cell Dev Biol* **9**, 583-9.

Leybaert, L., Braet, K., Vandamme, W., Cabooter, L., Martin, P.E. and Evans, W.H. (2003) Connexin channels, connexin mimetic peptides and ATP release. *Cell Commun Adhes* **10**, 251-7.

Livesey, F.J. and Cepko, C.L. (2001) Vertebrate neural cell-fate determination: lessons from the retina. *Nat Rev Neurosci* **2**, 109-18.

Lo Turco, J.J. and Kriegstein, A.R. (1991) Clusters of coupled neuroblasts in embryonic neocortex. *Science* **252**, 563-6.

Lodish, H., Darnell, J. and Matsudaira, P.T. (2000) Molecular cell biology. 4th ed. edn, New York, NY ; Basingstoke : W. H. Freeman : Macmillan.

Lopez, T., Lopez-Colome, A.M. and Ortega, A. (1998) Changes in GluR4 expression induced by metabotropic receptor activation in radial glia cultures. *Brain Res Mol Brain Res* **58**, 40-6.

LoTurco, J.J., Blanton, M.G. and Kriegstein, A.R. (1991) Initial expression and endogenous activation of NMDA channels in early neocortical development. *J Neurosci* **11**, 792-9.

LoTurco, J.J., Owens, D.F., Heath, M.J., Davis, M.B. and Kriegstein, A.R. (1995) GABA and glutamate depolarize cortical progenitor cells and inhibit DNA synthesis. *Neuron* **15**, 1287-98.

Lowe, G. (2003) Flash photolysis reveals a diversity of ionotropic glutamate receptors on the mitral cell somatodendritic membrane. *J Neurophysiol* **90**, 1737-46.

Lumsden, A., Sprawson, N. and Graham, A. (1991) Segmental origin and migration of neural crest cells in the hindbrain region of the chick embryo. *Development* **113**, 1281-91.

Ma, W., Maric, D., Li, B.S., Hu, Q., Andreadis, J.D., Grant, G.M., Liu, Q.Y., Shaffer, K.M., Chang, Y.H., Zhang, L., Pancrazio, J.J., Pant, H.C., Stenger, D.A. and Barker, J.L. (2000) Acetylcholine stimulates cortical precursor cell proliferation in vitro via muscarinic receptor activation and MAP kinase phosphorylation. *Eur J Neurosci* **12**, 1227-40.

Macaione, S., Ruggeri, P., De Luca, F. and Tucci, G. (1974) Free amino acids in developing rat retina. *J Neurochem* **22**, 887-91.

Malatesta, P., Hartfuss, E. and Gotz, M. (2000) Isolation of radial glial cells by fluorescent-activated cell sorting reveals a neuronal lineage. *Development* **127**, 5253-63.

Mattson, M.P., Dou, P. and Kater, S.B. (1988) Outgrowth-regulating actions of glutamate in isolated hippocampal pyramidal neurons. *J Neurosci* **8**, 2087-100.

McGonnell, I.M., Green, C.R., Tickle, C. and Becker, D.L. (2001) Connexin43 gap junction protein plays an essential role in morphogenesis of the embryonic chick face. *Dev Dyn* **222**, 420-38.

McLaughlin, T., Torborg, C.L., Feller, M.B. and O'Leary, D.D. (2003) Retinotopic map refinement requires spontaneous retinal waves during a brief critical period of development. *Neuron* **40**, 1147-60.

McLoon, S.C. and Barnes, R.B. (1989) Early differentiation of retinal ganglion cells: an axonal protein expressed by premigratory and migrating retinal ganglion cells. *J Neurosci* **9**, 1424-32.

Meister, M., Wong, R.O., Baylor, D.A. and Shatz, C.J. (1991) Synchronous bursts of action potentials in ganglion cells of the developing mammalian retina. *Science* **252**, 939-43.

Mey, J. and Thanos, S. (2000) Development of the visual system of the chick. I. Cell differentiation and histogenesis. *Brain Res Brain Res Rev* **32**, 343-79.

Meyer, R.A., Laird, D.W., Revel, J.P. and Johnson, R.G. (1992) Inhibition of gap junction and adherens junction assembly by connexin and A-CAM antibodies. *J Cell Biol* **119**, 179-89.

Mills, S.L., O'Brien, J.J., Li, W., O'Brien, J. and Massey, S.C. (2001) Rod pathways in the mammalian retina use connexin 36. *J Comp Neurol* **436**, 336-50.

Miyata, T., Kawaguchi, A., Okano, H. and Ogawa, M. (2001) Asymmetric inheritance of radial glial fibers by cortical neurons. *Neuron* **31**, 727-41.

Montoro, R.J. and Yuste, R. (2004) Gap junctions in developing neocortex: a review. *Brain Res Brain Res Rev* **47**, 216-26.

Morris, V.B. and Cowan, R. (1995) An analysis of the growth of the retinal cell population in embryonic chicks yielding proliferative ratios, numbers of proliferative and non-proliferative cells and cell-cycle times for successive generations of cell cycles. *Cell Prolif* **28**, 373-91.

Mortensen, M., Kristiansen, U., Ebert, B., Frolund, B., Krogsgaard-Larsen, P. and Smart, T.G. (2004) Activation of single heteromeric GABA(A) receptor ion channels by full and partial agonists. *J Physiol* **557**, 389-413.

Murciano, A., Zamora, J., Lopez-Sanchez, J. and Frade, J.M. (2002) Interkinetic nuclear movement may provide spatial clues to the regulation of neurogenesis. *Mol Cell Neurosci* **21**, 285-300.

Nadarajah, B., Brunstrom, J.E., Grutzendler, J., Wong, R.O. and Pearlman, A.L. (2001) Two modes of radial migration in early development of the cerebral cortex. *Nat Neurosci* **4**, 143-50.

Nadarajah, B., Jones, A.M., Evans, W.H. and Parnavelas, J.G. (1997) Differential expression of connexins during neocortical development and neuronal circuit formation. *J Neurosci* **17**, 3096-111.

Nadarajah, B., Makarenkova, H., Becker, D.L., Evans, W.H. and Parnavelas, J.G. (1998) Basic FGF increases communication between cells of the developing neocortex. *J Neurosci* **18**, 7881-90.

Nadarajah, B., Thomaidou, D., Evans, W.H. and Parnavelas, J.G. (1996) Gap junctions in the adult cerebral cortex: regional differences in their distribution and cellular expression of connexins. *J Comp Neurol* **376**, 326-42.

Nadler, L.S., Rosoff, M.L., Hamilton, S.E., Kalaydjian, A.E., McKinnon, L.A. and Nathanson, N.M. (1999) Molecular analysis of the regulation of muscarinic receptor expression and function. *Life Sci* **64**, 375-9.

Nagele, R.G. and Lee, H.Y. (1979) Ultrastructural changes in cells associated with interkinetic nuclear migration in the developing chick neuroepithelium. *J Exp Zool* **210**, 89-106.

Nakanishi, S. (1994) Metabotropic glutamate receptors: synaptic transmission, modulation, and plasticity. *Neuron* **13**, 1031-7.

Naus, C.C. and Bani-Yaghoub, M. (1998) Gap junctional communication in the developing central nervous system. *Cell Biol Int* **22**, 751-63.

Nguyen, L., Malgrange, B., Breuskin, I., Bettendorff, L., Moonen, G., Belachew, S. and Rigo, J.M. (2003) Autocrine/paracrine activation of the GABA(A) receptor inhibits the proliferation of neurogenic polysialylated neural cell adhesion molecule-positive (PSA-NCAM+) precursor cells from postnatal striatum. *J Neurosci* **23**, 3278-94.

Noctor, S.C., Flint, A.C., Weissman, T.A., Dammerman, R.S. and Kriegstein, A.R. (2001) Neurons derived from radial glial cells establish radial units in neocortex. *Nature* **409**, 714-20.

O'Rourke, N.A., Chenn, A. and McConnell, S.K. (1997) Postmitotic neurons migrate tangentially in the cortical ventricular zone. *Development* **124**, 997-1005.

Okano, T., Fukada, Y. and Yoshizawa, T. (1995) Molecular basis for tetrachromatic color vision. *Comp Biochem Physiol B Biochem Mol Biol* **112**, 405-14.

Oppenheim, R.W. (1991) Cell death during development of the nervous system. *Annu Rev Neurosci* **14**, 453-501.

Owens, D.F., Boyce, L.H., Davis, M.B. and Kriegstein, A.R. (1996) Excitatory GABA responses in embryonic and neonatal cortical slices demonstrated by gramicidin perforated-patch recordings and calcium imaging. *J Neurosci* **16**, 6414-23.

Owens, D.F. and Kriegstein, A.R. (1998) Patterns of intracellular calcium fluctuation in precursor cells of the neocortical ventricular zone. *J Neurosci* **18**, 5374-88.

Parnavelas, J.G. and Nadarajah, B. (2001) Radial glial cells. are they really glia? *Neuron* **31**, 881-4.

Pearson, R., Catsicas, M., Becker, D. and Mobbs, P. (2002) Purinergic and muscarinic modulation of the cell cycle and calcium signaling in the chick retinal ventricular zone. *J Neurosci* **22**, 7569-79.

Pearson, R.A., Catsicas, M., Becker, D.L., Bayley, P., Luneborg, N.L. and Mobbs, P. (2004) Ca(2+) signalling and gap junction coupling within and between pigment epithelium and neural retina in the developing chick. *Eur J Neurosci* **19**, 2435-45.

Pearson, R.A., Dale, N., Llaudet, E. and Mobbs, P. (2005a) ATP released from the retinal pigment epithelium regulates neural retinal progenitor proliferation. *Neuron* (In Press)

Pearson, R.A., Lüneborg, N.L., Becker, D.L. and Mobbs, P. (2005b) Gap junctions modulate interkinetic nuclear migration in retinal progenitor cells. *J Neurosci* (In Press)

Pearson, R.A. (2003) The role of neurotransmitters in the regulation of cell proliferation in the embryonic chick retina. University College London. Thesis (Ph.D.)

Peracchia, C., Wang, X., Li, L. and Peracchia, L.L. (1996) Inhibition of calmodulin expression prevents low-pH-induced gap junction uncoupling in Xenopus oocytes. *Pflugers Arch* **431**, 379-87.

Perron, M. and Harris, W.A. (2000) Determination of vertebrate retinal progenitor cell fate by the Notch pathway and basic helix-loop-helix transcription factors. *Cell Mol Life Sci* **57**, 215-23.

Piccolino, M., Neyton, J. and Gerschenfeld, H.M. (1984) Decrease of gap junction permeability induced by dopamine and cyclic adenosine 3':5'-monophosphate in horizontal cells of turtle retina. *J Neurosci* **4**, 2477-88.

Pittack, C., Grunwald, G.B. and Reh, T.A. (1997) Fibroblast growth factors are necessary for neural retina but not pigmented epithelium differentiation in chick embryos. *Development* **124**, 805-16.

Pittack, C., Jones, M. and Reh, T.A. (1991) Basic fibroblast growth factor induces retinal pigment epithelium to generate neural retina in vitro. *Development* **113**, 577-88.

Prada, C., Puga, J., Perez-Mendez, L., Lopez, R. and Ramirez, G. (1991) Spatial and Temporal Patterns of Neurogenesis in the Chick Retina. *Eur J Neurosci* **3**, 559-569.

Price, M.T., Romano, C., Fix, A.S., Tizzano, J.P. and Olney, J.W. (1995) Blockade of the second messenger functions of the glutamate metabotropic receptor is associated with degenerative changes in the retina and brain of immature rodents. *Neuropharmacology* **34**, 1069-79.

Raff, M.C., Barres, B.A., Burne, J.F., Coles, H.S., Ishizaki, Y. and Jacobson, M.D. (1993) Programmed cell death and the control of cell survival: lessons from the nervous system. *Science* **262**, 695-700.

Raff, M.C., Williams, B.P. and Miller, R.H. (1984) The in vitro differentiation of a bipotential glial progenitor cell. *EMBO J* **3**, 1857-64.

Rakic, P. (1972) Mode of cell migration to the superficial layers of fetal monkey neocortex. *J Comp Neurol* **145**, 61-83.

Rakic, P., Knyihar-Csillik, E. and Csillik, B. (1996) Polarity of microtubule assemblies during neuronal cell migration. *Proc Natl Acad Sci U S A* **93**, 9218-22.

Rakic, P. and Komuro, H. (1995) The role of receptor/channel activity in neuronal cell migration. *J Neurobiol* **26**, 299-315.

Rauen, T., Rothstein, J.D. and Wassle, H. (1996) Differential expression of three glutamate transporter subtypes in the rat retina. *Cell Tissue Res* **286**, 325-36.

Reese, B.E. and Tan, S.S. (1998) Clonal boundary analysis in the developing retina using X-inactivation transgenic mosaic mice. *Semin Cell Dev Biol* **9**, 285-92.

Reh, T.A. (1987) Cell-specific regulation of neuronal production in the larval frog retina. *J Neurosci* **7**, 3317-24.

Reid, C.B., Liang, I. and Walsh, C. (1995) Systematic widespread clonal organization in cerebral cortex. *Neuron* **15**, 299-310.

Revilla, A., Bennett, M.V. and Barrio, L.C. (2000) Molecular determinants of membrane potential dependence in vertebrate gap junction channels. *Proc Natl Acad Sci U S A* **97**, 14760-5.

Rivera, C., Voipio, J., Payne, J.A., Ruusuvuori, E., Lahtinen, H., Lamsa, K., Pirvola, U., Saarma, M. and Kaila, K. (1999) The K+/Cl- co-transporter KCC2 renders GABA hyperpolarizing during neuronal maturation. *Nature* **397**, 251-5.

Robinson, D.W. and Wang, G.Y. (1998) Development of intrinsic membrane properties in mammalian retinal ganglion cells. *Semin Cell Dev Biol* **9**, 301-10.

Robinson, S.R., Rapaport, D.H. and Stone, J. (1985) Cell division in the developing cat retina occurs in two zones. *Brain Res* **351**, 101-9.

Rook, M.B., de Jonge, B., Jongsma, H.J. and Masson-Pevet, M.A. (1990) Gap junction formation and functional interaction between neonatal rat cardiocytes in culture: a correlative physiological and ultrastructural study. *J Membr Biol* **118**, 179-92.

Rosen, L.B., Ginty, D.D., Weber, M.J. and Greenberg, M.E. (1994) Membrane depolarization and calcium influx stimulate MEK and MAP kinase via activation of Ras. *Neuron* **12**, 1207-21.

Rossi, D.J. and Slater, N.T. (1993) The developmental onset of NMDA receptor-channel activity during neuronal migration. *Neuropharmacology* **32**, 1239-48.

Saito, K., Kawaguchi, A., Kashiwagi, S., Yasugi, S., Ogawa, M. and Miyata, T. (2003) Morphological asymmetry in dividing retinal progenitor cells. *Dev Growth Differ* **45**, 219-29.

Sakaki, Y., Fukuda, Y. and Yamashita, M. (1996) Muscarinic and purinergic Ca2+ mobilizations in the neural retina of early embryonic chick. *Int J Dev Neurosci* **14**, 691-9.

Santos, P.F., Caramelo, O.L., Carvalho, A.P. and Duarte, C.B. (1999) Characterization of ATP release from cultures enriched in cholinergic amacrine-like neurons. *J Neurobiol* **41**, 340-8.

Santos, P.F., Carvalho, A.L., Carvalho, A.P. and Duarte, C.B. (1998) Differential acetylcholine and GABA release from cultured chick retina cells. *Eur J Neurosci* **10**, 2723-30.

Sauer, F.C. (1935) Mitosis in the neural tube. *The Journal of Comparative Neurology* **62**, 377-405.

Scemes, E., Duval, N. and Meda, P. (2003) Reduced expression of P2Y1 receptors in connexin43-null mice alters calcium signaling and migration of neural progenitor cells. *J Neurosci* **23**, 11444-52.

Sernagor, E. and Grzywacz, N.M. (1996) Influence of spontaneous activity and visual experience on developing retinal receptive fields. *Curr Biol* **6**, 1503-8.

Seymour, R.M. and Berry, M. (1975) Scanning and transmission electron microscope studies of interkinetic nuclear migration in the cerebral vesicles of the rat. *J Comp Neurol* **160**, 105-25.

Sidman, R.L., Miale, I.L. and Feder, N. (1959) Cell proliferation and migration in the primitive ependymal zone: an autoradiographic study of histogenesis in the nervous system. *Exp Neurol* **1**, 322-33.

Sieghart, W. (2000) Unraveling the function of GABA(A) receptor subtypes. *Trends Pharmacol Sci* **21**, 411-3.

Silveira dos Santos Bredariol, A. and Hamassaki-Britto, D.E. (2001) Ionotropic glutamate receptors during the development of the chick retina. *J Comp Neurol* **441**, 58-70.

Skaliora, I., Robinson, D.W., Scobey, R.P. and Chalupa, L.M. (1995) Properties of K+ conductances in cat retinal ganglion cells during the period of activity-mediated refinements in retinofugal pathways. *Eur J Neurosci* **7**, 1558-68.

Skaliora, I., Scobey, R.P. and Chalupa, L.M. (1993) Prenatal development of excitability in cat retinal ganglion cells: action potentials and sodium currents. *J Neurosci* **13**, 313-23.

Snellman, J. and Nawy, S. (2002) Regulation of the retinal bipolar cell mGluR6 pathway by calcineurin. *J Neurophysiol* **88**, 1088-96.

Snow, R.L. and Robson, J.A. (1994) Ganglion cell neurogenesis, migration and early differentiation in the chick retina. *Neuroscience* **58**, 399-409.

Spitzer, N.C. and Lamborghini, J.E. (1976) The development of the action potential mechanism of amphibian neurons isolated in culture. *Proc Natl Acad Sci U S A* **73**, 1641-5.

Spitzer, N.C. and Ribera, A.B. (1998) Development of electrical excitability in embryonic neurons: mechanisms and roles. *J Neurobiol* **37**, 190-7.

Spitzer, N.C., Root, C.M. and Borodinsky, L.N. (2004) Orchestrating neuronal differentiation: patterns of Ca2+ spikes specify transmitter choice. *Trends Neurosci* **27**, 415-21.

Spitzer, N.C., Vincent, A. and Lautermilch, N.J. (2000) Differentiation of electrical excitability in motoneurons. *Brain Res Bull* **53**, 547-52.

Sterling P., Freed, M. and Smith, R.G. (1986) Microcircuitry and functional architecture of the cat retina. *Trends in Neurosciences* **9**, 186-192 .

Sturman, J.A. (1993) Taurine in development. *Physiol Rev* **73**, 119-47.

Sugioka, M., Fukuda, Y. and Yamashita, M. (1996) Ca2+ responses to ATP via purinoceptors in the early embryonic chick retina. *J Physiol* **493 (Pt 3)**, 855-63.

Sugioka, M., Zhou, W.L., Hofmann, H.D. and Yamashita, M. (1999) Involvement of P2 purinoceptors in the regulation of DNA synthesis in the neural retina of chick embryo. *Int J Dev Neurosci* **17**, 135-44.

Sun, W., Seigel, G.M. and Salvi, R.J. (2002) Retinal precursor cells express functional ionotropic glutamate and GABA receptors. *Neuroreport* **13**, 2421-4.

Sutherland, M.L., Delaney, T.A. and Noebels, J.L. (1996) Glutamate transporter mRNA expression in proliferative zones of the developing and adult murine CNS. *J Neurosci* **16**, 2191-207.

Syed, M.M., Lee, S., He, S. and Zhou, Z.J. (2004) Spontaneous waves in the ventricular zone of developing mammalian retina. *J Neurophysiol* **91**, 1999-2009.

Takahashi, T., Nowakowski, R.S. and Caviness, V.S. Jr (1993) Cell cycle parameters and patterns of nuclear movement in the neocortical proliferative zone of the fetal mouse. *J Neurosci* **13**, 820-33.

Takahashi, T., Nowakowski, R.S. and Caviness, V.S. Jr (1996) Interkinetic and migratory behavior of a cohort of neocortical neurons arising in the early embryonic murine cerebral wall. *J Neurosci* **16**, 5762-76.

Takahashi, T., Nowakowski, R.S. and Caviness, V.S. Jr (1994) Mode of cell proliferation in the developing mouse neocortex. *Proc Natl Acad Sci U S A* **91** , 375-9.

Tessier-Lavigne, M., Attwell, D., Mobbs, P. and Wilson, M. (1988) Membrane currents in retinal bipolar cells of the axolotl. *J Gen Physiol* **91**, 49-72.

Thomas, M.A., Zosso, N., Scerri, I., Demaurex, N., Chanson, M. and Staub, O. (2003) A tyrosine-based sorting signal is involved in connexin43 stability and gap junction turnover. *J Cell Sci* **116**, 2213-22.

Thompson, S. (1982) Aminopyridine block of transient potassium current. *J Gen Physiol* **80**, 1-18.

Tian, N. and Copenhagen, D.R. (2003) Visual stimulation is required for refinement of ON and OFF pathways in postnatal retina. *Neuron* **39**, 85-96.

Turner, D.L. and Cepko, C.L. (1987) A common progenitor for neurons and glia persists in rat retina late in development. *Nature* **328**, 131-6.

Turner, D.L., Snyder, E.Y. and Cepko, C.L. (1990) Lineage-independent determination of cell type in the embryonic mouse retina. *Neuron* **4**, 833-45.

Veenstra, R.D. and DeHaan, R.L. (1986) Measurement of single channel currents from cardiac gap junctions. *Science* **233**, 972-4.

Vessey, J.P., Lalonde, M.R., Mizan, H.A., Welch, N.C., Kelly, M.E. and Barnes, S. (2004) Carbenoxolone inhibition of voltage-gated Ca channels and synaptic transmission in the retina. *J Neurophysiol* **92**, 1252-6.

Vincent, A., Lautermilch, N.J. and Spitzer, N.C. (2000) Antisense suppression of potassium channel expression demonstrates its role in maturation of the action potential. *J Neurosci* **20**, 6087-94.

Waid, D.K. and McLoon, S.C. (1998) Ganglion cells influence the fate of dividing retinal cells in culture. *Development* **125**, 1059-66.

Waid, D.K. and McLoon, S.C. (1995) Immediate differentiation of ganglion cells following mitosis in the developing retina. *Neuron* **14**, 117-24.

Walcott, J.C. and Provis, J.M. (2003) Muller cells express the neuronal progenitor cell marker nestin in both differentiated and undifferentiated human foetal retina. *Clin Experiment Ophthalmol* **31**, 246-9.

Wang, D.D., Krueger, D.D. and Bordey, A. (2003) Biophysical properties and ionic signature of neuronal progenitors of the postnatal subventricular zone in situ. *J Neurophysiol* **90**, 2291-302.

Wang, D.D., Krueger, D.D. and Bordey, A. (2003) GABA depolarizes neuronal progenitors of the postnatal subventricular zone via GABAA receptor activation. *J Physiol* **550**, 785-800.

Wei, C.J., Xu, X. and Lo, C.W. (2004) Connexins and cell signaling in development and disease. *Annu Rev Cell Dev Biol* **20**, 811-38.

Weise, B., Janet, T. and Grothe, C. (1993) Localization of bFGF and FGF-receptor in the developing nervous system of the embryonic and newborn rat. *J Neurosci Res* **34**, 442-53.

Weissman, T.A., Riquelme, P.A., Ivic, L., Flint, A.C. and Kriegstein, A.R. (2004) Calcium waves propagate through radial glial cells and modulate proliferation in the developing neocortex. *Neuron* **43**, 647-61.

Wheeler-Schilling, T.H., Marquordt, K., Kohler, K., Guenther, E. and Jabs, R. (2001) Identification of purinergic receptors in retinal ganglion cells. *Brain Res Mol Brain Res* **92**, 177-80.

Wheeler-Schilling, T.H., Marquordt, K., Kohler, K., Jabs, R. and Guenther, E. (2000) Expression of purinergic receptors in bipolar cells of the rat retina. *Brain Res Mol Brain Res* **76**, 415-8.

Wilkinson, M.G. and Millar, J.B. (2000) Control of the eukaryotic cell cycle by MAP kinase signaling pathways. *FASEB J* **14**, 2147-57.

Williams, M. and Jarvis, M.F. (2000) Purinergic and pyrimidinergic receptors as potential drug targets. *Biochem Pharmacol* **59**, 1173-85.

Wong, W.T., Sanes, J.R. and Wong, R.O. (1998) Developmentally regulated spontaneous activity in the embryonic chick retina. *J Neurosci* **18**, 8839-52.

Xu, X., Li, W.E., Huang, G.Y., Meyer, R., Chen, T., Luo, Y., Thomas, M.P., Radice, G.L. and Lo, C.W. (2001) Modulation of mouse neural crest cell motility by N-cadherin and connexin 43 gap junctions. *J Cell Biol* **154**, 217-30.

Yamashita, M. and Fukuda, Y. (1993) Calcium channels and GABA receptors in the early embryonic chick retina. *J Neurobiol* **24**, 1600-14.

Yang, X.L. (2004) Characterization of receptors for glutamate and GABA in retinal neurons. *Prog Neurobiol* **73**, 127-50.

Young, R.W. (1984) Cell death during differentiation of the retina in the mouse. *J Comp Neurol* **229**, 362-73.

Young, R.W. (1985) Cell differentiation in the retina of the mouse. *Anat Rec* **212**, 199-205.

Young, T.L. and Cepko, C.L. (2004) A role for ligand-gated ion channels in rod photoreceptor development. *Neuron* **41**, 867-79.

Zhou, Z.J. and Fain, G.L. (1995) Neurotransmitter receptors of starburst amacrine cells in rabbit retinal slices. *J Neurosci* **15**, 5334-45.